

STUDY OF ENVIRONMENTAL FRIENDLY DIAMOND LIKE COATING ON TOOL INSERTS FOR PRECISION MACHINING

A Thesis submitted to the Delhi Technological University, Delhi in fulfilment of the requirements for the award of the degree of

DOCTOR OF PHILOSOPHY

in

Mechanical Engineering

By

RAMAKANT RANA
(2K16/PhD/ME/18)

Under the Supervision of

Dr. Qasim Murtaza

Professor,
Department of Mechanical Engineering
Delhi Technological University,
Delhi, India

Dr. R.S. Walia

Professor and Head,
Department of Production and Industrial Engineering,
Punjab Engineering College,
Chandigarh, India



DEPARTMENT OF MECHANICAL ENGINEERING

DELHI TECHNOLOGICAL UNIVERSITY

SHAHBAD, DAULPUR, BAWANA ROAD, DELHI-110042, INDIA

July, 2022

DECLARATION

I hereby declare that the thesis work entitled “**STUDY OF ENVIRONMENTAL FRIENDLY DIAMOND LIKE COATING ON TOOL INSERTS FOR PRECISION MACHINING**” is an original work carried out by me under the supervision of Dr. Qasim Murtaza, Professor, Department of Mechanical Engineering, Delhi Technological University, Delhi and Dr. R.S. Walia, Professor and Head, Production and Industrial Engineering, Punjab Engineering College (Deemed to be University), Chandigarh. This thesis has been prepared in conformity with the rules and regulations of the Delhi Technological University, Delhi. The research work presented and reported in the thesis has not been submitted either in part or in full to any other university or institute for the award of any other degree or diploma.

RAMAKANT RANA

(Regd. No: 2K16/PhD/ME/18)

Deptt. of Mechanical Engineering

Delhi Technological University,

Delhi

Date: 07.07.2022

Place: Delhi

CERTIFICATE

This is to certify that the thesis entitled, “**STUDY OF ENVIRONMENTAL FRIENDLY DIAMOND LIKE COATING ON TOOL INSERTS FOR PRECISION MACHINING**” submitted by **Mr. Ramakant Rana** to the Delhi Technological University, Delhi for the award of the degree of **Doctor of Philosophy in Mechanical Engineering** is a bonafide record of original research work carried out by him under our supervision in accordance with the rules and regulations of the university. The results presented in this thesis have not been submitted, in part or full, to any University or Institute for the award of any degree or diploma.

Dr. Qasim Murtaza
Professor,
Department of Mechanical Engineering
Delhi Technological University,
Delhi, India

Dr. R.S. Walia,
Professor and Head,
Department of Production and Industrial Engineering,
Punjab Engineering College
(Deemed to be University),
Chandigarh, India

Dedicated

to

My Son, Rudransh Rana and My Father, Dr. Roop Lal

ACKNOWLEDGMENTS

I would like to express my deep gratitude, sincere thanks, and appreciation to my supervisors Prof. Qasim Murtaza and Prof. R.S. Walia, for their valuable guidance during my Ph.D. work. I am thankful from bottom of my heart for all the help, encouragement, and support he generously extended to me.

I would like to express, sincere gratitude to Prof. S.K. Garg, Head and Chairman DRC, Mechanical Engineering Department, Delhi Technological University, for his valuable help, motivation, and extending all the necessary processing and experimental facilities during my research work.

Thanks, are also due to Dr. Abid Ali Khan, Dr. Sanjeev Kumar, and Dr. Saurabh Aggarwal for serving my SRC committee and for much critical help without which I would not be able to complete my thesis in time.

I am also grateful to Dr. Lucky Krishnia, for all the motivation and support, without that I would not be able to finish my thesis work. My sincere thanks to all the faculty and staff members of the Department of Mechanical Engineering (DTU), who supported me during my entire course work and research work. I am grateful to Mr. Virender, Mr. Rajesh Bohra, Mr. Tekchand, Mr. Manmohan, and Mr. Ashok Dangi (MAIT) for their technical support.

I would like to express my sincere thanks to my HODs of MAIT, Dr. V. N. Mathur, and Dr. Vaibhav Jain, along with them Mr. Ashwni, Dr. Vipin Kumar Sharma, Dr. Sidharth, Dr. Sumit

Joshi, Dr. Garima Sharma, and Ms. Surabhi Lata of MAIT for their support and encouragement throughout this period.

I am always in debt to my parents Dr. Roop Lal and Mrs. Veena Devi, for providing me with all the energy booster thoughts, opportunities, and motivation that helped me to complete my Ph.D.

I am unable to express my sincere gratitude in words for the affection, encouragement, and support of my wife Mrs. Sakshi Raghuvanshi, during the entire research work, without her support I could not have completed my work. She happily permitted me to focus all my attention on my research work and continuously provided me the encouragement to complete my Ph.D.

Last but not the least; I would like to thank the Almighty for giving me the strength to complete this work in all respects and myself for not giving up.

(Ramakant Rana)

Place: New Delhi

July 2022

ABSTRACT

In this research work, attempts have been made to improve the machining parameters. For this, diamond-like carbon (DLC) coated tool inserts were used. The DLC coating on the tungsten carbide (WC) tool inserts were coated using the thermal chemical vapor deposition (CVD) method. For the growth of DLC coating, sugarcane bagasse was used as a carbon precursor. For characterization of the DLC coated tool inserts, Raman spectroscopy, a field emission scanning electron microscope (FESEM), and X-ray diffraction (XRD) were used, to confirm the presence of DLC coating on the tungsten carbide tool inserts.

For inspecting the hardness of the self-developed DLC coated and uncoated tool inserts, the tests of micro-hardness were also executed. The average values of the Vickers hardness for the uncoated and the DLC coated substrates were found to be 953.95 HV to 1478.78 HV respectively. It was observed that the hardness of the WC was increased by a factor of 1.5 after the coating process.

As per ASTM G-99 standards, the tribological behaviour of the self-developed DLC coated substrate was considered in the scope of this research work using a pin-on-disc tribometer. The tribological tests showed improvement in the wear resistance of the DLC coated WC tool inserts as there was a decrease in the value of wear by 58.02 %. The value of the coefficient of friction (COF) was also found to be decreased by 51.48%.

The coated tool inserts were evaluated for the crater wear, cutting force, surface roughness, and temperature in the cutting zone using conventional lathe machine tools and computer numeric control (CNC) lathe machine tools at different levels of the type of tools, feed, speed, and depth

of cut. It was found that for precision machining, computer numeric control (CNC) machine tools exhibit better results as compared to conventional ones. Further, the process parameters were optimized using TOPSIS and the Genetic Algorithm method. While optimizing the process parameters of the turning process on the conventional lathe machine tool using TOPSIS, the optimum values of cutting speed, feed, and depth of cut for achieving the minimum value of the selected response variables were found to be 60.52 m/min, 0.15 mm/rev and 0.192 mm respectively and from the Genetic Algorithm, the obtained optimized value of crater wear was found to be 461.07(μm), at a feed of 0.375mm/rev, a speed of 360m/min and a depth of cut of 0.2 mm.

Further, the performance of the coated tool inserts was enhanced by utilizing the surface texturing technique. Four shapes of the surface textures were fabricated on the coated tool inserts. These were line and wave texturing placed parallel and perpendicular to the tool nose radius. The textured tools were evaluated for the crater wear, cutting force, surface roughness, and temperature in the cutting zone. After optimizing the parameters, it was found that the tool inserts with wave texture parallel to the tool nose radius exhibit the best results when compared to the other texturing pattern and placement.

List of Publications

International Journals

1. R. Rana, R. S. Walia, and Q. Murtaza, “Characterization and parametric optimization of performance parameters of DLC-coated tungsten carbide (WC) tool using TOPSIS,” *Coatings*, vol. 11, no. 7, 2021, DOI: <https://doi.org/10.3390/coatings11070760>.
(SCIE Indexed, Impact Factor: 3.26)
2. R. Rana, L. Krishnia, R. S. Walia, and Q. Murtaza, “CVD Diamond Coated Tungsten Carbide (WC) Tool Inserts,” *J. Eng. Res.*, Oct. 2021, DOI: <https://doi.org/10.36909/jer.ICARI.15319>.
(SCIE Indexed, Impact Factor: 0.9)
3. R. Rana, L. Krishnia, Q. Murtaza, and R. S. Walia, “Optimizing the Machining performance of CNC tools inserts coated with Diamond-like Carbon Coatings under the dry cutting environment,” *J. Eng. Res.*, Oct. 2021, DOI: <https://doi.org/10.36909/jer.ICARI.15327> .
(SCIE Indexed, Impact Factor: 0.9)
4. R. Rana, Q. Murtaza, and R. S. Walia, “Optimization using genetic algorithm of tribological behaviour of WC tool material,” *Indian J. Eng. Mater. Sci.*, vol. 27, no. 4, pp. 889–896, 2020.
(SCIE Indexed, Impact Factor: 0.881)
5. R. Rana, W. R.S., and Q. Murtaza, “Characterizing and Analyzing the Tribological Behaviour of Diamond Coated Tungsten Carbide (WC),” *J. Eng. Res.*, Mar. 2022, DOI: <https://doi.org/10.36909/jer.ICAPIE.15107>.
(SCIE Indexed, Impact Factor: 0.9)
6. R. Rana, Q. Murtaza, and R. S. Walia, “GA based optimization of tri-biological behaviour of diamond coated tungsten carbide,” *World J. Eng.*, vol. 17, no. 3, pp. 335–346, May 2020, DOI: <https://doi.org/10.1108/WJE-08-2019-0220>.
(ESCI & SCOPUS Indexed, Impact Factor: 1.20)
7. R. Rana, Q. Murtaza, and R. S. Walia, “Studying and Analysing the Properties of the CVD and PVD Coated Tools used in Conventional Lathe Machine Tools and CNC Machine Tools for Turning Processes,” *Int. J. Adv. Prod. Ind. Eng.*, vol. 6, no. 1, pp. 53–83, 2021, DOI: <https://doi.org/10.35121/ijapie202101156>.

International Conferences

1. R. Rana, Q. Murtaza, and R. S. Walia, “*Experimental Analysis of various process parameters in CNC Turning Using TOPSIS*”, International Conference of Advance Research and Innovation (ICARI-2021), New Delhi, India, 19 January 2021, ISBN 978-93-5346-324-3.
2. R. Rana, Q. Murtaza, and R. S. Walia, “*Optimizing the Surface Roughness in CNC Turning Process using Coated Tools*”, International Conference of Advance Research and Innovation (ICARI-2020), New Delhi, India, 19 January 2020, ISBN 978-93-5346-324-3.
3. R. Rana, Q. Murtaza, and R. S. Walia, “*Study and Analysis of Tribological Behaviour of Coated and Uncoated tool material using a Pin on Disc Testing Rig*”, International Conference of Advance Research and Innovation (ICARI-2019), New Delhi, India, 20 January 2019, ISBN 978-93-5346-324-3.
4. R. Rana, Q. Murtaza, and R. S. Walia, “*Analyzing the temperature at the cutting zone while machining in the CNC using TAGUCHI*”, International Conference on Advanced Production and Industrial Engineering (ICAPIE-2019), Delhi, India, 20th - 21st December, 2019.

Table of Content

Page No.

	Declaration	i
	Certificate	ii
	Acknowledgments	iv
	Abstract	vi
	List of Publication	viii
	Table of Contents	x
	List of Figures	xiii
	List of Tables	xvii
Chapter 1	Introduction	1-32
1	Introduction	1
1.1	Manufacturing: An Introduction	4
1.2	Materials of Tool	5
1.2.1	High-Speed Steel (HSS)	7
1.2.2	High Carbon Steel (Tool Steel)	7
1.2.3	Cemented Carbides (Carbide Tool)	8
1.2.4	UCON	8
1.2.5	CBN (Cubic Boron Nitride)	8
1.3.6	SiAlON	9
1.2.7	Polycrystalline Diamond (PCD)	9
1.2.8	Ceramics	9
1.3	Tool Coatings	10
1.4	Texturing on Tools Inserts	12
1.5	Coating Techniques	13
1.5.1	Chemical Vapour Deposition (CVD) Process	15
1.5.2	Physical Vapour Deposition (PVD) Process	16
1.6	Precision Machining	18
1.7	Properties of Diamond	19
1.8	Application of Diamond	20
1.8.1	Wear and Cutting Applications	21
1.8.2	Acoustic Applications	21
1.8.3	Thermal Applications	22
1.8.4	Optical Applications	22
1.8.5	Electronic Applications	22
1.8.6	Electrochemical Applications	23
1.8.7	MEMS Applications	23
1.8.8	Biotechnology Applications	24
1.9	Different forms of Diamond	25
1.9.1	Natural Diamond	25
1.9.2	HPHT Method for the Formation of Diamond	26
1.9.3	CVD Method for the Formation of Diamond	27
1.9.4	Single Crystal Diamond	27
1.9.5	Polycrystalline Diamond	28
1.9.6	Nanocrystalline Diamond	29
1.9.7	Ultrananocrystalline Diamond	31
1.10	Summary	32

Chapter 2		Literature Review	33-59
2		Introduction	33
2.1		Coating Variants	33
2.2		Coating Thickness	36
2.3		Coating Wear Resistance	38
2.4		Analysis of Coatings	40
2.5		Effect of Coatings	40
4	2.5.1	Tool Life	44
	2.5.2	Tool Wear	45
2.6		Coating Failure	48
2.7		Texturing on Tool Inserts	50
2.8		Market Trend	52
	2.8.1	Market trends for coated cutting materials	52
2.9		Impact of coatings on Production Cost	53
2.10		Summary	59
Chapter 3		Problem Formulation	60-65
3		Introduction	60
3.1		Problem Formulation	61
3.2		Research Gap	62
3.3		Research Objectives	63
3.4		Scheme of Research Work	63
3.5		Summary	65
Chapter 4		Materials and Method	66-82
4		Introduction	66
4.1		Material	66
	4.1.1	Tool	66
	4.1.2	Workpiece	67
4.2		Coating Procedure	68
4.3		Experimental Plan	70
	4.3.1	Selection of Process Parameters	70
	4.3.2	Selection of Response Variables	72
	4.3.3	Design of Experiment	74
4.5		Optimization Techniques	77
	4.5.1	Genetic Algorithm (GA)	78
	4.5.2	Technique for Order of Preference by Similarity to Ideal Solution (TOPSIS)	80
Chapter 5		Result and Discussion	83-155
5		Introduction	83
5.1		Coating Characterization	83
	5.1.1	EDAX	83
	5.1.2	XRD	86
	5.1.3	RAMAN	86

5.1.4	FESEM	88
5.2	Mechanical Properties of Coating	92
5.2.1	Micro Hardness	92
5.2.2	Residual Stress	94
5.3	Tribological behaviour of Coating	97
5.3.1	Wear	100
5.3.2	Friction	101
5.4	Experimentation on Conventional Lathe Machine Tool	103
5.4.1	TOPSIS	106
5.4.2	Discussion	118
5.5	Experimentation on CNC Machine Tool	119
5.5.1	Genetic Algorithm (GA)	124
5.5.1.1	Crater Wear (CW)	126
5.5.1.2	Flank Wear (FW)	129
5.5.1.3	Cutting Forces (CF)	131
5.5.1.4	Surface Roughness (SR)	134
5.5.1.5	Temperature in the Cutting Zone (T)	136
5.6	Experimentation using Developed Coated Textured Tool on CNC Machine Tool	139
	5.6.1. TOPSIS	142
	5.6.2. Discussion	154
Chapter 6		
Conclusions and Future Works		156-160
6	Introduction	156
6.1	Conclusions	156
6.2	Limitations of Research Work	159
6.3	Future Scope	159
6.4	Summary	160
References		161-179

List of Figures

Figure No.	Title	Page No.
Figure 1.1	Classification of Tool Materials	6
Figure 1.2	Market distribution of Tool Materials	6
Figure 1.3	Classification of Tool Coatings	10
Figure 1.4	Classification of surface Texturing	12
Figure 1.5	Classification of Texturing Methods.	13
Figure 1.6	Classification of Tool Coating Techniques	14
Figure 1.7	Classification of Modern Methods of Coatings	14
Figure 1.8	Schematic Diagram of CVD Process	15
Figure 1.9	Stages of CVD Process	15
Figure 1.10	Schematic Diagram of PVD Process	16
Figure 1.11	Stages of PVD Process	16
Figure 1.12	Object size vs relative accuracy for the application for precision machining	18
Figure 1.13	Process technologies for precision machining	19
Figure 2.1	Variation of Coating Thickness on HSS and cemented Carbide	37
Figure 2.2	Variation of Coating Hardness on HSS and cemented Carbide	38
Figure 2.3	Global Market Share of Different Tools	52
Figure 2.4	Various Factors incurring the Production Cost	54
Figure 3.1	Sugarcane Grown in Farms.	61

Figure 3.2	Flowchart showing the scheme of experiments.	64
Figure 4.1	Un-Coated WC Tool Insert	66
Figure 4.2	EDX spectrum of Tungsten Carbide (WC) substrate	67
Figure 4.3	Workpiece used for the CNC Machining	67
Figure 4.4	Process used for thermal CVD of DLC coating from pyrolysis of sugarcane	69
Figure 4.5	Schematic of a cutting tool with crater wear and flank wear	73
Figure 4.6	Flowchart depicting the process of Genetic Algorithm	79
Figure 5.1	EDAX of the un-coated Tungsten Carbide (WC) tool insert	84
Figure 5.2	EDAX spectrum of the built-up edge (BUE) formation on coated tungsten carbide (WC) tool inserts.	85
Figure 5.3	The X-Ray Diffraction spectra of the self-developed DLC coating on the tungsten carbide (WC) insert.	86
Figure 5.4	Raman spectra of the self-developed DLC coating on the tungsten carbide (WC) insert.	87
Figure 5.5	FESEM images at different magnifications show the growth of diamond on the coated surface.	89
Figure 5.6	FESEM images of nucleation and growth of diamond coating.	90
Figure 5.7	FESEM images of the DLC coated tool inserts depicting the growth of diamond on the coated surface.	90
Figure 5.8	Cross-Sectional FESEM of Coating Thickness	91
Figure 5.9	Cross-Sectional FESEM of Coating Thickness at higher magnification	92
Figure 5.10	Loading and unloading profile graph obtained during the process of hardness measurement	93
Figure 5.11	Average Vickers hardness values of the uncoated tool inserts, market purchased coated tools and Self-developed DLC coated tool inserts.	93
Figure 5.12	Average residual stress values of the uncoated tool inserts, market purchased coated tools and self-developed DLC coated tool inserts.	95
Figure 5.13	Debye ring, distortion ring, and peak profile obtained while measuring the residual stress of the self-developed DLC coated tool inserts.	96

Figure 5.14	Debye ring, distortion ring, and peak profile obtained while measuring the residual stress of the market purchased coated tool inserts.	96
Figure 5.15	A schematic diagram of the Pin on Disc Tribometer test rig	97
Figure 5.16	Experimentation performed for the Tribological study.	99
Figure 5.17	Stereo microscopic image of DLC coated tungsten carbide (WC) pin after the tribological testing	99
Figure 5.18	Stereo microscopic image of Uncoated tungsten carbide (WC) pin after the tribological testing	99
Figure 5.19	Variation of wear with respect to sliding time.	101
Figure 5.20	Variation of the coefficient of friction with respect to sliding time.	102
Figure 5.21	Microscopic images of a few of the worn-out tool inserts.	105
Figure 5.22	The weight of the evaluated responses to the performance indicators.	111
Figure 5.23	Effect plot of crater wear vs Type of Tool, Feed, Speed and DOC.	116
Figure 5.24	Effect plot of cutting force vs Type of Tool, Feed, Speed and DOC.	117
Figure 5.25	Effect plot of Surface Roughness vs Type of Tool, Feed, Speed and DOC.	117
Figure 5.26	Effect plot of Temperature at Cutting Zone vs Type of Tool, Feed, Speed and DOC.	118
Figure 5.27	Experimentation on the CNC Machine Tool.	122
Figure 5.28	Microscopic images of a few of the worn-out tool inserts.	123
Figure 5.29	Genetic Algorithm Graph for the best value and the average value of Crater Wear.	128
Figure 5.30	Pareto Chart of the Standardized effects for the crater wear as response variable.	128
Figure 5.31	Genetic Algorithm Graph for the best value and the average value of Flank Wear.	130
Figure 5.32	Pareto Chart of the Standardized effects for the flank wear as the response variable.	131
Figure 5.33	Genetic Algorithm Graph for the best value and the average value of Cutting Force.	133

Figure 5.34	Pareto Chart of the Standardized effects for the cutting force as the response variable.	133
Figure 5.35	Genetic Algorithm Graph for the best value and the average value of surface roughness.	135
Figure 5.36	Pareto Chart of the Standardized effects for the surface roughness as the response variable.	136
Figure 5.37	Genetic Algorithm Graph for the best value and the average value of Temperature in the Cutting Zone.	138
Figure 5.38	Pareto Chart of the Standardized effects for the Temperature in the Cutting Zone as the response variable.	138
Figure 5.39	Microscopic images of the CNC tool inserts having Line and Sine Wave texturing perpendicular to the edge of the tool nose.	140
Figure 5.40	Microscopic images of the CNC tool inserts having Line and Sine Wave texturing parallel to the edge of the tool nose.	140
Figure 5.41	The weight of the evaluated responses to the performance indicators.	146
Figure 5.42	Effect plot of crater wear vs Type of Tool, Feed, Speed and DOC.	152
Figure 5.43	Effect plot of flank wear vs Type of Tool, Feed, Speed and DOC.	152
Figure 5.44	Effect plot of cutting force vs Type of Tool, Feed, Speed and DOC.	153
Figure 5.45	Effect plot of Surface Roughness vs Type of Tool, Feed, Speed and DOC.	153
Figure 5.46	Effect plot of Temperature at Cutting Zone vs Type of Tool, Feed, Speed and DOC.	154

List of Tables

Table No.	Title	Page No.
Table 1.1	Novelty of CVD Process and PVD Process	17
Table 2.1	Prominent attributes of the coatings	34
Table 2.2	Properties of various Coatings on different tool materials	41
Table 2.3	Fabrication Processes of Coating Technology	42
Table 2.4	Features of Coating Materials	45
Table 2.5	Tool Wear versus Coating Thickness	47
Table 2.6	Classification of textures on the rake face of the cutting tool inserts	51
Table 2.7	New findings over the past two decades	55
Table 4.1	Elemental composition of Tungsten Carbide (WC) substrate.	67
Table 4.2	Elemental composition of Aluminium (6061) workpiece.	68
Table 4.3	Levels of input parameters selected for Conventional Lathe Machine Tool	71
Table 4.4	Levels of input parameters selected for CNC Machine Tool	71
Table 4.5	Levels of input parameters selected for using the developed textured coated tools on the CNC Machine Tool	72
Table 4.6	The L27 OA (Parameters Assigned) for Machining on Conventional Lathe Machine Tool	75
Table 4.7	The L27 OA (Parameters Assigned) for Machining on CNC Machine Tool	76
Table 4.8	The L16 OA (Parameters Assigned) for Machining on CNC Machine Tool using the developed textured coated tools	77
Table 5.1	Elemental composition of the un-coated Tungsten Carbide (WC) tool insert	84
Table 5.2	Elemental composition at the Red Cross in figure 5.2	84
Table 5.3	Elemental composition at the Blue Cross in figure 5.2	85
Table 5.4	Experimental conditions for the tribological tests	100

Table 5.5	Levels of input parameters selected for Conventional Lathe Machine Tool	103
Table 5.6	The L27 OA for Machining on Conventional Lathe Machine Tool	104
Table 5.7	L27 Orthogonal Array using the input parameters along with the response variables in the form of initial decision matrices.	108
Table 5.8	Response variables in the form of obtained Normalised decision matrix	109
Table 5.9	Weights of the performance indicators.	111
Table 5.10	Performance indicator's standardized and weighted decision matrices.	113
Table 5.11	Positive Matrix for the performance indicators.	114
Table 5.12	Negative Matrix for the performance indicators.	114
Table 5.13	Standardized and weighted decision matrices for performance indicators.	114
Table 5.14	Best and worst combinations of the Input Parameters	115
Table 5.15	Best and worst combinations of the Response Variable	115
Table 5.16	Levels of input parameters selected for CNC Machine Tool	120
Table 5.17	The L27 OA for Machining on CNC Machine Tool	121
Table 5.18	Levels of input parameters selected for using the developed textured coated tools on the CNC Machine Tool	140
Table 5.19	The L16 OA for Machining on CNC Machine Tool using the developed textured coated tools.	141
Table 5.20	L16 Orthogonal Array using the input parameters along with the response variables in the form of initial decision matrices.	144
Table 5.21	Response variables in the form of obtained Normalised decision matrix	145
Table 5.22	Weights of the performance indicators.	146
Table 5.23	Performance indicator's standardized and weighted decision matrices.	147
Table 5.24	Positive Matrix for the performance indicators.	148
Table 5.25	Negative Matrix for the performance indicators.	148
Table 5.26	Standardized and weighted decision matrices for performance indicators.	149

Table 5.27	Best and worst combination of the Input Parameters	150
Table 5.28	Best and worst combinations of the Response Variable	150

Chapter 1: Introduction

1. Introduction

The foundations of any manufacturing or machining industry are the processes, production efficiencies, and safety measures and methods. Of these foundations, processes are accomplished efficiently with the use of various types of tools and techniques [1]. Material removal processes essentially require the cutting tools to shape the raw material into predetermined designs and dimensions. These are the building blocks of all other structures as they provide shape, dimension, and a meaningful existence to them [2]. The work executed in these industries necessitates the use of these cutting tools to enhance the efficiency and production of various machines, their parts, or any other form of structure [3,4].

Globally, the manufacturing industries employ various machining operations for the manufacturing of various parts irrespective of the size, shape, and dimensions. The design can be as simple as the needle to as intricate as an aircraft component [4-6]. The growing requirement for precise and efficient process plans has developed the need for accurate predictive models for various machining variables and output performance measures including the tool life, chip formation, dimensional accuracy, and the surface finish of the workpiece [7]. The essentiality of the cutting tool can be easily noted from the fact that the automotive industry in 2015 formed 44% of the share of metal parts. Expanding automotive fabrication in nations, such for example, the US, China, Japan, and Germany implied an expanded interest in advanced cutting tools [8].

The modern manufacturing sector is majorly using cutting inserts with various types of coatings to increase the tool life and lower the tool wear which directly influences the production cost. As the advancement unfolded new coating materials, the use of cemented carbides was the turning point in the field of cutting tool materials as these were processed with different types of thin coating films [8]. This helped in achieving higher tool life at a higher cutting speed which was previously not possible. Nowadays, approximately 80% of the cutting operations are accomplished using coated tools irrespective of which material removal process is considered. The new technology has virtually coated the tools of all processes viz. turning, shaping, milling, reaming, and drilling [9, 10].

Major material contribution to the metal cutting tools has been the tool steels manufactured from the conventional metallurgical process i.e. the powder metallurgy [11, 12]. Lind et al. [13] examined the blanking process for tool wear and eventually inferred its three basic stages. Tool wear initiated with abrasive wear which led to adhesive wear following its last stage of failure. The rate of tool wear was controlled by controlling the chemical composition of steel and the use of alloying elements such as vanadium, chromium, tungsten, molybdenum, etc. The tool wear was suppressed through the ceramic coatings which are the forms of carbides or nitrides of transition metals [14]. These coatings include TiC, TiN, TiCN, and TiAlN, which protect the tool from heat and corrosion and simultaneously provide good adhesion to the substrate. They also demonstrated high hardness when used on various mechanical components and as a coating on cutting tools [15].

Over the passing decade, the tungsten-based and HSS tools are coated with TiN through the process of physical vapor deposition method and are extensively used for various cutting

operations [16]. The tools coated with TiN are being successfully used as hobs and shaper cutters during gear cutting operations. Along with TiN coating, many other coatings have been developed over time such as TiCN, TiAlN, Al₂O₃, TiC, etc. The effectiveness of the coatings can be estimated by the exclusive use of TiN coating on conventional cutting tools. The coating of TiN on the conventional HSS tool has enhanced the tool life resulting in a high productivity rate at high cutting speeds [17]. Multi-point cutting tools like drills and taps are also coated to increase their life. Experiments in various other cutting processes had shown noteworthy results. It can be inferred from the previous experiments that the properties of the coatings and the cutting conditions significantly govern the tool life and delay the wearing of the tooltip [18].

The alarming rate of improvement in manufacturing technologies has necessitated the understanding of the fundamental properties of the coatings applied to the cutting tools along with their mechanism of protecting its surface [19]. It is a multidisciplinary field that includes the study of chemical, physical, and tribological properties. The amalgamation of these properties defines the performance of uncoated and coated tools. The major change in performance of coated tools is governed by the region of the chip-tool interface as this is the major area that is affected by high temperature and affects the tool wear in the cutting zone [20].

To comprehend the properties of coatings, numerous experiments have been performed before inferring the reasons for the performance enhancement of the cutting tools. Another aspect of the fabrication method i.e. chemical vapor deposition (CVD) is extensively being researched for the diamond coating which is to be utilized in the cutting processes in near future [21]. The diamond-coated tools exhibit incredible potential during various machining operations with the advantage

of being produced with complex geometry such as a reamer, drills, etc. Expanded utilization of lightweight high-quality parts has significantly developed an interest in these coated tools. A commonly used process for diamond coatings is the hot-filament CVD process which has the efficiency of depositing a film as thick as 50 μm on different tool materials such as HSS, tool steels, cobalt cemented tungsten carbide (WC-Co) [22, 23].

1.1. Manufacturing: An Introduction

Manufacturing is the production of work pieces having defined geometric shapes. It is the economic term for making goods and services available to satisfy human needs. It converts the raw materials (from nature or industry) to finished products to be used for some purpose [24]. The development of the finished product from raw material undergoes a number of processes such as selecting a material, reviewing the basic design model, selecting the parameters, type of operations to be performed, the economics involved, quality testing and inspection, assembling, and final testing [25].

The manufacturing processes are the methods that are required to produce parts and then assemble them to develop a finished product [26]. These processes are mainly categorized as:

- i. Primary Shaping Processes
- ii. Forming or Metal Working Processes
- iii. Machining (Metal removal) Processes
- iv. Joining and Assembly processes
- v. Surface Finishing Processes

1.2. Materials of Tool

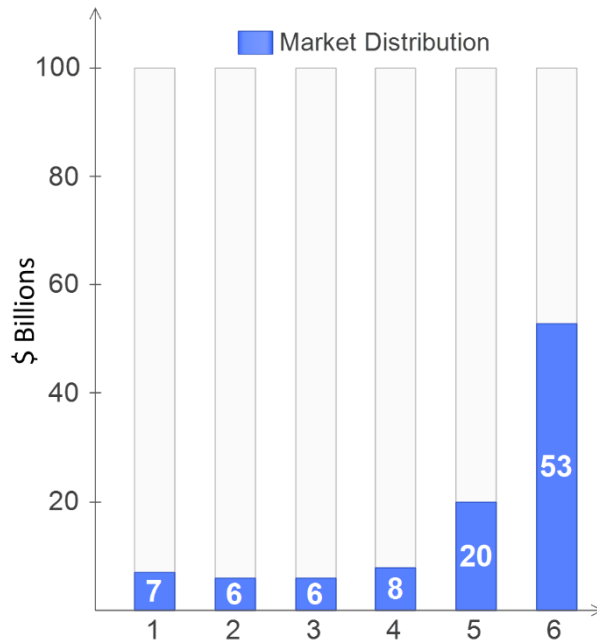
The advancements in the field of tool materials along with the coatings are a success only if the tool material selected is of proper microstructure and morphology. Hence, the selection of tool material has always been the initial requirement in the designing of a coated cutting tool [27].

The market distribution of various tool materials across the globe in terms of cost is depicted in Figure 1.2, while Figure 1.1 shows the classification of tool materials both conventional and modern [28]. Along with the conventionally available tool materials, a new highly researched material is powder steel owing to its properties and grain structure. It is a structure of fine-grained metal carbides that are uniformly distributed in the matrix of steel thereby developing better mechanical properties such as toughness and hardness [29].

Proper heat treatment of the tools should be carried out to curb the decarburization and oxidation at the surface [30]. They should be hardened to release any stresses developed by a thermal change in the structure of the tool material and should be able to obtain a hardness within a range of 55 - 64 HRC. There are various tool materials that are being used in the manufacturing sector, educational institutes, and the upcoming small enterprises in accordance with their application and usage [31]. Out of the materials depicted in Figure 1.1, some of the tool materials have been discussed in the following section.



Figure 1.1: Classification of Tool Materials [28]



[1: Diamond PCD, 2: CBN / PcBN, 3: Ceramics, 4: Cermets, 5: High-Speed Steel, 6: Cemented Carbide]

Figure 1.2: Market distribution of Tool Materials [32]

1.2.1. High-Speed Steel (HSS)

An extensively used tool material irrespective of the place of application is high-speed steel. These tools are coated to increase the mechanical properties viz. hardness, toughness; reduce friction, increase corrosion and wear resistance. Numerous coatings are available which include ceramics, soft, organic, metallic, hard, and glasses [33, 34].

Usually, metallic, ceramic, and intermetallic compounds are used as surface coatings which can be individual or multi-layered. A thorough selection of coatings is dependent on the applicability, dimension, cutting conditions, temperatures of the cutting zone, work material, coating thickness, and production costs [35].

1.2.2. High Carbon Steel (Tool Steel)

The tool steels when coated with the CVD technique have a high deposition rate. CVD technology is extensively used where heavy forming and stamping tools are used [36]. It has the advantage of coating any complex geometry of cutting tool uniformly. Due to the exposure to high temperature, the cutting tool made of tool steels undergoes a second heat treatment to relieve stress and attain thermal stability [36, 37].

The vacuum heat treatment tends to allow changes in the dimensions of the tools, this should be taken into account during the machining processes. For attaining the desired qualities, the maximum coating temperature must be below the quenching temperature of the tool steel. This helps in choosing the coating technology for PVD or PA-CVD [38].

1.2.3. Cemented Carbides (Carbide Tool)

Carbide tools exhibit high machinability during machining of hard work material. These tools are brazed onto the steel shank or are available in the form of inserts. They have higher tool life than the available HSS tool [39]. The life of the carbide tool had been increased through the use of various coatings such as chromium nitride (CrN), titanium nitride (TiN), titanium aluminium nitride (TiAlN), titanium carbonitride (TiCN), and their multi-layered structures [40 - 42]. Physical vapor deposition (PVD), chemical vapor deposition (CVD), cathode arc evaporation physical vapor deposition (CAE-PVD), electron beam-assisted physical vapor deposition, etc. are the various methods that are used for the development of the surface coated carbide tools [42-46].

1.2.4. UCON

It is a nitrided refractory metal alloy having the composition of 50% columbium, 30% titanium, and 20% tungsten with no carbide [47]. It has excellent thermal shock resistance, high hardness, and toughness. It exhibits excellent resistance to diffusion and chip welding. It is available in the form of throwaway inserts having 3-5 times more edge life than conventional carbides. It operates in the speed range of 250-500 m/min on steels of 200 BHN [48].

1.2.5. CBN (Cubic Boron Nitride)

It consists of atoms of nitrogen and boron, with a special structural configuration similar to diamond. It has high hardness and high thermal conductivity. It is chemically inert. It is used as a grinding wheel for HSS tools [49]. These are available in the form of indexable inserts and are

capable of machining hardened tool steel, chilled cast iron, high strength alloys. It is the hardest material next to diamond [49-51].

1.2.6. SiAlON

The word Si Al ON stands for silicon nitride-based materials with aluminium and oxygen additions. It is produced by milling Si_3N_4 , aluminium nitride, and alumina. The mixture is dried, pressed to shape, and sintered at 1800°C . This tool material is tougher than alumina and thus suited for interrupted cuts. Aerospace alloys and nickel-based gas turbine discs can be machined using a sialon tool bit at a cutting speed of 200-300 m/mt [52-55].

1.2.7. Polycrystalline Diamond (PCD)

High-speed machining operations make use of PCD and CBN tools for best results. In the motor vehicle and aircraft manufacturing industries, parts of non-metallic materials are being used extensively. PCD cutters achieve exceptional standards of surface quality at high feed and material removal rates with such materials. PCD tools are extensively used for machining aluminium components [55-57].

1.2.8. Ceramics

Ceramics consist mainly of sintered oxides (Al_2O_3) and are prepared in the form of clamped tips and as throw-away inserts. These can be used at very high speed (beyond carbide tools), resist built-up edge, and produce a good surface finish [58]. These are extremely brittle, so their use is limited for continuous cuts. Friction at rake face is usually lower as compared to carbide tools but the temperature is higher because these are poor conductors of heat. To strengthen the cutting edge,

a small chamfer or radius is often stoned on the cutting edge and a negative rake of about 15-20° is provided [59].

1.3. Tool Coatings

The conventional cutting tools have been modified as per the ongoing demands of the manufacturing sector for the processing of advanced materials. These conventional tools have been coated with various types of compounds to increase the life of tools and decrease the wear rate. The application of the coating aims to increase the performance of the tool during the cutting processes where coating thicknesses ranging from microns to millimetres play a vital role [60].

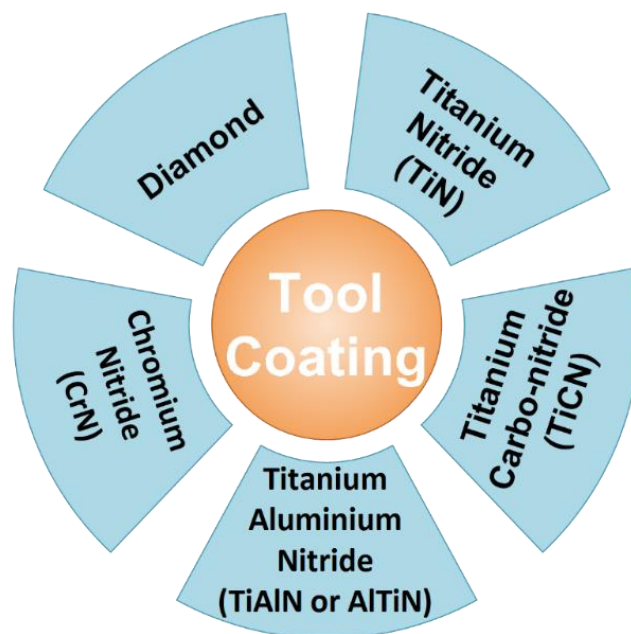


Figure 1.3: Classification of Tool Coatings. [28]

A coating can be defined as the surface covering layer applied on the machine component or the cutting tools in the sector of manufacturing and which is referred to as the “substrate” in connection

to the coating. The formation of an interface layer in the coating structure helps in enhancing the adhesion of the coating with the substrate [61]. This is the transition layer that governs the bonding between the coating layers improving the chemical and mechanical properties [62]. A substantial increase in the tool life at high cutting speed is governed by the thickness of coatings and the number of layers of coatings. TiC, Al₂O₃, TiAlN, TiCN, and TiN are some of the examples of hard and refractory coatings which can be applied as a monolayer or in multi-layer forms. Figure 3 shows the broad classification of tool coatings used in industries [63].

The most frequently used metals for coating purposes are titanium (Ti) and silver (Ag) which improve hardness and lower tool failure. Previous research shows a significant effect of coatings on tool life and tool wear [64]. Titanium nitride (TiN) coatings applied on the drill bits and milling cutters enhance the tool life by three times protecting the cutting edge, retaining its cutting ability and corrosion resistance of the cutting tip [64 - 66]. These coatings exhibit a hardness of 2400 HV, hence helping in the reduction of abrasive wear, showing excellent bonding of coating with the substrate, chemical inertness, low maintenance cost, resistance to high temperatures and eventually increasing productivity. They enhanced the tool life by 1000% when drilled stainless steel workpieces [66].

New coatings are being developed especially diamond coatings for difficult-to-machine materials like glass or fibre-reinforced composites and aluminium-silicon alloys [67 - 70]. Diamond coatings are developed using CVD technology and have been successful to some extent under working conditions. This owes to the increase in density of diamond nucleation and a further increase in its film growth along with improved diamond crystallinity [71 - 73]. These diamond-coated tools

showed superior performance in comparison to other coated tools and uncoated tools during their testing in various operations [74 -75]. The resistance to wear of the diamond compact tool and the diamond coated tools was comparable during the machining processes viz. milling and turning [76, 77].

1.4. Texturing on Tools Inserts

The usage of textured tool inserts during machining operations reduces the crater wear, flank wear, cutting forces, surface roughness, and temperature at the cutting zone [78]. The decision of surface texturing depends on three major factors i.e. Area of texturing, the direction of cutting edge, and patterns of the texture [79, 80]. These further can be categorized and have been shown in the form of a flow chart in Figure 1.4. The surface texturing can be performed using the various texturing methods viz. laser texturing, electro-chemical machining, micro grinding, and electro-discharge machining. A flow chart classifying all the methods of texturing is shown in Figure 1.5.

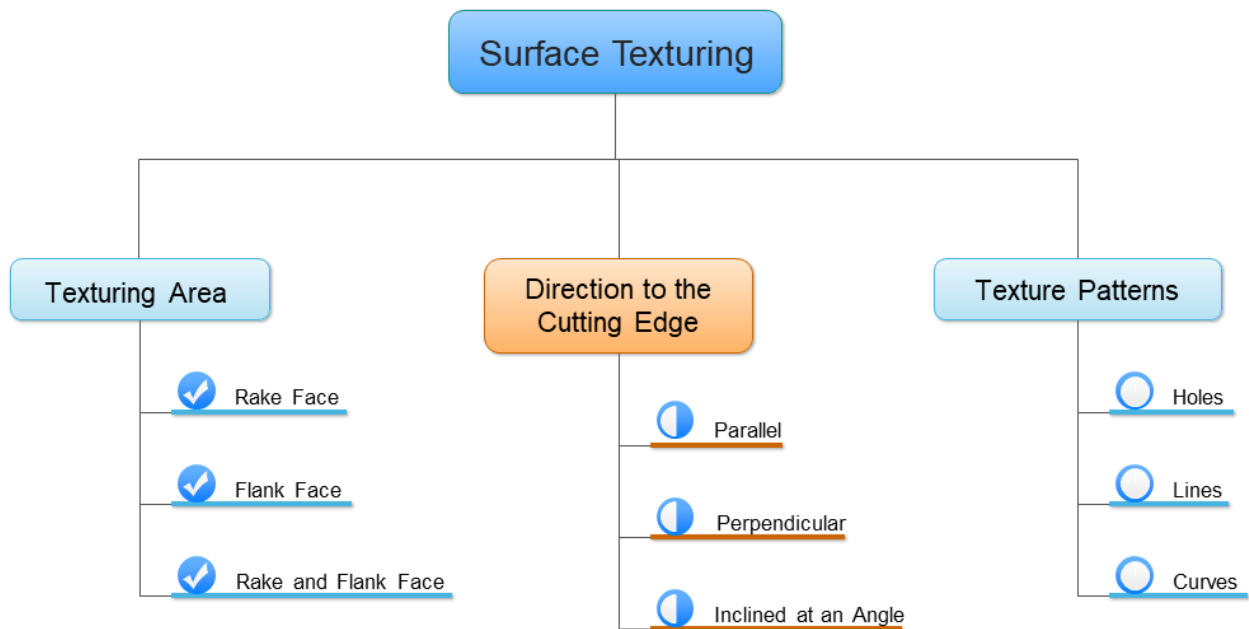


Figure 1.4: Classification of surface Texturing [28]

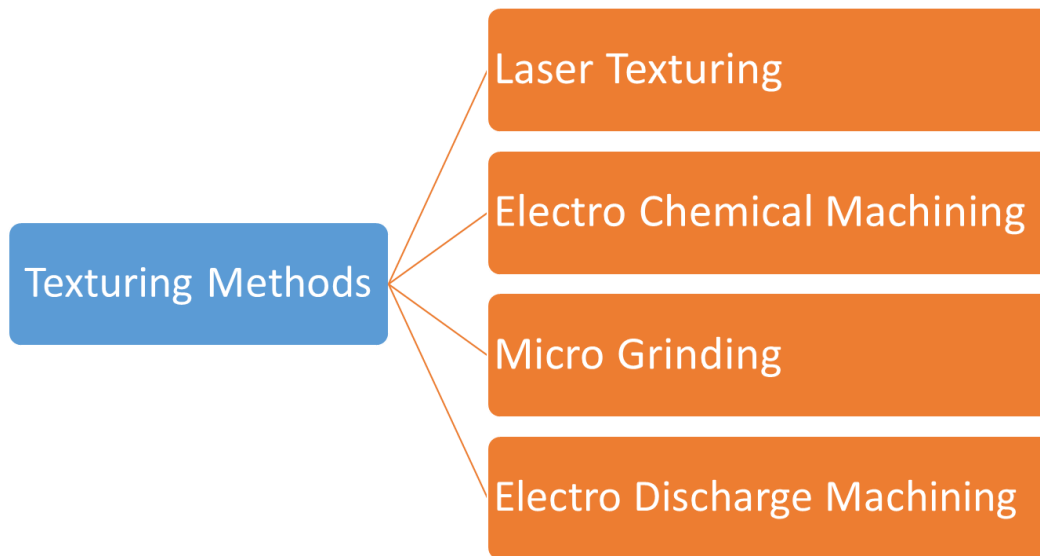


Figure 1.5: Classification of Texturing Methods.

1.5. Coating Techniques

The most frequently used metals for coating the tool inserts are titanium (Ti) and diamond-like carbon (DLC) which improve the hardness as well as decrease the tool failure rate. Titanium nitride (TiN) coatings applied on the tool inserts, drill bits, and milling cutters enhance the tool life by three times while protecting the cutting edge and retaining its cutting ability as well as resisting the cutting tip from corrosion [81, 82]. The coatings can be as hard as 2400 HV, hence helping in the reduction of abrasive wear, excellent bonding of coating with the substrate, chemical inertness, low maintenance cost, resistance to high temperatures and eventually increasing productivity. The tool coating techniques have been classified in Figure 1.6, these techniques include Chemical conversion, thermal and plasma spraying, galvanizing and electroless process, and modern methods [83].

The classification of modern methods of coatings is depicted in Figure 1.7, which includes diffusion, implantation, chemical vapour deposition (CVD), and physical vapour deposition (PVD) methods [28].

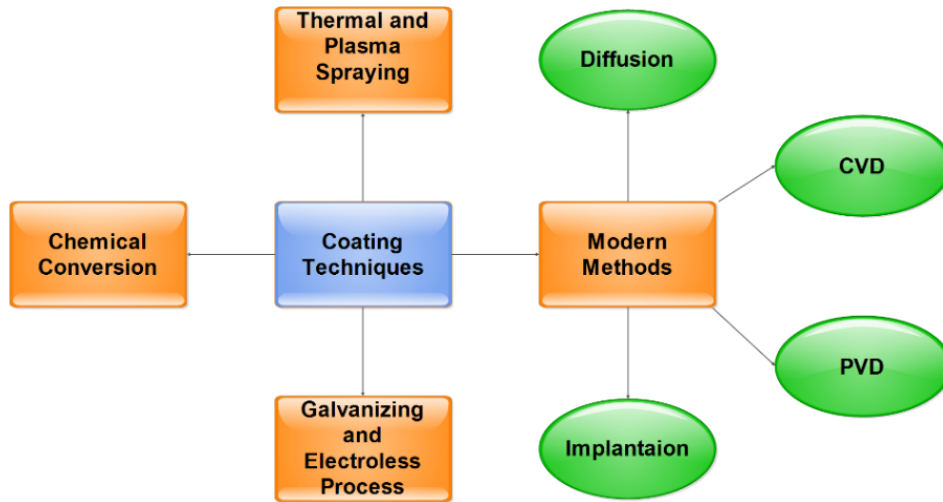


Figure 1.6: Classification of Tool Coating Techniques [28]

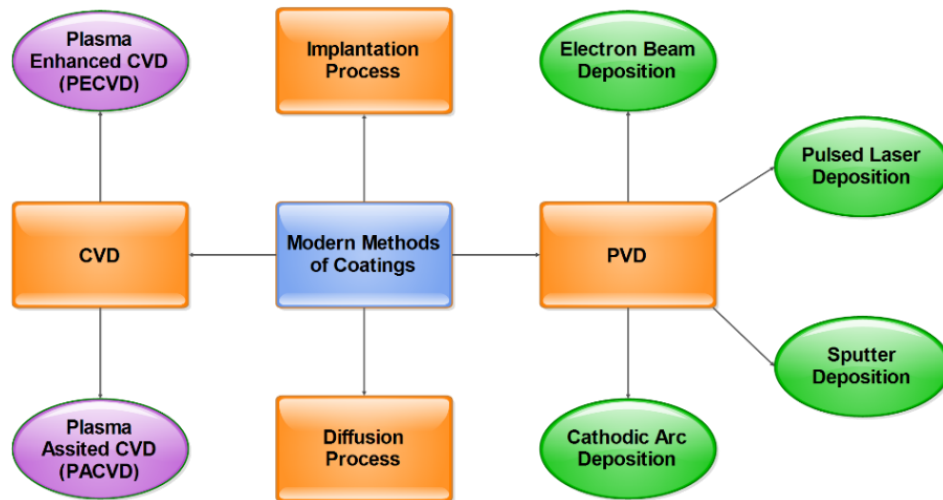


Figure 1.7: Classification of Modern Methods of Coatings [28]

The two principal methods of depositing the surface coating on the substrate are chemical vapor deposition (CVD) and physical vapor deposition (PVD) [84-86]. These modern methods are

capable of developing thin films (at micron and nano-level) which, have now become the backbone for advanced applications such as optical devices, cutting tool inserts, and environmental applications [87].

1.5.1. Chemical Vapour Deposition (CVD) Process

Chemical Vapour Deposition (CVD) is a coating technique to develop thin films on any base material. The chemical reaction occurs between reactants in the gaseous state which are deposited on the heated surface of the substrate [88]. The schematic diagram of the CVD process is shown in Figure 1.8 and the four stages in the CVD method are shown in Figure 1.9 [28, 89].

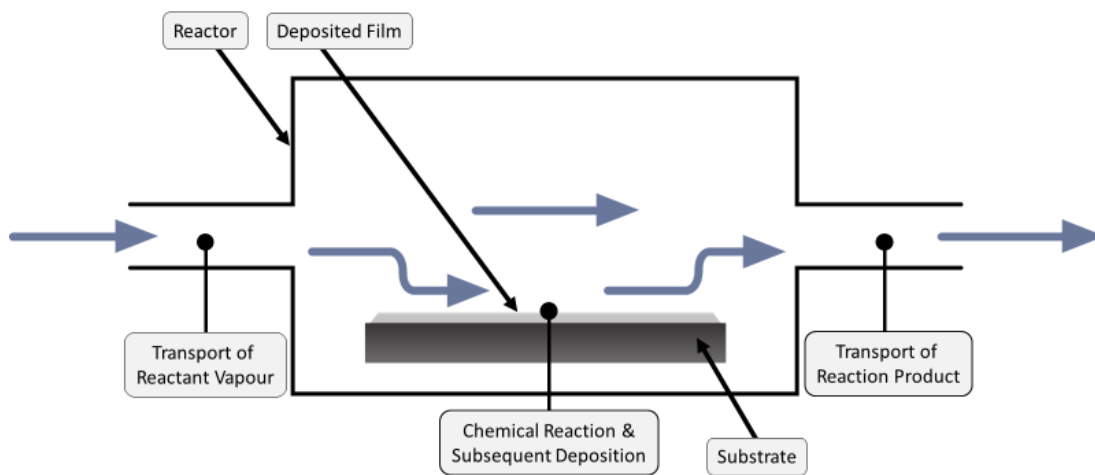


Figure 1.8: Schematic Diagram of CVD Process [89]

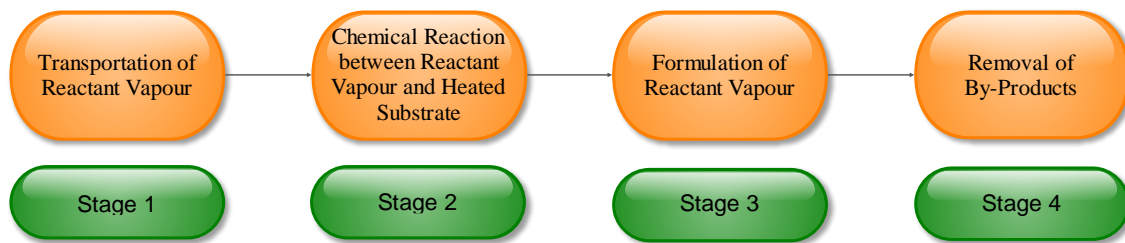


Figure 1.9: Stages of CVD Process [28]

1.5.2. Physical Vapour Deposition (PVD) Process

Physical vapour deposition is a coating technique that deposits thin films on the substrate by condensation of the vapours of the material. There are many vacuum deposition techniques for depositing these thin films. It is a process of transfer of material at the atomic level from solid to vapour phase and then again to the solid phase in terms of a thin film coating [88]. The schematic diagram of the PVD process is shown in Figure 1.10 and the four stages in the PVD method are shown in Figure 1.11 [28, 89].

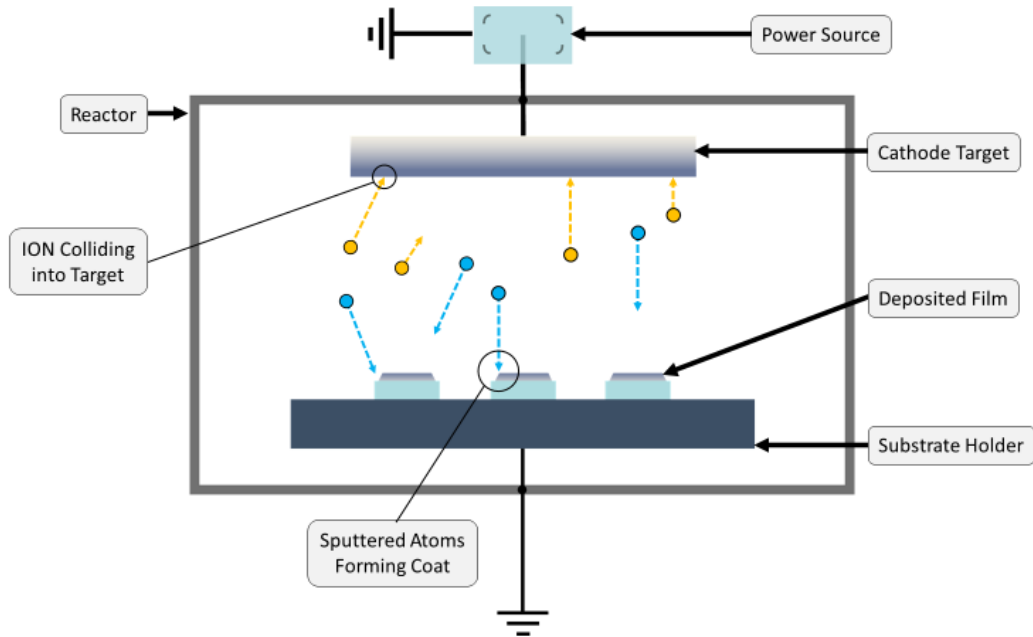


Figure 1.10: Schematic Diagram of PVD Process [89]

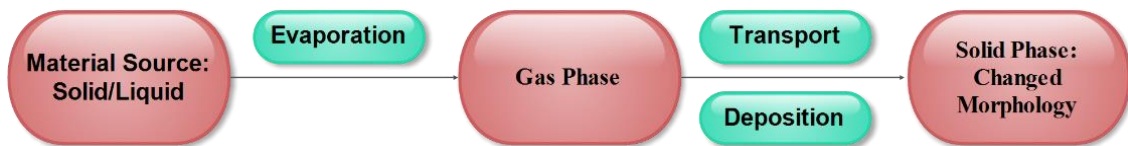


Figure 1.11: Stages of PVD Process [28]

Table 1.1: Novelty of CVD Process and PVD Process

S. No.	CVD Process	PVD Process	References
1	Uniform thick coatings (10 μm to 1mm) can be deposited at low temperatures with the minimum usage of gas.	It has excellent adhesion properties due to the penetration of the coating into the main material owing to exposure to high thermal expansion.	[88, 90, 91]
2	Coatings have fewer defects and are dense in structure with high strength, toughness, hardness, chemical inertness, and low coefficient of friction.	It exhibits improved hardness (3000 – 4000 HV about 85 – 90 HRC), decreased coefficient of friction on the cutting edge, increased lubricity level, improved oxidation, and wear resistance.	[88 – 90, 92]
3	It allows irregular shapes to be coated due to high throwing power.	No harmful by-products are produced, hence no damage to the environment.	[89]
4	Its process parameters can manage the morphology of the surface, structures of crystal, and CVD products orientations.	Coatings are deposited at low temperatures (200 - 300°C), hence a wide range of materials including polymers can be coated.	[89, 90]
5	Deposition rates can be adjusted easily.	Coatings developed are thin (2-15 μm) and very dense.	[89, 90]
6	It favours the development of thin films at a low deposition for microelectronic applications.	Smooth surfaces are generated as thermal transmittance of coating is on a low level leading to the high penetration of the coating into the main material.	[90]
7	It is used for depositing thin films of diamond on hard metal substrates such as tungsten carbide tools (cobalt-based).	It is used for depositing coatings of TiN, TiCN, CrN, and TiAlN.	[92 - 96]

1.6. Precision Machining

In modern times, precision engineering was initially pushed by nuclear programs and eventually by semiconductor manufacturing [97]. By the 1980s demands from electronics, defence, and energy applications led to pioneering work on diamond turning from Lawrence Livermore National Laboratory and Oak Ridge National Lab [98, 99]. In Figure 1.12 we have shown in a most generalized form, human manufactured objects in terms of absolute size and relative tolerances. Mechanical engineers define precision machining as machining in which the relative accuracy is 10^{-2} . “Precision machining,” when used by mechanical engineers, has typically been reserved for material removal processes only [100].

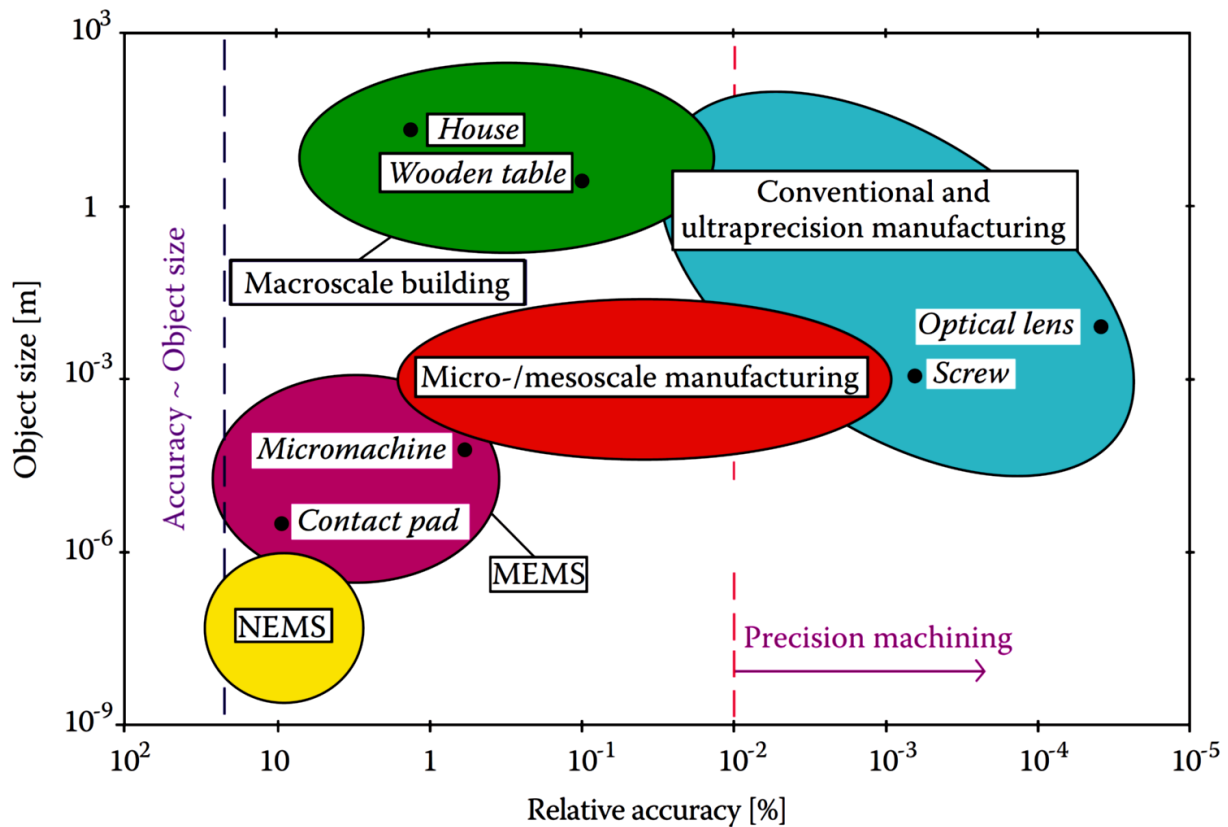


Figure 1.12: Object size vs relative accuracy for the application for precision machining [99]

The precision machining of microstructures and parts can majorly be divided into two general categories viz. Microsystem technologies (MST) and micro-engineering technologies (MET). These categories can be further be categorized into Micro Electro Mechanical Systems (MEMS) processes and Mechanical processes and the further categorization is shown in Figure 1.13 [101].

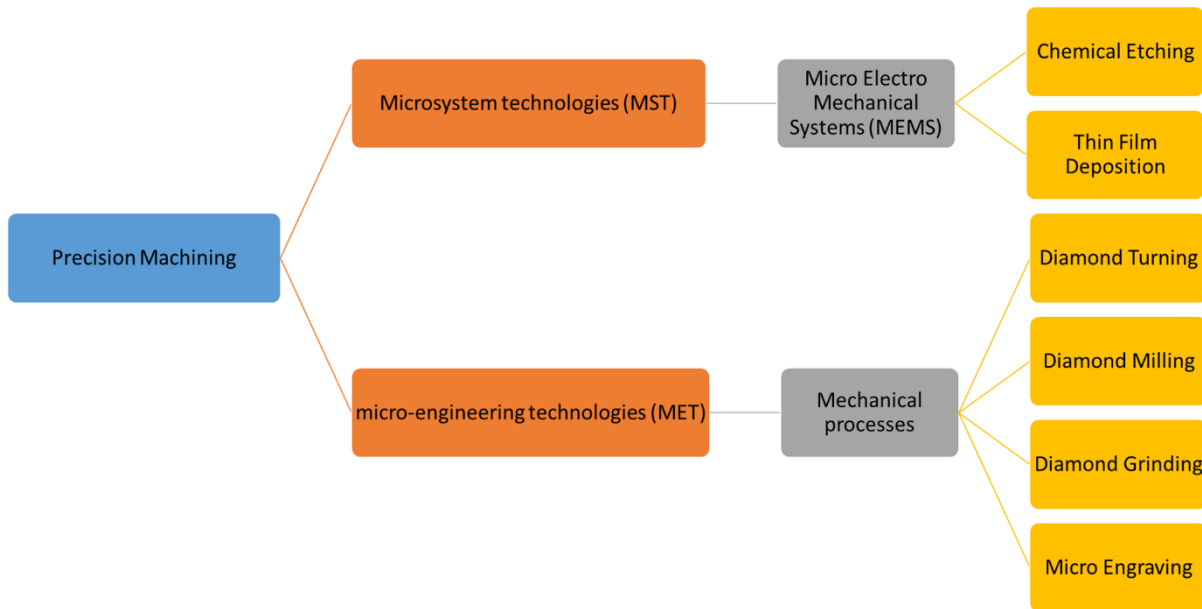


Figure 1.13: Process technologies for precision machining [101].

1.7. Properties of Diamond

The structure of diamond exhibits strong chemical bonding leading to special mechanical and elastic properties [102]. The hardness, molar density, thermal conductivity, longitudinal sound velocity, and the elastic and Young's modulus of diamond are the highest of all known materials while its compressibility is the lowest of all materials. The dynamic friction coefficient of the diamond is only 0.05 as low as that of Teflon [103].

Diamond possesses the highest thermal conductivity and it can be increased by five times if it is fabricated using isotropically pure carbon on account of decreased phonon scattering by different isotopes [104]. The chemical property is that diamond does not react with common acids at elevated temperatures. On treatment with the hot chromic acid cleansing mixture or a mixture of sulphuric and nitric acids, graphite slowly oxidizes while diamond is chemically inert. It, however, oxidizes (graphite) readily at high temperatures in an oxygen atmosphere and air. Molten hydroxides salts of oxy-acids and some metals (Fe, Ni, Co, etc.) have a corrosive effect on a diamond. At temperatures above 600°C, the diamond reacts with water vapour and CO₂ [105-107].

A diamond chemically reacts with metals such as tungsten, titanium, tantalum, and zirconium to form carbides while it dissolves in the metals like iron, cobalt, nickel, manganese, and chromium. Hence, diamond or diamond coated tools are unsuitable for machining ferrous metals. It can be used for machining non-ferrous metals and alloys such as aluminium, copper, and graphite owing to the poor weldability/wettability property [108]. Recent years witnessed the increased use of aluminium alloys which on machining with conventional carbide tools formed built-up edges easily. Diamond having poor weldability to such materials gives a very good finish without any built-ups [109, 110].

1.8. Application of Diamond

Diamond-coated through CVD (Chemical Vapour Deposition) process possesses many properties which are in high demand by the manufacturing industries [111]. The CVD diamond unleashes the beginning of the new age of industrial diamond. The major applications are given below:

1.8.1. Wear and Cutting Applications

Diamond-coated cutting tools are being used extensively nowadays owing to their excellent hardness and low coefficient of friction (in the range of 0.05- 0.1) They find use in the machining of aluminium, aluminium alloys, copper, copper alloys, chlorides, fluorides, polycarbonates, plastics, quartz, sapphire, NaCl, SiC, Ti, WC, ZnS, and ZnSe. Highly abrasive nonferrous material and metal matrix composites are employed in the automotive and aerospace industries which has increased the demand for diamond-coated tools in manufacturing processes [112-114].

Diamond-coated cutting tools display excellent resistance to thermal oxidation and high thermal conductivity making them suitable for both high speed and dry machining. Diamond cutting tool applications also include dressers for wheel dressing, special knives, burnishing tools and wire drawing dies. CVD diamond enables a diamond to be electrically conductive and hence can be easily machined using electrical discharge machining (EDM). Industrial cutting applications can be the diamond water jet nozzles used for cutting nappies, cloth, paper, cardboard, frozen foods, semiconductors, etc. which can be >100 h compared to tens of hours for more standard ruby or sapphire nozzles [115-119].

1.8.2. Acoustic Applications

The high stiffness of diamond makes it suitable for use as micro-mechanical oscillators, surface acoustic wave (SAW) devices, and tweeter domes for loudspeakers. Diamond tweeter components were envisaged and date back to 1987 [120]. The ideal tweeter acts as a perfect piston without deformation at all frequencies [119, 120].

1.8.3. Thermal Applications

The thermal conductivity of diamond is higher than any other material at room temperature contributing to applications such as windows for multi-kilowatt CO₂ lasers, megawatt gyrotrons, and cutting tools. Its high thermal conductivity is a key factor for its use at high temperatures. Diamond's extreme stiffness and low coefficient of thermal expansion are excellent for its use in high power transmission windows [121-123].

1.8.4. Optical Applications

Diamond exhibits the potential for both passive and active optical applications. Passive applications take advantage of its high thermal conductivity, corrosion resistance, hardness, its low absorption coefficient, and small coefficient of friction. The optical properties along with their thermal properties find exclusive use in optics such as CVD diamond beam exit windows in CO₂ lasers [124, 125].

1.8.5. Electronic Applications

Diamond is used as an electrically insulating thermal conductor for various electronics applications such as high-power laser diodes to increase the output power of diodes, and thick films used as heat spreaders for very large integrated circuits (VLSI) multiple chip module (MCM) to increase the packaging density [126]. Owing to the properties such as high carrier mobility, breakdown field, saturation velocity, thermal conductivity, and wide-bandgap, diamond is an ideal material for electronic devices. The utilization of synthetic crystals in photodetectors, light-emitting diodes, nuclear radiation detectors, thermistors, varistors, and negative resistance devices has been documented. In the basic field-effect transistor (FET) device operation with homoepitaxial

diamond films and boron-doped layers on insulating single crystal, diamond substances have been used [127].

1.8.6. Electrochemical Applications

In the field of electrochemistry, highly boron-doped diamond has been used in electro analysis and bulk oxidation of dissolved species in solution. Its chemical inertness, resistance to fouling, and large potential window in an aqueous solution make it a unique electrode material. The stability of the diamond surface, its chemical inertness, and the ability to apply large potentials before the electrolysis of water occurs are all factors in favour of selecting diamond as an electrode material. Most electrochemical synthesis and processing applications demand high volume capability and high reaction rates, in turn requiring large-area electrodes operating in very aggressive chemical environments [126].

Diamond is unparalleled in its ability to survive such environments without erosion and at the same time reduce the process cost. Trends in legislation are continually reducing the permitted levels of harmful chemicals in effluent and CVD diamond electrodes offer promising solutions to these new challenges [128].

1.8.7. MEMS Applications

Micro-electromechanical systems (MEMS) are a process technology used to create tiny integrated devices or systems that combine mechanical and electrical components. In the most general form, MEMS consist of mechanical microstructures, microsensors, microactuators, and microelectronics, all integrated onto the same silicon chip. After decades of research and

development, thin-film diamonds are used for wafer-scale applications and are available as a process module through the MEMS and Nanotechnology Exchange. The key issue to the wide adoption of diamond-based RFMEMS is cost. The integration of diamond into the process flow is small and several strategies have been developed to enable the diamond to be integrated into complex heterostructures including metals, oxides, and other functional materials. The recent state-of-the-art diamond technologies could only uniformly coat wafers 2-3 inches in diameter [129, 130].

The UNCD (ultrananocrystalline diamond) technology enables films as thin as 100 nm to be routinely deposited on wafers up to 200mm with excellent thickness and uniform property. Both diamond-on-silicon (DOSi) and diamond-on-insulator (DON) UNCD wafers are commercially available now and offer a means by which developers can fabricate prototype devices for their evaluation design. These wafers are manufactured using tools and processes that are fully insertable into a MEMS foundry environment and are available in wafers sizes ranging from 100 to 200 mm. Diamond has several intrinsic properties that make it an ideal candidate for GHz RF MEMS devices including having the highest acoustic velocity of any material, low dissipation, low-temperature coefficient of frequency, and linear frequency response at high frequencies/powers [131-133].

1.8.8. Biotechnology Applications

Diamond, the tetrahedral allotrope of carbon, has unusual properties defining it as a biomaterial. Its extreme chemical inertness makes it highly resistant to wet etching and other forms of degradation. It exhibits excellent biocompatibility and surface stability and has found application

as coating materials used for a prosthesis. New developments have witnessed its use to combat microbial biofilm formation on biomaterials. Diamond-like carbon-silver, diamond-like carbon-platinum, and diamond-like carbon-silver-platinum composite films have been prepared using a novel multi-component target pulsed laser deposition process. Silver and platinum form nanoparticle arrays within the diamond-like carbon matrix that can be attributed to the high surface energy of noble metals relative to carbon [134-136].

Diamond-like carbon-silver-platinum composites exhibit significant antimicrobial efficacy against *Staphylococcus* bacteria. Diamond-like carbon-metal composite films may provide higher hardness, corrosion resistance, and antimicrobial functionalities to next-generation cardiovascular, orthopaedic, biosensors, and other biomedical devices [137-139].

New applications of the antimicrobial properties of diamond-like carbon-silver-platinum nanocomposites may include catheters and other devices. Thin coatings of DLC (20-200 nm) for soft contact lenses and contact lens cases reduced the problems of biofilm formation. The microbial contamination of contact lenses is as major a problem as that of the lenses themselves and showed that lenses were stored in DLC coated cases were free from any contaminations [140-143].

1.9. Different forms of Diamond

1.9.1. Natural Diamond

Natural diamond crystals in the form of a single stone are created by geologic processes at great depth within the earth. This can be used as a cutting tool when the required shape of a piece is attached on the edge/tip for cutting glasses, stone, ceramics, FRP, etc. drill bits for mining, and oil

exploration. Single point cutting tool tips and small drills are used for high-speed machining of non-ferrous metals, ceramics, plastics, composites, etc., and effective machining of difficult-to-machine materials, super abrasive wheels for precision and critical grinding [144-146].

1.9.2. HPHT Method for the Formation of Diamond

In the 1950s, a successful attempt was made for producing synthetic diamond by converting graphite to diamond using high pressure and high temperature (HPHT) technology [147].

The HPHT process is an attempt to reproduce the conditions that create natural diamonds. Diamond is formed with large presses that can weigh hundreds of tons to produce a pressure of 5GPa at 1500°C, giving the conditions under which the bulk of the reported solution grown diamond stable region, crystallization of diamond has taken place. Diamond products are manufactured using alloys of transition metals, mainly iron-nickel, cobalt-iron, and to a lesser extent nickel-manganese for the grits and larger individual crystals and main cobalt for the polycrystalline products. Many solvent catalyzers are used to improve the quality of diamonds formed during high temperature and high-pressure synthesis of diamond [148-150].

The HPHT process takes only a few hours and produces tiny diamond bits and dust. These small diamonds, polycrystalline in structure (diamonds are single crystals) are too small for use as gemstones but as cutting tools they are extremely useful. Coated on edges of cutting tools drill bits and in resin, on a flexible backing these crystals can cut, drill, grind and polish a wide variety of materials. The high pressure, high temperature (HPHT) method of diamond formation is a major

contributor and research continues to improve both the creative process and its applications [150-152].

1.9.3. CVD Method for the Formation of Diamond

The chemical-vapour-deposition process involves the heterogeneous reaction of a gas-phase compound or compounds on or near a substrate surface to produce a solid deposit. The CVD technique for producing diamonds involves activating a mixture of H₂ or O₂ and carbon-containing gases to produce diamonds on a heated solid surface in a deposition chamber. The carbon-containing gases could be hydrocarbons such as CH₄, C₂H₂, or COs; various alcohols, or acetone. The activating source can be a hot filament, plasma (DC, RF or microwave), a combustion flame (oxyacetylene or plasma torches), an optical pumping source, or a laser. The basic mechanism in which the carbon phase is formed by the low-pressure process is by cracking hydrocarbon(s) (CH₄, C₂H₂, etc.) in the presence of hydrogen. The carbon species in the hydrocarbon gas have been activated since at low-pressure graphite is thermodynamically stable and without activation, only graphite is stable. The activation depends upon the temperature and chamber pressure. In the activation process, the mixture of reactants passes over a substrate that is heated either by radiation from the activated energy source or a separate self-heater. Under these conditions, carbon saturates the substrate surface as sp¹ bonded carbon diamond and sp² bonded carbon (graphite) in a competitive process [153-155].

1.9.4. Single Crystal Diamond

Single crystal CVD diamonds have been produced recently by several groups. This diamond contains the nitrogen-vacancy (N-V) and substitutional nitrogen, N_s, defects (which contribute to

the colour observed). Recent measurements on extremely pure CVD single-crystal diamonds indicate a quality much better than that of the best diamond found in nature or grown by HPHT processes. For extremely pure device grade CVD single crystals, with dimensions of the order of 3-5mm electron and hole mobilities (4400 and 3800 cm²/sec, respectively) exceeding twice the previously measured best values were reported recently [156, 157].

1.9.5. Polycrystalline Diamond

Polycrystalline diamond films and plates are grown on non-diamond materials, such as refractory metals or ceramics, e.g. W, Ta, Mo, WC, Si, SiO₂, and others, by seeding the surface with particles of diamond or by specific treatments that evolve into small diamond particles, e.g. biased enhanced nucleation followed by homoepitaxial growth on the surface of these particles until they coalesce into a continuous coating [158]. As a result of this growth process, the grain size is smallest on the nucleation surface (substrate side) and coarsens into larger grains as the film thickens due to overgrowth of slower growing surfaces (grains) by more rapidly growing surfaces (grains). Additionally, impurity incorporation and intentional doping (with B, N, P, Si, etc.) depend on the specific growth mechanisms on each local facet [typically a (111) or (100) surface], resulting in different incorporation rates on each surface (or growth sector under each surface) [159]. The polycrystalline (PCD) tools consist of layers of 0.5-1.0mm of fine grain size, randomly oriented diamond particles sintered with a suitable binder, usually cobalt, and then metallurgically bonded to a suitable substrate like cemented carbide or Si₃N₄, inserts. PCD exhibits excellent wear resistance, holds a sharp edge, generates less friction, and has high thermal conductivity. These properties contribute to PCD tooling's long life in conventional and high-speed machining of soft non-ferrous materials (Al, Mg, and Cu, etc.), advanced composites, eta-matrix composites,

superalloys, and nonmetallic materials. PCD is well suited for machining abrasive materials (drilling and reaming metal matrix composites) where it provides 100 times the life of carbides. It is not recommended for machining ferrous materials because of the high solubility of diamond (carbon) at elevated temperatures [160]. The main advantage of such a PCD tool is greater toughness due to finer microstructure with random orientation of the grains and reduced cleavage. The presence of binder cobalt/nickel reduces wear resistance and thermal stability. Freestanding plates of polycrystalline diamond have been made industrially with dimensions up to 30 cm in diameter and several mm in thickness [161]. The colour of such materials can vary from transparent for optical applications, to blue for electrically conductive applications, to grey/black found generally in cutting tools or thermal management applications [162].

1.9.6. Nanocrystalline Diamond

Nanocrystalline CVD diamond (NCD) is a form of polycrystalline diamond in which the initial seeds are of nanometer dimensions resulting in extremely high nucleation densities, typically between 10^{10} nuclei/cm² to over 10^{12} nuclei/cm². As with polycrystalline CVD diamond, the grain size coarsens with growth, reaching 100s of nm with films of several microns thickness [163]. The purity of individual growth sectors in a nanocrystalline diamond can approach that of the single crystal CVD diamond resulting in optically transparent or coloured doped films. But the existence of incoherent cluster boundaries and higher-order twin boundaries often causes localized stress and sp² bonded carbon regions, which in turn results in higher dislocation densities [164].

Since the invention of the low-pressure synthesis of the diamond from gas phases, continuous efforts were being made to use it as a coating on a cutting tool [165]. Various methods were

invented to synthesize diamonds from the gas phase (hydrocarbons with the help of a reducer like H_2 and O_2 , etc.). The coating thickness rate can vary from 0.1 $\mu\text{m}/\text{hour}$ to 1.0 mm/hour . This method is less expensive, free from the binder, and cleavage. It also permits use in the wide application range of cutting tools with complex shapes like milling cutters and drills. Nanocrystalline CVD diamond differs from polycrystalline CVD diamond in that the critical dimension of the growth sector or grain cluster (nanometers to hundreds of nanometers) is less than typical characteristic dimensions for various transport properties, e.g. phonon scattering electrical carrier scattering, crack propagation length [164, 166]. Hence there are important differences in some of the properties of these two classes of materials. The improved properties of nanocrystalline CVD diamond films are higher toughness and lower light scattering, while other properties such as carrier mobility and thermal diffusivity are decreased. Surprisingly, in fully dense nanocrystalline CVD diamond films, Young's modulus is nearly that of a single crystal diamond. In addition, many other properties of diamond are retained, such as corrosion resistance, surface termination and chemistry, density, optical transparency, and others [166 - 168]. Recently, nanocrystalline CVD diamond materials have been exploited for applications in micro-electro-mechanical systems (MEMS) and the nano variant MEMS, where the mechanical, electrical, and corrosion properties of these fully dense films extend the range and application of these novel devices. For example, the high stiffness (Young's Modulus) of the diamond can push resonant structures of a given dimension to much higher frequencies than achievable in more traditional MEMS material (Si, SiO_2 , Si_3N_4 , etc.) or relax the lithographic constraints required to achieve a particular frequency. Diamond MEMS/NEMS prove to be more durable, capable of surviving harsh chemical, radiation, or mechanical shock environments [169 - 172].

1.9.7. Ultrananocrystalline Diamond

Ultrananocrystalline diamond (UNCD) is a nanomaterial consisting of diamond grains only 2-5 nm in size (20 carbon atom diameters) separated by atomically abrupt grain boundaries. The grain boundaries consist of a mixture of diamond and graphite-bonded carbon [165]. Thus, UNCD is not a pure diamond but a nanostructured hybrid of different carbon allotropes (i.e., different forms of the same substance, in this case, carbon) that retains most of the desirable extreme properties of diamond and in some cases, exceeds the properties of natural diamond (e.g., fracture strength, electrical transport, field-induced electron emission, electrochemistry, and bio-inertness). Such films also retain the superior hardness, chemical inertness, and ultralow friction characteristics of natural diamonds [169]. UNCD films exhibit a unique set of complementary mechanical and tribological properties such as hardness (98 GPa) and Young's modulus (980 GPa) close to corresponding values for single crystal diamond (100 GPa and 1200 GPa, respectively). Close correlations were observed between the hydrogen content in diamond (UNCD) films, measured by elastic recoil detection (ERD), and their electrical conductivity and capacitance-frequency (C-f) behaviours [168, 171]. The addition of hydrogen gas in the Ar/ CH₄ gas mixture used to grow the diamond films appears to have two main effects depending on the film microstructure, in the UNCD films, hydrogen incorporates into the atomically abrupt grain boundaries [172]. Recent work has shown that electric field-induced emission of electrons from nanocarbon-based emitter surfaces, ND films, and carbon nanotubes (CNT) can be used to produce a new generation of electron emission devices, specifically, nanodiamond film- based lateral field-emission (FE) diodes and gated carbon nanotube (CNT) triodes, which are new configurations for robust nanoelectronic devices [165-172].

1.10.Summary

With the extensive study of standard handbooks and analysis of ongoing research, market analysis along with the demand of manufacturing sectors, the following inferences have been made:

1. A brief overview has been presented about the market trend of cutting tools across the globe.
2. An insight detail has been provided about the cutting tool materials and the coating types.
3. Primary fabrication techniques and their characteristics, used for coating cutting tools have been discussed.
4. A discussion is presented on the properties of diamond and its governing factors on its use as the coating material.
5. Lastly, applications have been listed to mark their increasing use in emerging fields.

Chapter 2: Literature Review

2. Introduction

Day by day, there has been a huge demand for better and long-life tools used in the manufacturing industry. These tools are required for the machining of various hard materials like metal-based composites and aluminium–silicon-based alloys because of their extensive use in the automobile and aerospace industries [91, 92]. It is a challenge to achieve extreme tolerances with operations of high volume for these materials as they are difficult to machine using conventional cutting tools [93, 94]. A large amount of literature is available on the determination of tool life, the effect of tool materials, tool coatings and cutting parameters on the output performance parameters such as surface topology, dimensional accuracy, etc. [176, 177]. A comprehensive literature review has been carried out and presented in the following subsections of this chapter.

2.1. Coating Variants

Nowadays, there exist numerous variants of the coatings which are being employed on conventional cutting tools [178]. The conventional tools are manufactured using the technique of high-temperature high-pressure sintering involving the powdered tungsten carbide and cobalt as binders. The substrate i.e. the surface of the conventional cutting tool carries the coating which is in contact with the work material in the cutting zone forming the active cutting edge. Due to the formation of an active edge, the need for a fine grain size of tungsten carbide arises which is to be sintered on the cemented carbide [178-180]. The interlocking between the coating and the substrate is favoured with fine grain size at the grain boundary lattices. The TiC, VC, NbC, ZrC, and TaC particles act as inhibitors when mixed in WC-Co matrix during the process of sintering [28, 181,

182]. While coating the substrate with the TiN and TiCN, the adhesion was increased using the TiC, TaC and NbC as grain growth inhibitors [183, 184].

Another research finding shows that the DLC coated tool's effectiveness depends upon the adhesion of the DLC coating with the substrate and which ultimately governs the output parameters such as surface roughness at high cutting speeds [185]. Table 2.1 shows the quantitative attributes of coating materials.

Table 2.1: Prominent attributes of the coatings [183, 186, 187].

Coating Material	TiN	TiCN	DLC
Friction coefficient against steel (dry)	0.4	0.4	0.1
Micro-hardness (HV 0.05)	2300	3000	3000
Maximum service temperature (°C)	600	400	800

Principally four types of coating materials are governing the global manufacturing sectors [188].

These are:

- Al_2O_3 : alumina-based ceramic coatings.
- Lubricant coatings deposited on hard coatings (pure graphite and Molybdenum Disulphide (MoS_2))
- Solid lubricant coatings (amorphous metal-carbon (Me-C:H)) and super hard coatings (CVD-DLC)
- TiN, TiAlN, TiCN, and TiC: Titanium-based coatings.

The recent research showed the extensive study of the DLC coated tools and their wear mechanism during the machining process. Oles et al. [189] investigated the CVD DLC coated tools during the machining process and concluded that the wear on the flank face of the tool was due to abrasive wear, a form of progressive failure of the tool. But, in the latest research, it was also shown in other studies that the life of DLC coated tools was restricted by the coating interface delamination (insufficient adhesion between the substrate (carbide) and coating (DLC)) [190] or the coating fractures [200]. Polini et al. [201] inferred during their research that the presence of cobalt in carbide tools decreases the adhesion of coating with the substrate due to non-diamond carbon layer formation at the interface. These tests were conducted with tungsten carbide tools coated with DLC coating using the CVD technique. It was also observed that the diamond being brittle, there exists a tendency of catastrophic failure of the DLC coated tool due to local fractures. A DLC film on the cutting tools may also fracture if the development of high tensile or shear stresses takes place [202-205].

In order to overcome the difficulties faced due to local fractures, numerous attempts have been made to modify the DLC coatings for better efficiency and effectiveness. The multi-interface structures can contribute to the hardness and toughness while reducing the internal stress by restricting the crack formation and propagation, which helps to improve the cutting performance and prevents catastrophic failure of DLC coated tools [206]. Also introducing graded transition layers can lower the gap between coating and substrate thereby redistributing the internal stress and enhancing the adhesion to the substrate. The addition of chemical elements can also be a helping tool for residual stress reduction and adhesion improvement and enhances the toughness by suppressing the deformation and propagation of cracks [205-207].

2.2. Coating Thickness

One of the significant variables in the coating system of cutting tools is the thickness of the coating on the substrate. An extensive study had been carried out on the tribological performance of the coating during the machining operations [208]. Variations of the coating thickness on HSS and cemented Carbide are shown in Figure 2.1 with the help of a bar chart.

Brief research findings have been discussed inferring that the coating thickness plays a vital role in governing the tool geometry and controlling the tribological properties of the coated tools during the cutting operation at various cutting parameters [209].

Thick coatings showed better resistance to scratch and wear during the working conditions when compared to the thin film-coated tools. This result was dependent on the high load-carrying capacity of the thickly coated tools [210, 211]. Dorner et al. [212] inferred the thickness of DLC coating, would not influence the wear resistance of DLC–Ti6Al4V if the thickness was from 0.7 to 3.5 μm . However, Kanda et al. [213] performed various machining tests with DLC coated tools and concluded that increased film thickness favours the tool life. It was also discovered that an increase in thickness was also associated with the lower transverse rupture strength which was one of the performance parameters during the interrupted machining and higher cutting forces were recorded because of the increment in the radius of the cutting-edge [214]. Silva et al. [215] showed with their experimental investigation that multilayer DLC coatings prevent catastrophic coating delamination, thereby increasing the tool life. Huang et al. [216] also displayed improvement in

the tool performance and tool life when tools were coated with a C:H and a C coatings while machining aluminium alloys.

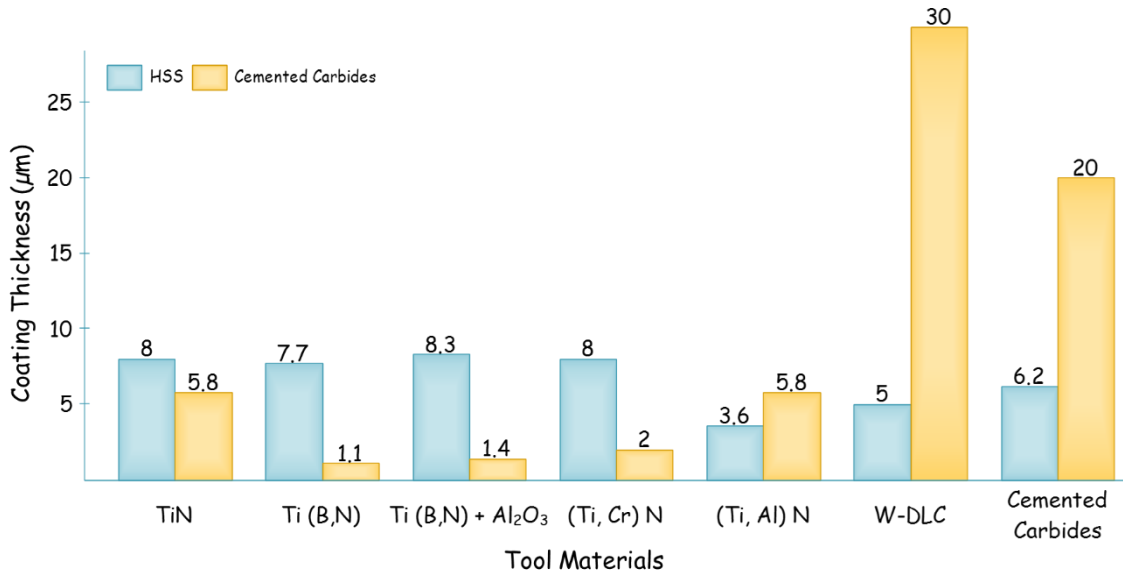


Figure 2.1: Variation of Coating Thickness on HSS and cemented Carbide

The TiN coating thickness on tool steels varies from 2 to 10 µm. These can be thicker (7–9 µm) if deposited using the CVD technique while these can be 3–5 µm thick if deposited by the PVD method [66]. The hardness of coating materials increased as the film thickness on the substrate increased which increased the life span of the cutting tool [64]. Though when considering the multi-layer coating systems, the thickness of the coating did not have much significance on the machining performance and machining parameters [217]. Variations of the coating hardness on HSS and cemented Carbide are shown in Figure 2.2 with the help of a bar chart.

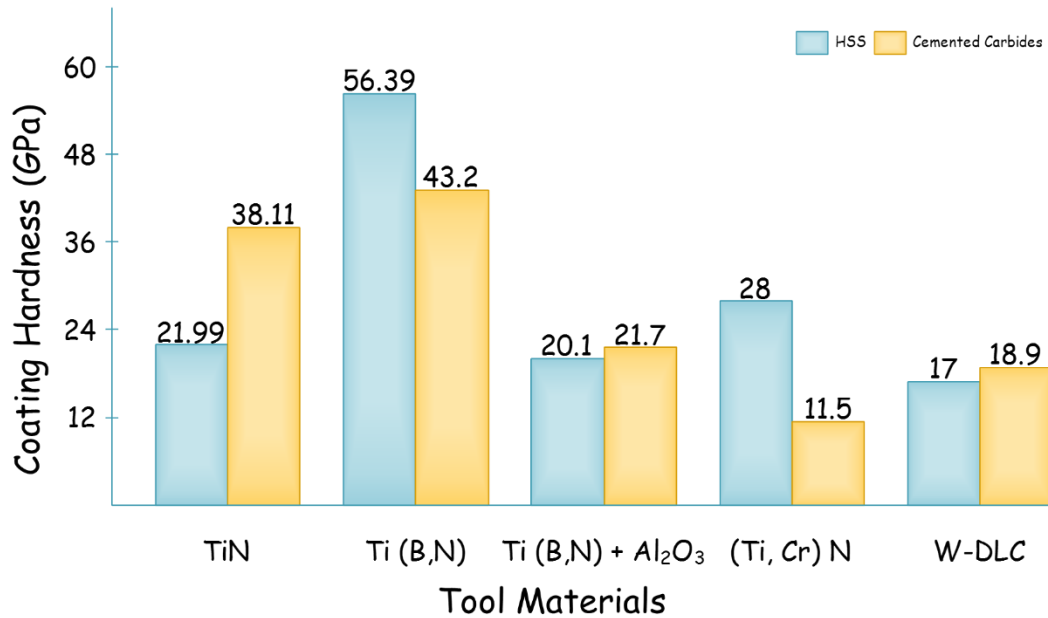


Figure 2.2: Variation of Coating Hardness on HSS and cemented Carbide [Table 2.2]

During experimentation by various researchers, it had been deduced that the rate of wear of uncoated tools was very high and the coating was promoting high resistance to wear and corrosion [218-222]. Another research observed that the PVD DLC coated insert showed low tribological properties in comparison to the CVD DLC coated insert when operating under the same cutting and environmental conditions [227]. This shows that the coating method along with the coating parameters decides the tribological properties and the working life of the coated cutting tools.

2.3. Coating Wear Resistance

Day-to-day increasing demands of the manufacturing industries have necessitated high performance of the cutting tools. The conventional tool material quality along with the type of surface coatings play a vital role in tool wear resistance [225-228]. In recent years, new materials as substrates are also being developed for the machining of new high strength sheets steels such

as TRIP steel, dual-phase steel, and martensite steel as it is difficult to perform forming processes on them [229]. These coatings should possess better resistance to wear with a less coefficient of friction and also should not deposit work material during the machining process. The property of high hardness curbs the abrasive wear and associates lubrication with a low friction coefficient [230].

Adhesion between the substrate and coating is a quantity that relies on several factors such as the substrate's surface roughness, composition, stress level and structure and thickness of coating [231]. The various methods of adhesion included mechanical bonding of coating with the substrate roughness, pores, and dendrite growth initiated at substrate level and movement towards coating; physical bonding through van der Waals, electrostatic forces and hydrogen; and chemical, i.e. covalent and ionic atomic bonds [232-234].

Another research conducted on the DLC coated tools shows that micro and nanocrystalline DLC coatings can be obtained by deposition in a microwave plasma (2.45 GHz) from methane–hydrogen mixtures to improve adhesion which will lead to higher wear resistance and inhibit the early crack formation and propagation in DLC coated tools [235].

An attempt has also been made to study the connection between the crystal structure and tribological properties of thin DLC coatings to ensure the enhancement of the tribological properties [236]. It can be inferred from the previous research that coating materials, coating methods, layer thickness, single or multi-layered coatings, and structure of coatings collectively

govern the performance of the cutting tools [237]. They can reduce and delay the wear and prevent crack propagation thereby enhancing the cutting tool life.

Tabulated information of different tool materials, coating materials, and their properties deduced from the work conducted in yesteryears are precisely displayed in Table 2.2, while Table 2.3 depicts the combinations of coating materials with cutting tool materials used in different machining operations along with the associated fabrication technique used for coating the tool material.

2.4. Analysis of Coatings

Ever since the development of metal cutting tools, there has been an urge to revolutionize to attain higher productivity at low production costs. This urge led to the change from conventional tools to coated tools which fulfil the demands of modern manufacturing sectors. Research on coating has mostly been assisted by its analysis and mechanisms. This section deals with the various effects of the surface coatings on the cutting tool materials [113, 128, 135].

2.5. Effect of Coatings

There are numerous effects of coatings that are applied to conventional cutting tool materials. Some of them are discussed in the following section [138].

Table 2.2: Properties of various Coatings on different tool materials

S. No.	Coating Type		Tool Material	Properties	Reference
1	Ti N		HSS	Thickness: 4 μm	[238]
2	DLC		WC/Co	Thickness: 1 mm	[239]
3	Textured DLC		WC/5% Co	Thickness: 20 μm	
4	Textured Diamond		Cemented Carbide	Thickness: 17 μm	
5	Si_3N_4	Composition: $\text{Al}_2\text{O}_3+\text{TiN}$	Ceramic	Thickness: 6 μm	[240]
				Hardness: 26.25 Gpa	
				Thickness: 2.6 μm	
6	TiN		Cemented Carbide	Thickness: 5 μm	[241]
7	TiN		WC–Co 6 wt.%	Hardness: 22.52 GPa	[242]
				Thickness: 5.8 μm	
8	TiN + nc-(Ti1-xAlx)N/a-Si ₃ N ₄ +TiN		WC–Co 6 wt.%	Hardness: 31.34 GPa	
			Thickness: 5.9 μm		
9	DLC Coating		Fine-grain WC/6 wt.% Co	Thickness: 5, 10, 15, 30 μm	[244]
10	TiN		Cemented Carbides	Hardness: 24.8 GPa	[245]
				Thickness: 2 μm	
11	DLC/TiAlN		Tool Steel	Hardness: 3000 HV	[246]
				Thickness: 4 \pm 0.40 μm	
12	A-C:H		Cemented carbide	Hardness: 2000 – 4000 HV	[247]
				Thickness: 1.02 μm	

Table 2.3: Fabrication Processes of Coating Technology

S. No.	Coating		Tool Materials	Operation/ Apparatus	Fabrication Process	References
1.	TiN		HSS	Turning	PVD	[238]
2.	TiN, single-phase high nitride martensite (α -fe)		HSS	Turning and Milling	1. Ion Nitriding 2. TiN (PVD) 3. PEPE layer	[248]
3.	WC/C-TiAlN, TiCN, TiN		HSS + Carbide	Drilling	PVD	[249]
	MoS ₂ -TiAlN, TiAlN, TiN		WC Multilayer			
4.	TiN		Cemented Carbide	Turning	PVD	[241]
5.	TiN		HSS	Turning	Cathodic Arc Physical Vapour Deposition	[250]
6.	AlSiTiN AlSiCrN	Nano Composite	Tungsten Carbide	Milling	Cathodic Arc Physical Vapour Deposition	[243]
7.	Diamond		WC with 6% wt. cobalt	Turning	CVD	[244]
8.	TiN, Nano TiAlN Monolayer, TiAlN/TiN multilayer		HSS	Drilling	PVD, Monolayer, Multilayer	[251]
9.	W-DLC coatings		HSS Cemented Carbide	Turning	Pulsed Reactive Magnetron Sputtering	[252]
10.	TiSiN, CrC/C		Cemented Carbide	Tapping	Hybrid cathodic arc sputter PVD	[245]

11.	TiN Al ₂ O ₃ TiN/Al ₂ O ₃	Cemented Carbide	Turning	PVD and CVD	[253]
12.	Wear Resistant Coating (WRC)	HSS	Turning and Milling	Filtration Vapour Ion Flow with Cathodic Vacuum Arc Deposition	[254]
13.	TiN, TiAlN, CrAlN	HSS and WC	Drilling	PVD (ARC and SARC)	[255]
14.	CrTiAlN	Cemented Carbide	Milling	Closed Field Unbalanced Magnetron Sputtering System PVD	[256]
15.	AlCrN	HSS	Pin-on-disc Test Rig	PVD	[257]
16.	Hydrogenated diamond-like carbon (H-DLC) CVD diamond	Tungsten Carbide (WC)	Drilling	CVD	[258]
17.	Si base layer +DLC	Cemented carbide	Drilling	PECVD	[259]
18.	DLC	Cemented carbide	Milling	Vacuum arc discharge	[260]
19.	TiB ₂ + DLC-WS ₂ Multilayer coating	Tungsten carbide	Milling	FCVA (graphite) MS (TiB ₂ , WS ₂)	[261]
20.	DLC coated tool	(WC-Co)	Milling	CVD	[262]
21.	DLC and DLC-WS ₂	Cemented carbide	Milling	Hybrid FVCA and magnetron sputtering PVD	[2]

2.5.1. Tool Life

Surface coatings on the cutting tools help in the wear resistance and corrosion resistance also simultaneously enhancing the tool life significantly. For the past three decades, these coated tools are employed successfully in the manufacturing sectors globally as they prove to be a helping hand in reducing the cutting forces and cutting zone temperatures. Statistics nearly 70% of the cemented carbide cutting tools had been coated to improve their life span [264, 265].

A coating thickness of 12-18 mm is the maximum upper limit as beyond this the integrity and stability of the coating weaken. A multi-layered coating has a better performance as it sums up the benefits of individual layers [266].

An accurate and proper selection of coating layers helps in suppressing the non-beneficial properties of individual coating layers and enhancing the useful properties in the integrated multi-layered coating on the substrate. The extensively used coating materials which have a substantial effect on the life of coated tools are TiN, TiC, Al₂O₃ and TiCN [110-115].

Table 2.4 shows that different coatings surface common results such as the decrease in crater wear, flank wear, lowering of coefficient of friction, and enhancement in tool life which eventually reduces the manufacturing costs and lowers the idle time of machine tools.

Table 2.4: Features of Coating Materials

Coating Type	Decrease in	Increase in	Reference
TiC	Crater wear	Tool Life	[241]
Al ₂ O ₃	Crater wear	Tool Life	[243]
Diamond	Crater wear	Tool Life, Hardness	[246]
TiN	Interfacial Friction	Tool Life, Layer Thickness	[267]
DLC	Adhesion Wear	Tool Life, Layer Thickness	[260]
DLC	Catastrophic Failure	Tool life, Coating hardness	[268]

2.5.2. Tool Wear

During the operations of machining/metal cutting, tool experiences wear in different forms. Among these wears, the most significant wear experienced by the cutting tool is crater and flank wear. Crater wear happens on the tool's rake face while flank wear happens on the tool's flank face [269].

In the cutting process, the zone of an interface of a tool chip is at high temperature and pressure and is the region where crater wear originates. As the cutting process progresses, the crater enlarges developing a sharper edge and high-stress zone at the cutting edge which leads to edge breakage. Obikawa et al. [270] looked into the characteristics of the crater wear during machining of AISI 1045 steel with the alumina coated carbide and ceramic tool. It was found through the experiments and their analysis that wear rate equations are functions of cutting zone temperature and normal stress. It was also discovered that the wearing of the coated tool was significantly dependent on

the substrate's thermal conductivity. Though ceramic tools showed high resistance to wear, the crater wear in both cases was found to be the same. The cutting temperature of the alumina coated carbide tool was lower than the alumina coated ceramic tool which became the reason for such an interpretation [270].

It is evident from the experiments performed by Garcia-Gonzalez et al. (2016) that tool wear (i.e. crater wear) is significantly affected by the maximum temperature in the cutting zone. The tool is heavily damaged at the cutting edge when the temperature was maximum at the chip-tool interface. Due to high temperature, a layer of base metal is deposited on the TiN coating at the cutting edge, beyond which a highly damaged region lies. This phenomenon is significantly governed by temperature [265].

Chowdhury et al. [271] performed machining of Ti6Al4V aerospace alloy with TiAlN, TiB₂ & DLC coated tools and inferred that tool coated with TiB₂ has the lowest wear intensity due to its dense, non-columnar microstructure which helps in dissipating frictional energy from cutting zone. On further analysis, it was concluded that TiB₂ coating chipped away in different ways. TiB₂ coating fails by plastic flow while TiAlN has an abrupt failure and also deformation in TiB₂ is localised [238].

Flank wear initiates at the interface of the tool flank and newly machining surface. It begins at the cutting edge and continues to grow away from the edge. This wear was easily predicted and had a stable cutting tool life [201]. Qin et al. (2009) [86] inferred that the effect on wear resistance of

flank hard coating thickness was significant. Table 2.5 reflects the conclusion that 3-7 μm is the optimum coating thickness in order to maximize the tool life [86, 110].

Table 2.5: Tool Wear versus Coating Thickness

Results	References
The increase in coating thickness up to 6 μm increases the resistance towards flank wear but decreases drastically at the thickness of 10 μm	[89]
With the increase in thickness of the coating, the resistance towards tool wear also gets increased uninterruptedly	[98]
The optimum coating thickness of 3.5 μm maximizes the resistance towards tool wear and enhances the tool life	[99]
Tool life increased when thickness ranged between 7.5 and 10.5 μm	[110]

Few studies worked on the pin-on-disc tribometer to investigate the effects of the thickness of the coating on the substrate and the surface roughness of the substrate [232]. The shape of the pins was spheres and they were made of alumina and 100C6 steel [175] or bearing AISI 52100 steel [135] which were loaded against discs made of materials either ferritic 35CD4 steel or AISI 440C steel, respectively. The discs roughness ranged from 0.01–1 μm Ra with a coating of titanium nitride (TiN) or Molybdenum disulfide/Titanium (MoS₂/Ti) possessing a thickness range as 0.1–5 μm thickness. Takadoum and Bennani [272], and Siu and Li [273] worked on pin-on-disc tribometer and not on cutting tools or cutting processes. McCool [274] identified surface roughness on three parameters i.e. and the area density of the asperities η , the radius of curvature of their summits r , and the standard deviation of asperities heights σ_s . No predictive or theoretical models

have been found in the literature which extensively discusses the effect of thickness of coating or surface roughness on resistance to wear during the operation.

Few studies revealed the weakening effect of the very thin hard coatings during the tribological performance of coated and uncoated materials. The coated case showed worse results as compared to the uncoated materials [167]. However, M'Saoubi et al. [275] showed a case of low wear resistance of a coated tool in comparison to the uncoated tool.

2.6. Coating Failure

In 1984 Laugier was one of the first to discuss and developed the energy description model of coating removal using scratch [276]. The failure mechanism of the coating can be easily categorized during adhesion evaluation techniques depending upon the coatings types (ductile or brittle), the material of the substrate and the stress developed in an adhesion test. Hedenqvist et al. [277] analysed the modes of failure of thin TiN film on the HSS substrate using scratch tests with variable coating thickness and substrate hardness [115]. The coating detachment mechanism is discussed in the following points:

- a. Initially, at critical normal force, no seeable damage on the surface is observed.
- b. An increase in normal force extended deformation to the plastic state from coating to substrate. Transverse surface cracks were observed as a result of the generation of tensile stresses.
- c. On further increase of normal force, internal and external cross cracking increases.
- d. Flaking occurred preponderantly outside the scratch range.

Coating failure relies on the thickness of the coating. As the thickness increases, the chances of chipping increase which makes the coating ineffective. The thickness of the Coating and level of its adhesiveness governs the failure of coated tools. Usually well adhered coated tools fail due to progressive wear. Catastrophic failure of coated tools is due to delamination of the coating due to increased stress in the cutting zone. Flank and crater wear is low in wet machining as the coating remains protected from the high temperature in the cutting zone.

During the experimental work conducted by Kumar and Patel in 2017 [278], it was observed that micro-grooves were formed due to abrasion and adhesion wear which delaminated the coating layer and led to spalling of the tool [187, 278]. Spalling of tool occurred because of poor adhesion of coating and material of substrate which was supported with values of critical load during a scratch test.

Bouzakis et al. [279] studied the failure mechanism of coating a TiAlN coated tool. A number of patterns of flank wear were obtained at various cutting speeds which governed the coating failures. The condition of failure of the coating through cracking is that the mechanical work of the brittle failure equalises the energy release rate from cracks of the coating. So, the compressive stresses developed around the surface of the coating transcend a critical value [193, 278, 279]. Research is ongoing through the simulations of the scratch test to overcome the challenges and develop a better understanding of the interface behaviour, coating brittle failures etc.

Many researchers have found various reasons for the failure of DLC Coatings. For instance, Lieberman [280] found that the reason for the failure of the DLC coating was the dissimilarity

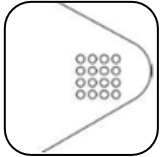
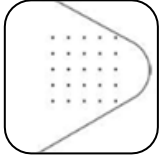


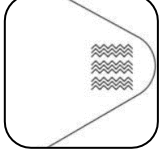
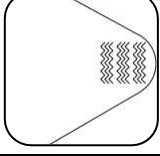
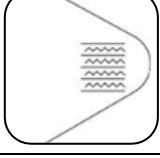
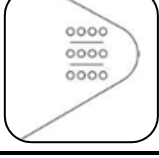
between the thermal expansion coefficients of DLC coating and the substrate material. Whereas, Wang (2022) [207] conducted research and concluded that the high internal compressive strength developed in the DLC coating was the reason for the coating failure.

2.7. Texturing on Tool Inserts

The beginning of textured tool inserts in the research papers was not known till 2009. Two research papers were published elaborating on the effectiveness and possibility of employing textures on the surfaces of the tool inserts [119]. It has been found that the texturing on the surface of tool inserts has benefits over non-textured tool inserts viz. reduction in cutting force [121,126], diminishing the length of contact [9], enhancing resistance against adhesion [10], improved quality of machining [11] and resistance towards tool wear [12].

Sugihara and Enomoto [281] analyzed the effect of micro-laser texturing on the flank faces of the carbide tool. They had performed experimentation on steel using textured and non-textured tool inserts for wet and dry machining conditions. They found reduced crater wear in as comparison to the non-textured tool inserts. Xie et al. [13] obtained approx. 33% of decrease in the cutting forces for machining using the micro-textured tool inserts. Sugihara et al. [14] have found that confederated textures decrease the coefficient of friction on the rake face of the tool inserts. Kim et al. [15] concluded that the air gaps in the tool-chip interface induce hydrophobicity i.e. it tends to repel fluid which results in the reduction of adherence. These research shows immense potential in the field of coating technology in terms of surface texturing at micro-scale and nano-scale. After carefully going through the research, we have classified the various texturing patterns and their placement on the tool inserts in Table 2.6.

Table 2.6: Classification of textures on the rake face of the cutting tool inserts

S. No.	Texturing Pattern	Placement of Texture	Diagram	References
1.	Circular Holes	Perpendicular or Parallel		[11]
2.	Indentations	Perpendicular or Parallel		[12]
3.	Linear	Parallel		[15]
4.	Linear	Perpendicular		[78]
5.	Waves	Perpendicular		[89]
6.	Waves	Parallel		[116]
7.	Hybrid (Linear and Waves)	Perpendicular or Parallel		[128]
8.	Hybrid (Linear and Holes)	Perpendicular or Parallel		[147]

2.8. Market Trend

The cutting tools market is sectioned into two categories i.e. linear cutting tools and rotary cutting tools. The cutting tools market has been progressively expanding owing to their application in various sectors such as power generation, aircraft industry, construction, oil and gas and automotive industry [110].

2.8.1. Market trends for coated cutting materials

Ever since the development in the field of coating, it has aimed to protect the surface from adhesion and abrasive wear during the cutting processes. Figure 2.3 shows the distribution of various tool materials over the past decade [136].

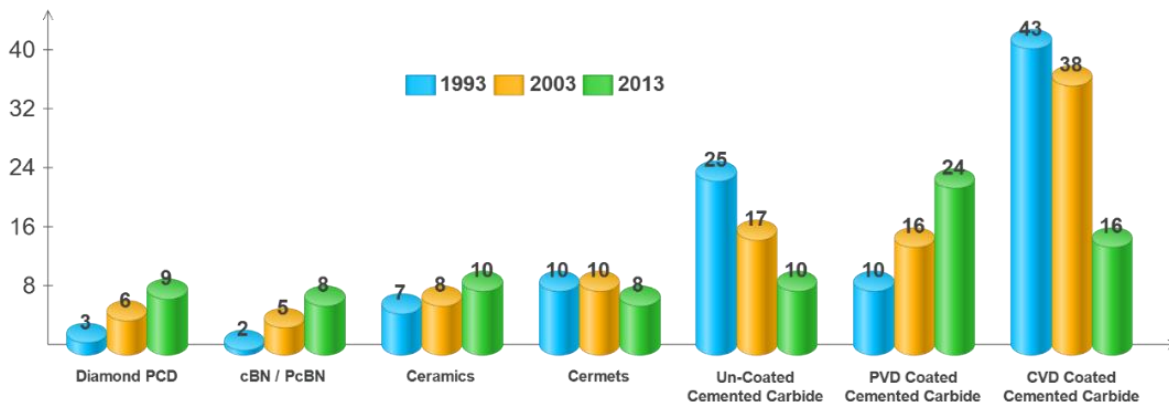


Figure 2.3: Global Market Share of Different Tools [123]

A dip is recorded in the percentage of cemented carbides due to the recent developments of cutting tool materials viz. ceramic, PcBN/cBN and PCD. Though cemented carbide's share has decreased carbides coated through the PVD process have captured the global market in recent times. PVD coated tools accounted for nearly 60% of the global manufacturing sector while the nanostructured

PVD coatings on cemented carbides emerged recently as a promising layer for the reduction in tool wear. The nanostructured PVD coatings date back to the late 90s and have grown at a faster rate conquering the 15% of the market in the manufacturing sector. A shift has been observed in materials of cutting tools from HSS to cemented carbides to nanostructured PVD coated carbide tools in the form of indexable inserts. According to the statistics, in 2013, nearly 74% of milling tools were accommodated with indexable inserts which were coated with the PVD process [124].

According to the latest survey report, the DLC coating market is estimated to reach USD 1052.5 million in 2022 and will further attain a value of USD 1362.7 million by 2028 globally. The DLC coating market is majorly led by Europe and Asia-Pacific capturing 36% and 33% of global consumption of DLC coating [161]. Globally, the major driving force behind the DLC coating market is the unending demands of the automotive and aerospace industries. These sectors account for 56% of the total downstream consumption of DLC coatings [162].

2.9. Impact of coatings on Production Cost

The production cost of any product in the manufacturing sector consists of nearly 3% of the cost incurred by the cutting tools. The statistics conducted by Dedalus Consulting [124] show that an increase in tool life due to the development of coatings and their material has a negligible effect on production costs incurred by the manufacturing firm. Nearly 1% of production cost per product is reduced by increasing the life of the cutting tool by 50%. Adjusting the machine parameters along with the coated cutting tools can reduce the production cost by 15% per component. The tool setting cost and tool regrinding cost can also be reduced by the use of tools coated with hard and super-hard coatings. It is quite evident that the new coating materials and the coating techniques are significantly affecting the productivity rate in every manufacturing sector. The

tribological analysis conducted on the advanced materials of coatings such as nanostructured layers has shown the excellent effect of protecting the cutting tool irrespective of variation in machining parameters and hence improving the productivity in machining [123]. The various factors incurring the production cost are shown in the form of a donut pie chart in Figure 2.4. [125].

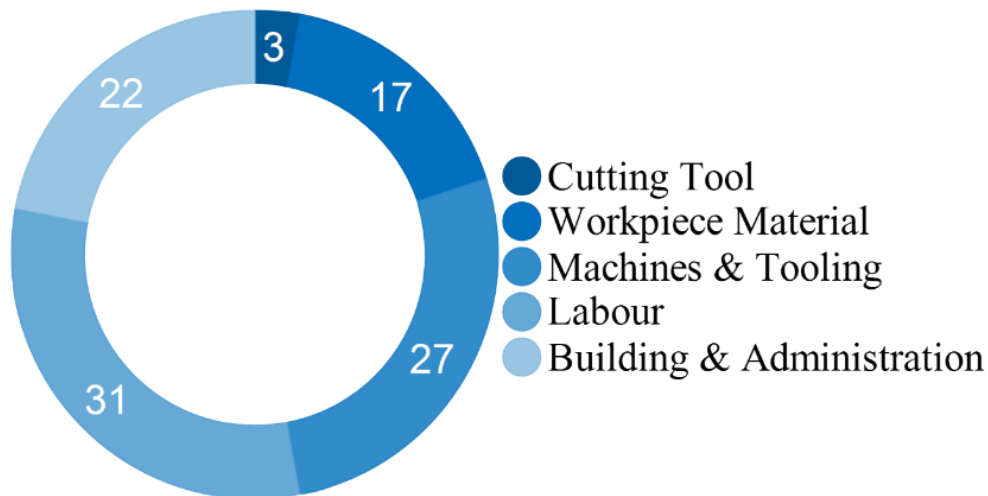


Figure 2.4: Various Factors incurring the Production Cost [N.N. Cutting Tools (2014)].

The study of cutting tools dates back to primitive ages. As time changed, with industrialization and technological growth, new cutting tool materials were introduced. A gradual change in their improvement was observed with the development of the difficult-to-machine metals in terms of the application of the coating on the cutting face. The experimental investigation carried out over the years provides the platform for deposition of the coating on the substrate, entrap the wear rate of the tool flank and face [129]. Table 2.7 shows the new findings over the past two decades in terms of tool material, tool coating, and changes in properties due to new findings.

Table 2.7: New findings over the past two decades

S. No.	Tool Material and Tool Coating	Properties Analysed	Investigation for New Findings	Change in Properties due to New Findings	Year	Reference
1.	Diamond coating on tungsten carbide (WC) tool substrates	Composite layer formation of TiC or TiN	Growth of continuous diamond film on the ceramic embedded discontinuous coat of diamond film.	<ol style="list-style-type: none"> 1. Improvement is significantly shown in the adhesion property of coated substrate due to the presence of TiC composite layers. 2. Enhancement in adhesion is a result of the change in thermal stresses. 	1995	[113]
2.	Diamond coatings on WC-Co tools	Coated tools presented 69%–79% better performance in comparison to the conventional PCD tool	Machining of various materials	<ol style="list-style-type: none"> 1. Machining of fibre reinforced plastics: A coated tool is equivalent to conventional PCD. 2. Turning Al-Si alloy, A380: Coated tools surpassed conventional tools by 200 %. 	2003	[103]
3.	Development of Ti/ TiN/ TiCN coatings on cemented carbide inserts	Enhanced tool life at high-speed turning operations	Formation of a single layer of TiC, Formation of multilayer composite coating Ti/ TiN/ TiCN	<ol style="list-style-type: none"> 1. Increased tool life 2. Good results at high-speed turning operation 	2003	[113]
4.	Al ₂ O ₃ +TiN and with TiN+Al ₂ O ₃ coatings on ceramics tools	Better adhesion and hardness along with very good resistance to abrasive wear	Investigation to increase the cutting tool flank life	Thermos-mechanically stable Al ₂ O ₃ layers acted as a barrier between the flow of the chip and tool inserts, leading to improvement in coated tool's resistance to wear while TiN layers facilitate easy chip flow by decreasing the friction.	2007	[114]

5.	Coated tools	Thermal and mechanical properties improved the wear behaviour of the tool	Reconditioning of worn coated solid cutting tools	<ol style="list-style-type: none"> 1. Macro-blasting with various grain shapes and sizes help in strengthening the coating. 2. Micro-blasting increased the coating adhesion. 	2012	[115]
6.	PVD-coated carbide cutting tools	Increased life of tool while preventing the cohesive damage of tool.	Investigation of the manufacturing process of coated carbide tools at each step of the conventional machining process.	<ol style="list-style-type: none"> 1. A transfer of residual stresses is observed in the direction of tensile stress which is governed only by thermal component loads. 2. The compressive stress of the substrate is released during the etching process. 	2013	[116]
7.	PVD-coated TiAlN carbide tool and CVD-coated multilayer TiN/TiCN/Al ₂ O ₃	The temperature at the interface of Chip-Tool significantly influences feed and cutting speed.	Study of effects of heat generation of temperature at the interface of chip-tool.	For PVD coated tools an observation of low temperature was found than when compared to the CVD-coated tool.	2014	[117]
8.	DLC and nano-crystalline diamond coatings on solid carbide tools	Excellent wear resistance and adhesion with high adaptability of tool geometry	Diamond coatings of Nano-crystalline size.	A very little influence was found on the feed and cutting velocity on tool lifetime	2014	[118]
9.	TiAlN films with Cemented carbide tool inserts	An investigation of coefficient of friction, tool wear and cutting forces.	Machining in starved lubrication and full lubricated conditions.	<ol style="list-style-type: none"> 1. Improvement of cutting performance of textured tools in lubrication regime owing to reduction of cutting forces by 22-35% at high speed. 2. Surface texturing improved cutting performance as grooves served like a small reservoir of liquid. 	2015	[119]

10.	Tungsten carbide (WC/Co-based) tool with Ti55Al45N coating layer	How tool wear and cutting performance were affected by the nano-scale texturing.	<ol style="list-style-type: none"> 1. Nano surface textured tool at the rake face followed by depositing the Ti55Al45N hard-coatings (NCT). 2. Deposition of Ti55Al45N hard-coatings on tool surface followed by nano-scale surface texturing (CNT). 	<ol style="list-style-type: none"> 1. Nano-scale textures help in the reduction of coefficient of friction, the temperature at the cutting zone, wear of the tool and also the forces developed while cutting. 2. The geometry of textures governs the cutting performance. 3. Texturing reduced the reach of chips at the rake face of the tool interface 4. NCT tools were not as effective as CNT tools were found to be. 	2015	[120]
11.	PVD coated cemented carbide (TiN + TiAlSi Nnanocomposite + TiN)	Nanolayer structure greatly improved the hardness in comparison to the structure of nanocomposite	Nanostructure and Nanolayer coatings	<ol style="list-style-type: none"> 1. Hardness was improved by the increase in Al ratio in AlTiN layers, but only up to 60:40 = Ti: Al. 2. Nanolayers differ in Al: Ti ratio. 3. Flank wear governed the durability while abrasion was the predominant wear mechanism. 	2016	[121]
12.	Carbide tool coated with TiAlN coating and TiN coating	Observation of similar results for both coated tools was found to be lowest for TiAlN coated tool.	<ol style="list-style-type: none"> 1. Wear mechanism majorly comprised of adhesion wear due to intermittent cutting. 2. Representation of flank wears through logarithmic curves. 	<ol style="list-style-type: none"> 1. The wear rate of the TiN coated tool was high above 400°C of annealing temperature. 2. Recrystallization led to a decrease in hardness and above 550°C it oxidised. 3. The wear rate of TiAlN coated tool was low as hardness increased in the temperature ranging from 600°C to 950°C and it has the self-adapting ability towards the applied thermal load during cutting. 4. Images obtained through SEM and EDS mapping confirmed the partial loss of the coating layer. 	2017	[122]

13.	Self-lubricated nano-micro textures coated cutting tools	Coated micro-textures tools are more effective than uncoated.	The flank face and rake face of the cutting tool was used for the micro texturing.	<ol style="list-style-type: none"> 1. Enhancement in tribological properties due to the presence of micro-textures. 2. Reduced machining forces, coefficient of friction, the temperature at the cutting zone, crater wear and flank wear. 	2018	[123]
14.	Carbide tools coated with TiAlN and TiN and coating	An increase in the cutting speed increases the wear at the flank face of the tool, resulting in a changed wear rate for the shorter distance.	An empirical relationship was developed between the increase in wear rate and the worn-out coating layer.	<ol style="list-style-type: none"> 1. Suppression of tool wear until coating layer prevails (coating worn-out layer prevents wear) 2. Increase in wear rate due to dependency of wear resistance on substrate material when coating at cutting edge is worn out. 	2019	[124]

2.10.Summary

An extensive study of previous literature quotes that the coated tools inserts were largely significantly established more resistance towards wear than uncoated tool inserts. Nevertheless, very less research was observed on the effect of thickness of the coating on the resistance towards flank wear. It was also observed during the literature review that very little study has been conducted on the effect of textures on the tool inserts on coating and tool life for the turning process. After an extensive review of previously conducted research on the cutting tool materials, their coating, processing of coatings and the number of layers of coating, majorly research is performed on the cobalt-based carbide tools or tungsten carbide tool inserts. Hence, the goal of future experimental research will be the development of coating for the tungsten carbide tool inserts for the turning process. On the basis of the above-mentioned literature, it has been found that limited researchers have reported the application of the TOPSIS and Genetic Algorithm (GA) method for the application of DLC coated tools in the turning process. Therefore, in this research, we have tried to estimate and optimize the selected input parameters using the self-developed DLC-coated tungsten carbide (WC) tool inserts and self-developed DLC-coated textured tungsten carbide (WC) tool inserts in the turning process.

Chapter 3: Problem Formulation

3. Introduction

A huge amount of bio residual is produced every year just through agricultural waste. If these residuals are relinquished into the environment without a suitable procedure of disposal, then these will cause environmental pollution and harmful effect on human and animal health. The majority of the agro-based residuals are not treated and are left underused, consequently, in most places, it is disposed of either by unplanned landfilling, dumping, or burning [33]. These untreated wastes create different problems with climate change by increasing the number of greenhouse gases [282]. These wastes cause a serious disposal problem [283]. For example, the juice industries produced a huge amount of waste as peels, the coffee industry produced coffee pulp as waste, cereal industries produced husks and the sugar industry produces sugarcane bagasse. Figure 3.1 shows the image of sugarcane grown on farms.

Across the earth, approximately 148,000,000 metric tons of fiber sources are obtained, also 710,000,000 and 680,000,000 metric tons of wheat residuals and sugarcane residues are estimated, respectively [284]. The sugarcane bagasse has always been one of the major waste generated from agricultural sources. After Brazil, India is the 2nd largest producer of sugarcane. 90 million tons of sugarcane bagasse is produced as agricultural waste from the sugarcane industries of India. This waste is sometimes further reduced as biofuel for applications on power plants and industrial boilers or is just burned as normal waste. The amount of sugarcane bagasse burned is approximately 7–8% of the total consumption of sugarcane bagasse [19]. The burnt residue of sugarcane bagasse has no possibility of any further reduction [20]. Hence, reasons for considering sugarcane bagasse as a carbon precursor for the growth of

polycrystalline diamond films in the used thermal CVD method. Interestingly, pyrolysis of sugarcane bagasse produces effluent gases having good thermal dissociation which, produces the right chemical as well as thermodynamic equilibrium for diamond formation [21].



Figure 3.1: Sugarcane Grown in Farms.

3.1. Problem Formulation

In the present industrial scenario, a humongous research gap can be contemplated for the development of an eco-friendly way of depositing the coating using the thermal CVD technique.

- Trends in the industry are shifting from conventional to sustainable manufacturing. Hence there is a need for an environmentally friendly coating method.
- Use of bio-waste products, as carbon precursors for the production of the diamond coating.

- As we know the cost of machining is a major element of the mechanical industry, hence tools wearing off rapidly while machining also increases the cost. So, in the industry, we need tool inserts with higher wear resistance and hardness along with lower friction of coefficient for machining applications at higher speed.
- Bulk use of coolant in machining industries is not only causing the economical problem but also increases the environmental damage. Hence, there is a need for such coated tools which can be used in a dry machining environment.

With this background, the present research work aims to develop, characterize and analyze the environment-friendly DLC coated CNC tool inserts through a thermal CVD technique for industrial applications. The upcoming sections explain research gaps and thesis objectives.

3.2. Research Gap

After carefully going through the literature mentioned in chapter 2 the following research gaps were formulated:

- In the present scenario, new advances in coated CNC tools are replacing conventional CNC tools for advanced engineering applications and industrial purposes.
- By going through the various literature it is found that most of the methods applied for the coatings of DLC are based on conventional CVD, very limited research has been based on environment-friendly methods such as the Thermal CVD process. So this area needs to be explored.
- Also, most of the literature has been done using single response optimization for optimizing the various parameters viz. crater wear (CW), flank wear (FW), cutting forces (CF), surface roughness (SR), and temperature in the cutting zone (T). Hence, there is a

need to optimize the various parameters together using a Multi-response optimization technique.

- Apart from the above, very less attempts have been made to optimize the machining process parameters using a genetic algorithm (G.A.). So, this technique needs to be explored more for the precision machining process.

3.3. Research Objectives

After going through the above-mentioned research gaps, the following research objectives were formulated:

1. Development of diamond-like coating on tool inserts using the environment-friendly method.
2. Comparison of tool performance for coated tools fabricated by conventional CVD and eco-friendly CVD process.
3. Morphology and characterization of developed tool inserts.
4. Study of mechanical properties of developed tool inserts.
5. Study of wear and tool life of developed tool inserts for precision machining.
6. Experimental study of the effect of various process parameters on precision machining and to develop the empirical relationships between important process parameters and response characteristics.
7. Multi-response optimization of the process parameters of the precision machining process using developed inserts.

3.4. Scheme of Research Work

The following Figure 3.2 displays the flow chart of experimentation that was carried out to accomplish the objectives of the work.

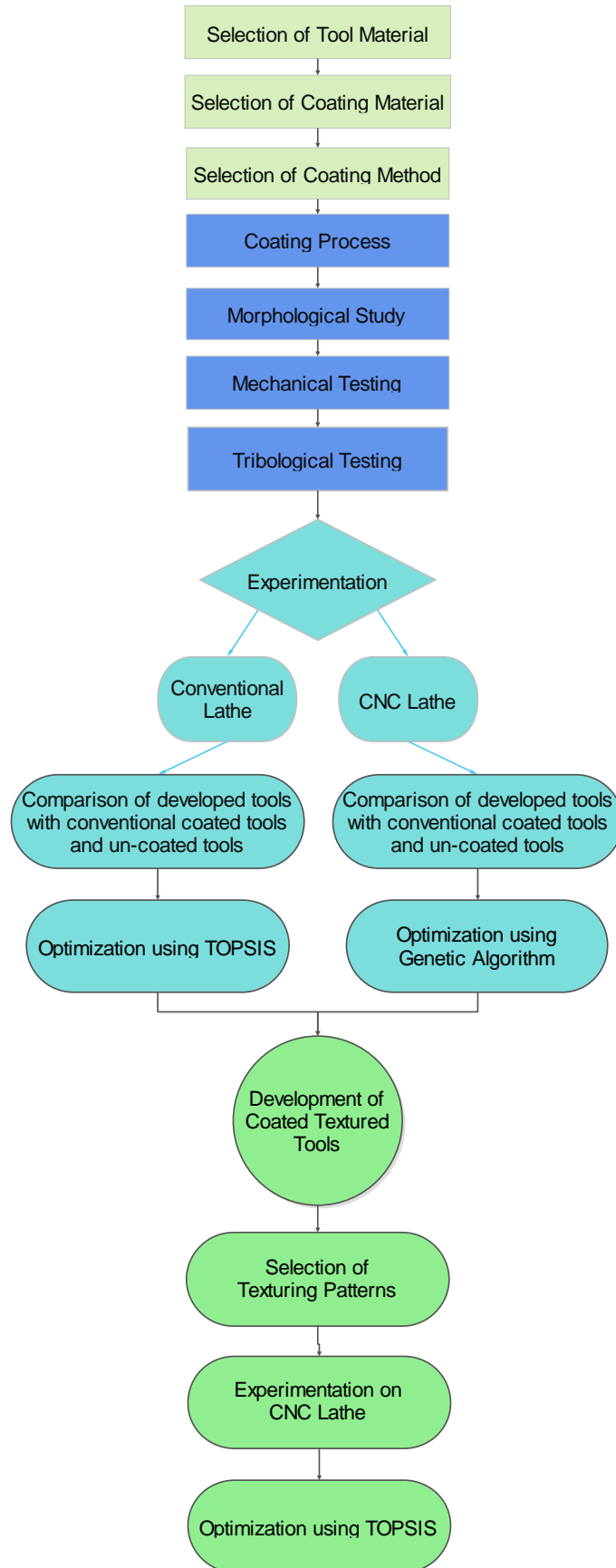


Figure 3.2: Flowchart showing the scheme of experiments.

The initial work was accomplished by the selection of cutting tool material, coating materials, and coating techniques. This was followed by characterization of the coated cutting tool which includes mechanical and tribological testing. Once the cutting tool was developed, experimentation was carried out on conventional and CNC lathe machine tools. The results so obtained were utilized to develop predictive models for optimization.

Two techniques of optimization i.e. TOPSIS and Genetic Algorithm were used to optimize the output parameters. Also further, coated textured tools were developed and used for experimentation on the CNC lathe machine tool. These results were also optimized using the TOPSIS method. A concise flowchart has been shown in Figure 3.2.

3.5. Summary

This chapter consisted of problem formulation, research gaps, and research objectives of the thesis. Also, the chapter gives a concise flowchart of the experimentation which is carried out to fulfil all the listed objectives of the project.

Chapter 4: Materials and Method

4. Introduction

This chapter provides the precise details of the development of DLC coating on the tungsten carbide (WC) tool inserts along with the process of turning in machining operations.

4.1. Material

This section will cover the materials used for the tool and workpiece. In this research work, tungsten carbide was used as the substrate for developing the diamond-like coating on the tungsten carbide (WC) tool inserts and aluminium (6061) was used as a workpiece.

4.1.1. Tool

In this research work, commercially available tungsten carbide cutting tool inserts were used as substrate material for coating. The selected cutting tool insert is in the form of a triangular shape as shown in Figure 4.1. The average hardness measured through the micro-hardness tester for the uncoated insert was 953.95 HV i.e. Vicker's Hardness number.

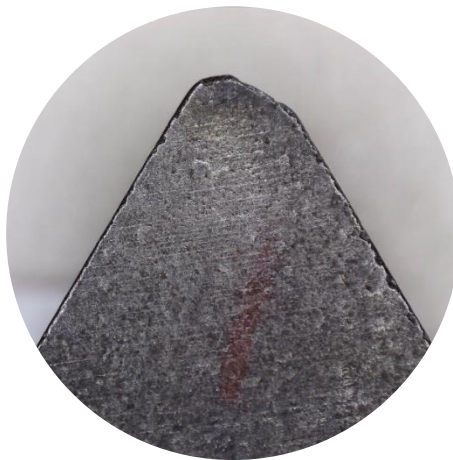


Figure 4.1: Un-Coated WC Tool Insert

The elemental composition of the tool insets is shown in Table 4.1 and the EDX spectrum of the same is shown in Figure 4.2.

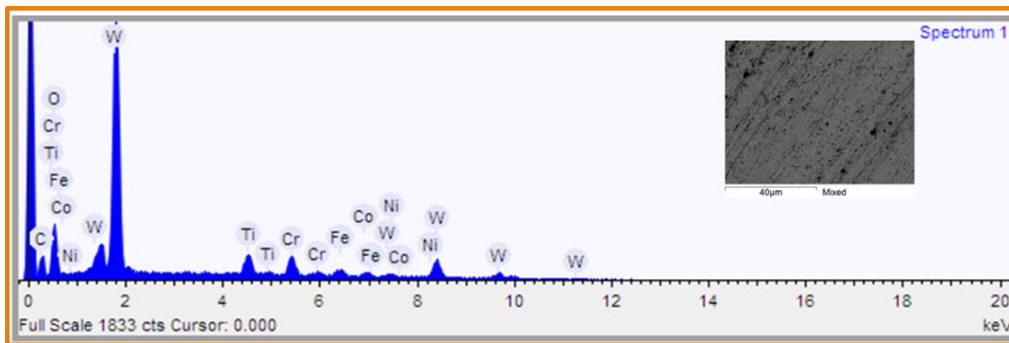


Figure 4.2: EDX spectrum of Tungsten Carbide (WC) substrate

Table 4.1: Elemental composition of Tungsten Carbide (WC) substrate.

Element	W	C	O	Fe	Ti	Co	Ni	Cr
% Weight	44.18	17.46	14.53	8.82	4.27	3.86	3.34	2.27

4.1.2. Workpiece

In this research work, aluminium (6061) was taken as a workpiece, as they are the best fit for the non-ferrous materials for the diamond coated tools. The workpiece used had a diameter of 50 mm and a length of 610 mm. The image of the same can be seen in figure 4.3 and the elemental composition of the Aluminium (6061) workpiece is shown in Table 4.2.



Figure 4.3: Workpiece used for the CNC Machining

Table 4.2: Elemental composition of Aluminium (6061) workpiece.

Element	AL	Mg	Si	Cu	Cr	Ti	Zn
% Weight	94.18	1.46	0.94	0.56	1.32	0.81	0.73

4.2. Coating Procedure

Tungsten carbide (WC) inserts were used as a substrate material for the coating process. In the present work, DLC films were coated on the tungsten carbide tools inserts at atmospheric pressure using the thermal chemical vapour deposition (CVD) technique. The substrates were cleaned (pre-treated) using concentrated sulphuric acid (H_2SO_4) and acetone ($(CH_3)_2CO$) for 7–10 min before depositing the film. At the same time, sugarcane bagasse (SBg) (obtained from sugarcane) was used to produce pyrolyzed sugarcane bagasse (p-SBg) by placing sugarcane bagasse (SBg) in the split furnace set on a controlled temperature of $550^\circ C$, at atmospheric pressure [18].

The activated carbon was produced from the pyrolyzed sugarcane bagasse (p-SBg) after chemical treatment [18, 26]. After that, the cleaned substrates of tungsten carbide tool inserts and produced activated carbon were loaded into the reaction chamber of the thermal CVD system for the growth of the DLC coating. This process of coating was carried out at atmospheric pressure in the thermal CVD system at $\sim 900^\circ C$. Sugarcane bagasse was used as a carbon precursor for the growth of DLC coating on WC substrates along with a mixture of Ar/ H_2 in the ratio of 2:1 to carry the effluent gases and to remove the presence of oxygen in the reactor chamber of the thermal CVD process.

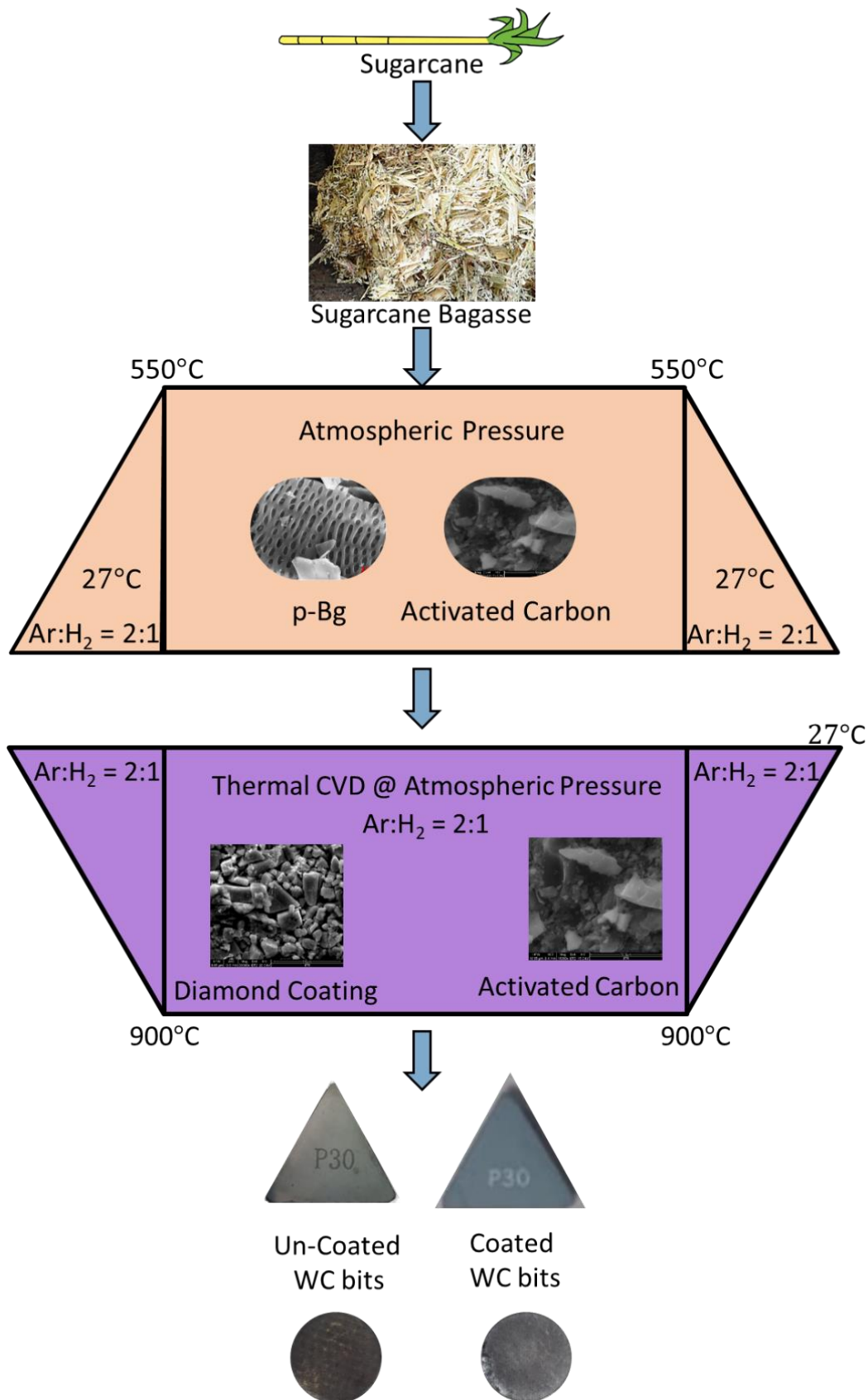


Figure 4.4: Process used for thermal CVD of DLC coating from pyrolysis of sugarcane [18, 26, 27-30]

As stated in the literature, sugarcane bagasse has been the major waste produced by sugar industries. Also, India is the 2nd largest sugarcane producer and has been producing 90 million tons of sugarcane bagasse as an agricultural waste [19]. Burning this waste is not an environment-friendly solution as the burnt residue of sugarcane bagasse has no possibility of any further reduction [20]. Fascinatingly, pyrolysis of sugarcane bagasse produces effluent gases that have good thermal dissociation. This thermal dissociation produces the right chemical and thermodynamic equilibrium, which is further responsible for the growth of DLC coating [18, 21]. In the process, the deposition rate was found to be $\sim 60 \mu\text{m/h}$ and the deposition time for the coating process was 10 min. As the deposition time was 10 min hence, the coating was having a thickness in the range of 8–10 μm . Figure 4.4 depicts the process conditions which were used for developing the films from the pyrolysis process of sugarcane bagasse on the tungsten carbide tool insert substrate [21, 22]. There is a high commercial value of activated carbon in industry and it may be used for the removal of chlorine as well [21, 27, 28].

4.3. Experimental Plan

In the section, the process parameters which may affect the machining characteristics such as Type of Tool, Feed (f), Cutting Speed (V_c), and Depth of Cut (DOC) are selected. The range of the process parameters for the experimentation was decided based on literature and past experience. The selection of the experimental plan is laid out. The experiments are conducted within the range of selected process parameters. The details of process parameters, their values and detailed experimentation are given in the subsequent sections.

4.3.1. Selection of Process Parameters

In order to obtain low crater wear, flank wear, cutting force, surface roughness, and temperature at the cutting zone, the working range of the various parameters is to be determined.

Table 4.3: Levels of input parameters selected for Conventional Lathe Machine Tool

S. No.	Input Parameters	Unit	Level 1	Level 2	Level 3
1	Type of Tool	---	Un-Coated	MDC (Market available diamond-coated tool)	DLC (Self-developed DLC coated tool)
2	Feed (f)	mm/rev	0.07	0.11	0.15
3	Cutting Speed (Vc)	m/min	30.26	60.52	90.78
4	Depth of Cut (DOC)	mm	0.192	0.384	0.576
Work Material: Aluminium 6061, Workpiece Diameter: 50 mm, Total length of the Workpiece: 610 mm, Temperature: Room Temperature, Machining: Dry Machining					

Table 4.4: Levels of input parameters selected for CNC Machine Tool

S. No.	Input Parameters	Unit	Level 1	Level 2	Level 3
1	Type of Tool	---	Un-Coated	MDC (Market available diamond coated tool)	DLC (Self-developed DLC coated tool)
2	Feed (f)	mm/rev	0.125	0.25	0.375
3	Cutting Speed (Vc)	m/min	360	480	600
4	Depth of Cut (DOC)	mm	0.2	0.4	0.6
Work Material: Aluminium 6061, Workpiece Diameter: 50 mm, Total length of the Workpiece: 610 mm, Temperature: Room Temperature, Machining: Dry Machining					

Table 4.5: Levels of input parameters selected for using the developed textured coated tools on the CNC Machine Tool

S. No.	Input Parameters	Unit	Level 1	Level 2	Level 3
1	Type of Tool	---	L ₁	L ₂	S ₁
2	Feed (f)	mm/rev	0.125	0.25	---
3	Cutting Speed (V _c)	m/min	360	480	---
4	Depth of Cut (DOC)	mm	0.2	0.4	---
Work Material: Aluminium 6061, Workpiece Diameter: 50 mm, Total length of the Workpiece: 610 mm, Temperature: Room Temperature, Machining: Dry Machining					

4.3.2. Selection of Response Variables

The following response variables are decided on the basis of the literature review:

1. Crater Wear,
2. Flank Wear,
3. Cutting Force,
4. Surface Roughness (SR)
5. Temperature at Cutting Zone

Crater wear happens on the tool face at a short distance from the cutting edge by the action of chip flow over the face at a very high temperature and speed. The crater wear is mainly due to diffusion and abrasion. They are commonly observed where the continuous chip is formed (usually in the ductile material). In the brittle material, the chip formation is in the shape of a small segment, this loosely fragmented chip has low abrasive action on the face as compared to the continuous chip formation. The depth of the crater measures the crater wear; the surface measuring instrument can measure it. The cutting edge may break from the tool due to excessive cratering.

Flank wear occurs at the tool flanks, where it gets in contact with the finished surface, as a result of abrasion and adhesion wear. The cutting force increases with flank wear. It affects the great extent of the mechanics of cutting. The flank wear region is known as wear land and is measured by the width of wear land. If the width of wear land exceeds 0.5-0.6mm the excessive cutting forces cause tool failure. The schematic diagram of crater wear and flank wear on the surface of the tool is shown in figure 4.5.

The cutting force in turning is referred to as the main cutting force F_c which is tangential and often the largest force. While F_c , the feed force F_f and the passive force F_p can be measured directly during turning, the active Force F_a and the resultant force R are calculated. The active force is the vector sum of the main cutting force F_c and feed force F_f .

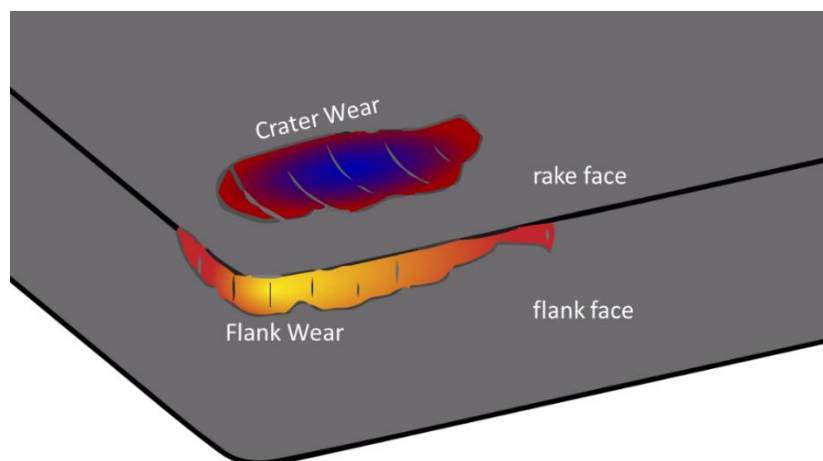


Figure 4.5: Schematic of a cutting tool with crater wear and flank wear.

As stated in 3.3.10, surface roughness, often shortened to roughness, is a component of surface texture. In surface metrology, roughness is typically considered to be the high-frequency, short-wavelength component of a measured surface. In tribology, rough surfaces usually wear more quickly and have higher friction coefficients than smooth surfaces [286]. Roughness is often a

good predictor of the performance of a mechanical component, since irregularities on the surface may form nucleation sites for cracks or corrosion. On the other hand, roughness may promote adhesion [286].

Measurement of temperatures during machining is very important because, along with the mechanical load, the thermal load also impacts the wear. The temperature in the cutting zone influences the accuracy of machined parts and the quality of machined surfaces. High temperatures in the cutting zone can lead to tensile residual stresses and structural changes in the machined surfaces.

4.3.3. Design of Experiment

The experiments were designed to study the effects of coated tools on the response characteristics. L_{27} Orthogonal Array was adopted for the design methodology in the experimentation. The experiments are conducted within the range of selected process parameters.

Table 4.6 and Table 4.7 shows the standard L_{27} OA with the assigned parameters for machining on the conventional lathe machine tool and CNC machine tool respectively. Whereas, table 4.8 shows the L_{16} OA with the assigned parameters for Machining on CNC Machine Tool using the developed textured coated tools.

While performing various experiments, the following precautionary measures are taken:

1. The order and replication of the experiment were randomized to avoid bias, if any, in the results.
2. Each set of experiments was performed at room temperature in a narrow range ($32\pm 2^\circ\text{C}$).

Table 4.6: The L₂₇ OA (Parameters Assigned) for Machining on Conventional Lathe
Machine Tool

Run No.	Exp. No.	Type of Tool	Feed (mm/rev)	Speed (m/min)	Depth of Cut (mm)
1	1	Bare	0.07	30.26	0.192
4	2	Bare	0.07	30.26	0.192
7	3	Bare	0.07	30.26	0.192
9	4	Bare	0.11	60.52	0.384
2	5	Bare	0.11	60.52	0.384
5	6	Bare	0.11	60.52	0.384
8	7	Bare	0.15	90.78	0.576
6	8	Bare	0.15	90.78	0.576
3	9	Bare	0.15	90.78	0.576
10	10	MDC	0.07	60.52	0.576
13	11	MDC	0.07	60.52	0.576
16	12	MDC	0.07	60.52	0.576
18	13	MDC	0.11	90.78	0.192
11	14	MDC	0.11	90.78	0.192
14	15	MDC	0.11	90.78	0.192
17	16	MDC	0.15	30.26	0.384
15	17	MDC	0.15	30.26	0.384
12	18	MDC	0.15	30.26	0.384
19	19	DLC	0.07	90.78	0.384
22	20	DLC	0.07	90.78	0.384
25	21	DLC	0.07	90.78	0.384
27	22	DLC	0.11	30.26	0.576
20	23	DLC	0.11	30.26	0.576
23	24	DLC	0.11	30.26	0.576
26	25	DLC	0.15	60.52	0.192
24	26	DLC	0.15	60.52	0.192
21	27	DLC	0.15	60.52	0.192

Table 4.7: The L₂₇ OA (Parameters Assigned) for Machining on CNC Machine Tool

Run No.	Exp. No.	Type of Tool	Feed (mm/rev)	Speed (m/min)	Depth of Cut (mm)
1	1	Bare	0.125	360	0.2
4	2	Bare	0.125	360	0.2
7	3	Bare	0.125	360	0.2
9	4	Bare	0.25	480	0.4
2	5	Bare	0.25	480	0.4
5	6	Bare	0.25	480	0.4
8	7	Bare	0.375	600	0.6
6	8	Bare	0.375	600	0.6
3	9	Bare	0.375	600	0.6
10	10	MDC	0.125	480	0.6
13	11	MDC	0.125	480	0.6
16	12	MDC	0.125	480	0.6
18	13	MDC	0.25	600	0.2
11	14	MDC	0.25	600	0.2
14	15	MDC	0.25	600	0.2
17	16	MDC	0.375	360	0.4
15	17	MDC	0.375	360	0.4
12	18	MDC	0.375	360	0.4
19	19	DLC	0.125	600	0.4
22	20	DLC	0.125	600	0.4
25	21	DLC	0.125	600	0.4
27	22	DLC	0.25	360	0.6
20	23	DLC	0.25	360	0.6
23	24	DLC	0.25	360	0.6
26	25	DLC	0.375	480	0.2
24	26	DLC	0.375	480	0.2
21	27	DLC	0.375	480	0.2

Table 4.8: The L₁₆ OA (Parameters Assigned) for Machining on CNC Machine Tool using the developed textured coated tools

Exp. No.	Type of Tool	Feed (mm/rev)	Speed (m/min)	Depth of Cut (mm)
1	L1	0.125	360	0.2
2	L1	0.125	360	0.2
3	L1	0.25	480	0.4
4	L1	0.25	480	0.4
5	L2	0.125	360	0.4
6	L2	0.125	360	0.4
7	L2	0.25	480	0.2
8	L2	0.25	480	0.2
9	S1	0.125	480	0.2
10	S1	0.125	480	0.2
11	S1	0.25	360	0.4
12	S1	0.25	360	0.4
13	S2	0.125	480	0.4
14	S2	0.125	480	0.4
15	S2	0.25	360	0.2
16	S2	0.25	360	0.2

4.4. Optimization Techniques

A scientific approach to plan the experiments is necessary for efficiently conducting the experimentation. By the statistical design of experiments, the process of planning the experiment is carried out, so that appropriate data will be collected and analyzed by statistical methods resulting in valid and objective conclusions.

When the problem involves data that are subjected to experimental error, a statistical methodology is the only objective approach to analysis.

4.4.1. Genetic Algorithm (GA)

A Genetic Algorithm (GA) is a metaheuristic inspired by the process of natural selection that belongs to the larger class of evolutionary algorithms (EA). Genetic algorithms are commonly used to generate high-quality solutions to optimization and search problems by relying on biologically inspired operators such as mutation, crossover and selection.

In a genetic algorithm, a population of candidate solutions to an optimization problem is evolved toward better solutions. Each candidate solution has a set of properties (its genotype) that can be mutated and altered.

The evolution usually starts from a population of randomly generated individuals, and is an iterative process, with the population in each iteration called a generation. In each generation, the fitness of every individual in the population is evaluated. The fitness is usually the value of the objective function in the optimization problem being solved. The more fit individuals are stochastically selected from the current population, and each individual's genome is modified to form a new generation. The new generation of candidate solutions is then used in the next iteration of the algorithm. Commonly, the algorithm terminates when either a maximum number of generations has been produced, or a satisfactory fitness level has been reached for the population. The same is shown as a flow chart in Figure 4.6.

A typical genetic algorithm requires:

1. A genetic representation of the solution domain,
2. A fitness function to evaluate the solution domain.

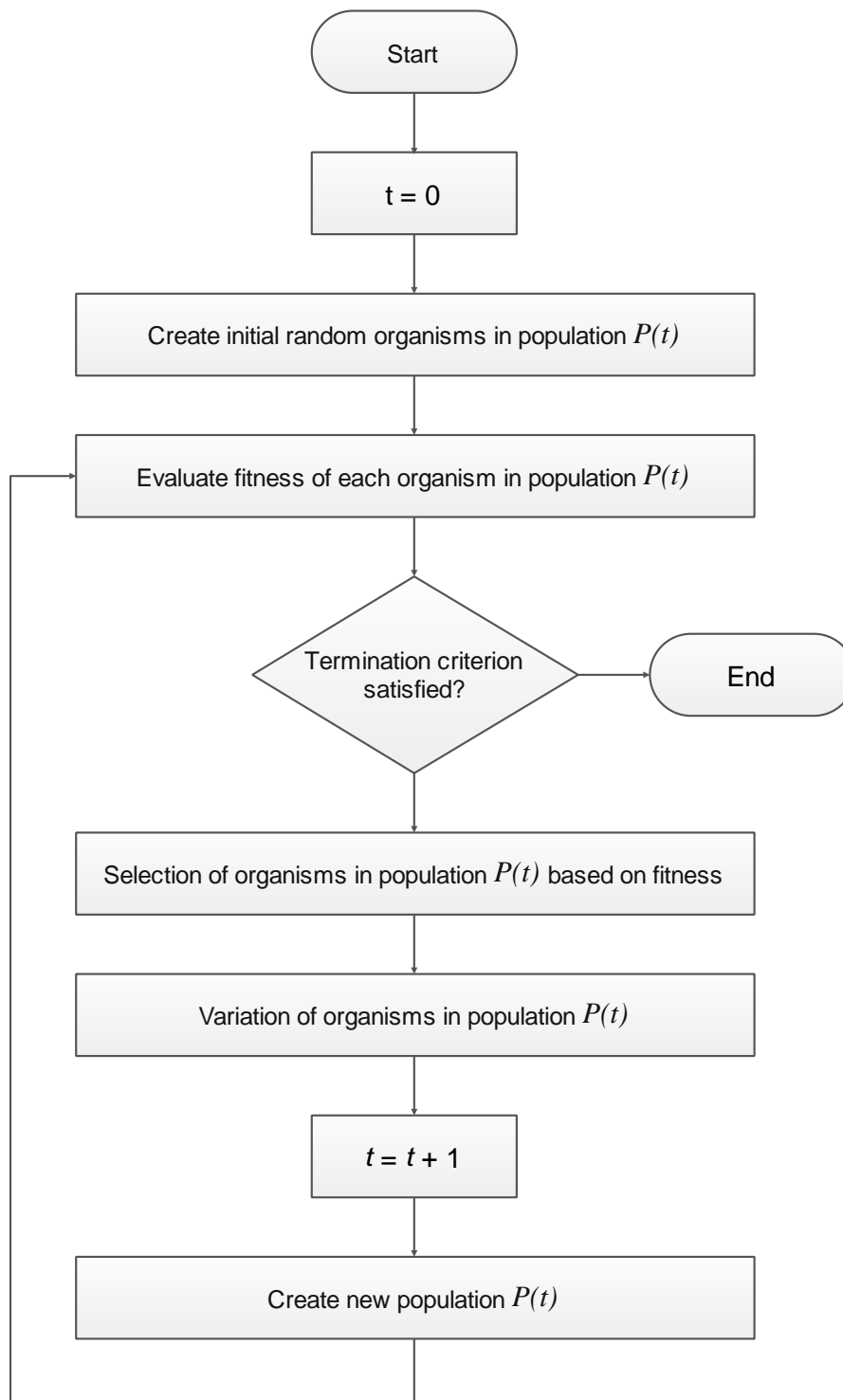


Figure 4.6: Flowchart depicting the process of Genetic Algorithm

A standard representation of each candidate solution is as an array of bits. Arrays of other types and structures can be used in essentially the same way. The main property that makes these genetic representations convenient is that their parts are easily aligned due to their fixed size,

which facilitates simple crossover operations. Variable-length representations may also be used, but crossover implementation is more complex in this case. Tree-like representations are explored in genetic programming and graph-form representations are explored in evolutionary programming; a mix of both linear chromosomes and trees is explored in gene expression programming.

Once the genetic representation and the fitness function are defined, a GA proceeds to initialize a population of solutions and then to improve it through repetitive application of the mutation, crossover, inversion and selection operators.

4.4.2. Technique for Order of Preference by Similarity to Ideal Solution (TOPSIS)

Technique for Order of Preference by Similarity to Ideal Solution (TOPSIS) is a multi-criteria decision analysis method, which was originally developed by Ching-Lai Hwang and Yoon in 1981 with further developments by Yoon in 1987 and Hwang, Lai and Liu in 1993. TOPSIS is based on the concept that the chosen alternative should have the shortest geometric distance from the positive ideal solution (PIS) and the longest geometric distance from the negative ideal solution (NIS).

Step 1

Create an evaluation matrix consisting of m alternatives and n criteria, with the intersection of each alternative and criteria given as x_{ij} , we therefore have a matrix $(x_{ij})_{m \times n}$.

Step 2

The matrix $(x_{ij})_{m \times n}$ is then normalised to form the matrix

$R = (r_{ij})_{m \times n}$, using the normalisation method

$$r_{ij} = \frac{x_{ij}}{\sqrt{\sum_{k=1}^m x_{kj}^2}}, i = 1, 2, \dots, m, j = 1, 2, \dots, n$$

Step 3

Calculate the weighted normalised decision matrix

$$t_{ij} = r_{ij} \cdot w_j, i = 1, 2, \dots, m, j = 1, 2, \dots, n$$

Where,

$w_j = \frac{W_j}{\sum_{k=1}^n W_k}, j = 1, 2, \dots, n$ so that $\sum_{i=1}^n w_i = 1$, and W_j is the original weight given to the indicator $v_j, j = 1, 2, \dots, n$.

Step 4

Determine the worst alternative (A_w) and best alternative (A_b):

$$A_w = \{ \langle \max(t_{ij} | i = 1, 2, \dots, m) | j \in J_- \rangle, \langle \min(t_{ij} | i = 1, 2, \dots, m) | j \in J_+ \rangle \} \equiv \{ t_{wj} | j = 1, 2, \dots, n \},$$

$$A_b = \{ \langle \min(t_{ij} | i = 1, 2, \dots, m) | j \in J_- \rangle, \langle \max(t_{ij} | i = 1, 2, \dots, m) | j \in J_+ \rangle \} \equiv \{ t_{bj} | j = 1, 2, \dots, n \},$$

Where,

$J_+ = \{ j = 1, 2, \dots, n | j \}$ associated with the criteria having a positive impact, and

$J_- = \{ j = 1, 2, \dots, n | j \}$ associated with the criteria having a negative impact.

Step 5

Calculate the L^2 – distance between the target alternative i and the worst condition A_w

$$d_{iw} = \sqrt{\sum_{j=1}^n (t_{ij} - t_{wj})^2}, i = 1, 2, \dots, m,$$

and the distance between the alternative i and the best condition A_w

$$d_{ib} = \sqrt{\sum_{j=1}^n (t_{ij} - t_{bj})^2}, i = 1, 2, \dots, m$$

Where, d_{iw} and d_{ib} and L^2 - norm distances from the target alternative i to the worst and best conditions, respectively.

Step 6

Calculate the similarity to the worst condition:

$$s_{iw} = \frac{d_{ib}}{(d_{iw} + d_{ib})}, 0 \leq s_{iw} \leq 1, i = 1, 2, \dots, m.$$

$s_{iw} = 1$ if and only if the alternative solution has the best condition; and

$s_{iw} = 0$ if and only if the alternative solution has the worst condition.

Step 7

Rank the alternatives according to s_{iw} ($i = 1, 2, \dots, m$)

Chapter 5: Result and Discussion

5. Introduction

This chapter provides the detail of the characterization of the self-developed DLC coating on the tungsten carbide (WC) tool inserts along with the testing for the mechanical properties of the developed tool inserts. Further tribological testing performed on those developed tool inserts and experimentation performed using the developed DLC coated tool inserts are discussed.

5.1. Coating Characterization

For characterization of the developed coating, a Field Emission Scanning Electron Microscope (FESEM), Raman Spectroscopy and X-ray diffraction (XRD), were used. These tests were used to affirm the existence of DLC coating on the tungsten carbide tool inserts and are discussed further in detail in the subsequent sub-sections.

5.1.1. EDAX

As discussed in section 4.3.1, a tabletop scanning electron microscope (TM3000) was used to perform Energy-dispersive X-ray spectroscopy (EDAX) on the un-coated samples of tungsten carbide (WC) tool inserts for identifying the elemental composition. The EDAX was also performed on the tool inserts after the experimentation to identify the presence of workpiece material on the tool inserts. The elemental composition and EDAX spectrum of the un-coated tungsten carbide (WC) substrate sample is shown in Table 5.1 and Figure 5.1 respectively.

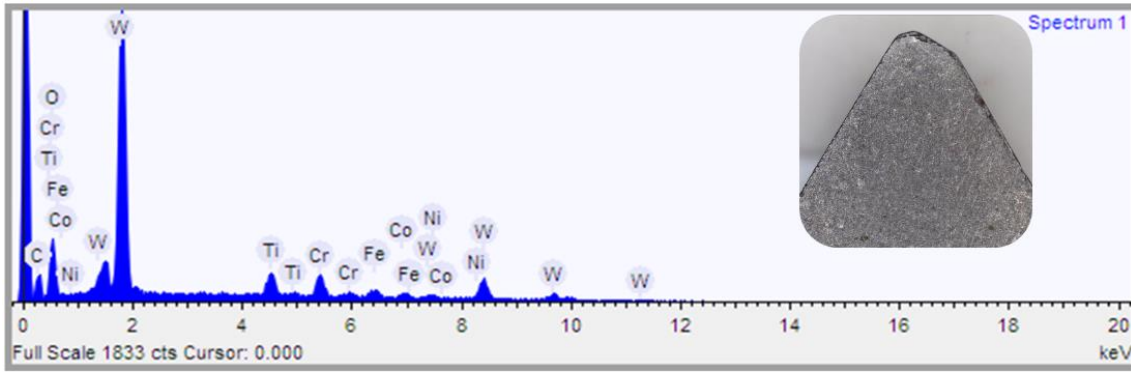


Figure 5.1: EDAX of the un-coated Tungsten Carbide (WC) tool insert

Table 5.1: Elemental composition of the un-coated Tungsten Carbide (WC) tool insert

Element	W	C	O	Fe	Ti	Co	Ni	Cr
% Weight	44.2	17.5	14.5	8.82	4.27	3.86	3.34	2.27

The elemental compositions and EDAX spectrums taken at the worn-out tool insert with a build-up edge are shown in Table 5.2, Table 5.3 and Figure 5.2 respectively. The region at the red cross of Figure 5.2 is depicting the presence of aluminium (Al) along with the tungsten carbide (WC). The presence of aluminium over this region is because of the movement of the chips over the surface of the tool inserts while machining [34]. The presence of the aluminium being deposited on the worn-out tool insert is clearly shown in Table 5.2. The presence of aluminium deposition on the tool surface is because of the formation of a built-up edge (BUE) on the tool. Whereas the elemental composition at the blue cross is also shown in Table 5.3.

Table 5.2: Elemental composition at the Red Cross in figure 5.2

Element	Cl	O	Al	Co	Ti	W
% Weight	0.23	7.16	50.68	0.52	6.72	34.69

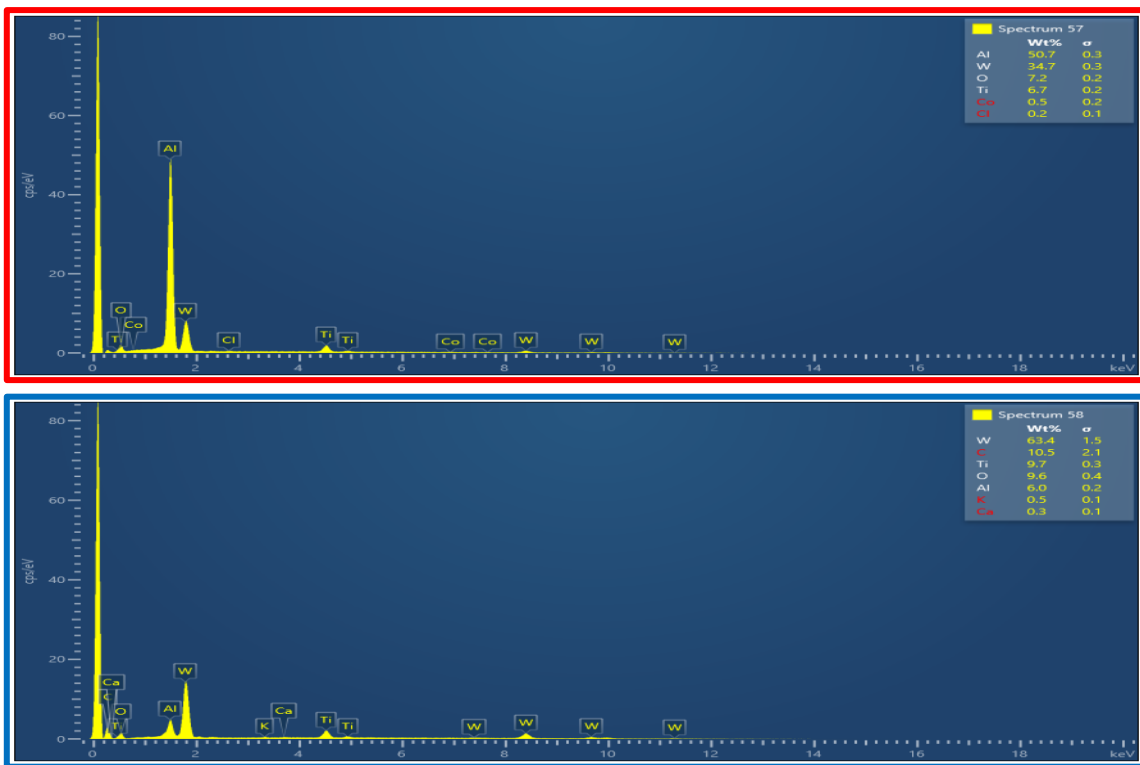
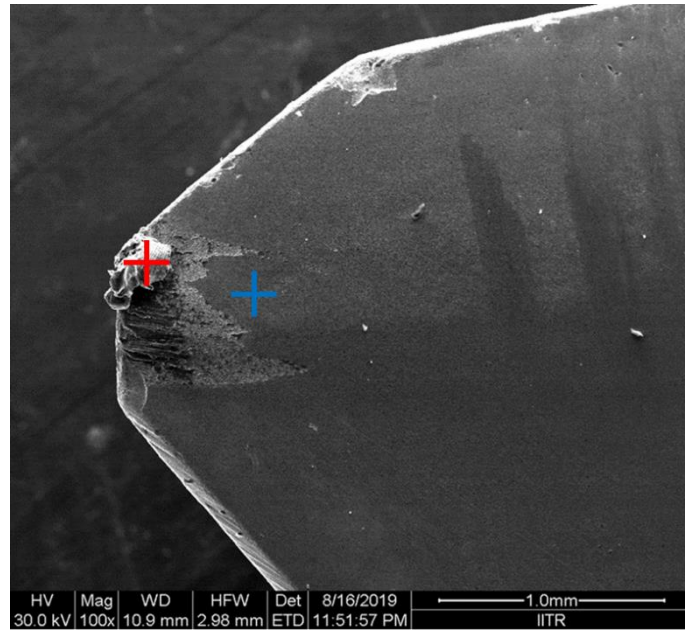


Figure 5.2: EDAX spectrum of the built-up edge (BUE) formation on coated tungsten carbide (WC) tool inserts.

Table 5.3: Elemental composition at the Blue Cross in figure 5.2

Element	C	O	Al	Ti	W
% Weight	10.48	9.62	5.99	9.73	64.18

5.1.2. XRD

As explained in section 4.3.2 of chapter 4, Rigaku make Ultima IV was used to perform the X-ray diffraction (XRD) on the self-developed DLC coating on the tungsten carbide (WC) insert. It was performed in the 2θ range from 5° to 80° and the results are presented in Figure 5.3. As can be seen in the XRD profile of coated WC tool in Figure 5.3, one visible peak is near $2\theta \sim 43.02^\circ$ which matches to the diamond $\{111\}$ plane and the other peak at $2\theta \sim 75.52^\circ$ which matched to the diamond $\{220\}$ plane. All the other peaks originating in the X-ray diffraction spectra are from tungsten carbide WC substrate [35].

5.1.3. RAMAN

We have already mentioned in section 4.3.3 of chapter 4, that the LabRAM Soleil™ Raman Microscope at the Nano Research facility of IIT Delhi was used to confirm the growth of the polycrystalline diamond coating by capturing the Raman spectra. The LabRAM Soleil™ Raman Microscope machine is shown in figure 5.4.

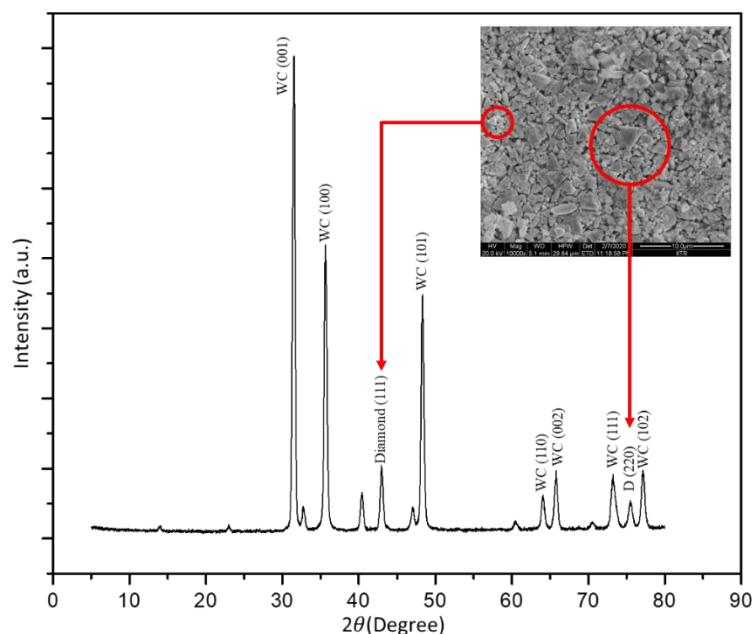


Figure 5.3: The X-Ray Diffraction spectra of the self-developed DLC coating on the tungsten carbide (WC) insert.

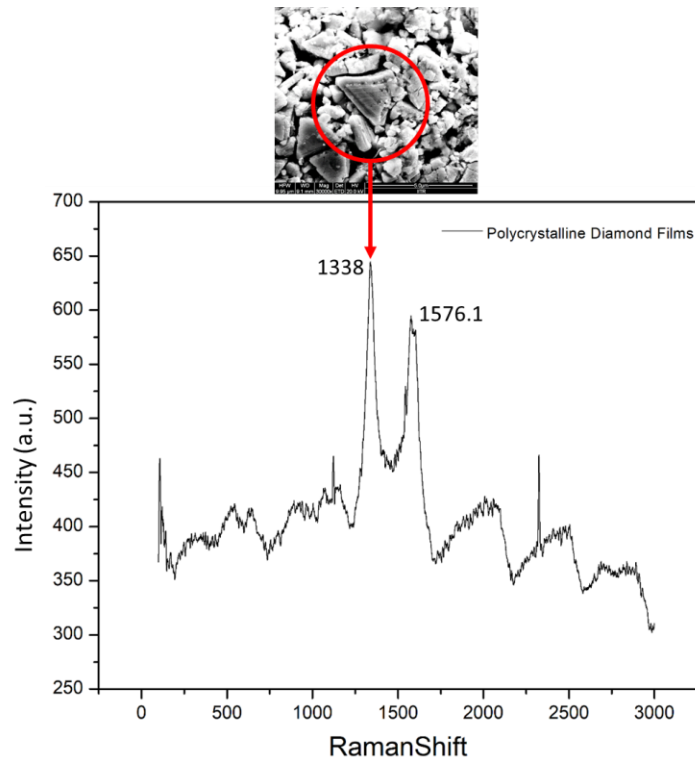


Figure 5.4: Raman spectra of the self-developed DLC coating on the tungsten carbide (WC) insert.

Diamond provides a single sharp peak of intensity at 1332 cm^{-1} because of its only active phonon [36]. LabRAM Soleil™ Raman Microscope was used to confirm the growth of the DLC coating by capturing the Raman spectra using a 514nm lamp. Obtained Raman spectra for the same are shown in Figure 8. The obtained Raman spectra depicted that the D and G band lies at 1338 cm^{-1} and 1576.5 cm^{-1} respectively. The sharp intensity of the peak is observed at 1338 cm^{-1} in the spectrum, taken from the flat top surface of the coated tungsten carbide inserts. The centre phonon mode of the as-developed DLC coating is the reason for the above-stated peak at 1338 cm^{-1} . As it is observed from the Raman spectra that there is an upshift in the peak from 1332 cm^{-1} to 1338 cm^{-1} . This up-shift occurs because of the compressive stress developed on the as-developed DLC coating. The compressive stress developed because of the thermal stress, which was generated during the cooling process of the substrate to room temperature [13, 18, 21] which arises as a result of the mismatch in thermal coefficients of both

diamond and tungsten carbide. The Development of the G band at 1576.5 cm^{-1} was due to the co-existence of the sp^2 -phases, called Trans-polyacetylene (Trans-PA). Trans-PA is an alternate chain of sp^2 carbon atoms, with single hydrogen bonded to each carbon [37].

5.1.4.FESEM

As mentioned in section 4.3.4 of chapter 4, FEI Quanta 200 FESEM machine was used in the Institute Instrumentation Centre (IIC) of Indian Institutes of Technology Roorkee (IITR) for studying the morphology of the WC inserts before and after the growth of the DLC coating. The FESEM micrographs were captured at different magnifications. The quality of the as-developed DLC coating on the WC tool insert's surface is almost the same on the whole substrate. The presence of faceted growth of DLC can be seen in Figure 5.5 [15, 40]. It is also clearly evident from the FESEM images in Figure 5.5 and Figure 5.7 that, the crystallites of the as-developed DLC coating get together to form clusters [17, 41]. The phenomenon of nucleation is very important in the process of determination of the growth of diamonds using the chemical vapour deposition (CVD) method. A diamond may nucleate on residual grains embedded into the surface after scratching with powders on an intermediate layer [155]. The nucleation growth on the surface of tungsten carbide (WC) tool inserts can be seen in Figure 5.6.

Cross-sectional FESEM images of the DLC coated tool inserts were taken and are shown in Figure 5.8. The average thickness of the coating was in the range of $11\text{-}12\mu\text{m}$, whereas the minimum and maximum thickness observed in FESEM images were $8.5\mu\text{m}$ and $15\mu\text{m}$ respectively. The FESEM image of the coating thickness at the magnification of $50,000\times$ is shown in figure 5.9.

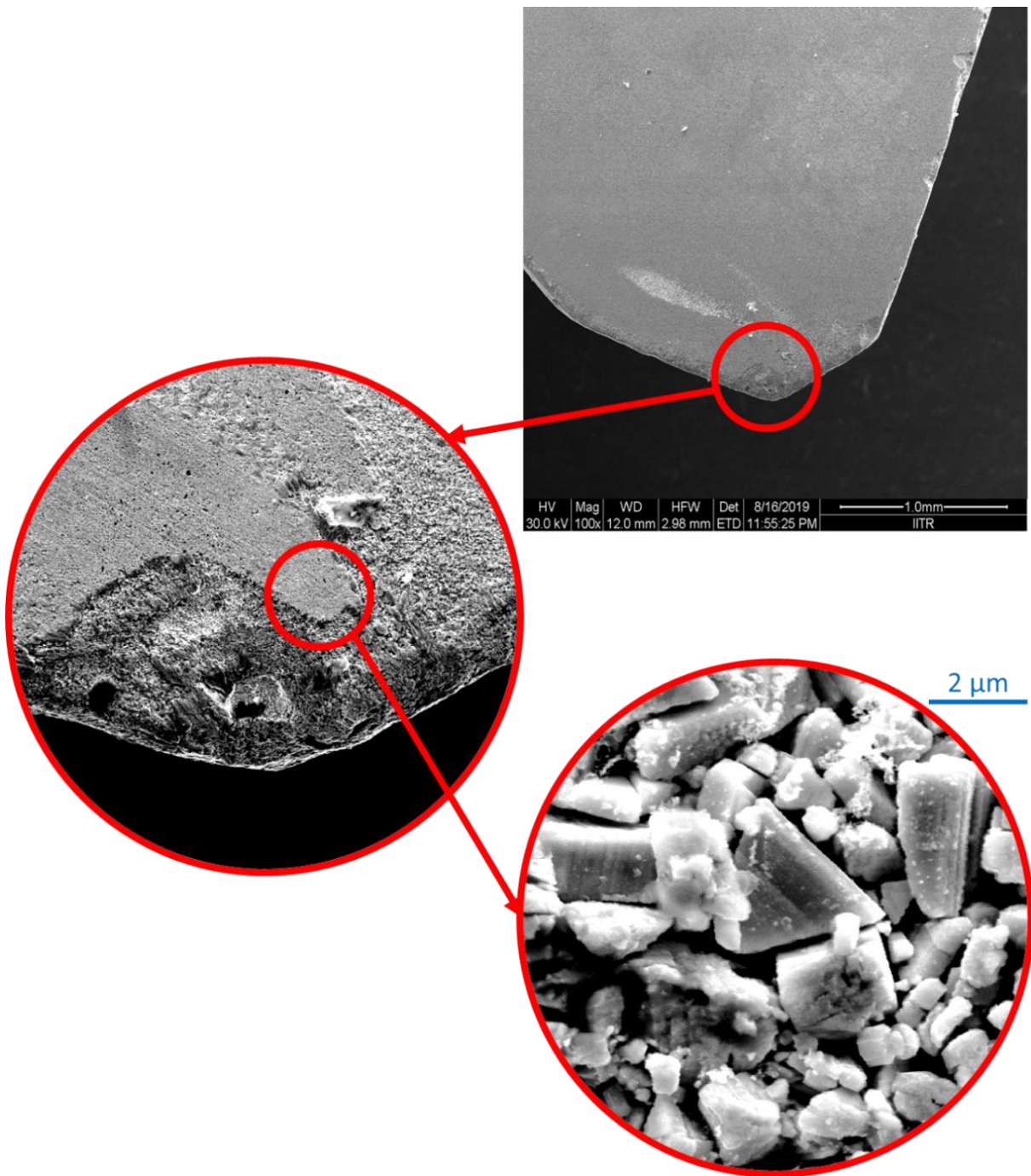


Figure 5.5: FESEM images at different magnifications show the growth of diamond on the coated surface.

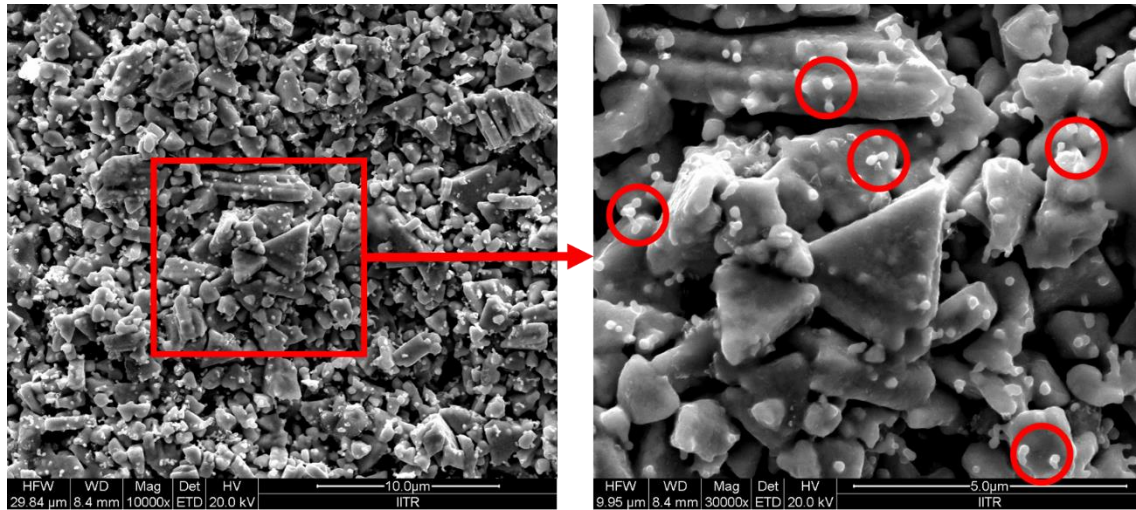


Figure 5.6: FESEM images of nucleation and growth of diamond coating.

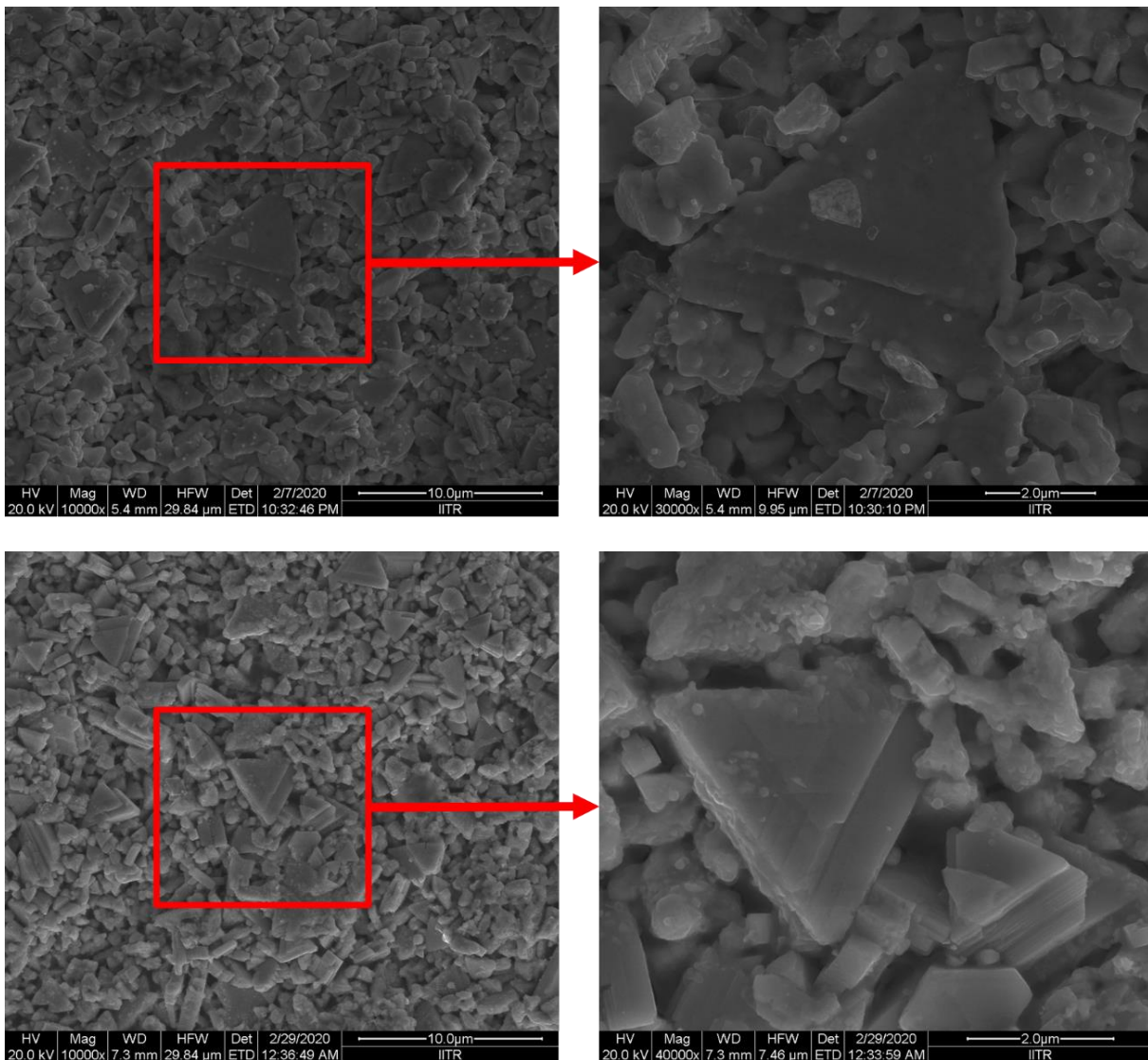


Figure 5.7: FESEM images of the DLC coated tool inserts depicting the growth of diamond on the coated surface.

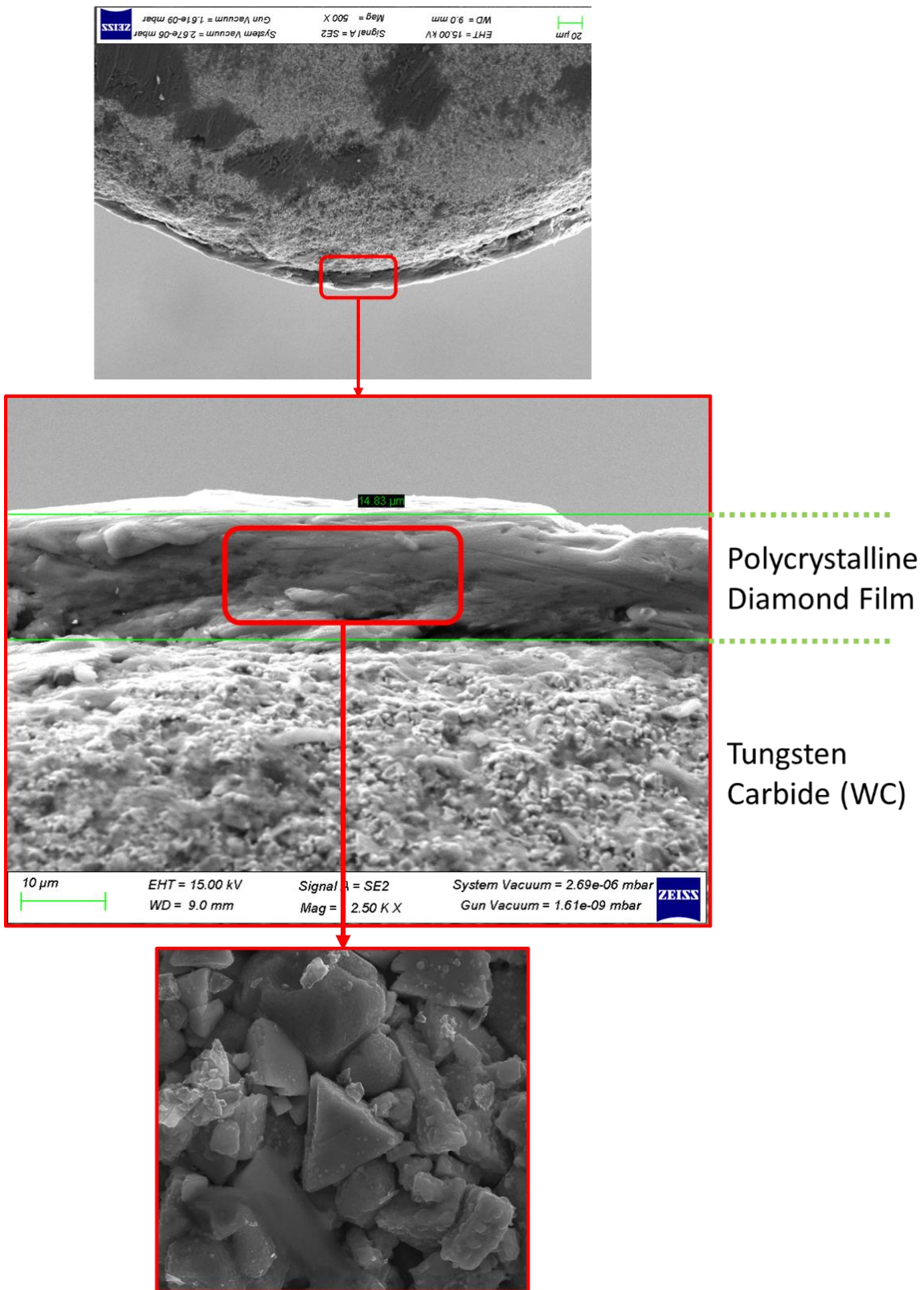


Figure 5.8: Cross-Sectional FESEM of Coating Thickness

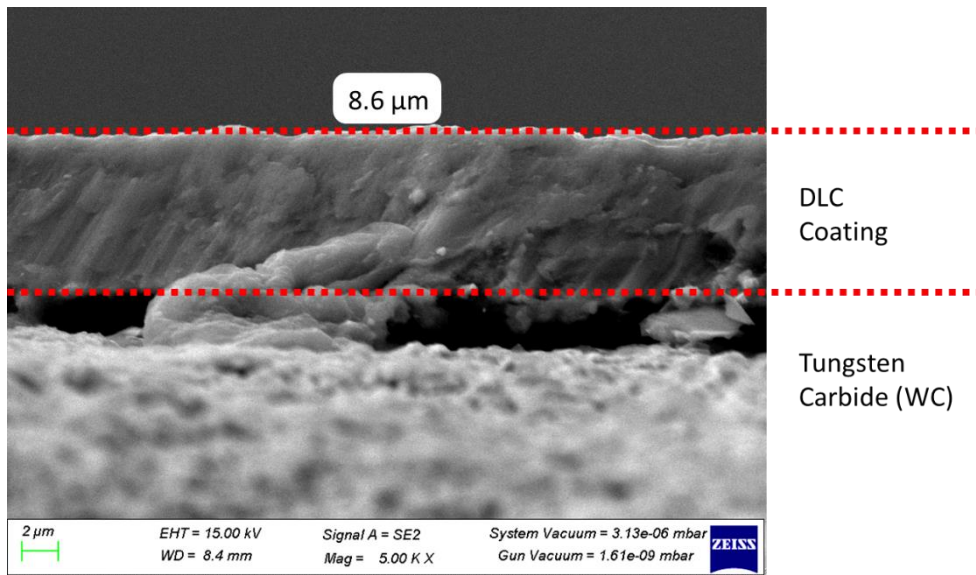


Figure 5.9: Cross-Sectional FESEM of Coating Thickness at higher magnification

5.2. Mechanical Properties of Coating

5.2.1. Micro Hardness

As mentioned in section 4.3.5 of chapter 4, Fischerscope HM2000s was used to perform the micro-hardness test on the market purchased coated, self-coated, and uncoated WC inserts. Figure 5.10 depicts the loading and unloading profile in form of a graph obtained during the indentation testing process of measuring the hardness. The hardness was measured on the flank face of the tool insert before and after the coating process on the same WC substrate. Figure 5.10 shows one out of many measurement processes performed on the samples at various locations on the flank face of the tool inserts. The average evaluated Vickers Hardness number was found to be 953.95 HV for un-coated tool inserts. The average evaluated Vickers Hardness number was found to be 1365.4 HV and 1478.78 HV for both market purchased coated tools and Self-developed DLC coated tool inserts, respectively. These values have been plotted and shown as a graph in Figure 5.11. The surface hardness values were measured by taking 4 measurements along the flank face of the tool inserts. The applied tests have shown that the

hardness of the un-coated WC inserts has been increased by a factor of 1.5 after the coating process [38, 39].

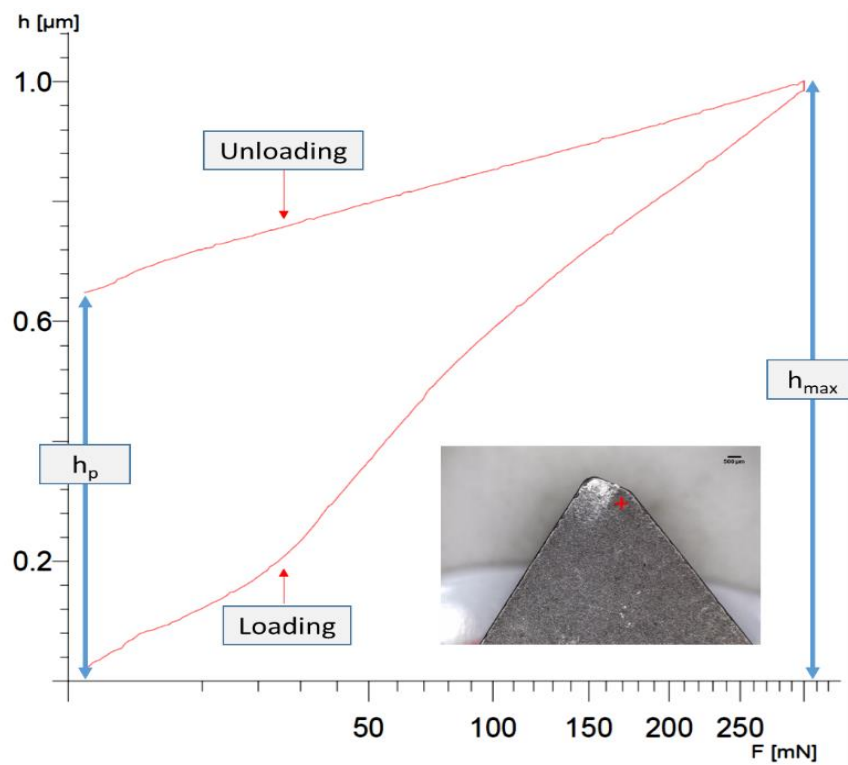


Figure 5.10: Loading and unloading profile graph obtained during the process of hardness measurement

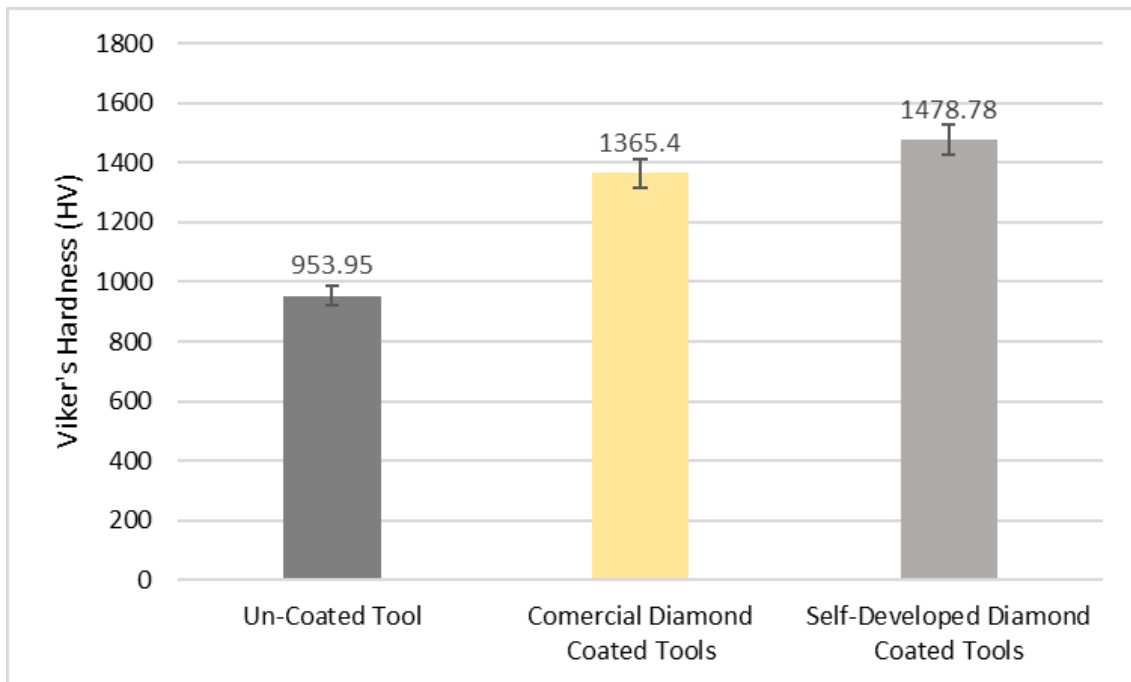


Figure 5.11: Average Vickers hardness values of the uncoated tool inserts, market purchased coated tools and Self-developed DLC coated tool inserts.

5.2.2. Residual Stress

As explained in section 4.3.6 of chapter 4, an X-ray residual analyzer (Pulstec limited model- μ X-360n) was used in the precision manufacturing lab of the Mechanical Engineering Department at Delhi Technological University. This X-ray analyzer was used to measure the residual stress of the uncoated WC tool inserts, market purchased coated tools and self-developed DLC coated tool inserts.

The measurement of residual stresses is an important parameter that directly affects the performance of the coating. The higher stresses will lead to cracking and spallation of coatings. The X-ray analyzer works on the principle of Bragg's law [37]. For the measurement, the radiation time, voltage and current of the X-ray tube were set at 30 s, 30 kV and 1mA respectively. The wavelength of the X-ray was set at 2.29 Å while keeping the angle of incidence of the X-ray at 35°. The samples were mounted at a distance of 39 mm from the incident rays.

The average evaluated residual stress was found to be -162 (MPa) for the uncoated tool inserts, whereas the average value of residual stresses was found to be -239.36 (MPa) and -409.73 (MPa) for the market purchased coated tools and self-developed DLC coated tool inserts, respectively. These values have been plotted and shown as a graph in Figure 5.12.

It is seen that the residual stress in DLC coated samples and uncoated samples were -0.39 GPa and -0.28 GPa [38]. There was a decrease of 39.28 % in the residual stress generation in the DLC coated sample. Such a decrease in the residual stress of the deposited DLC films is in agreement with the literature [39, 40]. It is clear from the literature that the reason for the decrease in residual stresses is largely dependent upon the sp^2 concentration in the deposited polycrystalline diamond film [38, 41].

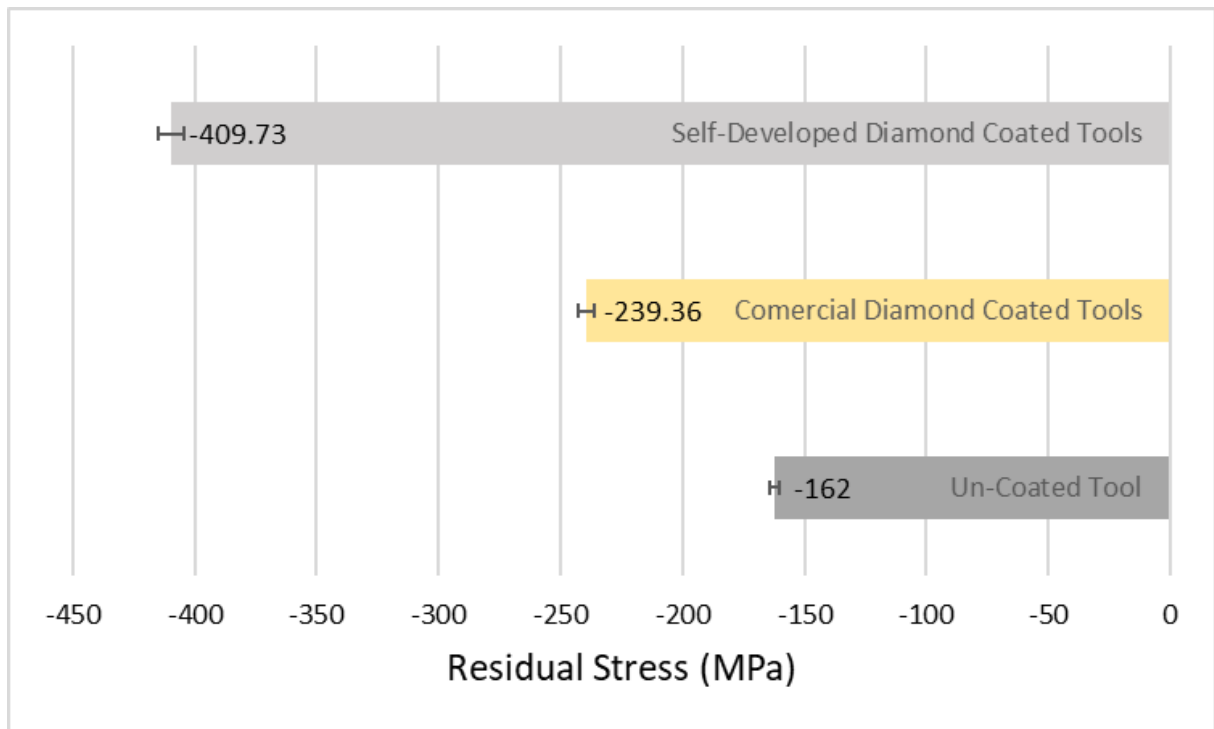


Figure 5.12: Average residual stress values of the uncoated tool inserts, market purchased coated tools and self-developed DLC coated tool inserts.

Figure 5.13 and Figure 5.14 represent the profile graph along with distortion and Debye ring (3D) of the market purchased coated tools and self-developed DLC coated tool inserts respectively. These were obtained while analyzing residual tests on the samples. The residual stress concentration distribution (from red to blue colour) over the machined surface is indicated by the Debye ring [42, 43]. The region on the sample where maximum stress concentration is observed is signified by the red ring while the region on the sample where comparatively lower stress concentration is induced in the samples is shown with a yellow ring and the blue ring signifies the region of minimum induced stress on the samples [22, 37]. The damage caused to the samples during the process is indicated by the obtained distortion images damage. These distortion images are used to see whether any structural changes have occurred within the samples.

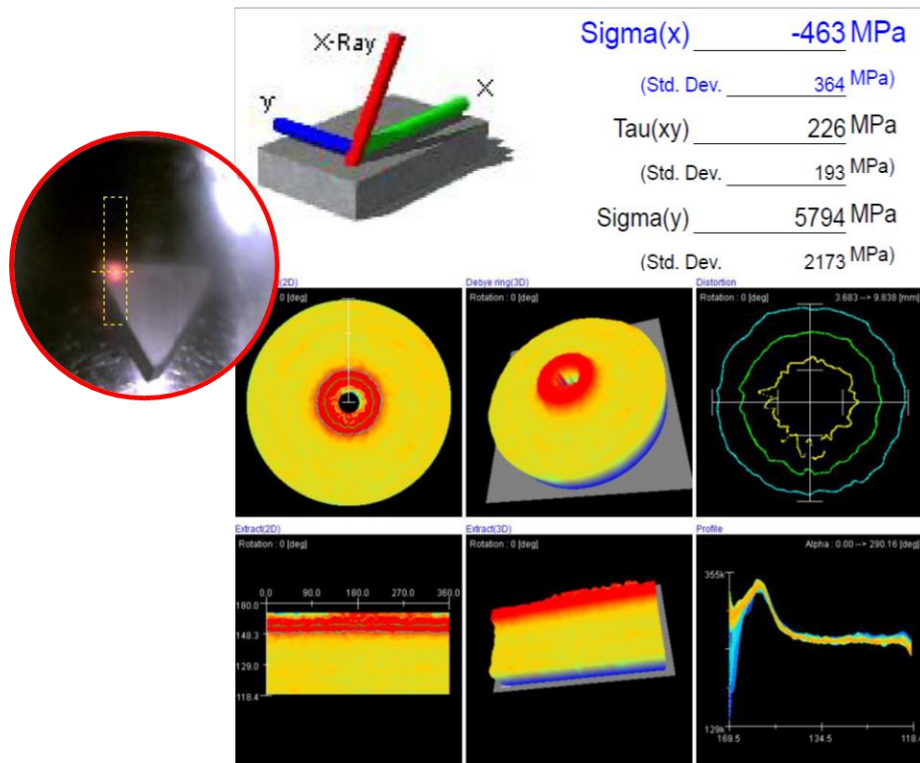


Figure 5.13: Debye ring, distortion ring, and peak profile obtained while measuring the residual stress of the self-developed DLC coated tool inserts.

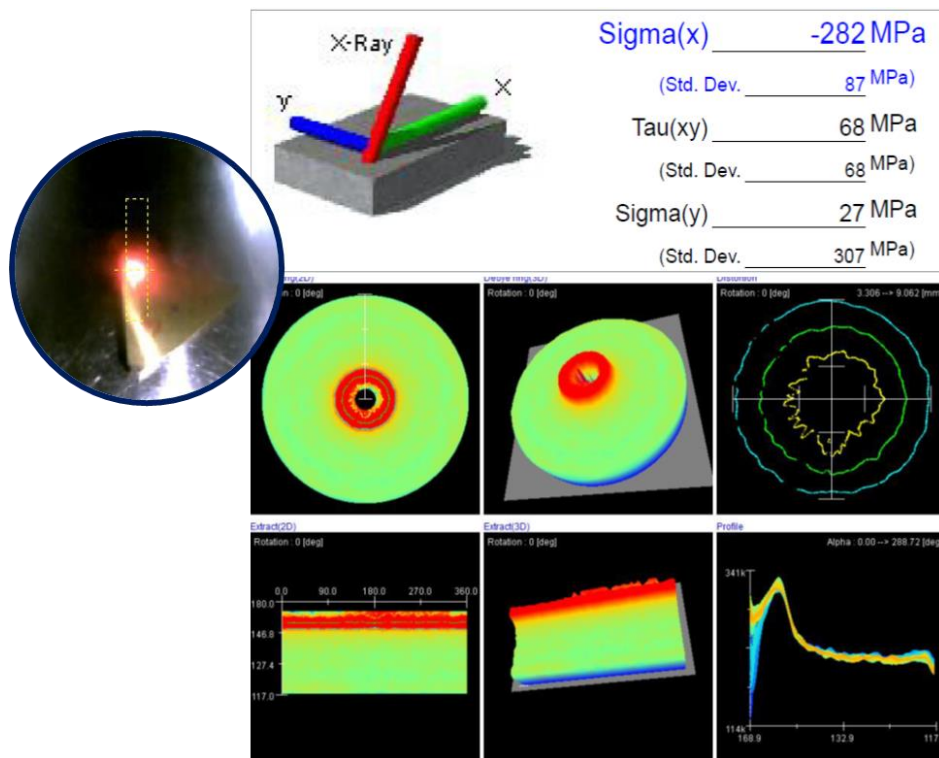


Figure 5.14: Debye ring, distortion ring, and peak profile obtained while measuring the residual stress of the market purchased coated tool inserts.

5.3. Tribological behaviour of Coating

As explained in section 4.3.7 of chapter 4, A DUCOM™ made Tribometer (TR-20L-PHM800-DHM850) was used as a pin-on-disc setup to measure the coefficient of frictional and wear. It was used in the precision manufacturing lab of the mechanical engineering department, at Delhi Technological University, Delhi. A schematic diagram of the Pin on Disc Tribometer test rig used for the experimentation is shown in figure 5.15.

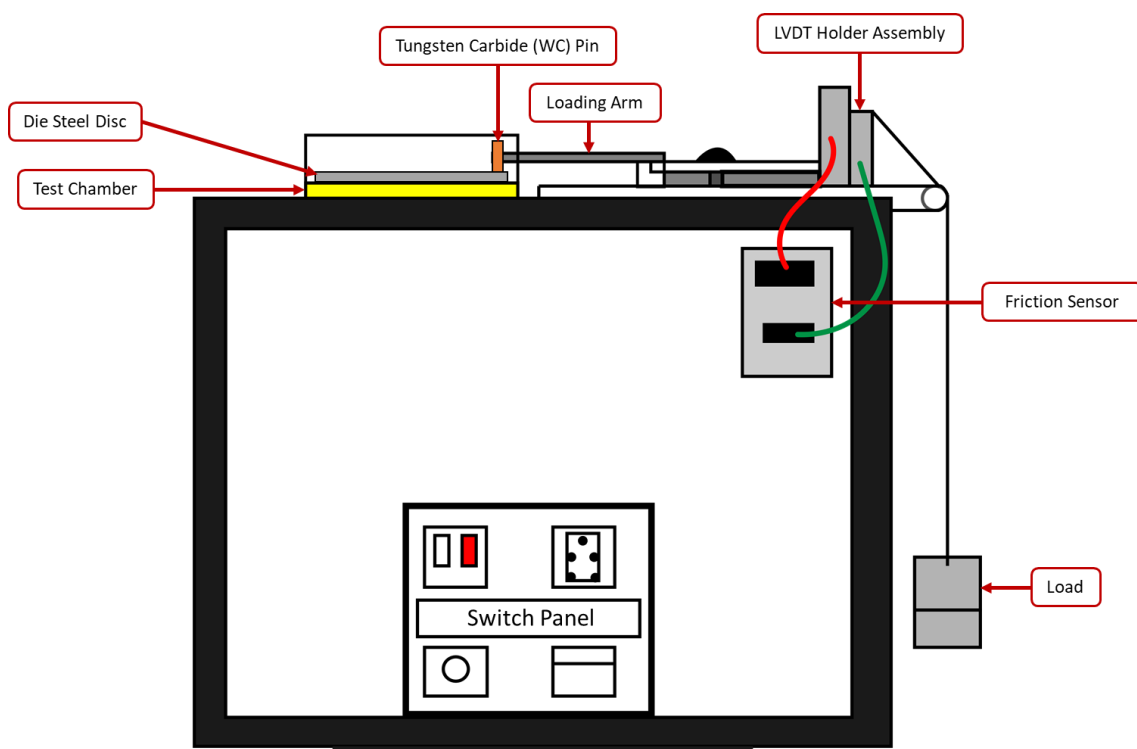


Figure 5.15: A schematic diagram of the Pin on Disc Tribometer test rig

The tribological behaviour of the as-deposited DLC coating on the WC inserts may vary as per the conditions of the sliding test. These conditions play a decisive role in their wear and friction. For mostly all other coating materials, there are plenty of factors that influence the behaviour of wear and friction of the developed coating. All these factors can be broadly classified into two types: intrinsic and extrinsic factors. Intrinsically for our as-deposited polycrystalline diamond films, the degree of sp^3 bonding on the sliding top flat surface of polycrystalline

diamond films can have a strong effect on their wear as well as friction behaviour [44]. Extrinsicly, mechanical interactions, physical interactions, and the chemical interactions between the sliding surfaces of the as-developed films and their surroundings influence the wear as well as frictional behaviour of the as-developed polycrystalline diamond films on the WC tool inserts [45, 46]. The tribological test measures the wear and coefficient of friction of the material at the contact point, this measuring property of these tests will be highly beneficial in understanding the self-developed DLC coated tool inserts. The tribological testing process was performed using the self-developed DLC coated tool insert pins were made and experiments were performed in dry conditions using a pin-on-disc machine as per the ASTM-G99 standards [25, 26].

The tribological tests have shown remarkable effects of wear and friction in the study of coated WC tool inserts. This study has helped researchers understand the life of coated samples in industrial applications also [27]. The pins were positioned in the perpendicular direction to the flat circular counter disc. In pin-on-disc, a flat circular counter disc rotates at a predefined rotational speed while the pin specimen is pressed against the disc at a specified load by the means of a lever with attached weights. The setup consists of two sensors for the measurement of the coefficient of friction and wear. Before initiating the tribological tests, it was made sure that the surfaces were cleaned properly using acetone and well dried after cleaning. The input parameters were used for performing the experimentation are mentioned in table 5.4.

The self-explanatory setup of the pin and disc for the experimentation is shown in figure 15.16. Stereo microscopic images of Uncoated WC and coated WC pins, taken after the tribological testing are shown in Figure 5.17 and Figure 5.18 respectively [27]. It is evident from the images that, the un-coated pin has undergone higher amounts of wear as compared to the coated pin.

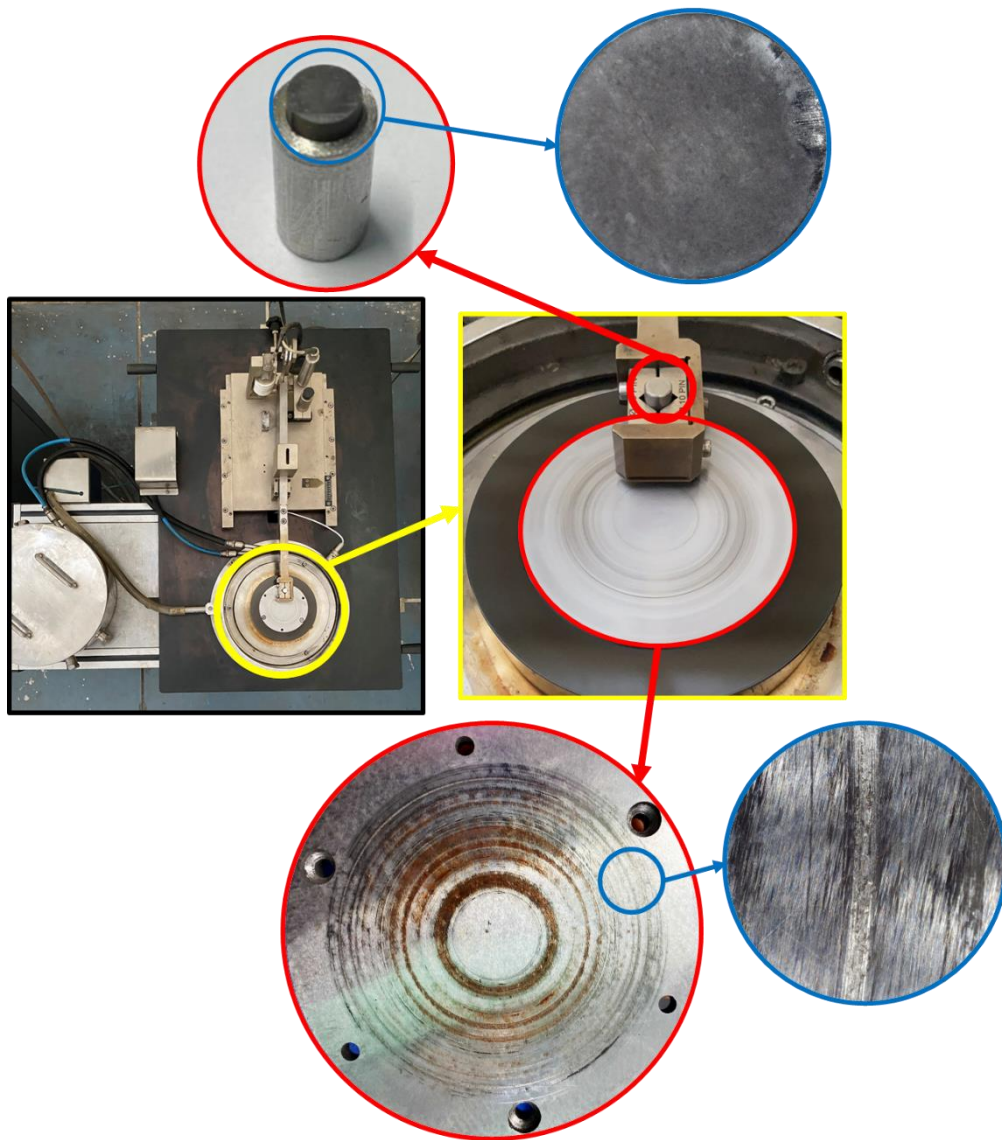


Figure 5.16: Experimentation performed for the Tribological study.

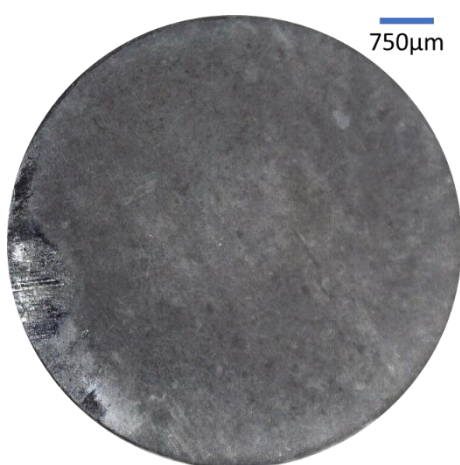


Figure 5.17: Stereo microscopic image of DLC coated tungsten carbide (WC) pin after the tribological testing

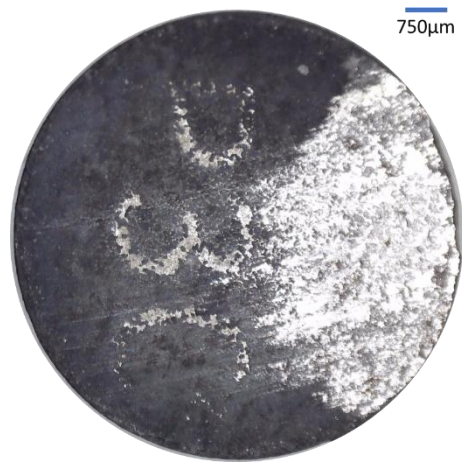


Figure 5.18: Stereo microscopic image of Uncoated tungsten carbide (WC) pin after the tribological testing

Table 5.4: Experimental conditions for the tribological tests

S. No.	Test Condition	Coated	Uncoated
1.	Sliding Speed (m/s)	2.0	2.0
2.	Load (N)	30	30
3.	Track Diameter (mm)	60	80
4.	Pin diameter (mm)	5.5	5.5
5.	Disc diameter (mm)	100	100
6.	Sliding distance (m)	200	200
7.	Temperature (°C)	20	20
8.	Humidity (%)	50-55	50-55

5.3.1. Wear

The wear curves of the sample pin have been shown as the function of the sliding time in figure 15.19, which were in contact with the counterface of the disc, under the dry sliding environment [27, 50].

The pin on disc setup measures the wear of the pin in the form of pin length, any changes to the length of the pin are measured with the help of wearable sensors. It is seen that the DLC coating plays a vital role in improving the wear resistance of the WC material. The average value of the wear (μm) obtained for the DLC coated WC insert was $12.79 \mu\text{m}$, whereas the average value of the wear (μm) obtained for the un-coated WC insert was $30.47 \mu\text{m}$. This shows that the polycrystalline diamond films coated on the WC inserts have been able to decrease the wear by 58.02%.

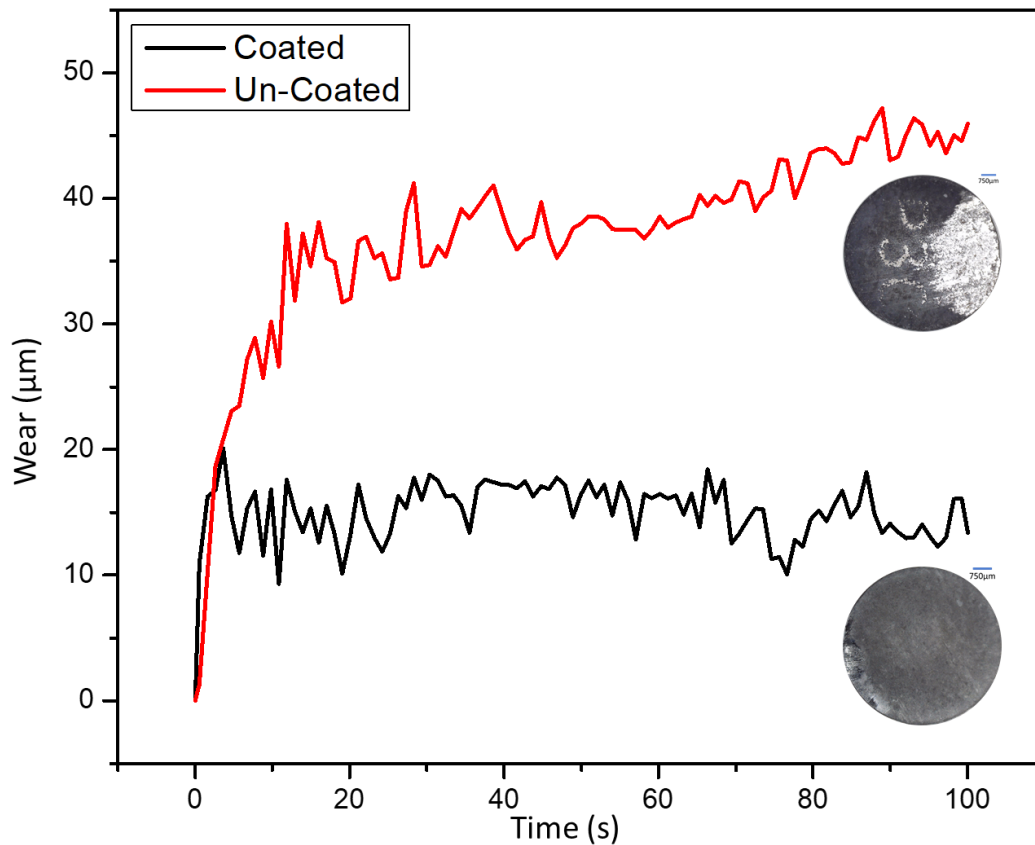


Figure 5.19: Variation of wear with respect to sliding time.

5.3.2. Friction

The coefficient of friction curves as a function of the sliding time for the coated and uncoated WC insert pins is presented in Figure 5.20. The coated and uncoated WC pins were in the contact with counterface of the disc, under the dry sliding environment [Prasad, 2020, Surya, 2020].

As it is evident from the plots of the coefficient of friction, the depicted curves of the coefficient of friction of the as-developed DLC coated WC pin exhibit similar plots [47-49]. These plots indicate that the whole process of sliding can be divided into two parts. There is an ephemeral peak in the graph of the coefficient of friction with comparatively very high amplitude, at the beginning of the sliding process. This peak characterizes the behaviour of the coefficient of

friction. The effect of initial mechanical interlocking occurring on the pin-disc interface results in the attribution of the presence of high initial friction. The occurrence of this initial interlocking makes it difficult to start the sliding movement between the pin and disc. While the sliding process repeats on the same track, the rigorousness in the sliding interface of pin and disc is worn out. In the meantime, the gaps developed on the disc are filled with the fragmentations of the coated WC tool inserts or with the microfractures of the uncoated WC tool inserts. These filling processes lead to smoother sliding movement, which further leads to stable wear and friction curves. The average value of the coefficient of friction (COF) obtained for the DLC coated WC pin was 0.196. Whereas the average value of the coefficient of friction (COF) obtained for the uncoated WC pin was 0.404. This shows that the DLC coated WC pins have been able to decrease the coefficient of friction (COF) by 51.48%.

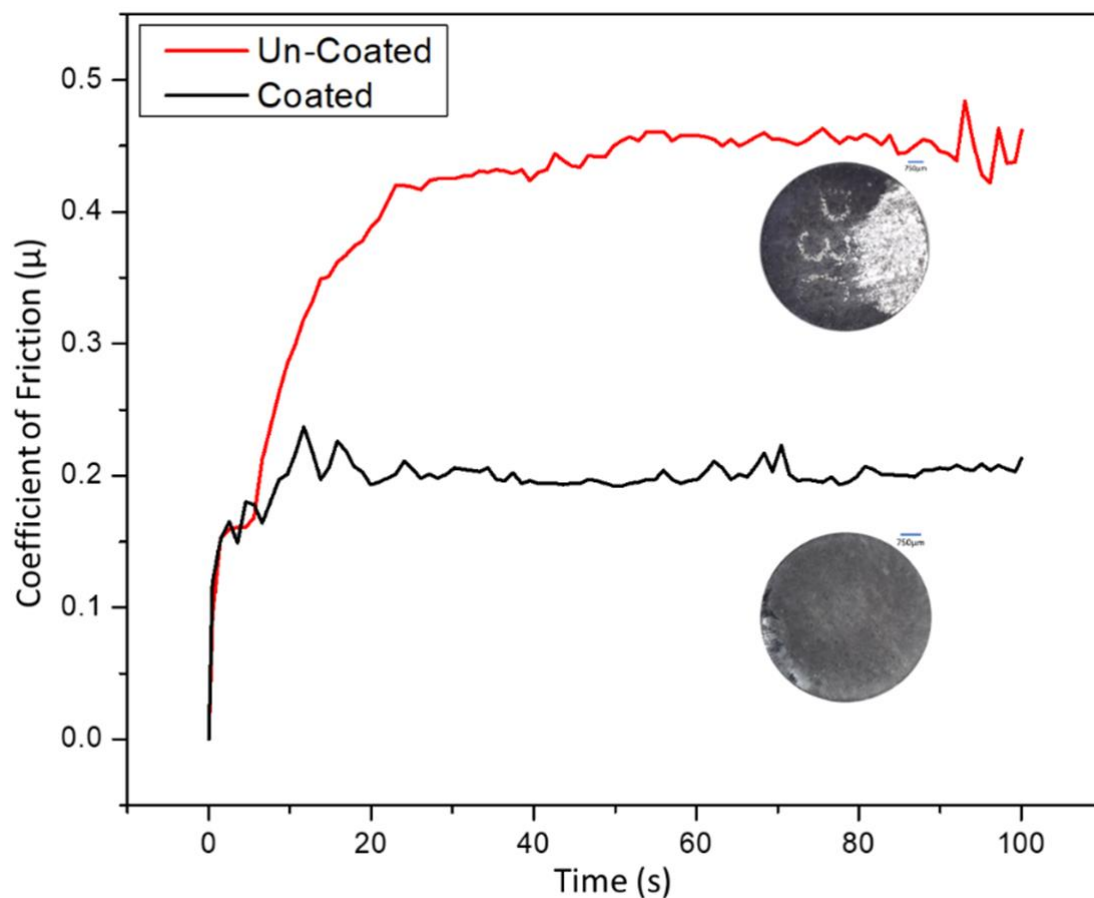


Figure 5.20: Variation of the coefficient of friction with respect to sliding time.

5.4. Experimentation on Conventional Lathe Machine Tool

As explained in section 4.3.11 of chapter 4, HARRISON LATHES make HARRISON 12' Lathe "Model L6" of Metal Cutting Lab in the mechanical engineering department at Delhi Technological University, Delhi, was used to perform the experimentation with the self-developed DLC coated tungsten carbide (WC) tool inserts.

A round bar of 50 mm in diameter and 610 mm in length was chosen for the turning process. The process of dry turning operation was performed on the lathe machine tool. The levels of input parameters selected for the experimentation are mentioned in Table 5.5. The levels were decided by going through the various literature as well as after doing the test runs on the machine tools.

Table 5.5: Levels of input parameters selected for Conventional Lathe Machine Tool

S. No.	Input Parameters	Unit	Level 1	Level 2	Level 3
1	Type of Tool	---	Un-Coated	MDC (Market available diamond coated tool)	DLC (Self-developed DLC coated tool)
2	Feed (f)	mm/rev	0.07	0.11	0.15
3	Cutting Speed (Vc)	m/min	30.26	60.52	90.78
4	Depth of Cut (DOC)	mm	0.192	0.384	0.576
	Work Material: Aluminium 6061, Workpiece Diameter: 50 mm, Total length of the Workpiece: 610 mm, Temperature: Room Temperature, Machining: Dry Machining				

The experimental set-up consists of a dynamometer was used for the measurement of cutting force and an infrared thermometer for measuring the temperature, as shown in section 4.3.8 of chapter 4. Detailed experimental conditions viz. the design of experiments selected for the experiments is an L_{27} orthogonal array (OA), which is depicted in Table 5.6.

Table 5.6: The L_{27} OA for Machining on Conventional Lathe Machine Tool

Run No.	Exp. No.	Type of Tool	Feed (mm/rev)	Speed (m/min)	Depth of Cut (mm)
1	1	Bare	0.07	30.26	0.192
4	2	Bare	0.07	30.26	0.192
7	3	Bare	0.07	30.26	0.192
9	4	Bare	0.11	60.52	0.384
2	5	Bare	0.11	60.52	0.384
5	6	Bare	0.11	60.52	0.384
8	7	Bare	0.15	90.78	0.576
6	8	Bare	0.15	90.78	0.576
3	9	Bare	0.15	90.78	0.576
10	10	MDC	0.07	60.52	0.576
13	11	MDC	0.07	60.52	0.576
16	12	MDC	0.07	60.52	0.576
18	13	MDC	0.11	90.78	0.192
11	14	MDC	0.11	90.78	0.192
14	15	MDC	0.11	90.78	0.192
17	16	MDC	0.15	30.26	0.384
15	17	MDC	0.15	30.26	0.384
12	18	MDC	0.15	30.26	0.384
19	19	DLC	0.07	90.78	0.384
22	20	DLC	0.07	90.78	0.384
25	21	DLC	0.07	90.78	0.384
27	22	DLC	0.11	30.26	0.576
20	23	DLC	0.11	30.26	0.576
23	24	DLC	0.11	30.26	0.576
26	25	DLC	0.15	60.52	0.192
24	26	DLC	0.15	60.52	0.192
21	27	DLC	0.15	60.52	0.192

Stereo microscopic images of the tools were captured after each set of experiments, using the optical coordinate measuring machines (CMM). As mentioned in section 4.3.9 of chapter 4, Sipcon made SVI Optical Coordinate Measuring Machine (SVI-OCMM-442) was used in the Center for Advanced Production and Industrial Engineering Research (CAPIER) Lab of the Mechanical Engineering Department at Delhi Technological University. A few of the images captured are shown in Figure 5.21.

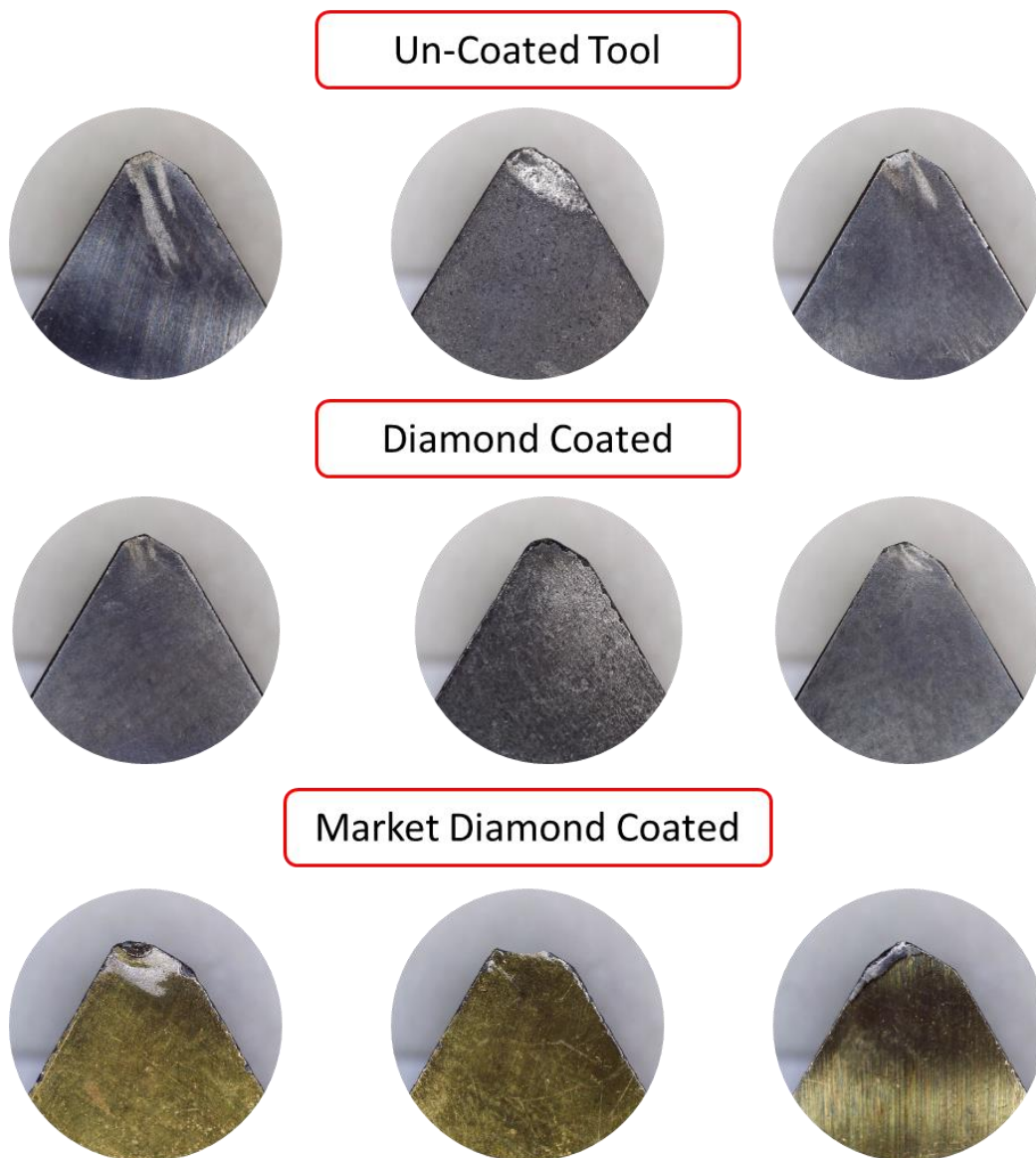


Figure 5.21: Microscopic images of a few of the worn-out tool inserts.

As multi-response optimization of the process parameters of the machining process was one of the objectives of our research work, hence, we used TOPSIS for doing the same. After carefully going through the literature we got to know that the TOPSIS method is used to get the optimum combination of process parameters using relative closeness value based on the ideal solution. We also got to know that when, compared to other multi-response optimization techniques such as Artificial Neural Network (ANN), TOPSIS (a technique for order of preference by similarity to ideal solution) method has fewer computational steps. This method provided an optimum solution with the shortest distance from the positive ideal solution and the farthest from the negative solution.

5.4.1. TOPSIS

To optimize the selected input parameters of the turning process for the self-developed DLC coated tungsten carbide (WC) tool inserts while using the TOPSIS method is one of the main objectives of our research. According to the TOPSIS (Technique for Order of Preference by Similarity to Ideal Solution) method, there should be a maximum value of the relative closeness for obtaining the optimum cutting conditions [43].

Selecting the Orthogonal Array OA

With the intention of deciding the optimum combination of the selected input parameters for decided response variables, we have used the Taguchi method. Keeping the aim to find out the effect of input parameters viz. type of tool, feed (f), cutting speed (V_c) and Depth of cut (DOC) on the response variables (performance indicators) viz. Crater Wear (μm), Cutting Force (N), Surface Roughness (μm) and Temperature at Cutting Zone ($^{\circ}\text{C}$), an appropriate orthogonal array (OA) was selected using the Taguchi method. The OA is selected to have a minimum number of experiments i.e. to have the least number of experimental runs.

In this research, we have used four input parameters ($P = 4$) having three levels ($L = 3$) for the experimentation. Hence, we opted for the L_{27} orthogonal array shown in Table 5.6.

TOPSIS based on entropy weight method

To accomplish the optimal solution we used a statistical tool. This method enlarges the distance from a negative ideal solution and also shortens the distance from a positive ideal solution. Moreover, this ranking method uses the closeness of the optimal solution from the positive ideal solution [41].

Formation of decision matrix

Using the responses, a decision matrix A is formed. This decision matrix is evaluated for n responses of variables containing m of values [42]. The response variables in the form of an initial decision matrix are also shown in Table 5.7.

$$A = (a_{ij})_{m \times n} = \begin{bmatrix} a_{11} & \cdots & a_{1n} \\ \vdots & \ddots & \vdots \\ a_{m1} & \cdots & a_{mn} \end{bmatrix} \quad (1)$$

Standardizing the decision matrix

To have the uniform units for all the responses viz. Crater Wear (μm), Cutting Force (N), Surface Roughness (μm) and Temperature at Cutting Zone ($^{\circ}\text{C}$), we have normalised the decision matrix [43]. In our research, we have used the criterion of “lower the better” for all the responses. Table 5.8 shows the response variables in the form of the obtained normalised decision matrix.

Table 5.7: L₂₇ Orthogonal Array using the input parameters along with the response variables in the form of initial decision matrices.

Input Parameters				Response Variables			
Type of Tool	Feed (mm/rev)	Speed (m/min)	Depth of Cut (mm)	Crater Wear (μm)	Cutting Force (N)	Surface Roughness (μm)	Temperature at Cutting Zone (°C)
Bare	0.07	30.26	0.192	1488.722	126.80	1.63	167.7
Bare	0.07	30.26	0.192	1508.459	121.23	1.651	112.2
Bare	0.07	30.26	0.192	1172.932	118.20	1.487	159.3
Bare	0.11	60.52	0.384	1531.015	132.52	1.515	161.3
Bare	0.11	60.52	0.384	1449.248	119.80	1.315	173.5
Bare	0.11	60.52	0.384	1545.113	122.36	1.462	153.5
Bare	0.15	90.78	0.576	1646.617	130.57	1.758	276.4
Bare	0.15	90.78	0.576	1624.06	134.57	1.867	286.1
Bare	0.15	90.78	0.576	1605.263	137.91	1.64	303.1
MDC	0.07	60.52	0.576	947.368	169.36	0.761	243.4
MDC	0.07	60.52	0.576	900.846	160.08	0.712	253.1
MDC	0.07	60.52	0.576	1131.579	159.33	0.804	270.1
MDC	0.11	90.78	0.192	1028.195	177.35	0.873	128.3
MDC	0.11	90.78	0.192	947.368	160.60	0.981	140.1
MDC	0.11	90.78	0.192	1125.94	163.47	1.074	120.5
MDC	0.15	30.26	0.384	944.549	166.53	0.744	134.7
MDC	0.15	30.26	0.384	1048.872	173.55	0.767	103.2
MDC	0.15	30.26	0.384	883.459	173.60	0.861	126.3
DLC	0.07	90.78	0.384	872.18	82.11	0.64	210.4
DLC	0.07	90.78	0.384	868.421	83.99	0.565	220.1
DLC	0.07	90.78	0.384	842.105	78.34	0.567	237.1
DLC	0.11	30.26	0.576	759.398	80.92	0.468	119.3
DLC	0.11	30.26	0.576	721.805	88.23	0.467	107.5
DLC	0.11	30.26	0.576	689.85	92.92	0.44	111.5
DLC	0.15	60.52	0.192	680.921	94.33	0.491	114.7
DLC	0.15	60.52	0.192	625.94	92.89	0.558	103.2
DLC	0.15	60.52	0.192	496.241	99.64	0.482	117.3

Table 5.8: Response variables in the form of obtained Normalised decision matrix

Run No.	Performance Indicators (Response Variables)			
	Crater Wear (μm)	Cutting Force (N)	Surface Roughness (μm)	Temperature at Cutting Zone ($^{\circ}\text{C}$)
1	0.253423733	0.185388302	0.288231568	0.175583504
2	0.256783543	0.177244668	0.291944981	0.117474473
3	0.199667101	0.172814648	0.262944995	0.166788624
4	0.26062323	0.193751245	0.267896212	0.168882643
5	0.246704111	0.175153932	0.232530375	0.18165616
6	0.263023119	0.178896788	0.258524265	0.160715969
7	0.280302048	0.190900242	0.310865703	0.289393444
8	0.276462192	0.196748453	0.330140084	0.299549437
9	0.273262396	0.20163171	0.28999986	0.3173486
10	0.161269555	0.247613272	0.134567008	0.254842129
11	0.153350159	0.234045421	0.125902378	0.264998122
12	0.192627619	0.232948882	0.142170663	0.282797284
13	0.175028659	0.259295074	0.154371876	0.134331328
14	0.161269555	0.234805689	0.173469428	0.14668604
15	0.191667697	0.239001781	0.189914542	0.126164653
16	0.160789679	0.243475662	0.131560912	0.141032189
17	0.178548485	0.253739273	0.135627983	0.108051387
18	0.150390387	0.253812376	0.152249926	0.132237308
19	0.148470373	0.12004916	0.113170677	0.220290813
20	0.147830482	0.12279782	0.099908488	0.230446806
21	0.143350735	0.114537221	0.100262147	0.248245968
22	0.1292716	0.118309317	0.082756057	0.124908241
23	0.12287218	0.128996924	0.082579228	0.112553529
24	0.11743251	0.135853952	0.07780484	0.116741567
25	0.115912535	0.137915446	0.086823129	0.120091997
26	0.106553172	0.13581009	0.098670684	0.108051387
27	0.084474634	0.145678947	0.085231666	0.122814222

If (a_{ij}) denotes the response variables for lower the better standard.

$$(r_{ij}) = \frac{a_{ij}}{\sqrt{\sum_{i=1}^n a_{ij}^2}} \quad (2)$$

Consequently, evaluating the obtained standardized decision matrix by

$$R = (r_{ij})_{m \times n} \quad (3)$$

Using the entropy method for determining the weight for the response variable

The entropy technique was used for calculating the weight for all the response variables. The calculation for the entropy of the performance indicator for the j^{th} response variable is done by:

$$e_j = -k \sum_{i=1}^m r_{ij} \ln r_{ij}, j = 1, 2, \dots, n \text{ and} \quad (4)$$

$$k = \frac{1}{\ln(m)} \quad (5)$$

Calculation of the performance indicator's total entropy done by

$$E = -\frac{1}{\ln(m)} * \sum_{j=1}^n \sum_{i=1}^m r_{ij} \ln(r_{ij}) \quad (6)$$

Calculation of the inequality for the j^{th} response variable is done by:

$$d_j = |1 - e_j|, j = 1, 2, 3, \dots, n \quad (7)$$

Whenever d_j will be larger, r_{ij} will be propagated more which in turn will make the response variable “ j ” the important one. Similarly, when r_{ij} , becomes comparatively saturated, it makes “ j ” the least important response variable.

Calculation of the weight factor was done by:

$$w_j = d_j / \sum_{j=1}^n d_j \quad (8)$$

The weight of the evaluated responses is shown in Table 5.9 and is also plotted in the form of a graph, depicted in Figure 5.22.

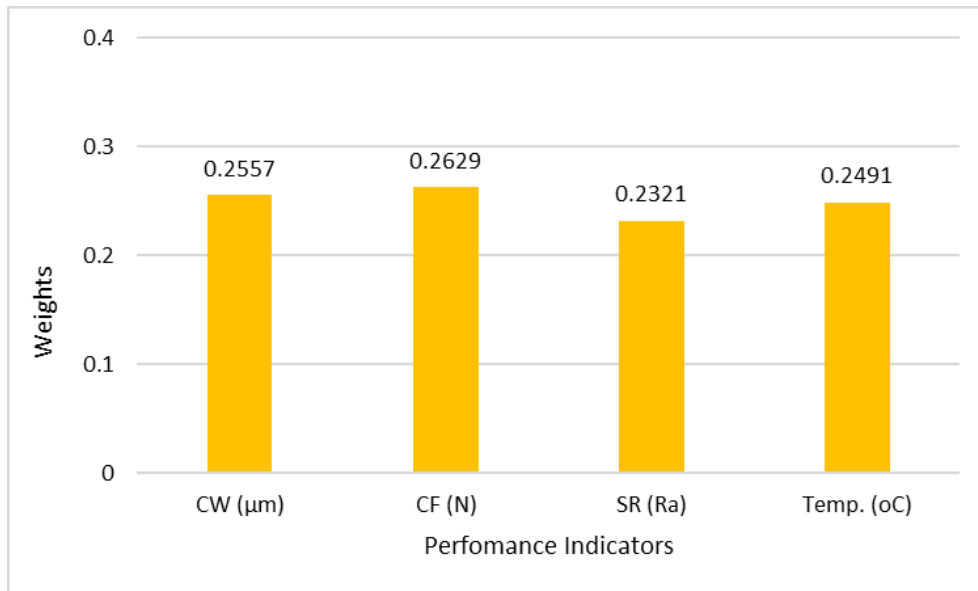


Figure 5.22: The weight of the evaluated responses to the performance indicators.

Table 5.9: Weights of the performance indicators.

Crater Wear	Cutting Force	Surface Roughness	Temperature at Cutting Zone
0.255755308	0.26293098	0.232198664	0.249115049

Determination of Weight

$R =$ Standardized decision matrix $= (r_{ij})_{m \times n}$,

$w_j =$ Calculated weight of the evaluated responses,

The weighted decision matrix of all the response variables was calculated by the following matrix and is shown in Table 5.10:

$$v = \begin{bmatrix} w_1 r_{11} & w_2 r_{12} \cdots & w_n r_{1n} \\ \vdots & \ddots & \vdots \\ w_1 r_{m1} & w_2 r_{m2} \cdots & w_n r_{mn} \end{bmatrix} = \begin{bmatrix} v_{11} & v_{12} \cdots & v_{1n} \\ \vdots & \ddots & \vdots \\ v_{m1} & v_{m2} \cdots & v_{mn} \end{bmatrix} \quad (9)$$

The calculation for finding the negative and positive ideal solution

The expression used for determining the positive ideal solution is mentioned below:

$$V^+ = \{v_1^+, v_2^+, \dots, v_n^+\} = \{(\max v_{ij} | j \in J_1), (\min v_{ij} | j \in J_2) | i = 1, 2, \dots, m\} \quad (10)$$

The expression used for determining the negative ideal solution is mentioned below:

$$V^- = \{v_1^-, v_2^-, \dots, v_n^-\} = \{(\min v_{ij} | j \in J_1), (\max v_{ij} | j \in J_2) | i = 1, 2, \dots, m\} \quad (11)$$

Where,

J_1 = variable for larger the better;

J_2 = variable for smaller the better.

Determination of the relative distance:

$$S_i^+ = \sqrt{\sum_{j=1}^n (v_{ij} - v_j^+)^2}, i = 1, 2, 3, \dots, m \quad (12)$$

$$S_i^- = \sqrt{\sum_{j=1}^n (v_{ij} - v_j^-)^2}, i = 1, 2, 3, \dots, m \quad (13)$$

Where,

S_i^+ = Relative distance between V_{ij} and positive ideal solution V_j^+

S_i^- = Relative distance between V_{ij} and negative ideal solution V_j^-

The positive and negative matrix for the performance indicators is shown in Table 5.11 and Table 5.12 respectively. Whereas, the relative distance of the considered performance indicators is shown in Table 5.13.

Table 5.10: Performance indicator's standardized and weighted decision matrices.

Run No.	Crater Wear	Cutting Force	Surface Roughness	Temperature at Cutting Zone
1	0.064814465	0.048744328	0.066926985	0.043740493
2	0.065673754	0.046603114	0.067789234	0.029264659
3	0.051065921	0.045438325	0.061055476	0.041549556
4	0.066655774	0.050943205	0.062205142	0.042071208
5	0.063095886	0.046053395	0.053993242	0.045253283
6	0.067269559	0.047037508	0.060028989	0.040036766
7	0.071688737	0.050193588	0.072182601	0.072092262
8	0.070706673	0.051731264	0.076658086	0.074622273
9	0.069888308	0.053015223	0.06733758	0.079056312
10	0.041245545	0.0651052	0.031246279	0.063485009
11	0.039220117	0.061537792	0.029234364	0.06601502
12	0.049265536	0.061249478	0.033011838	0.070449059
13	0.044764508	0.068176708	0.035844943	0.033463955
14	0.041245545	0.06173769	0.040279369	0.0365417
15	0.049020031	0.062840972	0.044097903	0.031429514
16	0.041122814	0.064017294	0.030548268	0.035133241
17	0.045664723	0.066715916	0.031492636	0.026917227
18	0.03846314	0.066735137	0.035352229	0.032942303
19	0.037972086	0.031564643	0.02627808	0.054877757
20	0.037808431	0.032287351	0.023198617	0.057407767
21	0.036662711	0.030115384	0.023280736	0.061841806
22	0.033061898	0.031107185	0.019215846	0.031116523
23	0.031425212	0.033917288	0.019174786	0.028038778
24	0.030033988	0.035720213	0.01806618	0.029082081
25	0.029645246	0.036262243	0.020160214	0.029916724
26	0.027251539	0.03570868	0.022911201	0.026917227
27	0.021604836	0.038303508	0.019790679	0.030594871

Formation of sequence table while evaluating the TOPSIS value

The calculated preferred value “C_j” and assigned rank of the experimental value are also shown in Table 5.13.

$$C_j = S_i^- / (S_i^+ + S_i^-) \quad (15)$$

Table 5.11: Positive Matrix for the performance indicators.

Crater Wear	Cutting Force	Surface Roughness	Temperature at Cutting Zone
0.021604836	0.030115384	0.01806618	0.026917227

Table 5.12: Negative Matrix for the performance indicators.

Crater Wear	Cutting Force	Surface Roughness	Temperature at Cutting Zone
0.071688737	0.068176708	0.076658086	0.079056312

Table 5.13: Standardized and weighted decision matrices for performance indicators.

Run No.	S _i ⁺	S _i ⁻	C _j	Rank
1	0.06988927	0.042033015	0.375555369	24
2	0.068496769	0.055312432	0.446755425	20
3	0.056257735	0.05091692	0.475083594	18
4	0.068126913	0.043578778	0.390121374	23
5	0.060020765	0.047112822	0.43975772	21
6	0.06560964	0.047596709	0.420442049	22
7	0.088774446	0.019796984	0.182340641	25
8	0.092666173	0.017061002	0.15548566	27
9	0.089453068	0.017888097	0.166647128	26
10	0.055865575	0.056929077	0.504714328	17
11	0.054323399	0.05930743	0.521930804	16
12	0.062071243	0.050297776	0.447612484	19
13	0.048414656	0.066852746	0.579979639	14

14	0.044404774	0.064024621	0.590472917	13
15	0.050205263	0.062215896	0.55341803	15
16	0.041875965	0.070759649	0.628217369	10
17	0.045812082	0.073741341	0.616806606	11
18	0.044275476	0.070275842	0.613487853	12
19	0.033454652	0.07483317	0.691058039	7
20	0.034975547	0.075911102	0.684582883	8
21	0.038388247	0.076295266	0.665267954	9
22	0.012296494	0.09200009	0.882100706	6
23	0.010648058	0.093284392	0.897548281	4
24	0.010351391	0.093375465	0.900205292	3
25	0.010761693	0.091612755	0.894879108	5
26	0.0093083	0.092930346	0.908955172	2
27	0.00914026	0.094779842	0.912045316	1

Table 5.14: Best and worst combinations of the Input Parameters

	Input Parameters			
	Type of Tool	Feed	Speed	Depth of Cut
Best combination	DLC	0.15	60.52	0.192
Worst combination	Bare	0.15	90.78	0.576

Table 5.15: Best and worst combinations of the Response Variable

	Response Variable			
	Crater Wear	Cutting Force	Surface Roughness	Temperature at Cutting Zone
Best combination	496.241	99.64	0.482	117.3
Worst combination	1624.06	134.57	1.867	286.1

The effects plots of all the response variables viz. Crater Wear, Cutting Force, Surface Roughness, and Temperature at Cutting Zone vs all the input parameters viz. Type of Tool, Feed, Speed, and Depth of Cut have been plotted separately in Figure 5.23, Figure 5.24, Figure 5.25 and Figure 5.26 respectively.

As can be seen in Figure 5.23, crater wear was at its lowest value when machining was done using DLC coated tool inserts. Crater wear was low with low values of speed and DOC but, it was lowest with the highest value of feed. These effects can also be seen in Table 5.14 of the Best and worst combinations of the Input Parameters.

Similarly, it is also observed that cutting force is also found to be at the lowest value when DLC coated tool inserts were used to perform the experimentations. Along with the DLC coated tool inserts, low feed, low cutting speed and average depth of cut were found to be the reasons behind the lower value of the cutting force. This is also evident in Figure 5.24.

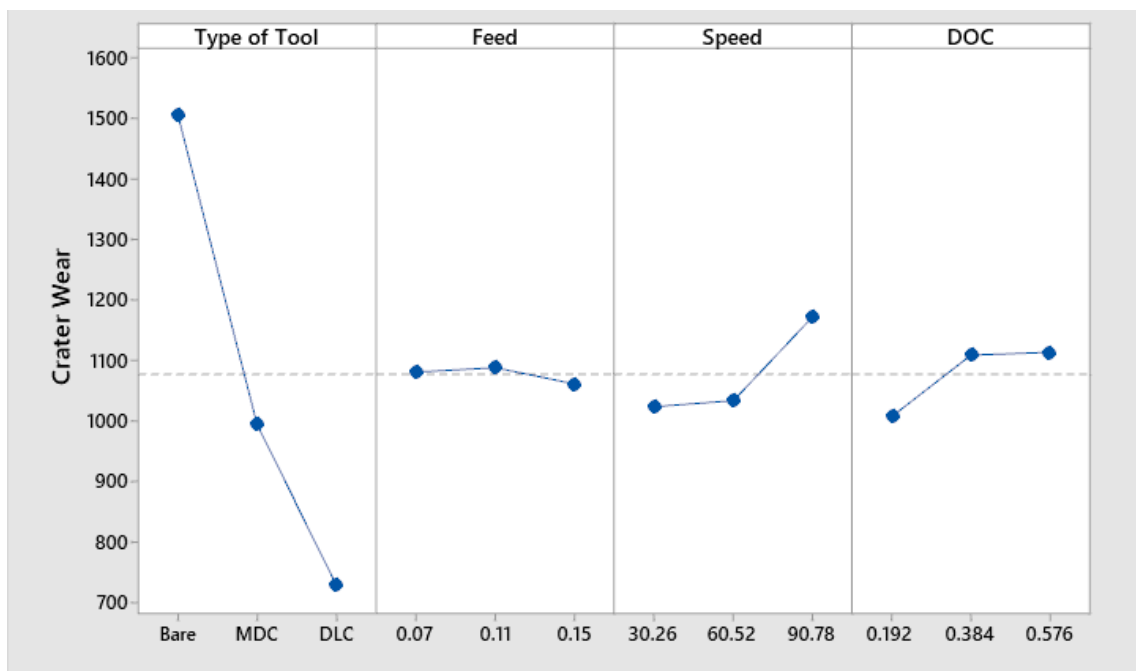


Figure 5.23: Effect plot of crater wear vs Type of Tool, Feed, Speed and DOC.

It is observed in Figure 5.25 that Surface Roughness is detected to be at the lowest value when the experimentation was performed using the DLC coated tool inserts. But, along with the DLC coated tool inserts, average feed, low cutting speed and depth of cut were the reasons behind the lower value of the surface roughness.

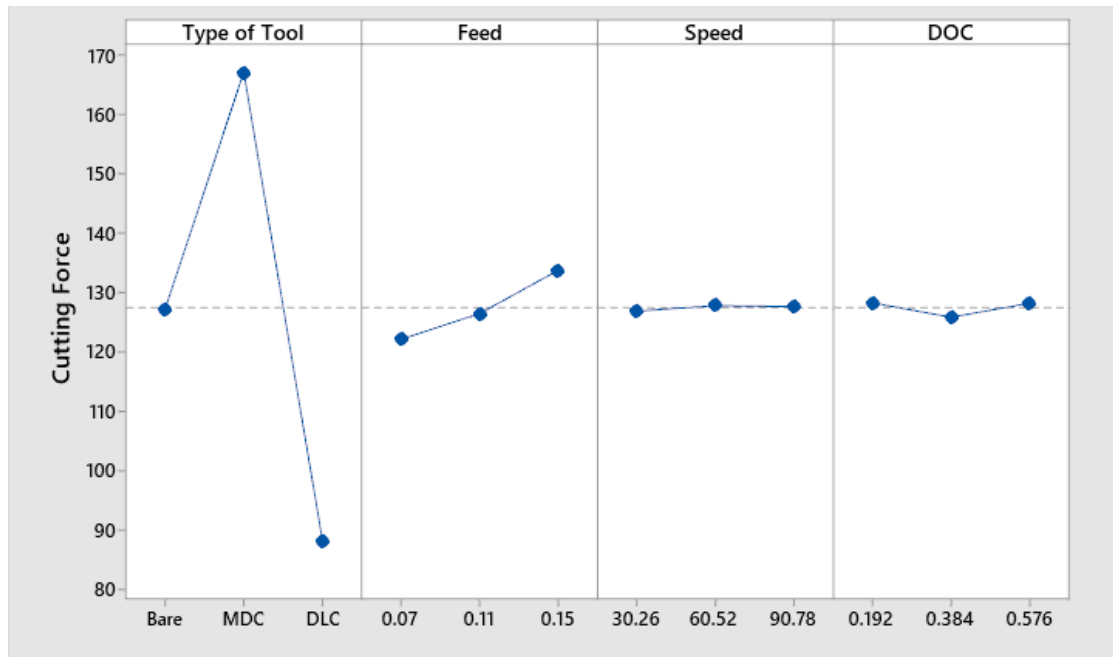


Figure 5.24: Effect plot of cutting force vs Type of Tool, Feed, Speed and DOC.

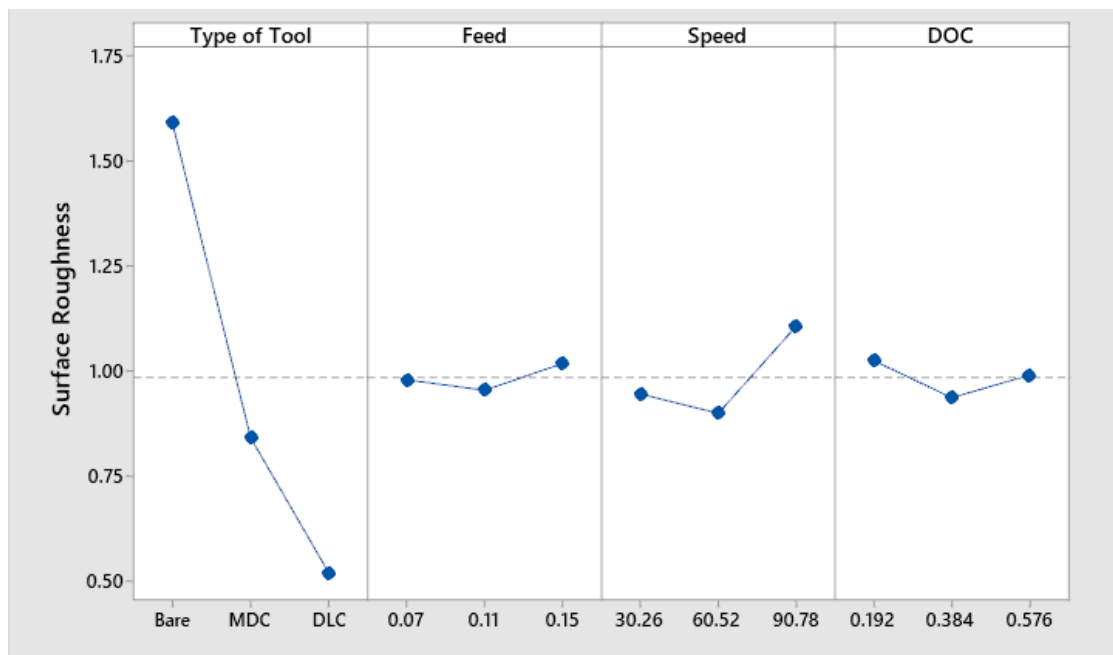


Figure 5.25: Effect plot of Surface Roughness vs Type of Tool, Feed, Speed and DOC.

It has been found and clearly shown in Figure 5.26 that the temperature obtained at the cutting zone is at the lowest range of value when the experimentations were performed using the DLC coated tool inserts. But, the low cutting speed and low depth of cut along with the average feed were the reasons behind the lower value of the temperature at the cutting zone.

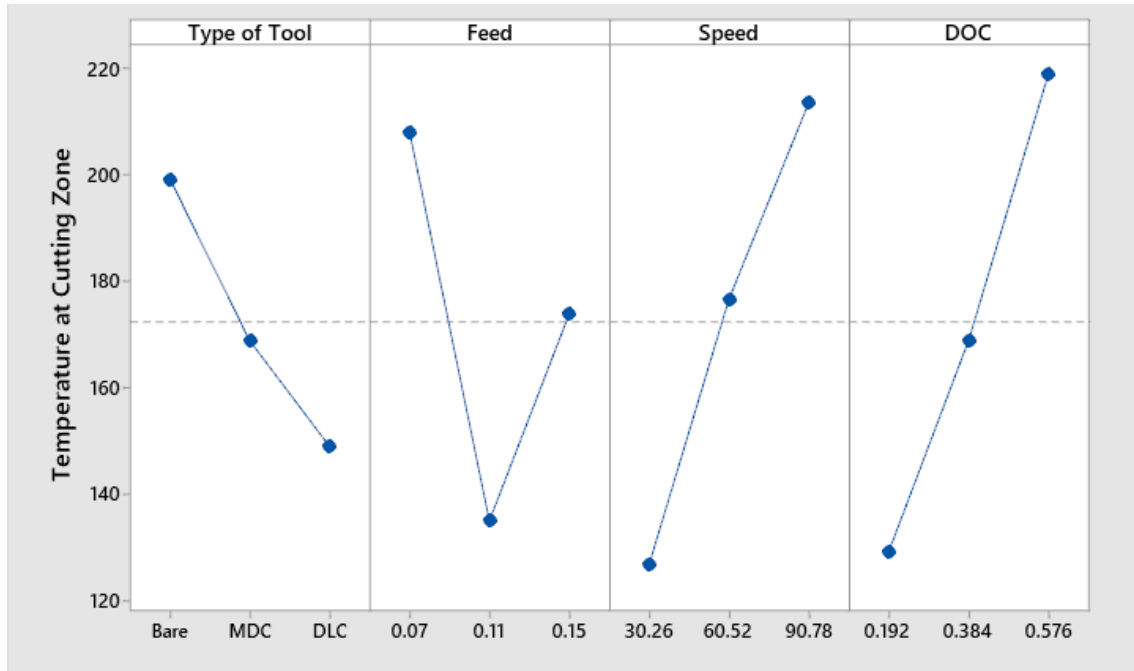


Figure 5.26: Effect plot of Temperature at Cutting Zone vs Type of Tool, Feed, Speed and DOC.

5.4.2. Discussion

In this research, for obtaining the optimal performance of the machining process the minimization characteristic for Crater Wear (μm), Cutting Force (N), Surface Roughness (μm) and Temperature at Cutting Zone ($^{\circ}\text{C}$) were taken. The obtained results of best and worst combinations for the input parameter and response variable are shown in Table 5.14 and Table 5.15 respectively.

As mentioned in above section 5.4.1, the minimum values of Crater Wear (μm), Cutting Force (N), Surface Roughness (μm) and Temperature at Cutting Zone ($^{\circ}\text{C}$) are indicated by the maximum relative closeness. The combination of a self-developed DLC coated tool insert with

the feed of 0.15 mm/rev, speed of 60.52 m/min and 0.192 mm depth of cut is the optimal values of input parameters for achieving the minimum values of response variables using the DLC coated tungsten carbide (WC) tool inserts in a turning process [31].

Generally, an increase in the cutting speed and feed, will either enhance the tool flank wear or creates the formation of a built-up edge (BUE) on the tool inserts [24]. Low rates of shear strain developed inside the shear zone of the tool insert in a corresponding manner at lower cutting speeds, which doesn't enhance the extension of the adiabatic shear band without the loss or gain of heat along the shear zone [43].

The optimum value indicates that while using the self-developed DLC coated tool inserts with the highest level of feed, normal level of cutting speed and the lowest level of depth of cut, we can reduce the Crater Wear (μm), Cutting Force (N), Surface Roughness (μm) and Temperature at Cutting Zone ($^{\circ}\text{C}$) [15].

5.5. Experimentation on CNC Machine Tool

As explained in section 4.3.12 of chapter 4, LMW® Machine Tool Division make “HORIZONTAL CNC LATHE - LL20T L3” of Metal Cutting Lab in the mechanical engineering department at Delhi Technological University, Delhi, was used to perform the experimentation.

As mentioned in section 4.1.2 of chapter 4, a round bar of 50 mm in diameter and 610 mm in length was selected for the turning process. The maximum turning length of the CNC machine tool was 580 mm. The process of dry turning operation was performed on the CNC machine tool. The levels of input parameters selected for the experimentation are mentioned in Table 5.16. The levels were decided by going through the various literature as well as after doing the

test runs on the CNC machine tool. Detailed experimental conditions viz. the design of experiments selected for the experiments is an L_{27} orthogonal array (OA), which is depicted in Table 5.17. Also, the measurement of temperature using an infrared thermal imaging camera while performing the machining process is shown in Figure 5.27.

Table 5.16: Levels of input parameters selected for CNC Machine Tool

S. No.	Input Parameters	Unit	Level 1	Level 2	Level 3
1	Type of Tool	---	Un-Coated	MDC (Market available diamond coated tool)	DLC (Self-developed DLC coated tool)
2	Feed (f)	mm/rev	0.125	0.25	0.375
3	Cutting Speed (Vc)	m/min	360	480	600
4	Depth of Cut (DOC)	mm	0.2	0.4	0.6
Work Material: Aluminium 6061, Workpiece Diameter: 50 mm, Total length of the Workpiece: 610 mm, Temperature: Room Temperature, Machining: Dry Machining					

Stereo microscopic images of the tools were captured just like it was done in the conventional lathe experimentation, i.e. after each set of experiments, using the optical coordinate measuring machines (CMM). A few of the images captured are shown in Figure 5.28.

As the development of empirical relationships between important process parameters and response characteristics along with studying the effect of various process parameters on machining was one of the objectives of our experimental research work, hence we used Genetic Algorithm (GA) for doing the same. After going through the literature we got to know that Genetic algorithms are commonly used to generate high-quality solutions to optimization and search problems by relying on biologically inspired operators such as mutation, crossover and selection.

Table 5.17: The L₂₇ OA for Machining on CNC Machine Tool

Run No.	Exp. No.	Type of Tool	Feed (mm/rev)	Speed (m/min)	Depth of Cut (mm)
1	1	Bare	0.125	360	0.2
4	2	Bare	0.125	360	0.2
7	3	Bare	0.125	360	0.2
9	4	Bare	0.25	480	0.4
2	5	Bare	0.25	480	0.4
5	6	Bare	0.25	480	0.4
8	7	Bare	0.375	600	0.6
6	8	Bare	0.375	600	0.6
3	9	Bare	0.375	600	0.6
10	10	MDC	0.125	480	0.6
13	11	MDC	0.125	480	0.6
16	12	MDC	0.125	480	0.6
18	13	MDC	0.25	600	0.2
11	14	MDC	0.25	600	0.2
14	15	MDC	0.25	600	0.2
17	16	MDC	0.375	360	0.4
15	17	MDC	0.375	360	0.4
12	18	MDC	0.375	360	0.4
19	19	DLC	0.125	600	0.4
22	20	DLC	0.125	600	0.4
25	21	DLC	0.125	600	0.4
27	22	DLC	0.25	360	0.6
20	23	DLC	0.25	360	0.6
23	24	DLC	0.25	360	0.6
26	25	DLC	0.375	480	0.2
24	26	DLC	0.375	480	0.2
21	27	DLC	0.375	480	0.2

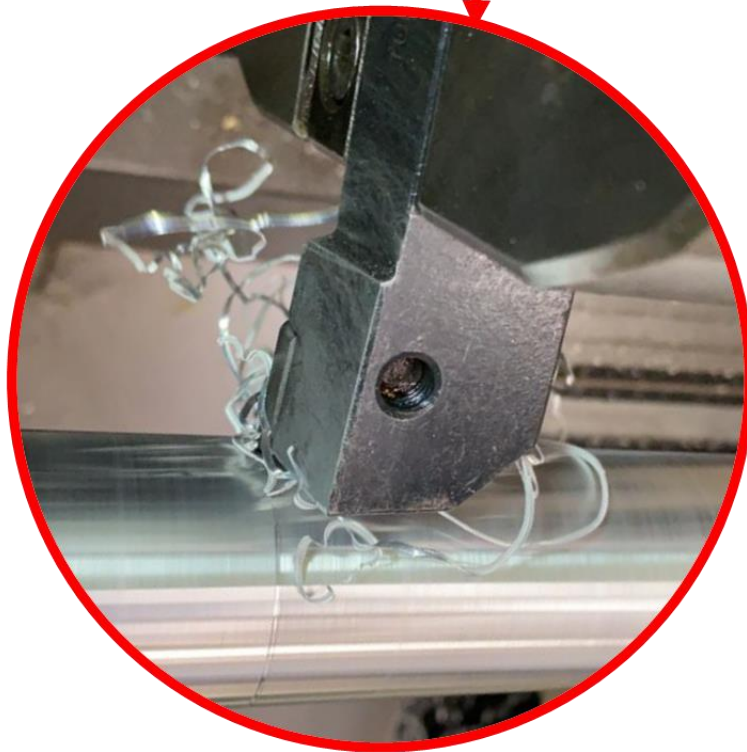


Figure 5.27: Experimentation on the CNC Machine Tool.

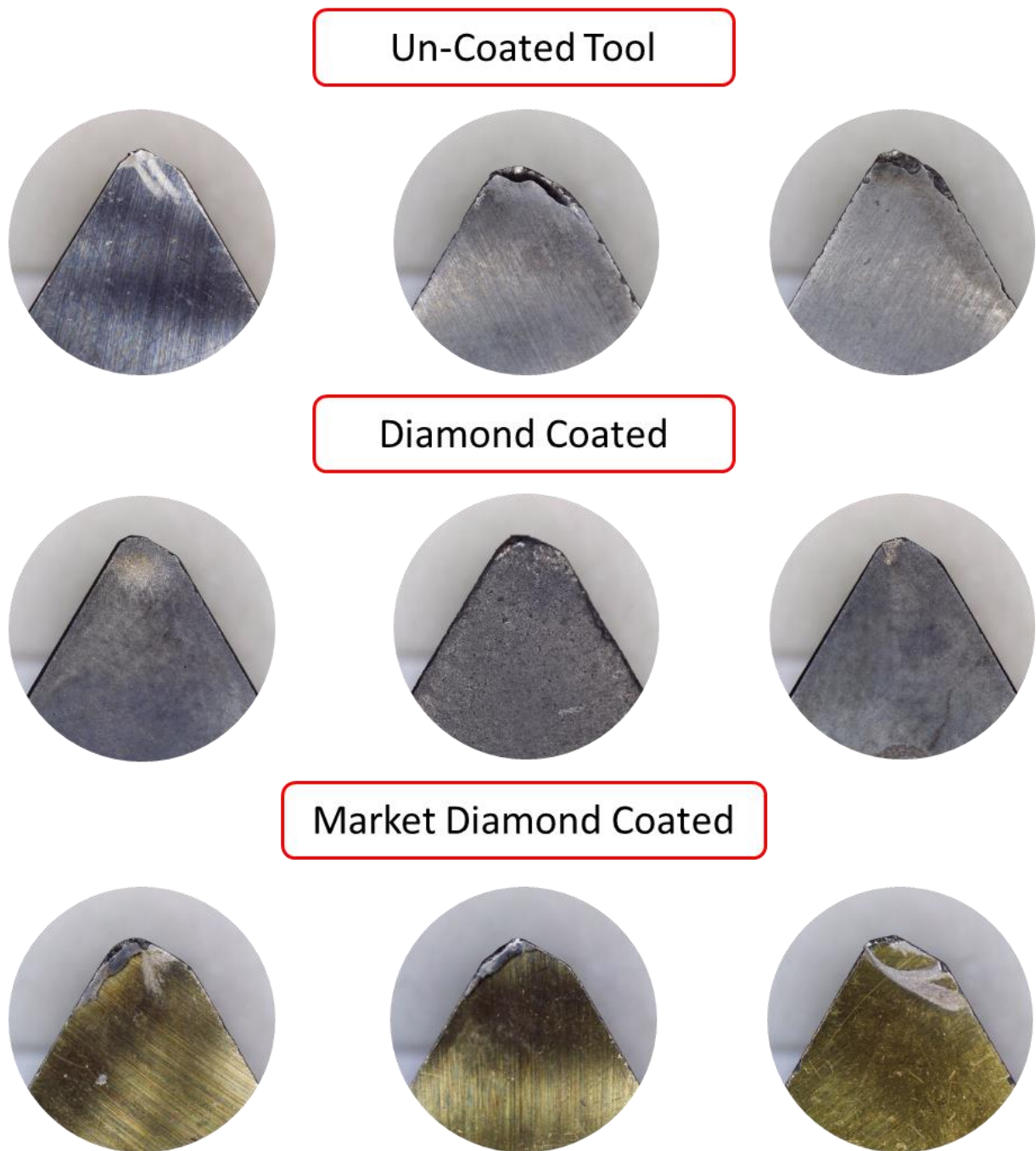


Figure 5.28: Microscopic images of a few of the worn-out tool inserts.

GA is one of the modern optimization techniques, which is heuristic in nature. It creates the population through reproduction via three methods; selection, crossover and mutation. After setting the fixed parameters such as elite population, crossover function, mutated population,

etc. the optimized output parameters were yielded. The population count considered was 50 and the elite, as well as the mutated population, was taken as 20 per cent from the previous population. Through the M-file, the GA model was run for the considered output parameters individually i.e. Crater Wear (μm), Flank Wear (μm), Cutting Force (N), Surface Roughness (μm) and Temperature at Cutting Zone ($^{\circ}\text{C}$), which have been discussed below.

5.5.1. Genetic Algorithm (GA)

GA predictive model was considered for optimization taking into account all the process parameters individually. This approach was adopted to analyze the individual effect of process parameters on the considered output parameters.

GA being a heuristic optimization technique develops its model based on the regression equations generated through regression analysis. As the main effects of process parameters are focused on in this experimentation, only the linear regression equations were generated. These equations are further transformed into predictive equations considering a specific range of the process parameters. In this section of our research, we are discussing a general form of GA based predictive equations. Hence, the lowest value of the range defines the lower bound while the highest value defines the upper bound for these predictive equations.

The GA parameters considered for the optimization are selected as Population type: Double Vector, Selection: Stochastic uniform, Elite count: 20%, Crossover fraction: 0.8, Mutation: 20% and Crossover function: Scattered. The Crater Wear, Flank Wear, Cutting Force, Surface Roughness and Temperature at Cutting Zone were expressed in terms of feed, speed and depth of cut. In the general form the response function can be expressed as follows:

$$Y = \Phi (F, V, D) \quad (1)$$

Where,

Y = Response (Crater Wear/Flank Wear/Cutting Force/Surface Roughness/Temperature at Cutting Zone);

F = feed (mm/rev);

V = Cutting Speed (m/min);

D = Depth of Cut (mm)

Using the following regression equation

$$Y = \beta_0 + \beta_1 F + \beta_2 V + \beta_3 D \quad (2)$$

where β_0 is constant while β_1 , β_2 , and β_3 are partial regression coefficients of the model from which the response functions were generated as given below:

$$CW = C_1 * F^{x1} * V^{x2} * D^{x3} \quad (3)$$

$$FW = C_2 * F^{x1} * V^{x2} * D^{x3} \quad (4)$$

$$CF = C_3 * V^{x1} * L^{x2} * D^{x3} \quad (5)$$

$$SR = C_4 * V^{x1} * L^{x2} * D^{x3} \quad (6)$$

$$T = C_5 * V^{x1} * L^{x2} * D^{x3} \quad (7)$$

Where,

CW = Crater Wear;

FW = Flank Wear;

CF = Cutting Force;

SR = Surface Roughness;

T = Temperature at Cutting Zone.

$C_1, C_2, C_3, C_4, C_5 = \text{Constant}$

F = feed (mm/rev);

V = Cutting Speed (m/min);

D = Depth of Cut (mm)

The unknown coefficients, namely, exponents of feed, cutting speed and depth of cut and constants involved in the above equations were determined by minimizing the least-squares error between experimental and predicted results obtained within the range of cutting conditions.

5.5.1.1. Crater Wear (CW)

The equation developed using regression analysis for the output parameter “Crater Wear” is given as follows [Rana et al. (2020)]:

Regression Equation:

$$\text{Crater Wear } (\mu\text{m}) = 422 - 79\text{feed} + 0.621\text{speed} + 264\text{DOC}$$

The predictive equation developed for the optimization model is as follows:

GA Predictive Equation:

$$CW = 489.31 * X_1^{(-0.604)} * X_2^{0.00081} * X_3^{0.408}$$

X_1, X_2 & X_3 are feed, cutting speed and depth of cut, respectively.

Hence,

GA Predictive Equation:

$$CW = 489.31 * feed^{(-0.604)} * speed^{0.00081} * DOC^{0.408}$$

Optimized Result:

$$CW = 461.06723(\mu\text{m}) \text{ at } feed = 0.375, speed = 360 \text{ and } DOC = 0.2 \text{ mm}$$

After setting the fixed parameters, the yielded optimized output parameter i.e. optimized crater wear (CW) was 461.067 μm . The value of the optimized crater wear (CW) is shown in figure 5.29 along with the genetic algorithm graph for the best value and the average value of crater wear. The optimized value of crater wear (CW) was obtained at a feed of 0.375 mm/rev, a cutting speed of 360 m/min and a depth of cut of 0.2 mm. Whereas, the Pareto chart of the standardized effects for the crater wear as the response variable is shown in Figure 5.30.

The graph between fitness value and generation reveals the average and mean fitness values of the output parameter i.e., crater wear for a given generation. The best fitness value represents that value beyond which the variation doesn't occur in the output parameter. The optimization cycle for the developed model ran for 170 generations, after which the best and mean values were recorded. The graph, individual vs. generation, depicts the development of 170 generations consisting of 2% of the elite population and 2% of the mutated population. These generations follow selection, mutation or crossover processes for forming the next generation. The Pareto graph explains the contribution or significance of the input parameters to a particular output parameter. The graph in Figure 5.30 shows that cutting speed has the maximum effect on crater wear followed by the depth of cut. Feed rate is the least significant parameter for evaluating crater wear.

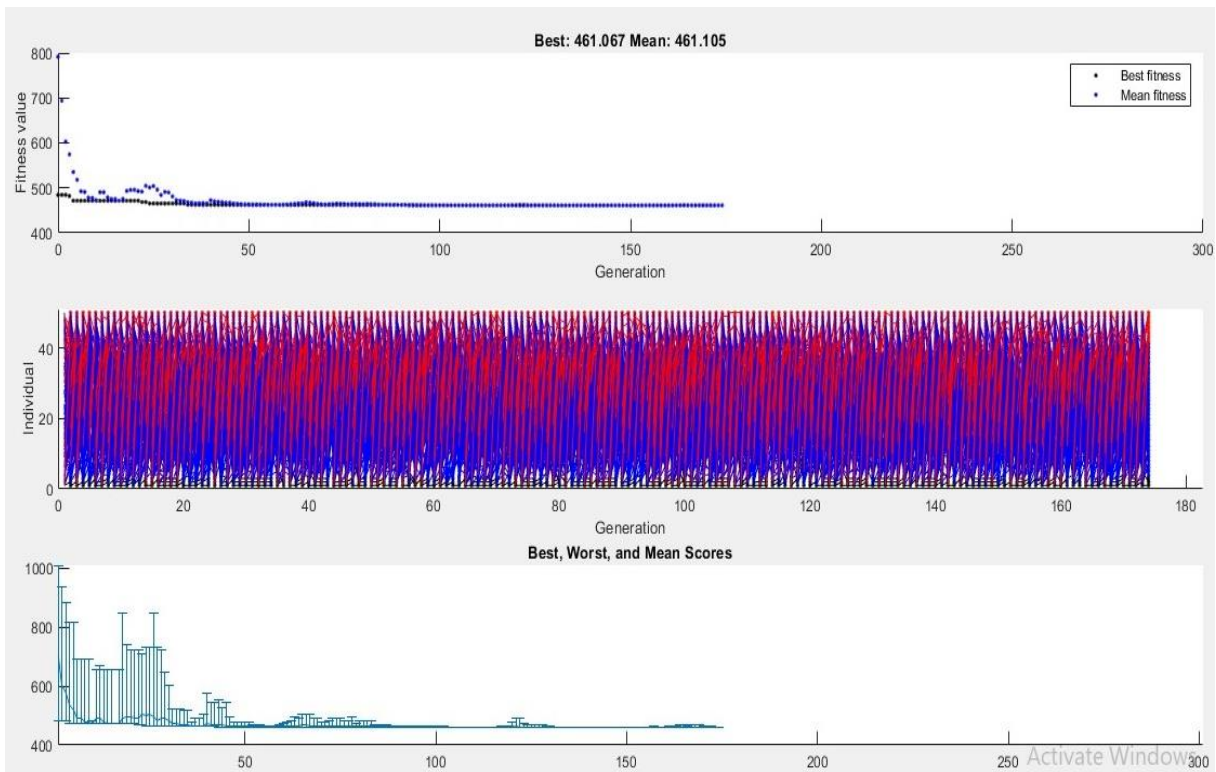


Figure 5.29: Genetic Algorithm Graph for the best value and the average value of Crater Wear.

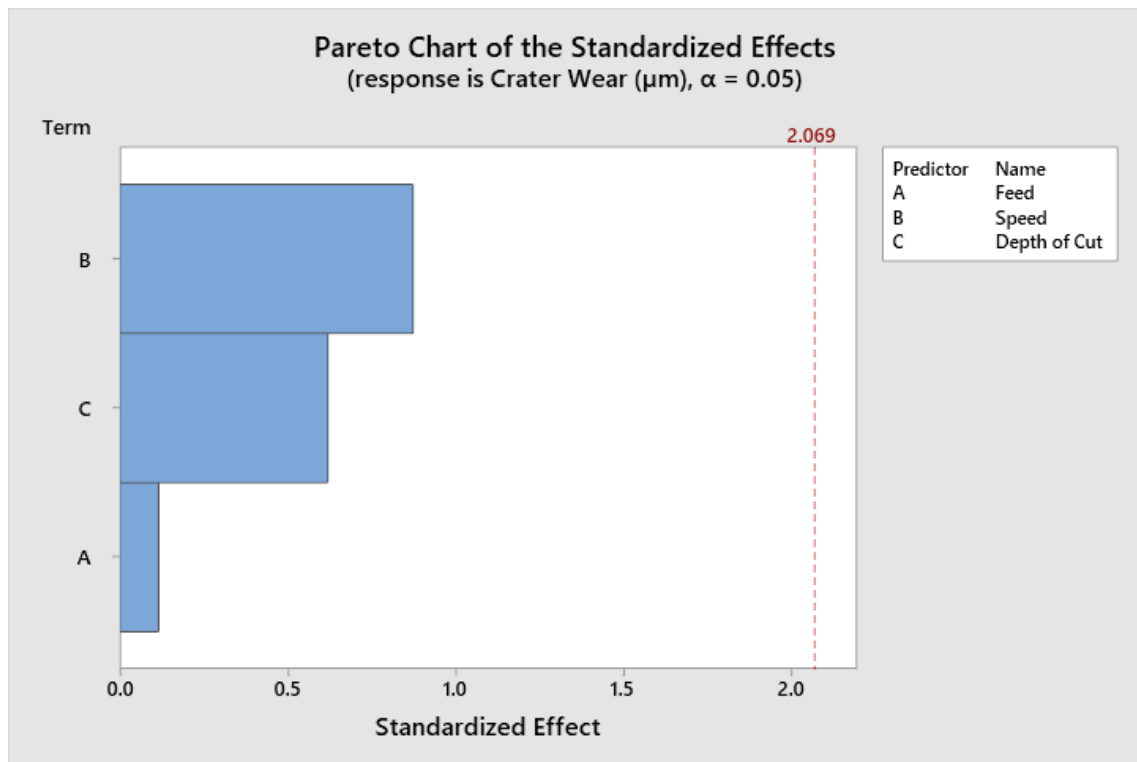


Figure 5.30: Pareto Chart of the Standardized effects for the crater wear as response variable.

5.5.1.2. Flank Wear (FW)

The equation developed using regression analysis for the output parameter “Flank Wear” is given as follows [Rana et al. (2020)]:

Regression Equation:

$$\text{Flank Wear } (\mu\text{m}) = 55 + 57 \textit{ feed} + 0.621 \textit{ speed} + 180 \textit{ DOC}$$

The predictive equation developed for the optimization model is as follows:

GA Predictive Equation:

$$FW = 123.97 * X_1^{(-1.71)} * X_2^{0.00234} * X_3^{0.42}$$

X_1 , X_2 & X_3 are feed, cutting speed and depth of cut, respectively.

Hence,

GA Predictive Equation:

$$FW = 123.97 * \textit{feed}^{(-1.71)} * \textit{speed}^{0.00234} * \textit{DOC}^{0.42}$$

Optimized Result:

$$FW = 342.0878(\mu\text{m}) \text{ at } \textit{feed} = 0.125, \textit{ speed} = 600 \text{ and } \textit{DOC} = 0.4 \text{ mm}$$

After setting the fixed parameters, the yielded optimized output parameter i.e. optimized flank wear (FW) was 342.087 μm . The value of the optimized flank wear (FW) is shown in figure 5.31 along with the genetic algorithm graph for the best value and the average value of flank wear. The optimized value of flank wear (FW) was obtained at a feed of 0.125 mm/rev, a cutting speed of 600 m/min and a depth of cut of 0.4 mm. Whereas, the Pareto chart of the standardized effects for the flank wear as the response variable is shown in Figure 5.32.

The graph between fitness value and generation in Figure 5.31 reveals that the average and mean fitness values of the output parameter i.e., flank wear for a given generation. The optimization cycle for the developed model ran for approximately 140 generations, after which the best and mean values were recorded as 342.88 μm and 342.103 μm respectively. The graph, individual vs. generation, depicts the development of 140 generations consisting of 2% of the elite population and 2% of the mutated population. These generations follow selection, mutation or crossover processes for forming the next generation.

The Pareto graph explains the contribution or significance of the input parameters to a particular output parameter. The graph in Figure 5.32 shows cutting speed has the maximum effect on flank wear followed by the depth of cut. Feed rate is the least significant parameter for evaluating flank wear.

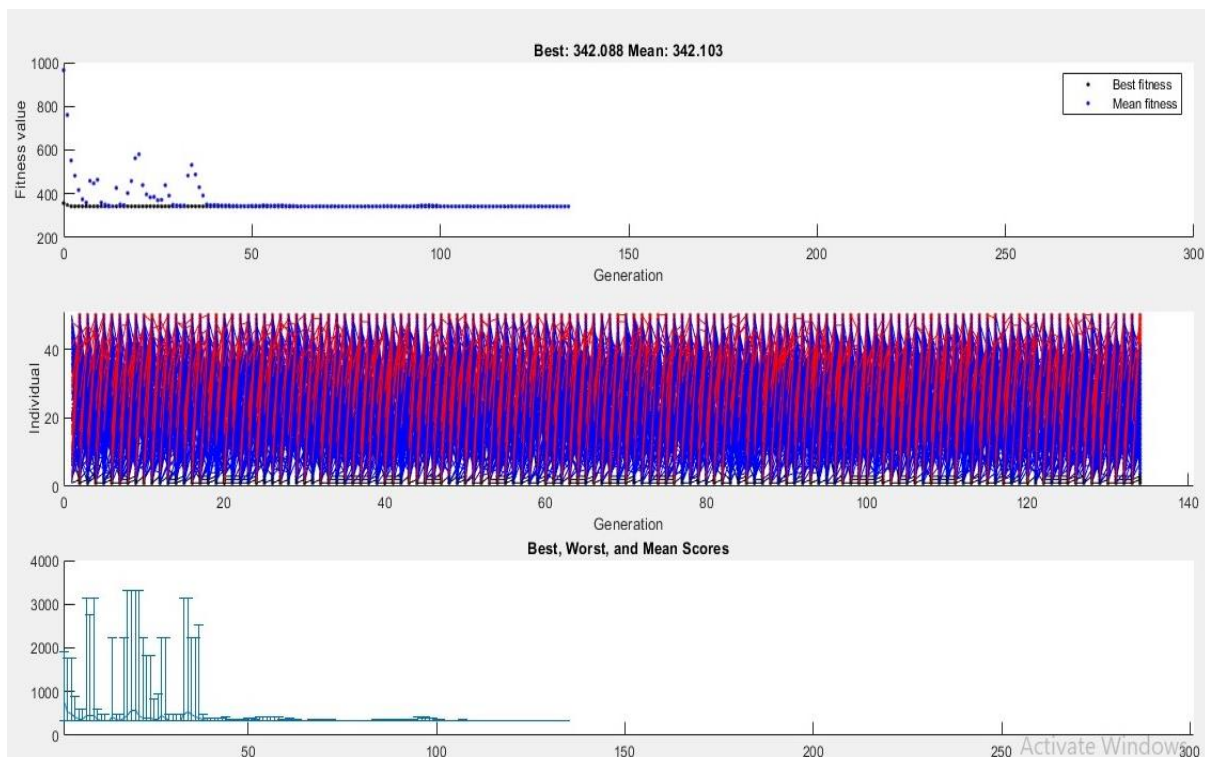


Figure 5.31: Genetic Algorithm Graph for the best value and the average value of Flank Wear.

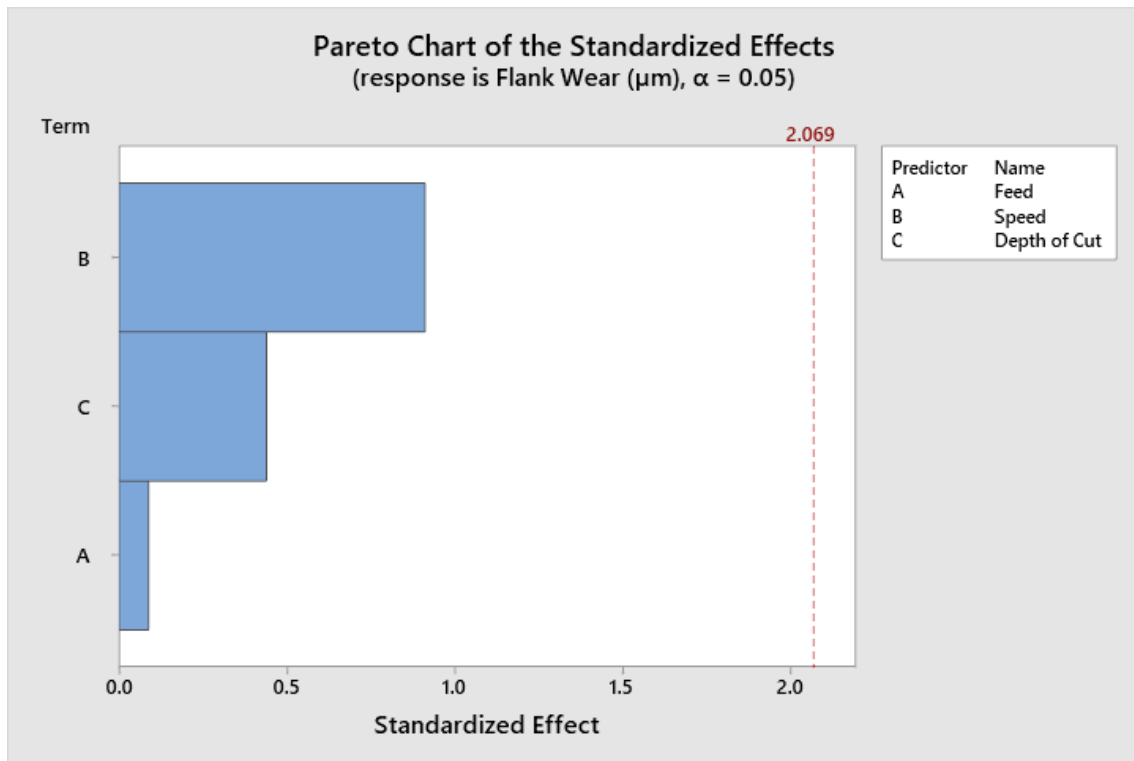


Figure 5.32: Pareto Chart of the Standardized effects for the flank wear as the response variable.

5.5.1.3. Cutting Forces (CF)

The equation developed using regression analysis for the output parameter “Cutting Force” is given as follows [Rana et al. (2020)]:

Regression Equation:

$$\text{Cutting Force (CF)} = 5.3 + 273.3 \text{ feed} + 0.5654 \text{ speed} - 1.2 \text{ DOC}$$

The predictive equation developed for the optimization model is as follows:

GA Predictive Equation:

$$\text{Cutting Force} = 110.06 * X_1^{(0.898)} * X_2^{0.001833} * X_3^{0.022}$$

X_1 , X_2 & X_3 are feed, cutting speed and depth of cut, respectively.

Hence,

GA Predictive Equation:

$$\text{Cutting Force} = 110.06 * \text{feed}^{(0.898)} * \text{speed}^{0.001833} * \text{DOC}^{0.022}$$

Optimized Result:

$$\text{CF} = 216.5949(\text{N}) \text{ at } \text{feed} = 0.25, \text{ speed} = 360 \text{ and } \text{DOC} = 0.6 \text{ mm}$$

After setting the fixed parameters, the yielded optimized output parameter i.e. optimized cutting force (CF) was 216.595 N. The value of the optimized cutting force (CF) is shown in figure 5.33 along with the genetic algorithm graph for the best value and the average value of cutting force. The optimized value of cutting force (CF) was obtained at a feed of 0.25 mm/rev, a cutting speed of 360 m/min and a depth of cut of 0.6 mm. Whereas, the Pareto chart of the standardized effects for the cutting force as the response variable is shown in Figure 5.34.

The graph between fitness value and generation in Figure 5.33 reveals the average and mean fitness values of the output parameter i.e. cutting force for a given generation. The optimization cycle for the developed model ran for 180 generations, after which the best and mean values were recorded. These values were 216.595 N and 216.596 N respectively. The graph, individual vs. generation, depicts the development of 180 generations consisting of 2% of the elite population and 2% of the mutated population from the previous generation.

The Pareto graph explains the contribution or significance of the input parameters to a particular output parameter. The graph in Figure 5.34 shows that the cutting speed has the maximum effect on cutting force followed by feed rate. It also depicts that the depth of cut has a negligible effect on cutting force.

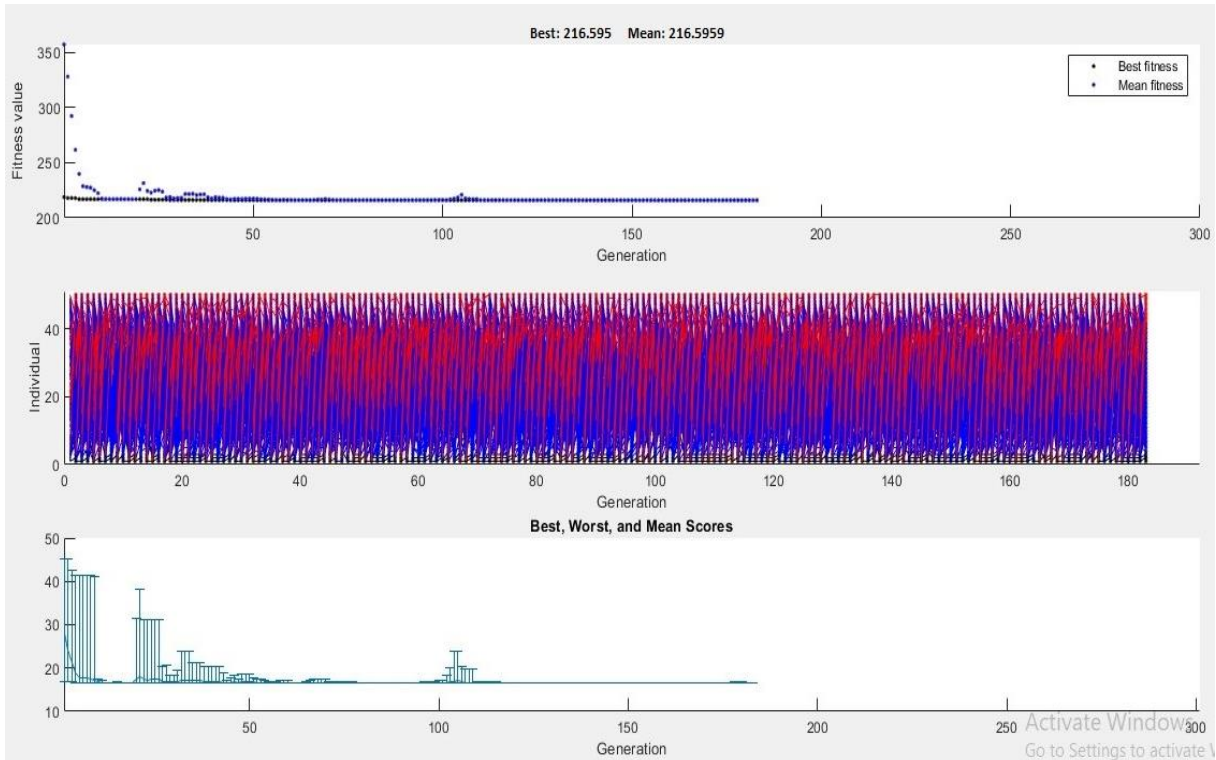


Figure 5.33: Genetic Algorithm Graph for the best value and the average value of Cutting Force.

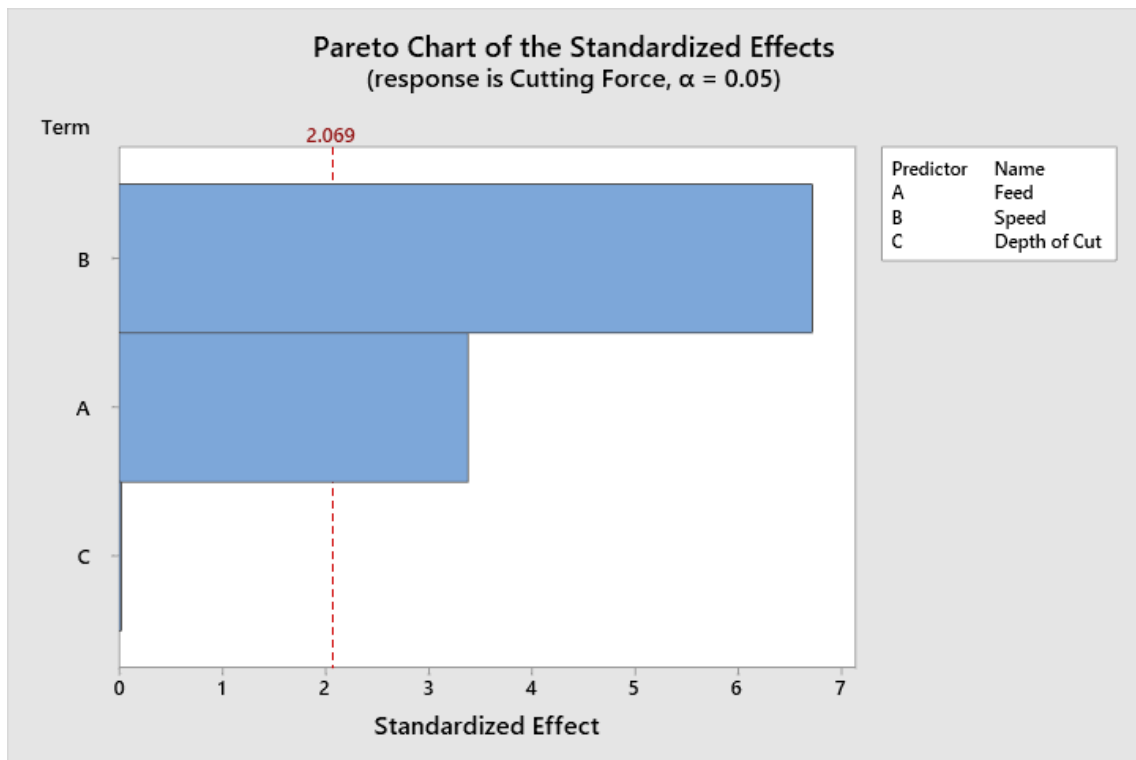


Figure 5.34: Pareto Chart of the Standardized effects for the cutting force as the response variable.

5.5.1.4. Surface Roughness (SR)

The equation developed using regression analysis for the output parameter “Surface Roughness” is given as follows [Rana et al. (2020)]:

Regression Equation:

$$\text{Surface Roughness } (\mu\text{m}) = 0.658 + 0.156 \text{ feed} + 0.000671 \text{ speed} - 0.086 \text{ Depth of Cut}$$

The predictive equation developed for the optimization model is as follows:

GA Predictive Equation:

$$\text{Surface Roughness} = 0.666 * X_1^{(-0.018)} * X_2^{0.00769} * X_3^{-0.217}$$

X_1 , X_2 & X_3 are feed, cutting speed and depth of cut, respectively.

Hence,

GA Predictive Equation:

$$\text{Surface Roughness} = 0.666 * \text{feed}^{(-0.018)} * \text{speed}^{0.00769} * \text{DOC}^{-0.217}$$

Optimized Result:

$$\text{SR} = 0.7607(\mu\text{m}) \text{ at } \text{feed} = 0.375, \text{ speed} = 360 \text{ and } \text{DOC} = 0.4 \text{ mm}$$

After setting the fixed parameters, the yielded optimized output parameter i.e. optimized surface roughness (SR) was 0.761 μm . The value of the optimized surface roughness (SR) is shown in figure 5.35 along with the genetic algorithm graph for the best value and the average value of surface roughness. The optimized value of surface roughness (SR) was obtained at a feed of 0.375 mm/rev, a cutting speed of 360 m/min and a depth of cut of 0.4 mm. Whereas, the Pareto chart of the standardized effects for the surface roughness as the response variable is shown in Figure 5.36.

The graph between fitness value and generation in Figure 5.35 reveals the average and mean fitness values of the output parameter i.e., surface roughness for a given generation. The

optimization cycle for the developed model ran for 70 generations, after which the best and mean values were recorded as 0.760 μm and 0.760 μm respectively. The graph, individual vs generation, depicts the development of 70 generations consisting of 2% of the elite population and 2% of the mutated population. These generations follow selection, mutation or crossover processes for forming the next generation.

The Pareto graph explains the contribution or significance of the input parameters to a particular output parameter. The graph in Figure 5.36 shows that the cutting speed has the maximum effect on surface roughness followed by feed rate. Depth of cut is the least significant parameter for evaluating surface roughness.

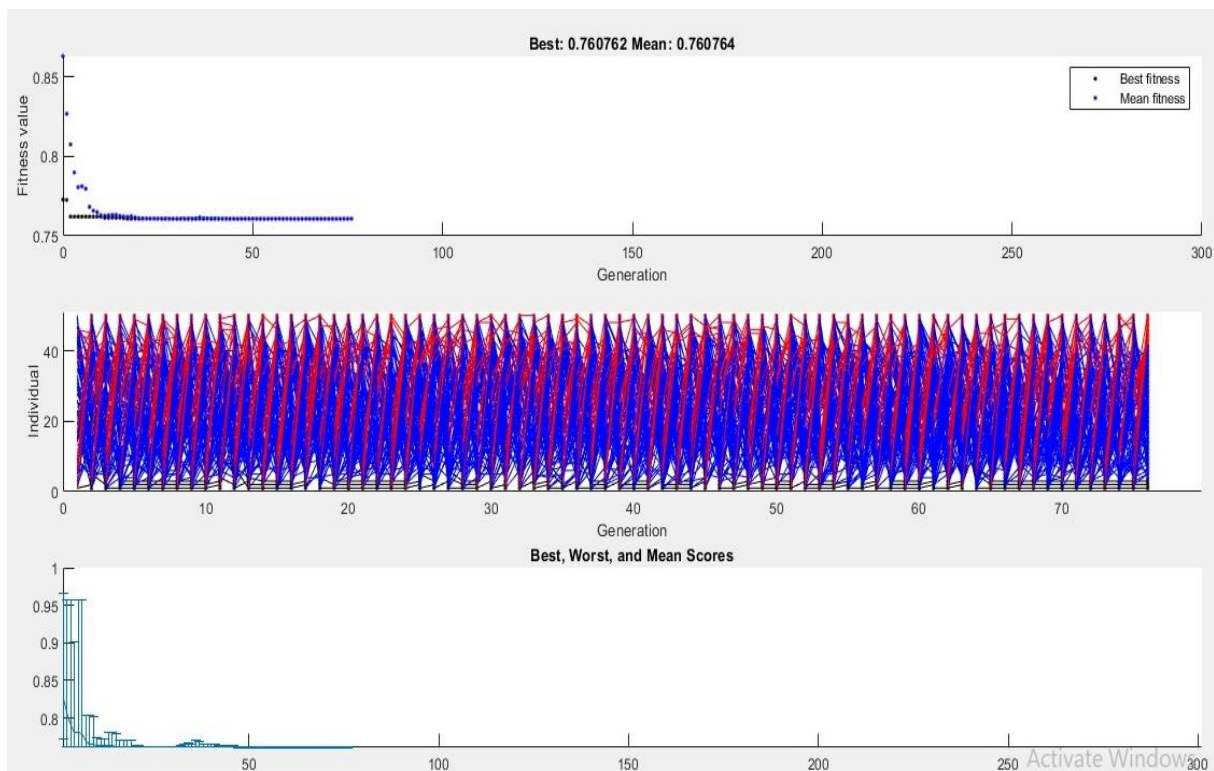


Figure 5.35: Genetic Algorithm Graph for the best value and the average value of surface roughness.

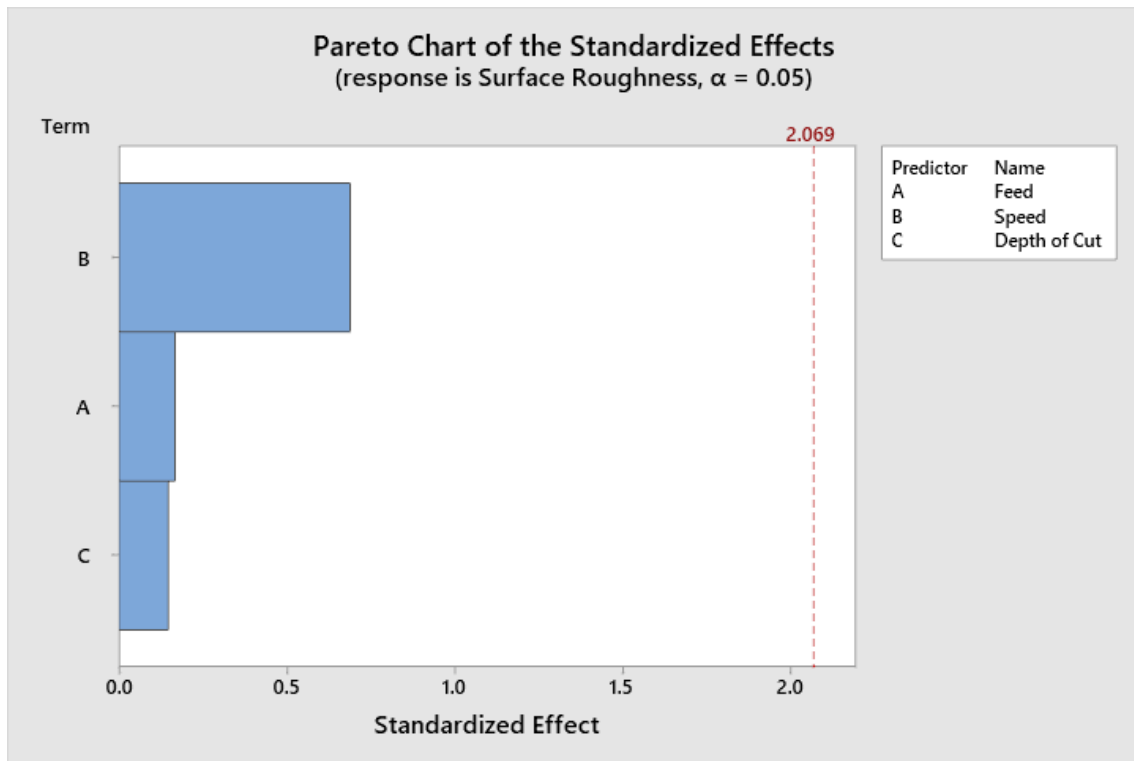


Figure 5.36: Pareto Chart of the Standardized effects for the surface roughness as the response variable.

5.5.1.5. Temperature in the Cutting Zone (T)

The equation developed using regression analysis for the output parameter “Temperature in the Cutting Zone (T)” is given as follows [Rana et al. (2020)]:

Regression Equation:

$$Temp = -32.9 - 131.0 \text{ Feed} + 0.3676 \text{ Speed} + 228.0 \text{ DOC}$$

The predictive equation developed for the optimization model is as follows:

GA Predictive Equation:

$$Temp = 232.293 * X_1^{(-0.385)} * X_2^{0.000878} * X_3^{0.525}$$

X_1 , X_2 & X_3 are feed, cutting speed and depth of cut, respectively.

Hence,

GA Predictive Equation:

$$Temp = 232.293 * feed^{(-0.385)} * speed^{0.000878} * DOC^{0.525}$$

Optimized Result:

$$T = 183.282^{\circ}\text{C at } feed = 0.25, speed = 360 \text{ and } DOC = 0.6 \text{ mm}$$

After setting the fixed parameters, the yielded optimized output parameter i.e. optimized Temperature in the Cutting Zone (T) was 183.282 °C. The value of the optimized Temperature in the Cutting Zone (T) is shown in figure 5.37 along with the genetic algorithm graph for the best value and the average value of Temperature in the Cutting Zone. The optimized value of Temperature in the Cutting Zone (T) was obtained at a feed of 0.25 mm/rev, a cutting speed of 360 m/min and a depth of cut of 0.6 mm. Whereas, the Pareto chart of the standardized effects for the Temperature in the Cutting Zone as the response variable is shown in Figure 5.38.

The graph between fitness value and generation in Figure 5.37 reveals the average and mean fitness values of the output parameter i.e. the temperature in the cutting zone for a given generation. The optimization cycle for the developed model ran for 220 generations, after which the best and mean values were recorded as 183.2821 °C and 183.286 °C respectively. The graph, individual vs generation, depicts the development of 220 generations consisting of 2% of the elite population and 2% of the mutated population from the previous generation.

The Pareto graph explains the contribution or significance of the input parameters to a particular output parameter. The graph in Figure 5.38 shows that the depth of cut significantly affects the temperature in the cutting zone which is followed by cutting speed. Feed rate is the least significant parameter for evaluating temperature in the cutting zone.

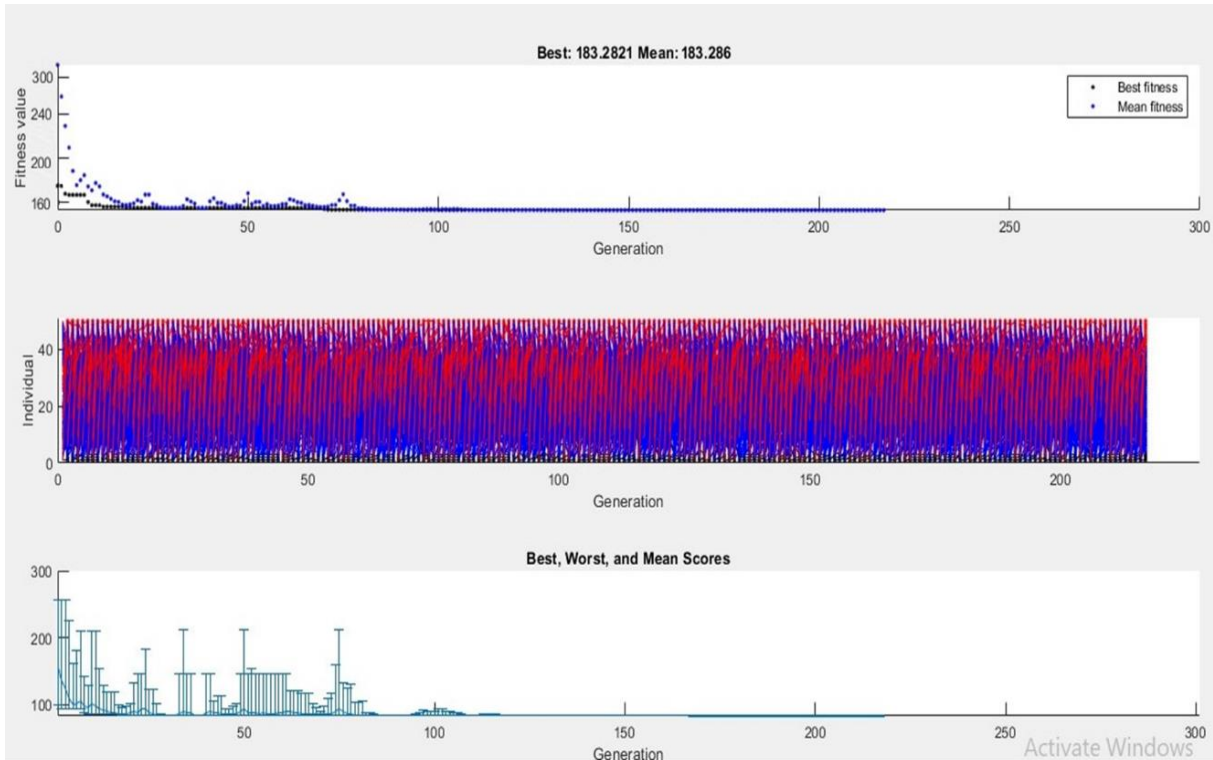


Figure 5.37: Genetic Algorithm Graph for the best value and the average value of Temperature in the Cutting Zone.

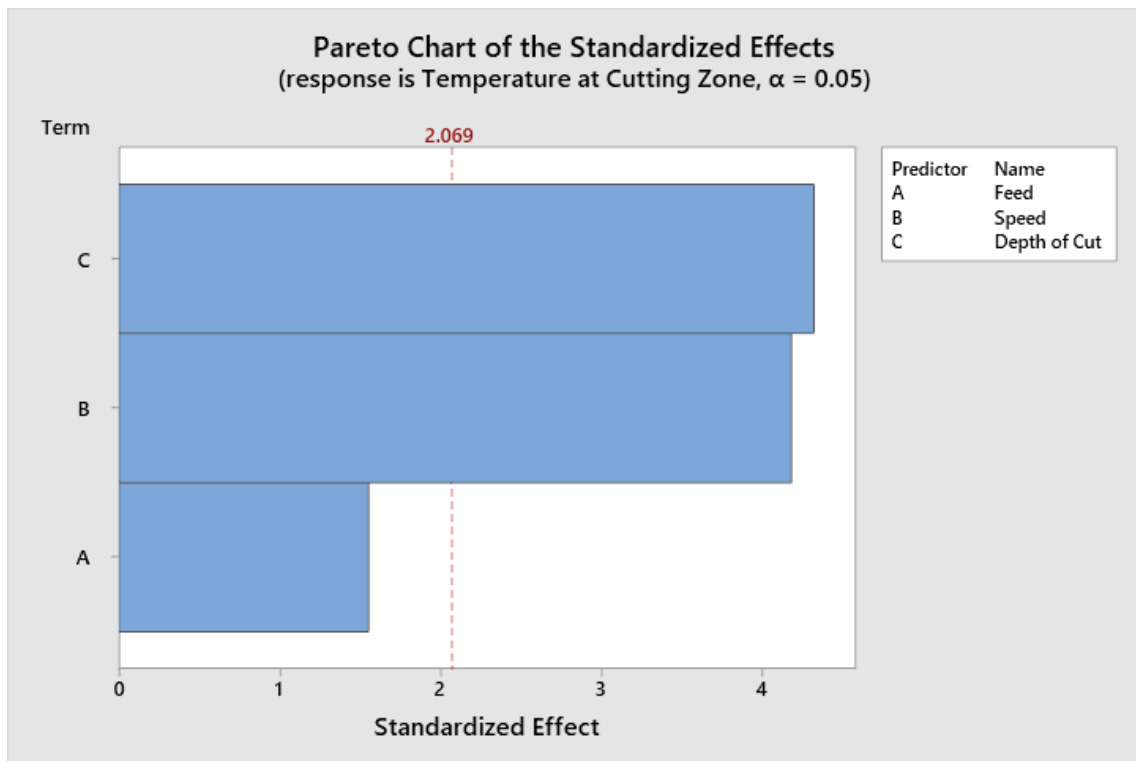


Figure 5.38: Pareto Chart of the Standardized effects for the Temperature in the Cutting Zone as the response variable.

5.6. Experimentation using Developed Coated Textured Tool on CNC

Machine Tool

While going through the extensive literature we got to know, texturing is being accommodated on the CNC tool inserts by researchers nowadays. After carefully considering the available resources we developed coating on the textured CNC tool inserts. We have generated four texturing patterns on the WC tool inserts.

The microscopic images of the four generated texturing patterns are shown in Figure 5.39 and Figure 5.40. The notation used for the generated four texturing patterns is as follows:

L_1 = Denoted to the Line texturing perpendicular to the edge of the tool nose;

S_1 = Denoted to the Sine Wave texturing perpendicular to the edge of the tool nose;

L_2 = Denoted to the Line texturing parallel to the edge of the tool nose;

S_2 = Denoted to the Sine Wave texturing parallel to the edge of the tool nose.

We have used LMW® Machine Tool Division make “HORIZONTAL CNC LATHE - LL20T L3” of the Metal Cutting Lab in the mechanical engineering department at Delhi Technological University, Delhi, to perform the experimentation using the self-developed textured tools.

We have used the same size workpiece i.e. a round bar of 50 mm in diameter and 610 mm in length for the machining process. The levels of input parameters selected for the experimentation are mentioned in Table 5.18. The levels were decided by analyzing the results obtained in the previous experimentations along with the literature. Detailed experimental conditions viz. the design of experiments selected for the experiments is an L_{16} orthogonal array (OA), which is depicted in Table 5.19.



Figure 5.39: Microscopic images of the CNC tool inserts having Line and Sine Wave texturing perpendicular to the edge of the tool nose.

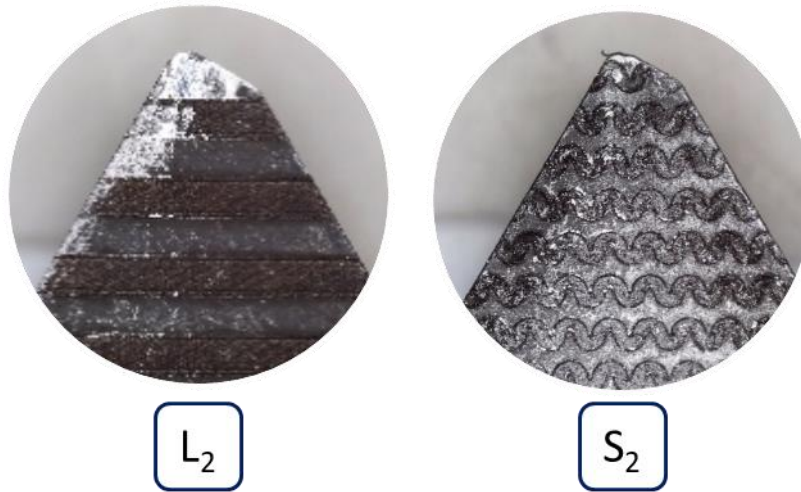


Figure 5.40: Microscopic images of the CNC tool inserts having Line and Sine Wave texturing parallel to the edge of the tool nose.

Table 5.18: Levels of input parameters selected for using the developed textured coated tools on the CNC Machine Tool

S. No.	Input Parameters	Unit	Level 1	Level 2	Level 3	Level 4
1	Type of Tool	---	L ₁	L ₂	S ₁	S ₂
2	Feed (f)	mm/rev	0.125	0.25	---	---
3	Cutting Speed (V _c)	m/min	360	480	---	---
4	Depth of Cut (DOC)	mm	0.2	0.4	---	---
Work Material: Aluminium 6061, Workpiece Diameter: 50 mm, Total length of the Workpiece: 610 mm, Temperature: Room Temperature, Machining: Dry Machining						

Table 5.19: The L₁₆ OA for Machining on CNC Machine Tool using the developed textured coated tools.

Exp. No.	Type of Tool	Feed (mm/rev)	Speed (m/min)	Depth of Cut (mm)
1	L1	0.125	360	0.2
2	L1	0.125	360	0.2
3	L1	0.25	480	0.4
4	L1	0.25	480	0.4
5	L2	0.125	360	0.4
6	L2	0.125	360	0.4
7	L2	0.25	480	0.2
8	L2	0.25	480	0.2
9	S1	0.125	480	0.2
10	S1	0.125	480	0.2
11	S1	0.25	360	0.4
12	S1	0.25	360	0.4
13	S2	0.125	480	0.4
14	S2	0.125	480	0.4
15	S2	0.25	360	0.2
16	S2	0.25	360	0.2

As already mentioned in section 5.4 of this chapter, as per the TOPSIS (Technique for Order of Preference by Similarity to Ideal Solution) method, there should be a maximum value of the relative closeness for obtaining the optimum cutting conditions [43]. Here in this set of experiments, we have used mixed levels of input parameters for designing the OA for the experimentation.

As we already know that when compared to other multi-response optimization techniques such as Artificial Neural Network (ANN), TOPSIS (a technique for order of preference by similarity to ideal solution) method has fewer computational steps. This method provided an optimum solution with the shortest distance from the positive ideal solution and the farthest from the negative solution.

5.6.1. TOPSIS

Selecting the Orthogonal Array OA

With the intention of deciding the optimum combination of the selected input parameters for decided response variables, we have used the Taguchi method. Keeping the aim to find out the effect of input parameters viz. type of tool, feed (f), cutting speed (V_c) and Depth of cut (DOC) on the response variables (performance indicators) viz. Crater Wear (μm), Flank Wear (μm) Cutting Force (N), Surface Roughness (μm) and Temperature at Cutting Zone ($^{\circ}\text{C}$), an appropriate orthogonal array (OA) was selected using the Taguchi method. The OA is selected to have a minimum number of experiments i.e. to have the least number of experimental runs.

In this research work, we have used four input parameters ($P = 4$) having mixed levels for the experimentation i.e. first parameter has four levels ($L = 4$) and all the remaining parameters have 2 levels ($L = 2$). Hence, we opted for the Mixed Level, L_{16} orthogonal array (OA), which is shown in Table 5.19.

TOPSIS based on entropy weight method

To accomplish the optimal solution we used a statistical tool. This method enlarges the distance from a negative ideal solution and also shortens the distance from a positive ideal solution.

Moreover, this ranking method uses the closeness of the optimal solution from the positive ideal solution [41].

Formation of decision matrix

Using the responses, a decision matrix A is formed. This decision matrix is evaluated for n responses of variables containing m of values [42]. The response variables in the form of an initial decision matrix are also shown in Table 5.20.

$$A = (a_{ij})_{m \times n} = \begin{bmatrix} a_{11} & \cdots & a_{1n} \\ \vdots & \ddots & \vdots \\ a_{m1} & \cdots & a_{mn} \end{bmatrix} \quad (1)$$

Standardizing the decision matrix

To have the uniform units for all the responses viz. Crater Wear (μm), Flank Wear (μm), Cutting Force (N), Surface Roughness (μm) and Temperature at Cutting Zone ($^{\circ}\text{C}$), we have normalised the decision matrix [43]. In our research, we have used the criterion of “lower the better” for all the responses. Table 5.21 shows the response variables in the form of the obtained normalised decision matrix.

If (a_{ij}) denotes the response variables for lower the better standard.

$$(r_{ij}) = \frac{a_{ij}}{\sqrt{\sum_{i=1}^n a_{ij}^2}} \quad (2)$$

Consequently, evaluating the obtained standardized decision matrix by

$$R = (r_{ij})_{m \times n} \quad (3)$$

Table 5.20: L₁₆ Orthogonal Array using the input parameters along with the response variables in the form of initial decision matrices.

Input Parameters				Response Variables				
Type of Tool	Feed (mm/rev)	Speed (m/min)	Depth of Cut (mm)	Crater Wear (μm)	Flank Wear (μm)	Cutting Force (N)	Surface Roughness (μm)	Temperature at Cutting Zone (°C)
L1	0.125	360	0.2	676.368	298.368	363.45	0.761	270.5
L1	0.125	360	0.2	629.846	251.846	372.79	0.712	280.2
L1	0.25	480	0.4	860.579	482.579	365.13	0.804	297.2
L1	0.25	480	0.4	757.195	379.195	406.6	0.873	155.4
L2	0.125	360	0.4	612.459	234.459	436.94	0.981	167.2
L2	0.125	360	0.4	601.18	223.18	425.37	1.074	147.6
L2	0.25	480	0.2	597.421	219.421	326.1	0.744	161.8
L2	0.25	480	0.2	571.105	193.105	338.44	0.767	130.3
S1	0.125	480	0.2	676.368	298.368	346.5	0.861	153.4
S1	0.125	480	0.2	854.94	476.94	350.11	0.64	231.7
S1	0.25	360	0.4	673.549	295.549	326.28	0.565	241.4
S1	0.25	360	0.4	777.872	399.872	351.09	0.567	258.4
S2	0.125	480	0.4	488.398	110.398	220.91	0.468	140.6
S2	0.125	480	0.4	450.805	72.805	228.15	0.467	128.8
S2	0.25	360	0.2	418.85	83.94	377.45	0.44	132.8
S2	0.25	360	0.2	409.921	45.759	365.27	0.491	136

Using the entropy method for determining the weight for the response variable

The entropy technique was used for calculating the weight for all the response variables. The calculation for the entropy of the performance indicator for the j^{th} response variable is done by:

$$e_j = -k \sum_i^m r_{ij} \ln r_{ij}, j = 1, 2, \dots, n \text{ and} \quad (4)$$

$$k = \frac{1}{\ln(m)} \quad (5)$$

Calculation of the performance indicator's total entropy done by

$$E = -\frac{1}{\ln(m)} * \sum_{j=1}^n \sum_{i=1}^m r_{ij} \ln(r_{ij}) \quad (6)$$

Calculation of the inequality for the j^{th} response variable is done by:

$$d_j = |1 - e_j|, \quad j = 1, 2, 3, \dots, n \quad (7)$$

Whenever d_j will be larger, r_{ij} will be propagated more which in turn will make the response variable “ j ” the important one. Similarly, when r_{ij} , becomes comparatively saturated, it makes “ j ” the least important response variable.

Table 5.21: Response variables in the form of obtained Normalised decision matrix

Run No.	Performance Indicators (Response Variables)				
	Crater Wear (μm)	Flank Wear (μm)	Cutting Force (N)	Surface Roughness (μm)	Temperature at Cutting Zone ($^{\circ}\text{C}$)
1	0.262876	0.260715	0.256259	0.262325	0.34031
2	0.244795	0.220063	0.262844	0.245434	0.352513
3	0.334471	0.421678	0.257443	0.277147	0.3739
4	0.29429	0.331341	0.286682	0.300933	0.195505
5	0.238037	0.204871	0.308074	0.338161	0.21035
6	0.233654	0.195015	0.299917	0.370219	0.185692
7	0.232193	0.19173	0.229924	0.256465	0.203557
8	0.221965	0.168736	0.238625	0.264393	0.163927
9	0.262876	0.260715	0.244308	0.296796	0.192989
10	0.33228	0.416751	0.246853	0.220615	0.291496
11	0.26178	0.258251	0.230051	0.194762	0.3037
12	0.302326	0.349409	0.247544	0.195451	0.325087
13	0.18982	0.096466	0.155758	0.161325	0.176886
14	0.175209	0.063617	0.160862	0.16098	0.16204
15	0.16279	0.073347	0.26613	0.151673	0.167073
16	0.159319	0.039984	0.257542	0.169253	0.171098

Calculation of the weight factor was done by:

$$w_j = d_j / \sum_{j=1}^n d_j \quad (8)$$

The weight of the evaluated responses is shown in Table 5.22 and is also plotted in the form of a graph, depicted in Figure 5.41.

Table 5.22: Weights of the performance indicators.

Crater Wear	Flank Wear	Cutting Force	Surface Roughness	Temperature at Cutting Zone
0.211515	0.1645	0.215906	0.206682	0.201397

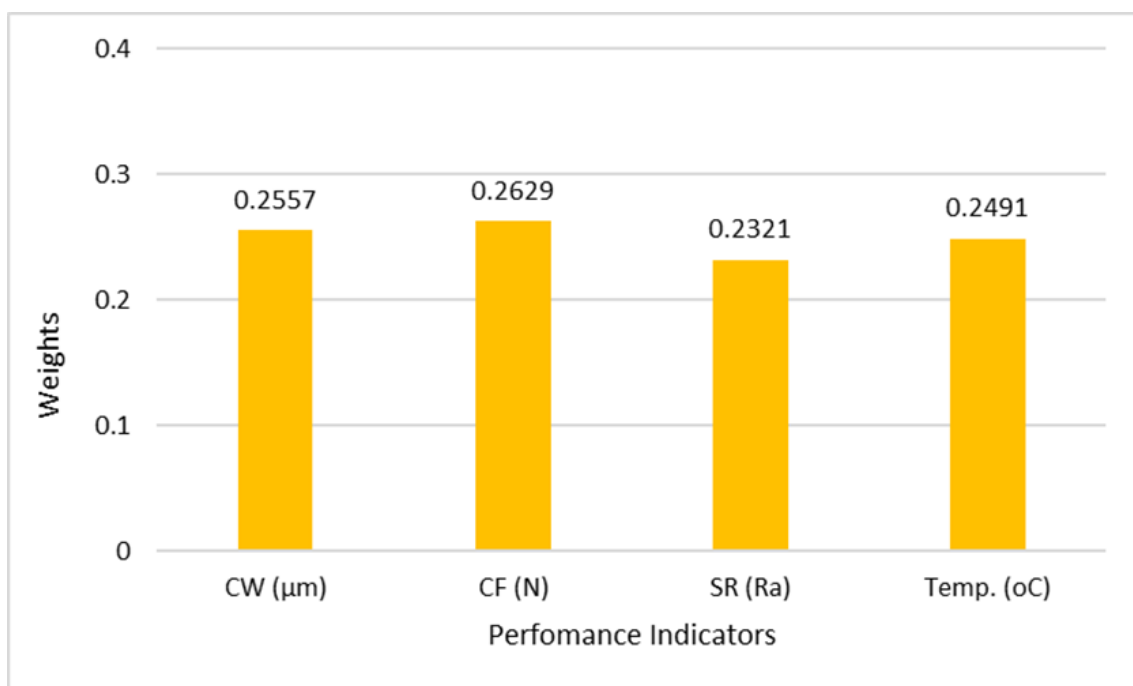


Figure 5.41: The weight of the evaluated responses to the performance indicators.

Determination of Weight

R = Standardized decision matrix = $(r_{ij})_{m \times n}$,

w_j = Calculated weight of the evaluated responses,

The weighted decision matrix of all the response variables was calculated by the following matrix and is shown in Table 5.23:

$$v = \begin{bmatrix} w_1 r_{11} & w_2 r_{12} \cdots & w_n r_{1n} \\ \vdots & \ddots & \vdots \\ w_1 r_{m1} & w_2 r_{m2} \cdots & w_n r_{mn} \end{bmatrix} = \begin{bmatrix} v_{11} & v_{12} \cdots & v_{1n} \\ \vdots & \ddots & \vdots \\ v_{m1} & v_{m2} \cdots & v_{mn} \end{bmatrix} \quad (9)$$

Table 5.23: Performance indicator's standardized and weighted decision matrices.

Run No.	Crater Wear	Flank Wear	Cutting Force	Surface Roughness	Temperature at Cutting Zone
1	0.055602	0.042888	0.055328	0.054218	0.068537
2	0.051778	0.0362	0.05675	0.050727	0.070995
3	0.070746	0.069366	0.055584	0.057281	0.075302
4	0.062247	0.054506	0.061897	0.062197	0.039374
5	0.050349	0.033701	0.066515	0.069892	0.042364
6	0.049421	0.03208	0.064754	0.076518	0.037398
7	0.049112	0.03154	0.049642	0.053007	0.040996
8	0.046949	0.027757	0.051521	0.054645	0.033014
9	0.055602	0.042888	0.052748	0.061342	0.038867
10	0.070282	0.068556	0.053297	0.045597	0.058706
11	0.055371	0.042482	0.049669	0.040254	0.061164
12	0.063947	0.057478	0.053446	0.040396	0.065471
13	0.04015	0.015869	0.033629	0.033343	0.035624
14	0.037059	0.010465	0.034731	0.033272	0.032634
15	0.034432	0.012066	0.057459	0.031348	0.033648
16	0.033698	0.006577	0.055605	0.034982	0.034459

The calculation for finding the negative and positive ideal solution

The expression used for determining the positive ideal solution is mentioned below:

$$V^+ = \{v_1^+, v_2^+, \dots, v_n^+\} = \{(\max v_{ij} | j \in J_1), (\min v_{ij} | j \in J_2) | i = 1, 2, \dots, m\} \quad (10)$$

The expression used for determining the negative ideal solution is mentioned below:

$$V^- = \{v_1^-, v_2^-, \dots, v_n^-\} = \{(\min v_{ij} | j \in J_1), (\max v_{ij} | j \in J_2) | i = 1, 2, \dots, m\} \quad (11)$$

Where,

J_1 = variable for larger the better;

J_2 = variable for smaller the better.

Table 5.24: Positive Matrix for the performance indicators.

Crater Wear	Flank Wear	Cutting Force	Surface Roughness	Temperature at Cutting Zone
0.033698	0.006577	0.033629	0.031348	0.032634

Table 5.25: Negative Matrix for the performance indicators.

Crater Wear	Flank Wear	Cutting Force	Surface Roughness	Temperature at Cutting Zone
0.070746	0.069366	0.066515	0.076518	0.075302

Determination of the relative distance:

$$S_i^+ = \sqrt{\sum_{j=1}^n (v_{ij} - v_j^+)^2}, i = 1, 2, 3, \dots, m \quad (12)$$

$$S_i^- = \sqrt{\sum_{j=1}^n (v_{ij} - v_j^-)^2}, i = 1, 2, 3, \dots, m \quad (13)$$

Where,

S_i^+ = Relative distance between V_{ij} and positive ideal solution V_j^+

S_i^- = Relative distance between V_{ij} and negative ideal solution V_j^-

The positive and negative matrix for the performance indicators is shown in Table 5.24 and Table 5.25 respectively. Whereas, the relative distance of the considered performance indicators is shown in Table 5.26.

Formation of sequence table while evaluating the TOPSIS value

The calculated preferred value “C_j” and assigned rank of the experimental value are also shown in Table 5.26.

$$C_j = S_i^- / (S_i^+ + S_i^-) \quad (15)$$

Table 5.26: Standardized and weighted decision matrices for performance indicators.

Run No.	S_i^+	S_i^-	C_j	Rank
1	0.063883	0.039983	0.384947	12
2	0.059883	0.047316	0.441384	11
3	0.091049	0.022125	0.195498	16
4	0.070059	0.042548	0.377843	13
5	0.060619	0.053074	0.466818	10
6	0.062684	0.057314	0.477621	9
7	0.040696	0.062556	0.605861	6
8	0.038564	0.069203	0.642157	5
9	0.055698	0.051747	0.481617	8
10	0.080307	0.037511	0.318381	15
11	0.053939	0.052515	0.493315	7
12	0.071124	0.04195	0.370992	14
13	0.011869	0.091203	0.88485	2
14	0.005597	0.096463	0.945161	1
15	0.024486	0.091975	0.789751	4
16	0.022349	0.093954	0.80784	3

Table 5.27: Best and worst combination of the Input Parameters

	Input Parameters			
	Type of Tool	Feed	Speed	Depth of Cut
Best combination	S2	0.125	480	0.4
Worst combination	L1	0.25	480	0.4

Table 5.28: Best and worst combinations of the Response Variable

	Response Variable				
	Crater Wear	Flank Wear	Cutting Force	Surface Roughness	Temperature at Cutting Zone
Best combination	450.805	72.805	228.15	0.467	128.8
Worst combination	860.579	482.579	365.13	0.804	297.2

The effects plots of all the response variables viz. Crater Wear, Flank Wear, Cutting Force, Surface Roughness, and Temperature at Cutting Zone vs all the input parameters viz. Type of Tool, Feed, Speed, and Depth of Cut have been plotted separately in Figure 5.42, Figure 5.43, Figure 5.44, Figure 5.45 and Figure 5.46 respectively.

As can be seen in Figure 5.42, crater wear was at its lowest value when machining was done using S₂ tool inserts i.e. textured coated tool inserts having sine wave texturing parallel to the edge of the tool nose. Crater wear was low with low values of feed, speed and DOC. These effects can also be seen in Table 5.27 of the Best and worst combinations of the Input Parameters.

Similarly, in Figure 5.43, it is also observed that flank wear was at its lowest value when machining was done using S_2 tool inserts i.e. textured coated tool inserts having sine wave texturing parallel to the edge of the tool nose. Flank wear was also low with low values of feed, speed and DOC. These effects can also be seen in Table 5.27 of the Best and worst combinations of the Input Parameters.

Similarly, in Figure 5.44, it is also observed that cutting force was at its lowest value when machining was done using S_2 tool inserts i.e. textured coated tool inserts having sine wave texturing parallel to the edge of the tool nose. The cutting force was also low with low values of feed, and DOC. But, it was low with the higher speed. These effects can also be seen in Table 5.27 of the Best and worst combinations of the Input Parameters.

Similarly, in Figure 5.45, it is also observed that surface roughness was at its lowest value when machining was done using S_2 tool inserts i.e. textured coated tool inserts having sine wave texturing parallel to the edge of the tool nose. The surface roughness was also low with low values of speed, and DOC. But, it was low with the higher feed. These effects can also be seen in Table 5.27 of the Best and worst combinations of the Input Parameters.

Similarly, in Figure 5.46, it is observed that the temperature obtained at the cutting zone was at its lowest value when machining was done using S_2 tool inserts i.e. textured coated tool inserts having sine wave texturing parallel to the edge of the tool nose. The temperature obtained at the cutting zone was also low with low values of DOC, and high values of speed. But, it was low with the average feed. These effects can also be seen in Table 5.27 of the Best and worst combinations of the Input Parameters.

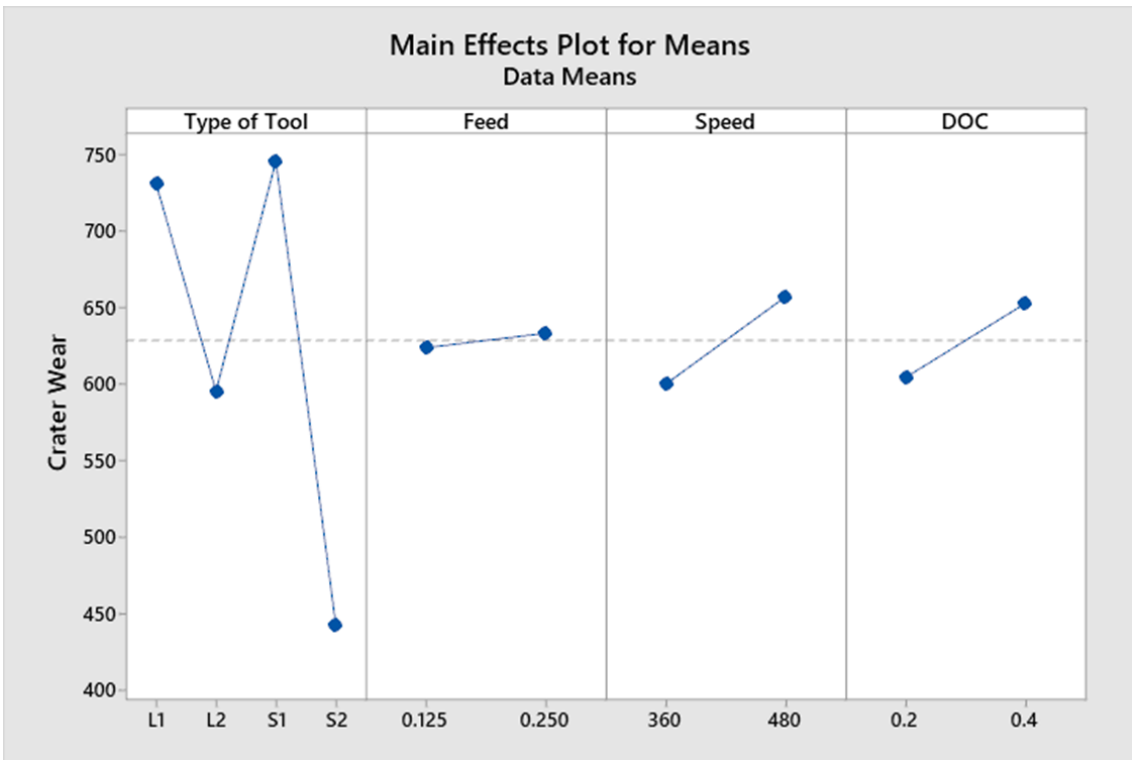


Figure 5.42: Effect plot of crater wear vs Type of Tool, Feed, Speed and DOC.



Figure 5.43: Effect plot of flank wear vs Type of Tool, Feed, Speed and DOC.

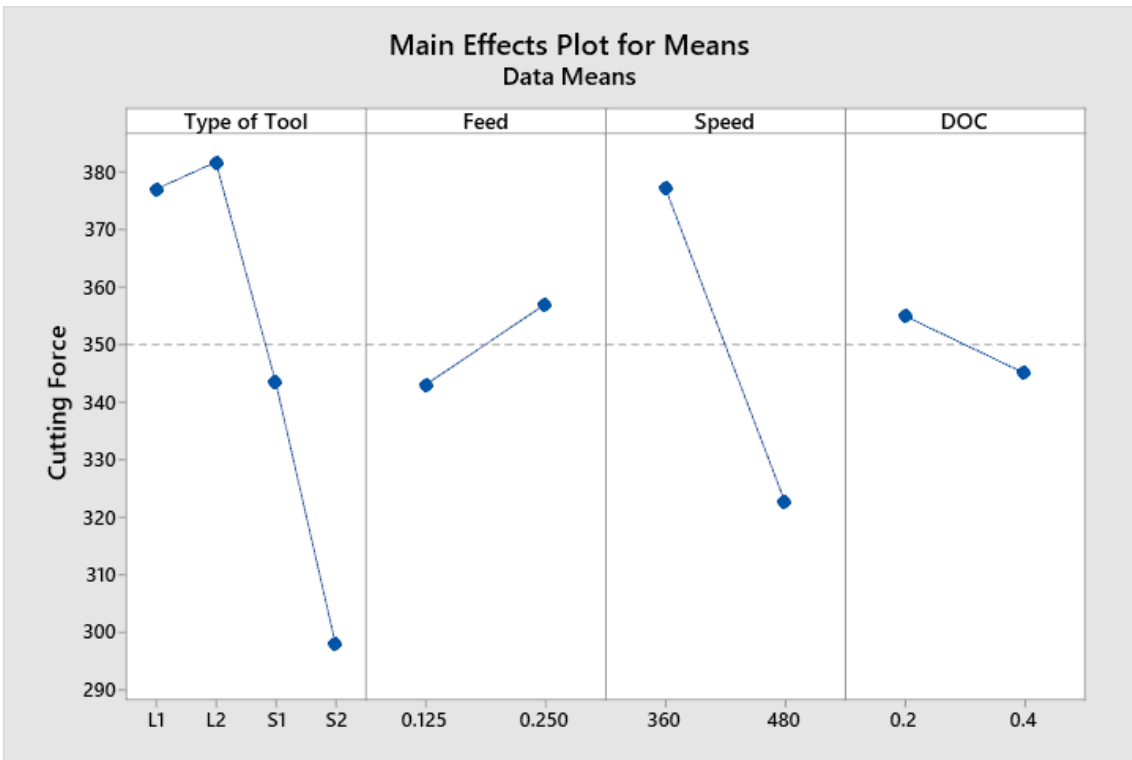


Figure 5.44: Effect plot of cutting force vs Type of Tool, Feed, Speed and DOC.

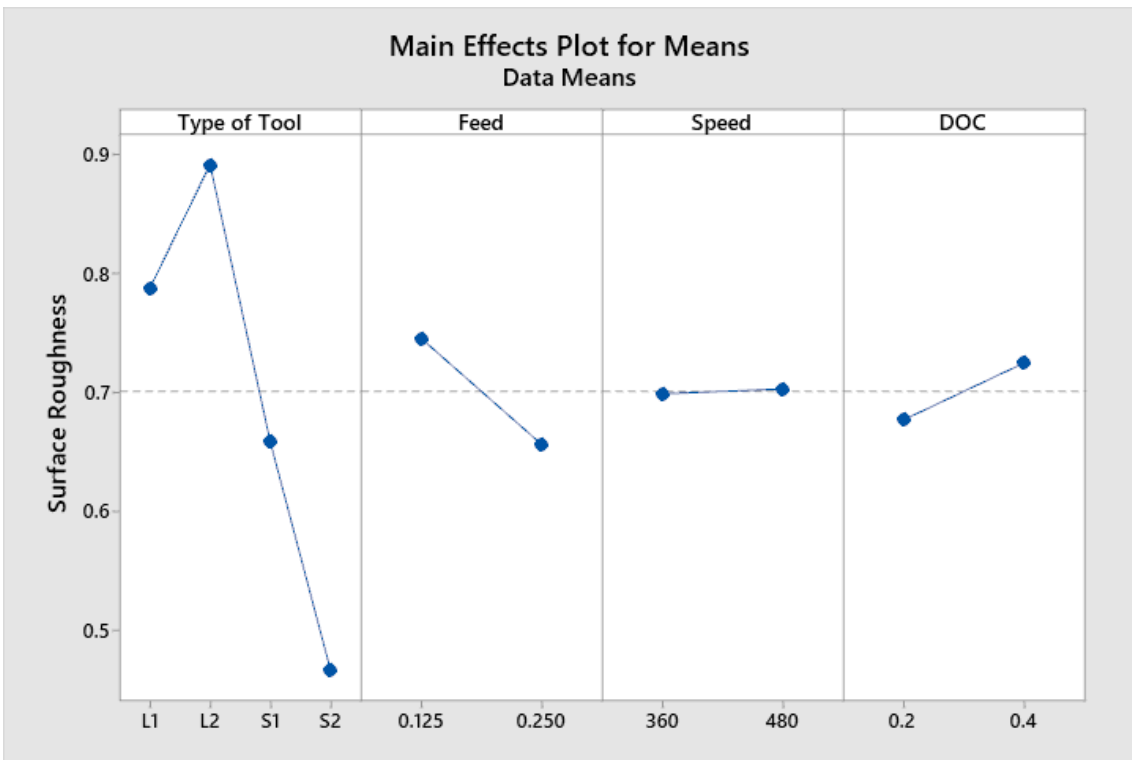


Figure 5.45: Effect plot of Surface Roughness vs Type of Tool, Feed, Speed and DOC.

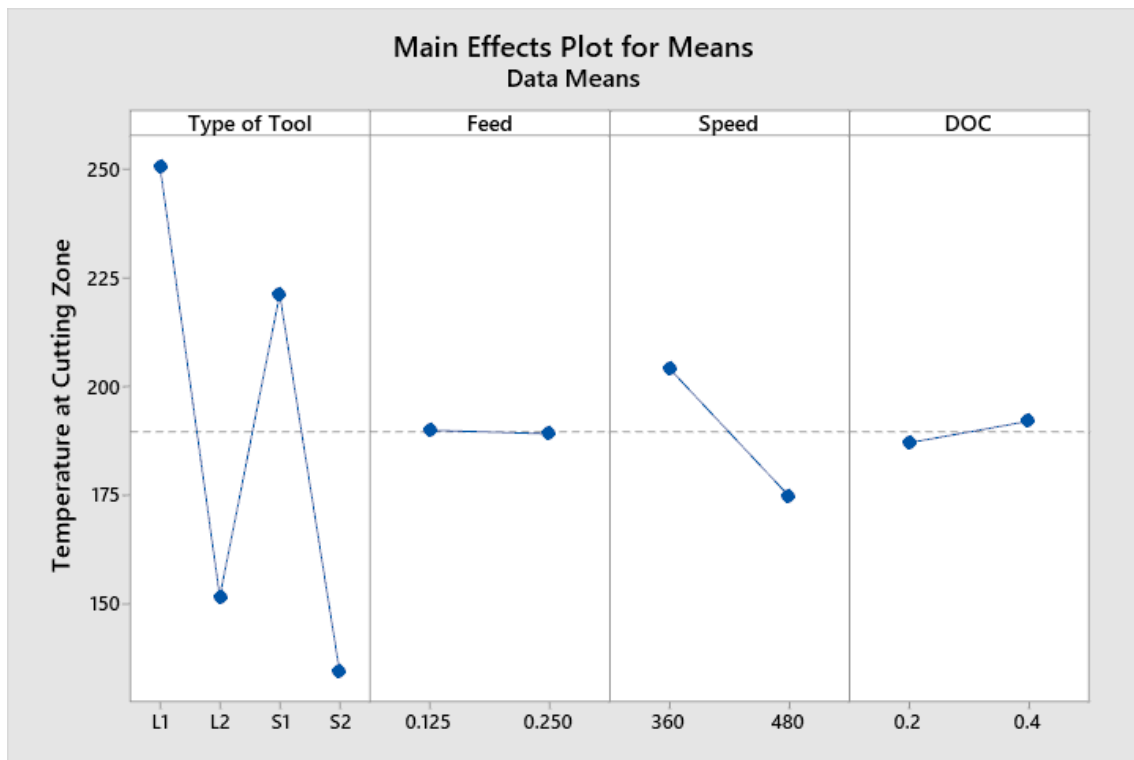


Figure 5.46: Effect plot of Temperature at Cutting Zone vs Type of Tool, Feed, Speed and DOC.

5.6.2. Discussion

In this research, for obtaining the optimal performance of the machining process the minimization characteristic for Crater Wear (μm), Flank Wear (μm), Cutting Force (N), Surface Roughness (μm) and Temperature at Cutting Zone ($^{\circ}\text{C}$) were taken. The obtained results of best and worst combinations for the input parameter and response variable are shown in Table 5.27 and Table 5.28 respectively.

As mentioned in above section 5.4.1, the minimum values of Crater Wear (μm), Flank Wear (μm), Cutting Force (N), Surface Roughness (μm) and Temperature at Cutting Zone ($^{\circ}\text{C}$) are indicated by the maximum relative closeness. The combination of self-developed DLC coated textured tool (S_2) insert with the feed of 0.125 mm/rev, speed of 480 m/min and 0.4 mm depth

of cut is the optimal values of input parameters for achieving the minimum values of response variables using the “S₂” Tool inserts in a turning process [31].

Generally, an increase in the cutting speed and feed, will either decrease the tool flank wear or creates the formation of a built-up edge (BUE) on the tool inserts [24]. But here the cutting force decreases with the decrease in cutting speed and depth of cut for the textured cutting inserts due to the thermal softening of the workpiece at the interface [115]. The chips get trapped in the gap widths of the texturing, increasing the stress on the rake surface, which increases the flank and crater wear but subsequently decreases the surface roughness and the temperature at cutting zone [115]. Surface roughness decreases due to the abrasive wear and delamination of coating material on the tool surface.

The optimum value indicates that while using the self-developed DLC coated textured tool (S₂) insert with the low level of feed, and cutting speed along with the high level of depth of cut, we can reduce the Crater Wear (μm), Flank Wear (μm), Cutting Force (N), Surface Roughness (μm) and Temperature at Cutting Zone ($^{\circ}\text{C}$) [15].

Chapter 6: Conclusions and Future Scope

6. Introduction

This chapter provides the conclusions obtained through detailed experimentation using the self-developed DLC coated tungsten carbide (WC) tool inserts.

6.1. Conclusions

In this research, the diamond-like coating was developed on the tungsten carbide (WC) tool inserts to minimize the selected response variables viz. crater wear, flank wear, cutting force, surface roughness, and temperature in the cutting zone. From this research, the following conclusions were drawn:

- ❑ Successfully able to develop diamond coating on the tungsten carbide (WC) tool inserts using an agro-waste, whose results are at par with commercial diamond-coated tool inserts.
- ❑ The FESEM images of the developed coated tools insert show us the presence of diamond crystals on the developed coated surface.
- ❑ X-Ray Diffraction (XRD) spectra for the coated tungsten carbide tool inserts also confirmed the presence of diamond in the developed coating on the tungsten carbide (WC) tool inserts.
- ❑ The peak at 1338 cm^{-1} in the Raman spectra also supported the presence of diamond in the developed coating on the tungsten carbide (WC) tool inserts. The result of the presence of diamond is in correlation with the SEM images.
- ❑ It was observed that the hardness of the WC was increased by a factor of 1.5 after the coating process. The average Vickers hardness was 953.95 HV for the uncoated

tungsten carbide (WC) and for the DLC coated WC, the hardness increased to 1478.78 HV.

- ❑ It was also noticed that the compressive residual stress of the WC was increased by 252.91% after the coating process in comparison to the uncoated tungsten carbide (WC) tool inserts. As the average values of residual stress for the uncoated tool inserts and DLC coated tool inserts were 162 MPa and 409.73 MPa respectively.
- ❑ Whereas the compressive residual stress of the WC was increased by 71.17% after the coating process compared to the commercial coated tool inserts. As the average value of residual stress for the market purchased coated tool inserts was 239.36 MPa.

While optimizing the process parameters of the turning process on the conventional lathe machine tool using TOPSIS, the following conclusions were drawn:

- ❑ The optimum values for attaining the minimum value of the selected response variables were achieved by the self-developed DLC coated inserts.
- ❑ The optimum value of depth of cut for achieving the minimum value of the selected response variables was found to be 0.192 mm.
- ❑ The optimum values of cutting speed and feed for achieving the minimum value of the selected response variables were found to be 60.52 m/min and 0.15 mm/rev respectively.

While optimizing the process parameters of the turning process on the CNC lathe machine tool using a Genetic Algorithm, the following conclusions were drawn:

- ❑ The obtained optimized value of crater wear was found to be 461.07(μm), at a feed of 0.375mm/rev, a speed of 360m/min and a depth of cut of 0.2 mm.

- ❑ The obtained optimized value of flank wear was found to be 342.08 (μm), at a feed of 0.125mm/rev, a speed of 600m/min, and a depth of cut of 0.4 mm.
- ❑ The obtained optimized value of cutting force was found to be 216.59 (N), at a feed of 0.25mm/rev, a speed of 360m/min, and a depth of cut of 0.6 mm.
- ❑ The obtained optimized value of surface roughness was found to be 0.761(μm), at a feed of 0.375mm/rev, a speed of 360m/min, and a depth of cut of 0.4 mm.
- ❑ The obtained optimized value of temperature at cutting zone was found to be 183.28($^{\circ}\text{C}$), at a feed of 0.25mm/rev, a speed of 360m/min, and a depth of cut of 0.6 mm.
- ❑ Incidentally, all these optimized results were obtained by the self-developed DLC coated tool inserts.

We developed the DLC coating on the various textured WC tool inserts. After optimizing the process parameters of the turning process on the CNC lathe machine tool using TOPSIS, the following conclusions were drawn:

- ❑ The best results for achieving the minimum value of the selected response variables were obtained using Tool S_2 i.e. tool where Sine Wave texturing was parallel to the edge of the tool nose.
- ❑ The optimum value of depth of cut, cutting speed and feed for achieving the minimum value of the selected response variables using the self-developed tool inserts in a turning process, was found to be 0.4mm, 480 m/min and 0.125 mm/rev respectively.

6.2. Limitations of Research Work

Complications confronted during the present experimental investigation include the following concerns:

- ❑ The CVD process is a critical process, and the major limitation was the size of the tube in which the substrate was inserted for the coating procedure. The limitation of tube size limits the size of the substrate hence, the substrate of a certain size can only be coated.
- ❑ As mentioned about the size of the tube. Hence, one can only insert a very limited number of substrate materials at one go for the coating procedure. Hence, that diminishes the chances of constant or same coating thickness on all the samples. This was observed during our research work.

The next section includes future research scopes in the extension of the present investigation.

6.3. Future Scope

Present research subject matter has been extremely impactful pertaining to the novel advancements in DLC coating using the environmentally friendly method. Though this research provides a comprehensive blend of development, characterizing, and parameter optimization of machining operation with enhanced properties of the developed coated tools, however, there is plausible scope for future research, which may lead to better scientific aspects in detail. The scope of diversified future works in perpetuation with the present study has been discussed below:

- ❑ There is scope to use other bio-waste materials as carbon precursors for the production of activated carbon, which can further be used in many places including the CVD process for diamond coating.

- ❑ One can use different tool materials like non-ceramics, as the substrate for the growth of diamond coating on the surface.
- ❑ The technology can be further changed a bit to accommodate the coating on more complex tools shapes like milling and drilling tools.
- ❑ The tribological test can be performed at various ranges of temperatures.

6.4. Summary

This chapter consisted of conclusions and limitations of our research work along with the future scope.

References

- [1]. P. Huang, X. Wu, S. To, L.M. Zhu, Z. Zhu, Deterioration of form accuracy induced by servo dynamics errors and real-time compensation for slow tool servo diamond turning of complex-shaped optics, *Int. J. Mach. Tools Manuf.* 154 (2020) 103556. <https://doi.org/10.1016/j.ijmachtools.2020.103556>.
- [2]. J.P. Davim, Diamond tool performance in machining metal–matrix composites, *J. Mater. Process. Technol.* 128 (2002) 100–105. [https://doi.org/10.1016/S0924-0136\(02\)00431-4](https://doi.org/10.1016/S0924-0136(02)00431-4).
- [3]. R. Rana, Q. Murtaza, R.S. Walia, GA based optimization of tri-biological behaviour of diamond coated tungsten carbide, *World J. Eng.* 17 (2020) 335–346. <https://doi.org/10.1108/WJE-08-2019-0220>.
- [4]. K. Bobzin, High-performance coatings for cutting tools, *CIRP J. Manuf. Sci. Technol.* 18 (2017) 1–9. <https://doi.org/10.1016/j.cirpj.2016.11.004>.
- [5]. Đ. Gorščak, P. Panjan, M. Čekada, L. Čurković, Comparison of mechanical properties of various PVD hard coatings for forming tools, *Surf. Eng.* 23 (2007) 177–182. <https://doi.org/10.1179/174329407X174452>.
- [6]. W. Huang, J. Yan, Surface formation mechanism in ultraprecision diamond turning of coarse-grained polycrystalline ZnSe, *Int. J. Mach. Tools Manuf.* 153 (2020) 103554. <https://doi.org/10.1016/j.ijmachtools.2020.103554>.
- [7]. I. S. Jawahir, A. K. Balaji, R. Stevenson, and C. A. van Luttervelt, “Towards Predictive Modeling and Optimization of Machining Operations,” in *Manufacturing Science and Engineering: Volume 2*, Nov. 1997, pp. 3–12, doi: 10.1115/IMECE1997-1129.
- [8]. Global Metal Forming Machine Tools Market 2016-2020, Jan 04, 2018, 03:06 ET, <https://www.prnewswire.com/news-releases/global-metal-forming-machine-tools-market-2016-2020-300198814.html>
- [9]. F. Klocke, T. Krieg, Coated Tools for Metal Cutting – Features and Applications, *CIRP Ann.* 48 (1999) 515–525. [https://doi.org/10.1016/S0007-8506\(07\)63231-4](https://doi.org/10.1016/S0007-8506(07)63231-4).
- [10]. Rana, Ramakant, Kunal Rajput, Rohit Saini, and Roop Lal. "Optimization of tool wear: a review." *Int J Mod Eng Res* 4, no. 11 (2014): 35-42.
- [11]. S. Kumar, S. Grover, R.S. Walia, Effect of hybrid wire EDM conditions on generation of residual stresses in machining of HCHCr D2 tool steel under ultrasonic vibration, *Int. J. Interact. Des. Manuf.* 12 (2018) 1119–1137. <https://doi.org/10.1007/s12008-018-0474-8>.
- [12]. N. Gupta, A.K. Agrawal, R.S. Walia, Taguchi based analysis of cutting force in hard turning EN 31 with indigenous developed Carbon Nano Tubes coated insert, *Mater. Today Proc.* 25 (2020) 827–832. <https://doi.org/10.1016/j.matpr.2019.10.001>.
- [13]. Lind, L., Peetsalu, P., Põdra, P., Adoberg, E., Veinthal, R., & Kulu, P. (2010, April). Description of punch wear mechanism during fine blanking process. In *Proc. 7th International Conference DAAAM Baltic Industrial Engineering* (pp. 504-509).
- [14]. N. Kawasegi, H. Sugimori, H. Morimoto, N. Morita, and I. Hori, “Development of cutting tools with microscale and nanoscale textures to improve frictional behavior,” *Precis. Eng.*, vol. 33, no. 3, pp. 248–254, Jul. 2009, doi: 10.1016/j.precisioneng.2008.07.005.
- [15]. S. Lei, S. Devarajan, and Z. Chang, “A study of micropool lubricated cutting tool in machining of mild steel,” *J. Mater. Process. Technol.*, vol. 209, no. 3, pp. 1612–1620, Feb.

- 2009, doi: 10.1016/j.jmatprotec.2008.04.024.R.L. Hatschek, Coatings, Revolution in HSS Tools”, American Machining, March, 1983, pp129–144.
- [16]. Deller, D. L. "Laboratory and Field Test Results on TiN Coated High-Speed Steel Cutting Tools." In National Machine Tool Builder's Assoc. Technical Conference, (1982), pp. 289–313.
- [17]. S. Lei, S. Devarajan, and Z. Chang, “A study of micropool lubricated cutting tool in machining of mild steel,” *J. Mater. Process. Technol.*, vol. 209, no. 3, pp. 1612–1620, Feb. 2009, doi: 10.1016/j.jmatprotec.2008.04.024.
- [18]. A. Fatima and P. T. Mativenga, “Assessment of tool rake surface structure geometry for enhanced contact phenomena,” *Int. J. Adv. Manuf. Technol.*, vol. 69, no. 1–4, pp. 771–776, Oct. 2013, doi: 10.1007/s00170-013-5079-6.
- [19]. [1] T. Obikawa, A. Kamio, H. Takaoka, and A. Osada, “Micro-texture at the coated tool face for high performance cutting,” *Int. J. Mach. Tools Manuf.*, vol. 51, no. 12, pp. 966–972, Dec. 2011, doi: 10.1016/j.ijmachtools.2011.08.013.
- [20]. T. Sugihara and T. Enomoto, “Improving anti-adhesion in aluminum alloy cutting by micro stripe texture,” *Precis. Eng.*, vol. 36, no. 2, pp. 229–237, Apr. 2012, doi: 10.1016/j.precisioneng.2011.10.002.
- [21]. W. Chang, J. Sun, X. Luo, J. M. Ritchie, and C. Mack, “Investigation of microstructured milling tool for deferring tool wear,” *Wear*, vol. 271, no. 9–10, pp. 2433–2437, Jul. 2011, doi: 10.1016/j.wear.2010.12.026.
- [22]. T. Sugihara and T. Enomoto, “Crater and flank wear resistance of cutting tools having micro textured surfaces,” *Precis. Eng.*, vol. 37, no. 4, pp. 888–896, Oct. 2013, doi: 10.1016/j.precisioneng.2013.05.007.
- [23]. J. Xie, M. J. Luo, K. K. Wu, L. F. Yang, and D. H. Li, “Experimental study on cutting temperature and cutting force in dry turning of titanium alloy using a non-coated micro-grooved tool,” *Int. J. Mach. Tools Manuf.*, vol. 73, pp. 25–36, Oct. 2013, doi: 10.1016/j.ijmachtools.2013.05.006.
- [24]. T. Ejieji, S.M. Adedayo, O.W. Bello, S. Abdulkareem, Effect of machining variables and coolant application on HSS tool temperature during turning on a CNC lathe, *IOP Conf. Ser. Mater. Sci. Eng.* 413 (2018) 012004. <https://doi.org/10.1088/1757-899X/413/1/012004>.
- [25]. A. Agrawal, R. Kaur, R.S. Walia, Response surface methodological evaluation of drilling for the optimization of residual compressive strength of bio-based RPUF composite, *Mater. Res. Express.* 6 (2020) 125372. <https://doi.org/10.1088/2053-1591/ab5ea4>.
- [26]. M. Padmakumar, J. Guruprasath, D. Dinakaran, Influence of cryo-processing on properties of tungsten carbide with low, medium and high cobalt content, *Mater. Res. Express.* 6 (2019) 106597. <https://doi.org/10.1088/2053-1591/ab3c97>.
- [27]. Grainger, S., & Blunt, J. (Eds.). (1998). *Engineering coatings: design and application*. Woodhead Publishing.
- [28]. R. Rana, Q. Murtaza, and R. S. Walia, “Studying and Analysing the Properties of the CVD and PVD Coated Tools used in Conventional Lathe Machine Tools and CNC Machine Tools for Turning Processes,” *Int. J. Adv. Prod. Ind. Eng.*, vol. 6, no. 1, pp. 53–83, 2021, DOI: <https://doi.org/10.35121/ijapie202101156>.
- [29]. Lehrich, K., & Kosmol, J. (2010). Trends in the development of machinery and associated technology. In of the 14th International research/expert conference, Mediterranean Cruise (pp. 45-48).

- [30]. C. Mitterer, F. Holler, D. Reitberger, E. Badisch, M. Stoiber, C. Lugmair, R. Nöbauer, T. Müller, R. Kullmer, Industrial applications of PACVD hard coatings, *Surf. Coatings Technol.* 163–164 (2003) 716–722. [https://doi.org/10.1016/S0257-8972\(02\)00685-0](https://doi.org/10.1016/S0257-8972(02)00685-0).
- [31]. H. Shi, F. Chen, Y. Zhou, The Development of Manufacturing Technology of CVD Diamond Thick Film Tools, *IOP Conf. Ser. Mater. Sci. Eng.* 592 (2019) 012064. <https://doi.org/10.1088/1757-899X/592/1/012064>.
- [32]. M.F. Othman, A.R. Bushroa, W.N.R. Abdullah, Evaluation techniques and improvements of adhesion strength for TiN coating in tool applications: a review, *J. Adhes. Sci. Technol.* 29 (2015) 569–591. <https://doi.org/10.1080/01694243.2014.997379>.
- [33]. T. Sakamoto, S. Shimada, H. Kiyono, J. Tsujino, I. Yamazaki, Water vapor-controlled thermal plasma chemical vapor deposition of double-layered TiN/PSZ coatings on Si and WC-Co substrates, *Mater. Sci. Eng. B.* 172 (2010) 201–206. <https://doi.org/10.1016/j.mseb.2010.05.010>.
- [34]. J. Deng, F. Wu, Y. Lian, Y. Xing, S. Li, Erosion wear of CrN, TiN, CrAlN, and TiAlN PVD nitride coatings, *Int. J. Refract. Met. Hard Mater.* 35 (2012) 10–16. <https://doi.org/10.1016/j.ijrmhm.2012.03.002>.
- [35]. K. Khlifi, A.B.C. Larbi, Mechanical properties and adhesion of TiN monolayer and TiN/TiAlN nanolayer coatings, *J. Adhes. Sci. Technol.* 28 (2014) 85–96. <https://doi.org/10.1080/01694243.2013.827094>.
- [36]. J.L. Mo, M.H. Zhu, Tribological oxidation behaviour of PVD hard coatings, *Tribol. Int.* 42 (2009) 1758–1764. <https://doi.org/10.1016/j.triboint.2009.04.026>.
- [37]. X. Chen, H. Liu, Q. Guo, S. Sun, Oxidation behavior of WC–Co hard metal with designed multilayer coatings by CVD, *Int. J. Refract. Met. Hard Mater.* 31 (2012) 171–178. <https://doi.org/10.1016/j.ijrmhm.2011.10.012>.
- [38]. L. Aihua, D. Jianxin, C. Haibing, C. Yangyang, Z. Jun, Friction and wear properties of TiN, TiAlN, AlTiN and CrAlN PVD nitride coatings, *Int. J. Refract. Met. Hard Mater.* 31 (2012) 82–88. <https://doi.org/10.1016/j.ijrmhm.2011.09.010>.
- [39]. S. Hogmark, S. Jacobson, M. Larsson, Design and evaluation of tribological coatings, *Wear.* 246 (2000) 20–33. [https://doi.org/10.1016/S0043-1648\(00\)00505-6](https://doi.org/10.1016/S0043-1648(00)00505-6).
- [40]. E. Kusano, M. Kitagawa, Y. Kuroda, H. Nanto, A. Kinbara, Adhesion and hardness of compositionally gradient TiO₂/Ti/TiN, ZrO₂/Zr/ZrN, and TiO₂/Ti/Zr/ZrN coatings, *Thin Solid Films.* 334 (1998) 151–155. [https://doi.org/10.1016/S0040-6090\(98\)01134-1](https://doi.org/10.1016/S0040-6090(98)01134-1).
- [41]. M. Zhang, Y. He, N. Lin, X. Kang, Effects of carbon addition on the microstructure, mechanical properties, corrosion resistance and tribological behaviour of Ti(C, N)-based cermets, *Mater. Res. Express.* 5 (2018) 126504. <https://doi.org/10.1088/2053-1591/aae00c>.
- [42]. D.B. Miracle, *Metal Matrix Composites for Space Systems: Current Uses and Future Opportunities*, in: *Afford. Met. Compos. High Perform. Appl. II*, John Wiley & Sons, Inc., Hoboken, NJ, USA, 2013: pp. 1–22. <https://doi.org/10.1002/9781118787120.ch1>.
- [43]. K. Mallika, R. Komanduri, Diamond coatings on cemented tungsten carbide tools by low-pressure microwave CVD, *Wear.* 224 (1999) 245–266. [https://doi.org/10.1016/S0043-1648\(98\)00337-8](https://doi.org/10.1016/S0043-1648(98)00337-8).
- [44]. E. Uhlmann, M. Brücher, Wear Behavior of CVD-Diamond Tools, *CIRP Ann.* 51 (2002) 49–52. [https://doi.org/10.1016/S0007-8506\(07\)61463-2](https://doi.org/10.1016/S0007-8506(07)61463-2).
- [45]. S. Shimada, H. Tanaka, M. Higuchi, T. Yamaguchi, S. Honda, K. Obata, Thermo-Chemical Wear Mechanism of Diamond Tool in Machining of Ferrous Metals, *CIRP Ann.* 53 (2004) 57–60. [https://doi.org/10.1016/S0007-8506\(07\)60644-1](https://doi.org/10.1016/S0007-8506(07)60644-1).

- [46]. K. Saijo, M. Yagi, K. Shibuki, S. Takatsu, DEPOSITION OF DIAMOND FOR CUTTING TOOL APPLICATIONS, *Mater. Manuf. Process.* 8 (1993) 59–73. <https://doi.org/10.1080/10426919308934813>.
- [47]. T.H. Huang, C.-T. Kuo, T.S. Lin, Tribological behaviour of chemical vapour deposition diamond films on various cutting tools, *Surf. Coatings Technol.* 56 (1993) 105–108. [https://doi.org/10.1016/0257-8972\(93\)90013-E](https://doi.org/10.1016/0257-8972(93)90013-E).
- [48]. K. Shibuki, K. Sasaki, M. Yagi, T. Suzuki, Y. Ikuhara, Diamond coating on WC-Co and WC for cutting tools, *Surf. Coatings Technol.* 68–69 (1994) 369–373. [https://doi.org/10.1016/0257-8972\(94\)90187-2](https://doi.org/10.1016/0257-8972(94)90187-2).
- [49]. K. Saijo, M. Yagi, K. Shibuki, S. Takatsu, Improvements in adhesive strength and cutting performance of diamond-coated tools, *Surf. Coatings Technol.* 47 (1991) 646–653. [https://doi.org/10.1016/0257-8972\(91\)90336-U](https://doi.org/10.1016/0257-8972(91)90336-U).
- [50]. K. Kanda, S. Takehana, S. Yoshida, R. Watanabe, S. Takano, H. Ando, F. Shimakura, Application of diamond-coated cutting tools, *Surf. Coatings Technol.* 73 (1995) 115–120. [https://doi.org/10.1016/0257-8972\(94\)02370-0](https://doi.org/10.1016/0257-8972(94)02370-0).
- [51]. S.G. Huang, R.L. Liu, L. Li, O. Van der Biest, J. Vleugels, NbC as grain growth inhibitor and carbide in WC–Co hardmetals, *Int. J. Refract. Met. Hard Mater.* 26 (2008) 389–395. <https://doi.org/10.1016/j.ijrmhm.2007.09.003>.
- [52]. G.S. Fox-Rabinovich, A.I. Kovalev, D.L. Wainstein, L.S. Shuster, G.K. Dosbaeva, Improvement of ‘duplex’ PVD coatings for HSS cutting tools by PFPE (perfluoropolyether ‘Z-DOL’), *Surf. Coatings Technol.* 160 (2002) 99–107. [https://doi.org/10.1016/S0257-8972\(02\)00378-X](https://doi.org/10.1016/S0257-8972(02)00378-X).
- [53]. Rana, Ramakant, Qasim Murtaza, and Ravinderjit Singh Walia. "Optimization using genetic algorithm of tribological behaviour of WC tool material." *Indian Journal of Engineering and Materials Sciences (IJEMS)* 27, no. 4 (2021): 889-896.
- [54]. A.A. Matei, I. Pencea, M. Branzei, D.E. Trancă, G. Țepeș, C.E. Sfât, E. Ciovisa (Coman), A.I. Gherghilescu, G.A. Stanciu, Corrosion resistance appraisal of TiN, TiCN and TiAlN coatings deposited by CAE-PVD method on WC–Co cutting tools exposed to artificial sea water, *Appl. Surf. Sci.* 358 (2015) 572–578. <https://doi.org/10.1016/j.apsusc.2015.08.041>.
- [55]. J.R. Sartori Moreno, G.L. da Silva, C.E. Silva Junior, J.F. Souza Gonçalves, Comparative performance analysis of Tung and Jatropa emulsions for development as cutting fluids, *Mater. Res. Express.* 7 (2019) 015503. <https://doi.org/10.1088/2053-1591/ab5f7e>.
- [56]. Pfouts, W. R. (2000). Cutting edge coatings. *Manufacturing Engineering*, 125(1), 98-107.
- [57]. Y.-C. Yen, A. Jain, P. Chigurupati, W.-T. Wu, T. Altan, Computer Simulation of Orthogonal Cutting using a Tool with Multiple Coatings, *Mach. Sci. Technol.* 8 (2004) 305–326. <https://doi.org/10.1081/MST-200029230>.
- [58]. E.J. Oles, A. Inspektor, C.E. Bauer, The new diamond-coated carbide cutting tools, *Diam. Relat. Mater.* 5 (1996) 617–624. [https://doi.org/10.1016/0925-9635\(95\)00347-9](https://doi.org/10.1016/0925-9635(95)00347-9).
- [59]. Chai, H. Fracture mechanics analysis of thin coatings under spherical indentation. *Int J Fract* 119, (2003) 263–285. <https://doi.org/10.1023/A:1023913927118>
- [60]. R. Polini, P. D’Antonio, S. Lo Casto, V.F. Ruisi, E. Traversa, Cutting performance and indentation behaviour of diamond films on Co-cemented tungsten carbide, *Surf. Coatings Technol.* 123 (2000) 78–83. [https://doi.org/10.1016/S0257-8972\(99\)00471-5](https://doi.org/10.1016/S0257-8972(99)00471-5).
- [61]. Y. Xie, H. Hawthorne, Effect of contact geometry on the failure modes of thin coatings in the scratch adhesion test, *Surf. Coatings Technol.* 155 (2002) 121–129. [https://doi.org/10.1016/S0257-8972\(02\)00064-6](https://doi.org/10.1016/S0257-8972(02)00064-6).

- [62]. R.E. Clausing, L.L. Horton, J.C. Angus, P. Koidl, eds., *Diamond and Diamond-like Films and Coatings*, Springer US, Boston, MA, 1991. <https://doi.org/10.1007/978-1-4684-5967-8>.
- [63]. D.F. Wang, K. Kato, Effect of coating thickness on friction for carbon nitride films in repeated sliding against a spherical diamond with nano-scale asperities, *Wear*. 252 (2002) 210–219. [https://doi.org/10.1016/S0043-1648\(01\)00875-4](https://doi.org/10.1016/S0043-1648(01)00875-4).
- [64]. F. Deuerler, O. Lemmer, M. Frank, M. Pohl, C. Heßing, Diamond films for wear protection of hardmetal tools, *Int. J. Refract. Met. Hard Mater.* 20 (2002) 115–120. [https://doi.org/10.1016/S0263-4368\(02\)00009-4](https://doi.org/10.1016/S0263-4368(02)00009-4).
- [65]. W.S. Yip, S. To, H.T. Zhou, Social network analysis for optimal machining conditions in ultra-precision manufacturing, *J. Manuf. Syst.* 56 (2020) 93–103. <https://doi.org/10.1016/j.jmsy.2020.03.011>.
- [66]. S. Zhang, W. Zhu, TiN coating of tool steels: a review, *J. Mater. Process. Technol.* 39 (1993) 165–177. [https://doi.org/10.1016/0924-0136\(93\)90016-Y](https://doi.org/10.1016/0924-0136(93)90016-Y).
- [67]. W.-J. Chou, G.-P. Yu, J.-H. Huang, Mechanical properties of TiN thin film coatings on 304 stainless steel substrates, *Surf. Coatings Technol.* 149 (2002) 7–13. [https://doi.org/10.1016/S0257-8972\(01\)01382-2](https://doi.org/10.1016/S0257-8972(01)01382-2).
- [68]. C.H.R.V. Kumar, P.K. Nair, B. Ramamoorthy, Characterization of multilayer pvd nanocoatings deposited on tungsten carbide cutting tools, *Int. J. Adv. Manuf. Technol.* 38 (2008) 622–629. <https://doi.org/10.1007/s00170-007-1059-z>.
- [69]. S. Lata, R. Rana, Hitesh, Investigation of Chip-Tool Interface Temperature: Effect of Machining Parameters and Tool Material on Ferrous and Non-Ferrous Metal, *Mater. Today Proc.* 5 (2018) 4250–4257. <https://doi.org/10.1016/j.matpr.2017.11.689>.
- [70]. F.A. Soliman, O.A. Abu-Zeid, M. Merdan, On the improvement of the performance of high speed steel turning tools by tin coatings, *Wear*. 119 (1987) 199–204. [https://doi.org/10.1016/0043-1648\(87\)90109-8](https://doi.org/10.1016/0043-1648(87)90109-8).
- [71]. W. König, R. Fritsch, D. Kammermeier, Physically vapor deposited coatings on tools: performance and wear phenomena, *Surf. Coatings Technol.* 49 (1991) 316–324. [https://doi.org/10.1016/0257-8972\(91\)90076-9](https://doi.org/10.1016/0257-8972(91)90076-9).
- [72]. A.A. Minevich, Wear of cemented carbide cutting inserts with multilayer Ti-based PVD coatings, *Surf. Coatings Technol.* 53 (1992) 161–170. [https://doi.org/10.1016/0257-8972\(92\)90118-T](https://doi.org/10.1016/0257-8972(92)90118-T).
- [73]. S.C. Lim, C.Y.H. Lim, K.S. Lee, The effects of machining conditions on the flank wear of tin-coated high speed steel tool inserts, *Wear*. 181–183 (1995) 901–912. [https://doi.org/10.1016/0043-1648\(95\)90214-7](https://doi.org/10.1016/0043-1648(95)90214-7).
- [74]. C.Y.. Lim, S.. Lim, K.. Lee, The performance of TiN-coated high speed steel tool inserts in turning, *Tribol. Int.* 32 (1999) 393–398. [https://doi.org/10.1016/S0301-679X\(99\)00066-3](https://doi.org/10.1016/S0301-679X(99)00066-3).
- [75]. A. Devillez, F. Schneider, S. Dominiak, D. Dudzinski, D. Larrouquere, Cutting forces and wear in dry machining of Inconel 718 with coated carbide tools, *Wear*. 262 (2007) 931–942. <https://doi.org/10.1016/j.wear.2006.10.009>.
- [76]. R.P. Martinho, F.J.G. Silva, A.P.M. Baptista, Wear behaviour of uncoated and diamond coated Si₃N₄ tools under severe turning conditions, *Wear*. 263 (2007) 1417–1422. <https://doi.org/10.1016/j.wear.2007.01.048>.
- [77]. Y.-J. Lin, A. Agrawal, Y. Fang, Wear progressions and tool life enhancement with AlCrN coated inserts in high-speed dry and wet steel lathing, *Wear*. 264 (2008) 226–234. <https://doi.org/10.1016/j.wear.2007.03.007>.

- [78]. K. Aslantas, İ. Uçun, A. Çicek, Tool life and wear mechanism of coated and uncoated Al₂O₃/TiCN mixed ceramic tools in turning hardened alloy steel, *Wear*. 274–275 (2012) 442–451. <https://doi.org/10.1016/j.wear.2011.11.010>.
- [79]. B. Podgornik, S. Hogmark, O. Sandberg, V. Leskovsek, Wear resistance and anti-sticking properties of duplex treated forming tool steel, *Wear*. 254 (2003) 1113–1121. [https://doi.org/10.1016/S0043-1648\(03\)00322-3](https://doi.org/10.1016/S0043-1648(03)00322-3).
- [80]. P. Carlsson, M. Olsson, PVD coatings for sheet metal forming processes—a tribological evaluation, *Surf. Coatings Technol.* 200 (2006) 4654–4663. <https://doi.org/10.1016/j.surfcoat.2004.10.127>.
- [81]. P. Pesch, S. Sattel, S. Woestmann, P. Masarczyk, K. Herden, T. Stucky, A. Martens, S. Ulrich, H. Holleck, Performance of hard coated steel tools for steel sheet drawing, *Surf. Coatings Technol.* 163–164 (2003) 739–746. [https://doi.org/10.1016/S0257-8972\(02\)00654-0](https://doi.org/10.1016/S0257-8972(02)00654-0).
- [82]. Madorsky Y. and Thompson M.: Proc. 2nd Annu. Stamp. J. Forum, Detroit, MI, USA, May 2004, FMA; Internet www.thefabricator.com:80/ToolandDie/ToolandDie_Article.cfm?ID51058
- [83]. J. Vetter, R. Knaup, H. Dweletzki, E. Schneider, S. Vogler, Hard coatings for lubrication reduction in metal forming, *Surf. Coatings Technol.* 86–87 (1996) 739–747. [https://doi.org/10.1016/S0257-8972\(96\)03063-0](https://doi.org/10.1016/S0257-8972(96)03063-0).
- [84]. J. Vetter, Vacuum arc coatings for tools: potential and application, *Surf. Coatings Technol.* 76–77 (1995) 719–724. [https://doi.org/10.1016/0257-8972\(95\)02499-9](https://doi.org/10.1016/0257-8972(95)02499-9).
- [85]. A. Gilewicz, B. Warcholinski, Tribological properties of CrCN/CrN multilayer coatings, *Tribol. Int.* 80 (2014) 34–40. <https://doi.org/10.1016/j.triboint.2014.06.012>.
- [86]. S.T. Gonczy, N. Randall, An ASTM Standard for Quantitative Scratch Adhesion Testing of Thin, Hard Ceramic Coatings, *Int. J. Appl. Ceram. Technol.* 2 (2005) 422–428. <https://doi.org/10.1111/j.1744-7402.2005.02043.x>.
- [87]. S. Ebnesajjad, E. Cyrus, *Surface Treatment of Materials for Adhesive Bonding*, Elsevier, 2014. <https://doi.org/10.1016/C2013-0-12914-5>.
- [88]. J. Narayan, R.D. Vispute, K. Jagannadham, Interfacial processing and adhesion of diamond, diamond-like, and TiN films on metallic and polymeric substrates, *J. Adhes. Sci. Technol.* 9 (1995) 753–767. <https://doi.org/10.1163/156856195X00653>.
- [89]. B. Ollivier, A. Matthews, Relationship between interlayer hardness and adhesion and pin-on-disc behaviour for fast atom beam source diamond-like-carbon films, *J. Adhes. Sci. Technol.* 9 (1995) 725–735. <https://doi.org/10.1163/156856195X00635>.
- [90]. W. König, R. Kauven, A. Droese, Improved HSS Tool Performance with Mechanically Resistant Coatings, *CIRP Ann.* 35 (1986) 31–35. [https://doi.org/10.1016/S0007-8506\(07\)61832-0](https://doi.org/10.1016/S0007-8506(07)61832-0).
- [91]. H. Ronkainen, I. Nieminen, K. Holmberg, A. Leyland, A. Matthews, B. Matthes, E. Broszeit, Evaluation of some titanium-based ceramic coatings on high speed steel cutting tools, *Surf. Coatings Technol.* 49 (1991) 468–473. [https://doi.org/10.1016/0257-8972\(91\)90102-3](https://doi.org/10.1016/0257-8972(91)90102-3).
- [92]. C.-P. Klages, M. Fryda, T. Matthée, L. Schäfer, H. Dimigen, Diamond coatings and cBN coatings for tools, *Int. J. Refract. Met. Hard Mater.* 16 (1998) 171–176. [https://doi.org/10.1016/S0263-4368\(98\)80100-5](https://doi.org/10.1016/S0263-4368(98)80100-5).
- [93]. C.Y.H. Lim, S.C. Lim, K.S. Lee, Wear of TiC-coated carbide tools in dry turning, *Wear*. 225–229 (1999) 354–367. [https://doi.org/10.1016/S0043-1648\(98\)00366-4](https://doi.org/10.1016/S0043-1648(98)00366-4).

- [94]. J. Nickel, A.. Shuaib, B.. Yilbas, S.. Nizam, Evaluation of the wear of plasma-nitrided and TiN-coated HSS drills using conventional and Micro-PIXE techniques, *Wear*. 239 (2000) 155–167. [https://doi.org/10.1016/S0043-1648\(99\)00352-X](https://doi.org/10.1016/S0043-1648(99)00352-X).
- [95]. G.. Fox-Rabinovich, N.. Bushe, A.. Kovalev, S.. Korshunov, L.S. Shuster, G.. Dosbaeva, Impact of ion modification of HSS surfaces on the wear resistance of cutting tools with surface engineered coatings, *Wear*. 249 (2001) 1051–1058. [https://doi.org/10.1016/S0043-1648\(01\)00829-8](https://doi.org/10.1016/S0043-1648(01)00829-8).
- [96]. Sokovic, M., J. Kopac, L. A. Dobrzanski, J. Mikula, K. Golombek, and D. Pakula. "Cutting characteristics of PVD and CVD-coated ceramic tool inserts." *Tribology in industry* 28, no. 1/2 (2006): 3-8.
- [97]. R. M'Saoubi, H. Chandrasekaran, Investigation of the effects of tool micro-geometry and coating on tool temperature during orthogonal turning of quenched and tempered steel, *Int. J. Mach. Tools Manuf.* 44 (2004) 213–224. <https://doi.org/10.1016/j.ijmachtools.2003.10.006>.
- [98]. G.S. Fox-Rabinovich, S.C. Veldhuis, G.C. Weatherly, A.I. Kovalev, S.N. Korshunov, V.N. Sevortsov, G.K. Dosbaeva, L.S. Shuster, D.L. Wainstein, Improvement of 'duplex' PVD coatings for HSS cutting tools by ion mixing, *Surf. Coatings Technol.* 187 (2004) 230–237. <https://doi.org/10.1016/j.surfcoat.2004.02.015>.
- [99]. L. Settineri, M.G. Faga, Laboratory tests for performance evaluation of nanocomposite coatings for cutting tools, *Wear*. 260 (2006) 326–332. <https://doi.org/10.1016/j.wear.2005.04.025>.
- [100]. A. Mubarak, E. Hamzah, M.R.M. Toff, Study of macrodroplet and growth mechanisms with and without ion etchings on the properties of TiN coatings deposited on HSS using cathodic arc physical vapour deposition technique, *Mater. Sci. Eng. A*. 474 (2008) 236–242. <https://doi.org/10.1016/j.msea.2007.04.030>.
- [101]. L. Settineri, M.G. Faga, G. Gautier, M. Perucca, Evaluation of wear resistance of AlSiTiN and AlSiCrN nanocomposite coatings for cutting tools, *CIRP Ann.* 57 (2008) 575–578. <https://doi.org/10.1016/j.cirp.2008.03.103>.
- [102]. F. Qin, Y.K. Chou, D. Nolen, R.G. Thompson, Coating thickness effects on diamond coated cutting tools, *Surf. Coatings Technol.* 204 (2009) 1056–1060. <https://doi.org/10.1016/j.surfcoat.2009.06.011>.
- [103]. A. Czyzniewski, Optimising deposition parameters of W-DLC coatings for tool materials of high speed steel and cemented carbide, *Vacuum*. 86 (2012) 2140–2147. <https://doi.org/10.1016/j.vacuum.2012.06.011>.
- [104]. W. Henderer, F. Xu, Hybrid TiSiN, CrC/C PVD coatings applied to cutting tools, *Surf. Coatings Technol.* 215 (2013) 381–385. <https://doi.org/10.1016/j.surfcoat.2012.06.092>.
- [105]. W.-J. Chou, G.-P. Yu, J.-H. Huang, Corrosion behavior of TiN-coated 304 stainless steel, *Corros. Sci.* 43 (2001) 2023–2035. [https://doi.org/10.1016/S0010-938X\(01\)00010-5](https://doi.org/10.1016/S0010-938X(01)00010-5).
- [106]. E. Lunarska, N. Ageeva, J. Michalski, Corrosion resistance of plasma-assisted chemical vapour deposition (PACVD) TiN-coated steel in a range of aggressive environments, *Surf. Coatings Technol.* 85 (1996) 125–130. [https://doi.org/10.1016/0257-8972\(95\)02735-1](https://doi.org/10.1016/0257-8972(95)02735-1).
- [107]. H.-E. Cheng, M.-H. Hon, Influence of TiN coating thickness on the wear of Si₃N₄-based cutting tools, *Surf. Coatings Technol.* 81 (1996) 256–261. [https://doi.org/10.1016/0257-8972\(95\)02535-9](https://doi.org/10.1016/0257-8972(95)02535-9).
- [108]. Singh, Abhishek. "Effect of pre and post mechanical treatment on pvd coated tools' characteristics and machining performance." PhD diss., (2014).

- [109].Montgomery, S., Kennedy, D., & O'Dowd, N. (2010). PVD and CVD coatings for the metal forming industry.
- [110].Shibe, Vineet, and Vikas Chawla. "An Overview of Research Work in Surface Coating." *IJRMET* 3, no. 2 (2013): 85-88.
- [111].L. Krishnia, P.K. Tyagi, Growth and characterization of polycrystalline diamond films on silicon using sugarcane bagasse as carbon precursor at atmospheric pressure by thermal chemical vapor deposition, *Diam. Relat. Mater.* 87 (2018) 18–26. <https://doi.org/10.1016/j.diamond.2018.05.001>.
- [112].J. Karner, M. Pedrazzini, I. Reineck, M.E. Sjöstrand, E. Bergmann, CVD diamond coated cemented carbide cutting tools, *Mater. Sci. Eng. A.* 209 (1996) 405–413. [https://doi.org/10.1016/0921-5093\(95\)10140-3](https://doi.org/10.1016/0921-5093(95)10140-3).
- [113].B. Eliasson, U. Kogelschatz, Nonequilibrium volume plasma chemical processing, *IEEE Trans. Plasma Sci.* 19 (1991) 1063–1077. <https://doi.org/10.1109/27.125031>.
- [114].T. Kivak, G. Samtaş, A. Çiçek, Taguchi method based optimisation of drilling parameters in drilling of AISI 316 steel with PVD monolayer and multilayer coated HSS drills, *Measurement.* 45 (2012) 1547–1557. <https://doi.org/10.1016/j.measurement.2012.02.022>.
- [115].Narasimha, M., R. Reiji Kumar, and Achamyehaemro Kassie. "Performance of Coated Carbide Tools." *The International Journal Of Engineering And Science (IJES)* 2, no. 6 (2013): 47-54.
- [116].A.A. Vereschaka, M.A. Volosova, S.N. Grigoriev, A.S. Vereschaka, Development of Wear-resistant Complex for High-speed Steel Tool when Using Process of Combined Cathodic Vacuum Arc Deposition, *Procedia CIRP.* 9 (2013) 8–12. <https://doi.org/10.1016/j.procir.2013.06.159>.
- [117].D. Kottfer, M. Ferdinandy, L. Kaczmarek, I. Maňková, J. Beňo, Investigation of Ti and Cr based PVD coatings deposited onto HSS Co 5 twist drills, *Appl. Surf. Sci.* 282 (2013) 770–776. <https://doi.org/10.1016/j.apsusc.2013.06.051>.
- [118].A. Pilkington, S.J. Dowey, J.T. Toton, E.D. Doyle, Machining with AlCr-oxinitride PVD coated cutting tools, *Tribol. Int.* 65 (2013) 303–313. <https://doi.org/10.1016/j.triboint.2013.03.020>.
- [119].L. LU, Q. WANG, B. CHEN, Y. AO, D. YU, C. WANG, S. WU, K.H. KIM, Microstructure and cutting performance of CrTiAlN coating for high-speed dry milling, *Trans. Nonferrous Met. Soc. China.* 24 (2014) 1800–1806. [https://doi.org/10.1016/S1003-6326\(14\)63256-8](https://doi.org/10.1016/S1003-6326(14)63256-8).
- [120].I. Cho, A. Amanov, J. Kim, The effects of AlCrN coating, surface modification and their combination on the tribological properties of high speed steel under dry conditions, *Tribol. Int.* 81 (2015) 61–72. <https://doi.org/10.1016/j.triboint.2014.08.003>.
- [121].S. Bhowmick, A. Banerji, A.T. Alpas, Tribological behavior of Al–6.5%, –12%, –18.5% Si alloys during machining using CVD diamond and DLC coated tools, *Surf. Coatings Technol.* 284 (2015) 353–364. <https://doi.org/10.1016/j.surfcoat.2015.08.073>.
- [122].A.F. Rousseau, J.G. Partridge, E.L.H. Mayes, J.T. Toton, M. Kracica, D.G. McCulloch, E.D. Doyle, Microstructural and tribological characterisation of a nitriding/TiAlN PVD coating duplex treatment applied to M2 High Speed Steel tools, *Surf. Coatings Technol.* 272 (2015) 403–408. <https://doi.org/10.1016/j.surfcoat.2015.03.034>.
- [123].T. Aiso, U. Wiklund, M. Kubota, S. Jacobson, Influence of Mn and Al additions to carbon steel on material transfer and coating damage mechanism in a sliding contact between steel and TiN coated HSS tool, *Tribol. Int.* 101 (2016) 414–424. <https://doi.org/10.1016/j.triboint.2016.04.036>.

- [124].A. Bahri, E. Kaçar, S.S. Akkaya, K. Elleuch, M. Ürgen, Wear protection potential of TiN coatings for 304 stainless steels used in rotating parts during olive oil extraction, *Surf. Coatings Technol.* 304 (2016) 560–566. <https://doi.org/10.1016/j.surfcoat.2016.07.067>.
- [125].Z. Zhu, S. To, W. Le Zhu, P. Huang, X. Zhou, Cutting forces in fast-/slow tool servo diamond turning of micro-structured surfaces, *Int. J. Mach. Tools Manuf.* 136 (2019) 62–75. <https://doi.org/10.1016/j.ijmachtools.2018.09.003>.
- [126].A.K. Balaji, V.S. Mohan, AN ‘EFFECTIVE CUTTING TOOL THERMAL CONDUCTIVITY’ BASED MODEL FOR TOOL–CHIP CONTACT IN MACHINING WITH MULTI-LAYER COATED CUTTING TOOLS, *Mach. Sci. Technol.* 6 (2002) 415–436. <https://doi.org/10.1081/MST-120016254>.
- [127].N. Gupta, A.K. Agrawal, R.S. Walia, Soft Modeling Approach in Predicting Surface Roughness, Temperature, Cutting Forces in Hard Turning Process Using Artificial Neural Network: An Empirical Study, in: 2019: pp. 206–215. https://doi.org/10.1007/978-981-15-1384-8_17.
- [128].Grzesik, W., & Nieslony, P. (1998). Thermal characterization of the tool–chip interface when using coated turning inserts. *Trans. NAMRI/SME*, 26, 189-194.
- [129].W. Grzesik, Experimental investigation of the cutting temperature when turning with coated indexable inserts, *Int. J. Mach. Tools Manuf.* 39 (1999) 355–369. [https://doi.org/10.1016/S0890-6955\(98\)00044-3](https://doi.org/10.1016/S0890-6955(98)00044-3).
- [130].W. Grzesik, The influence of thin hard coatings on frictional behaviour in the orthogonal cutting process, *Tribol. Int.* 33 (2000) 131–140. [https://doi.org/10.1016/S0301-679X\(00\)00072-4](https://doi.org/10.1016/S0301-679X(00)00072-4).
- [131].W. König, R. Fritsch, D. Kammermeier, New Approaches to Characterizing the Performance of Coated Cutting Tools, *CIRP Ann.* 41 (1992) 49–54. [https://doi.org/10.1016/S0007-8506\(07\)61150-0](https://doi.org/10.1016/S0007-8506(07)61150-0).
- [132].H.G. Prengel, W.R. Pfouts, A.T. Santhanam, State of the art in hard coatings for carbide cutting tools, *Surf. Coatings Technol.* 102 (1998) 183–190. [https://doi.org/10.1016/S0257-8972\(96\)03061-7](https://doi.org/10.1016/S0257-8972(96)03061-7).
- [133].D. Singh, S. Lata, R. Rana, Reverse Engineered Structure of Tool Post aiding Tool Tip Alignment with Work Center, *Mater. Today Proc.* 5 (2018) 6433–6443. <https://doi.org/10.1016/j.matpr.2017.12.256>.
- [134].T. Obikawa, T. Matsumura, T. Shirakashi, E. Usui, Wear characteristic of alumina coated and alumina ceramic tools, *J. Mater. Process. Technol.* 63 (1997) 211–216. [https://doi.org/10.1016/S0924-0136\(96\)02626-X](https://doi.org/10.1016/S0924-0136(96)02626-X).
- [135].J.C. Garcia-Gonzalez, W. Moscoso-Kingsley, V. Madhavan, Rake Face Temperature When Machining with Coated Cutting Tools, *Procedia Manuf.* 5 (2016) 815–827. <https://doi.org/10.1016/j.promfg.2016.08.066>.
- [136].M.S.I. Chowdhury, S. Chowdhury, K. Yamamoto, B.D. Beake, B. Bose, A. Elfizy, D. Cavelli, G. Dosbaeva, M. Aramesh, G.S. Fox-Rabinovich, S.C. Veldhuis, Wear behaviour of coated carbide tools during machining of Ti6Al4V aerospace alloy associated with strong built up edge formation, *Surf. Coatings Technol.* 313 (2017) 319–327. <https://doi.org/10.1016/j.surfcoat.2017.01.115>.
- [137].S.C. Lim, C.Y.H. Lim, K.S. Lee, Crater wear of TiN coated high speed steel tool inserts, *Surf. Eng.* 13 (1997) 223–226. <https://doi.org/10.1179/sur.1997.13.3.223>.
- [138].V.G. Sargade, S. Gangopadhyay, S. Paul, A.K. Chattopadhyay, Effect of Coating Thickness on the Characteristics and Dry Machining Performance of TiN Film Deposited on Cemented

- Carbide Inserts Using CFUBMS, *Mater. Manuf. Process.* 26 (2011) 1028–1033. <https://doi.org/10.1080/10426914.2010.526978>.
- [139].L. Rogström, M.P. Johansson-Jõesaar, L. Landälv, M. Ahlgren, M. Odén, Wear behavior of ZrAlN coated cutting tools during turning, *Surf. Coatings Technol.* 282 (2015) 180–187. <https://doi.org/10.1016/j.surfcoat.2015.10.029>.
- [140].C. Sateesh Kumar, S.K. Patel, Experimental and numerical investigations on the effect of varying AlTiN coating thickness on hard machining performance of Al₂O₃-TiCN mixed ceramic inserts, *Surf. Coatings Technol.* 309 (2017) 266–281. <https://doi.org/10.1016/j.surfcoat.2016.11.080>.
- [141].E. Posti, I. Nieminen, Influence of coating thickness on the life of TiN-coated high speed steel cutting tools, *Wear.* 129 (1989) 273–283. [https://doi.org/10.1016/0043-1648\(89\)90264-0](https://doi.org/10.1016/0043-1648(89)90264-0).
- [142].K. Tuffy, G. Byrne, D. Dowling, Determination of the optimum TiN coating thickness on WC inserts for machining carbon steels, *J. Mater. Process. Technol.* 155–156 (2004) 1861–1866. <https://doi.org/10.1016/j.jmatprotec.2004.04.277>.
- [143].D. Petersen, R. Link, J.-D. Kim, Effect of Carbide and Oxide Coating Thickness on Cutting Tool Wear in the Turning Process, *J. Test. Eval.* 23 (1995) 311. <https://doi.org/10.1520/JTE10431J>.
- [144].J. Hu, Y.K. Chou, Characterizations of cutting tool flank wear-land contact, *Wear.* 263 (2007) 1454–1458. <https://doi.org/10.1016/j.wear.2007.01.080>.
- [145].S.K. Khrais, Y.J. Lin, Wear mechanisms and tool performance of TiAlN PVD coated inserts during machining of AISI 4140 steel, *Wear.* 262 (2007) 64–69. <https://doi.org/10.1016/j.wear.2006.03.052>.
- [146].A. Mkaddem, A. Ben Soussia, M. El Mansori, Wear resistance of CVD and PVD multilayer coatings when dry cutting fiber reinforced polymers (FRP), *Wear.* 302 (2013) 946–954. <https://doi.org/10.1016/j.wear.2013.03.017>.
- [147].S. Chinchankar, S.K. Choudhury, Evaluation of Chip-tool Interface Temperature: Effect of Tool Coating and Cutting Parameters during Turning Hardened AISI 4340 Steel, *Procedia Mater. Sci.* 6 (2014) 996–1005. <https://doi.org/10.1016/j.mspro.2014.07.170>.
- [148].J. Takadom, H.H. Bennani, Influence of substrate roughness and coating thickness on adhesion, friction and wear of TiN films, *Surf. Coatings Technol.* 96 (1997) 272–282. [https://doi.org/10.1016/S0257-8972\(97\)00182-5](https://doi.org/10.1016/S0257-8972(97)00182-5).
- [149].J.H.. Siu, L.K.. Li, An investigation of the effect of surface roughness and coating thickness on the friction and wear behaviour of a commercial MoS₂-metal coating on AISI 400C steel, *Wear.* 237 (2000) 283–287. [https://doi.org/10.1016/S0043-1648\(99\)00349-X](https://doi.org/10.1016/S0043-1648(99)00349-X).
- [150].J.I. McCool, Relating Profile Instrument Measurements to the Functional Performance of Rough Surfaces, *J. Tribol.* 109 (1987) 264–270. <https://doi.org/10.1115/1.3261349>.
- [151].R. Goltsberg, I. Etsion, G. Davidi, The onset of plastic yielding in a coated sphere compressed by a rigid flat, *Wear.* 271 (2011) 2968–2977. <https://doi.org/10.1016/j.wear.2011.06.025>.
- [152].W. Song, L. Li, A. Ovcharenko, D. Jia, I. Etsion, F.E. Talke, Plastic yield inception of an indented coated flat and comparison with a flattened coated sphere, *Tribol. Int.* 53 (2012) 61–67. <https://doi.org/10.1016/j.triboint.2012.04.022>.
- [153].R. Goltsberg, I. Etsion, A model for the weakening effect of very thin hard coatings, *Wear.* 308 (2013) 10–16. <https://doi.org/10.1016/j.wear.2013.09.019>.

- [154].X. Huang, H. Kasem, H.F. Shang, T.M. Shao, I. Etsion, Experimental study of a potential weakening effect in spheres with thin hard coatings, *Wear*. 296 (2012) 590–597. <https://doi.org/10.1016/j.wear.2012.08.018>.
- [155].R. M'Saoubi, M.P. Johansson, J.M. Andersson, Wear mechanisms of PVD-coated PCBN cutting tools, *Wear*. 302 (2013) 1219–1229. <https://doi.org/10.1016/j.wear.2013.01.074>.
- [156].F. Klocke, C. Nobel, D. Veselovac, Influence of Tool Coating, Tool Material, and Cutting Speed on the Machinability of Low-Leaded Brass Alloys in Turning, *Mater. Manuf. Process*. 31 (2016) 1895–1903. <https://doi.org/10.1080/10426914.2015.1127944>.
- [157].A. Miletić, P. Terek, L. Kovačević, M. Vilotić, D. Kakaš, B. Škorić, D. Kukuruzović, Influence of substrate roughness on adhesion of TiN coatings, *J. Brazilian Soc. Mech. Sci. Eng.* 36 (2014) 293–299. <https://doi.org/10.1007/s40430-013-0102-2>.
- [158].Dini, J. W. "Ion plating can improve coating adhesion." *METAL FINISHING-NEW JERSEY*- 91 (1993): 15-15.
- [159].S.J. Bull, E.G. Berasetegui, An overview of the potential of quantitative coating adhesion measurement by scratch testing, *Tribol. Int.* 39 (2006) 99–114. <https://doi.org/10.1016/j.triboint.2005.04.013>.
- [160].J. Stallard, S. Poulat, D.G. Teer, The study of the adhesion of a TiN coating on steel and titanium alloy substrates using a multi-mode scratch tester, *Tribol. Int.* 39 (2006) 159–166. <https://doi.org/10.1016/j.triboint.2005.04.011>.
- [161].T. Nsongo, M. Gillet, Adhesion characterization of titanium and titanium nitride thin coatings on metals using the scratch test, *Int. J. Adhes. Adhes.* 15 (1995) 191–196. [https://doi.org/10.1016/0143-7496\(95\)91631-F](https://doi.org/10.1016/0143-7496(95)91631-F).
- [162].S.J. Bull, Failure modes in scratch adhesion testing, *Surf. Coatings Technol.* 50 (1991) 25–32. [https://doi.org/10.1016/0257-8972\(91\)90188-3](https://doi.org/10.1016/0257-8972(91)90188-3).
- [163].D. Müller, Y.R. Cho, S. Berg, E. Fromm, Fracture mechanics tests for measuring the adhesion of magnetron-sputtered TiN coatings, *J. Adhes. Sci. Technol.* 7 (1993) 837–843. <https://doi.org/10.1163/156856193X00466>.
- [164].Jakubéczyová, D., P. Hvizdos, M. Hagarová, and M. Kocik. "THE USE OF INDENTATION TESTS FOR EVALUATION OF THIN PVD COATINGS OF(Ti, Al) N TYPE." *Powder Metallurgy Progress* 11, no. 1-2 (2011): 165-172.
- [165].A.J. Perry, Scratch adhesion testing of hard coatings, *Thin Solid Films*. 107 (1983) 167–180. [https://doi.org/10.1016/0040-6090\(83\)90019-6](https://doi.org/10.1016/0040-6090(83)90019-6).
- [166].D. Barnes, S. Johnson, R. Snell, S. Best, Using scratch testing to measure the adhesion strength of calcium phosphate coatings applied to poly(carbonate urethane) substrates, *J. Mech. Behav. Biomed. Mater.* 6 (2012) 128–138. <https://doi.org/10.1016/j.jmbbm.2011.10.010>.
- [167].R. Jaworski, L. Pawlowski, F. Roudet, S. Kozerski, F. Petit, Characterization of mechanical properties of suspension plasma sprayed TiO₂ coatings using scratch test, *Surf. Coatings Technol.* 202 (2008) 2644–2653. <https://doi.org/10.1016/j.surfcoat.2007.09.044>.
- [168].J. von Stebut, F. Lapostolle, M. Bucsa, H. Vallen, Acoustic emission monitoring of single cracking events and associated damage mechanism analysis in indentation and scratch testing, *Surf. Coatings Technol.* 116–119 (1999) 160–171. [https://doi.org/10.1016/S0257-8972\(99\)00211-X](https://doi.org/10.1016/S0257-8972(99)00211-X).
- [169].P. Lu, X. Xiao, M. Lukitsch, A. Sachdev, Y.K. Chou, Interface characterizations of diamond-coated tools by scratch testing and simulations, *Surf. Coatings Technol.* 206 (2011) 1860–1866. <https://doi.org/10.1016/j.surfcoat.2011.08.022>.

- [170].F.X. Liu, F.Q. Yang, Y.F. Gao, W.H. Jiang, Y.F. Guan, P.D. Rack, O. Sergic, P.K. Liaw, Micro-scratch study of a magnetron-sputtered Zr-based metallic-glass film, *Surf. Coatings Technol.* 203 (2009) 3480–3484. <https://doi.org/10.1016/j.surfcoat.2009.05.017>.
- [171].Y.-Y. Chang, H.-M. Lai, Wear behavior and cutting performance of CrAlSiN and TiAlSiN hard coatings on cemented carbide cutting tools for Ti alloys, *Surf. Coatings Technol.* 259 (2014) 152–158. <https://doi.org/10.1016/j.surfcoat.2014.02.015>.
- [172].S.S. Gill, J. Singh, H. Singh, R. Singh, Investigation on wear behaviour of cryogenically treated TiAlN coated tungsten carbide inserts in turning, *Int. J. Mach. Tools Manuf.* 51 (2011) 25–33. <https://doi.org/10.1016/j.ijmachtools.2010.10.003>.
- [173].J. Liu, C. Ma, G. Tu, Y. Long, Cutting performance and wear mechanism of Sialon ceramic cutting inserts with TiCN coating, *Surf. Coatings Technol.* 307 (2016) 146–150. <https://doi.org/10.1016/j.surfcoat.2016.08.069>.
- [174].M.T. Laugier, An energy approach to the adhesion of coatings using the scratch test, *Thin Solid Films.* 117 (1984) 243–249. [https://doi.org/10.1016/0040-6090\(84\)90354-7](https://doi.org/10.1016/0040-6090(84)90354-7).
- [175].P. Hedenqvist, M. Olsson, S. Jacobson, S. Söderberg, Failure mode analysis of TiN-coated high speed steel: In situ scratch adhesion testing in the scanning electron microscope, *Surf. Coatings Technol.* 41 (1990) 31–49. [https://doi.org/10.1016/0257-8972\(90\)90128-Y](https://doi.org/10.1016/0257-8972(90)90128-Y).
- [176].K.-D. Bouzakis, N. Michailidis, N. Vidakis, K. Eftathiou, S. Kompogiannis, G. Erkens, Interpretation of PVD Coated Inserts Wear Phenomena in Turning, *CIRP Ann.* 49 (2000) 65–68. [https://doi.org/10.1016/S0007-8506\(07\)62897-2](https://doi.org/10.1016/S0007-8506(07)62897-2).
- [177].J. Wang, X. Zhang, F. Fang, R. Chen, Diamond cutting of micro-structure array on brittle material assisted by multi-ion implantation, *Int. J. Mach. Tools Manuf.* 137 (2019) 58–66. <https://doi.org/10.1016/j.ijmachtools.2018.10.005>.
- [178].K. You, F. Fang, G. Yan, Surface generation of tungsten carbide in laser-assisted diamond turning, *Int. J. Mach. Tools Manuf.* 168 (2021) 103770. <https://doi.org/10.1016/j.ijmachtools.2021.103770>.
- [179].dalus Cutting Tools, (2014), Dedalus Consulting, New York. www.dedalusconsulting.com.
- [180].Pakuła, D., and L. A. Dobrzański. "Investigation of the structure and properties of PVD and CVD coatings deposited on the Si₃N₄ nitride ceramics." *Journal of Achievements in Materials and Manufacturing Engineering* 24, no. 2 (2007): 79-82.
- [181].W.D. Fan, K. Jagannadham, J. Narayan, Improvement of Adhesion of Diamond Coatings to WC(CO) Tool Substrates, *MRS Proc.* 363 (1994) 163. <https://doi.org/10.1557/PROC-363-163>.
- [182].C.E. Bauer, A. Inspektor, E.J. Oles, A comparative machining study of diamond-coated tools made by plasma torch, microwave, and hot filament techniques, *Sadhana.* 28 (2003) 933–944. <https://doi.org/10.1007/BF02703323>.
- [183].Saini, D. P., & Ali, M. (2003). New generation coatings for high speed cutting tools.
- [184].K.-D. Bouzakis, N. Michailidis, G. Skordaris, E. Bouzakis, D. Biermann, R. M'Saoubi, Cutting with coated tools: Coating technologies, characterization methods and performance optimization, *CIRP Ann.* 61 (2012) 703–723. <https://doi.org/10.1016/j.cirp.2012.05.006>.
- [185].B. Breidenstein, B. Denkena, Significance of residual stress in PVD-coated carbide cutting tools, *CIRP Ann.* 62 (2013) 67–70. <https://doi.org/10.1016/j.cirp.2013.03.101>.
- [186].M. Henerichs, R. Voß, D. Harsch, F. Kuster, K. Wegener, Tool Life Time Extension with Nano-crystalline Diamond Coatings for Drilling Carbon-fibre Reinforced Plastics (CFRP), *Procedia CIRP.* 24 (2014) 125–129. <https://doi.org/10.1016/j.procir.2014.07.144>.

- [187].K. Zhang, J. Deng, Y. Xing, S. Li, H. Gao, Effect of microscale texture on cutting performance of WC/Co-based TiAlN coated tools under different lubrication conditions, *Appl. Surf. Sci.* 326 (2015) 107–118. <https://doi.org/10.1016/j.apsusc.2014.11.059>.
- [188].K. Zhang, J. Deng, R. Meng, P. Gao, H. Yue, Effect of nano-scale textures on cutting performance of WC/Co-based Ti55Al45N coated tools in dry cutting, *Int. J. Refract. Met. Hard Mater.* 51 (2015) 35–49. <https://doi.org/10.1016/j.ijrmhm.2015.02.011>.
- [189].V.S. Ivan Mrkvica, Miroslav Neslušan, Robert Čep, Properties and comparison of PVD coatings, *Teh. Vjesn. - Tech. Gaz.* 23 (2016). <https://doi.org/10.17559/TV-20140509105317>.
- [190].I. Martinez, R. Tanaka, Y. Yamane, K. Sekiya, K. Yamada, S. Yamada, M. Hasegawa, Effect of coating layer loss on the wear rate change of coated carbide tools in turning process, *Precis. Eng.* 50 (2017) 1–7. <https://doi.org/10.1016/j.precisioneng.2017.04.006>.
- [191].K.K. Gajrani, M. Ravi Sankar, State of the art on micro to nano textured cutting tools, *Mater. Today Proc.* 4 (2017) 3776–3785. <https://doi.org/10.1016/j.matpr.2017.02.274>.
- [192].I. Martinez, R. Tanaka, Y. Yamane, K. Sekiya, K. Yamada, T. Ishihara, S. Furuya, Wear mechanism of coated tools in the turning of ductile cast iron having wide range of tensile strength, *Precis. Eng.* 47 (2017) 46–53. <https://doi.org/10.1016/j.precisioneng.2016.07.003>.
- [193].E. L. Silva, S. Pratas, M. A. Neto, C. M. Fernandes, D. Figueiredo, and R. F. Silva, “Multilayer diamond coatings applied to micro-end-milling of cemented carbide,” *Materials (Basel)*, vol. 14, no. 12, pp. 1–12, 2021, doi: 10.3390/ma14123333.
- [194].L. Wang, Y. Liu, H. Chen, and M. Wang, “Modification Methods of Diamond Like Carbon Coating and the Performance in Machining Applications: A Review,” *Coatings*, vol. 12, no. 2, 2022, doi: 10.3390/coatings12020224.
- [195].X. C. Wang, C. C. Wang, C. Y. Wang, and F. H. Sun, “Approach for Polishing Diamond Coated Complicated Cutting Tool: Abrasive Flow Machining (AFM),” *Chinese J. Mech. Eng. (English Ed.)*, vol. 31, no. 1, 2018, doi: 10.1186/s10033-018-0296-4.
- [196].M. H. Sulaiman, R. N. Farahana, M. N. Mustafa, and K. Bienk, “Tribological properties of DLC coating under lubricated and dry friction condition,” *IOP Conf. Ser. Mater. Sci. Eng.*, vol. 670, no. 1, 2019, doi: 10.1088/1757-899X/670/1/012052.
- [197].M. Shabani, J. Sacramento, F. J. Oliveira, and R. F. Silva, “Multilayer CVD diamond coatings in the machining of an Al6061-15 vol % Al₂O₃ composite,” *Coatings*, vol. 7, no. 10, 2017, doi: 10.3390/coatings7100165.
- [198].Y. Lieberman, S. Lukinskikh, K. Kulpina, and Y. Sarvarova, “To the Question of the Reasons for Decrease in the Durability of Cutting Tools with a Diamond- Like Coating,” vol. 01008, 2021.
- [199].B. Huang, E. G. Zhang, Q. Zhou, R. C. Lin, and H. M. Du, “Research on the performance of diamond-like carbon coatings on cutting aluminum alloy: Cutting experiments and first-principles calculations,” *Coatings*, vol. 11, no. 1, pp. 1–11, 2021, doi: 10.3390/coatings11010063.
- [200].J. KOWALCZYK, M. MADEJ, K. MILEWSKI, L. NOWAKOWSKI, and D. OZIMINA, “The Influence of Cutting Fluid and Diamond-Like Carbon Coating on Cutting Tool Wear,” *DEStech Trans. Comput. Sci. Eng.*, no. fe, 2019, doi: 10.12783/dtcese/fe2019/30679.
- [201].A. Dev, S. Tandon, P. Kumar, and A. Dutt, “Effect of coating and polishing of cutting tool on machined surface quality in dry machining of aluminium alloy,” *Def. Sci. J.*, vol. 70, no. 3, pp. 299–305, 2020, doi: 10.14429/dsj.70.14831.

- [202].M. M. Butt, K. A. Najar, and T. H. Dar, “Experimental evaluation of multilayered cvd-and pvd-coated carbide turning inserts in severe machining of aisi-4340 steel alloy,” *J. Tribol.*, vol. 29, no. May, pp. 117–143, 2021.
- [203].E. E. Ashkinazi et al., “Effect of crystal structure on the tribological properties of diamond coatings on hard-alloy cutting tools,” *J. Frict. Wear*, vol. 38, no. 3, pp. 252–258, 2017, doi: 10.3103/S1068366617030047.
- [204].P. Fernández-Lucio, I. Villarón-Osorno, O. Pereira Neto, E. Ukar, L. N. López de Lacalle, and A. Gil del Val, “Effects of laser-textured on rake face in turning PCD tools for Ti6Al4V,” *J. Mater. Res. Technol.*, vol. 15, pp. 177–188, 2021, doi: 10.1016/j.jmrt.2021.08.004.
- [205].T. L. Brzezinka et al., “DLC and DLC-WS2 coatings for machining of aluminium alloys,” *Coatings*, vol. 9, no. 3, pp. 1–15, 2019, doi: 10.3390/COATINGS9030192.
- [206].M. Akgün and F. Kara, “Analysis and Optimization of Cutting Tool Coating Effects on Surface Roughness and Cutting Forces on Turning of AA 6061 Alloy,” *Adv. Mater. Sci. Eng.*, vol. 2021, 2021, doi: 10.1155/2021/6498261.
- [207].Brzezinka, T.; Rao, J.; Paiva, J.; Kohlscheen, J.; Fox-Rabinovich, G.; Veldhuis, S.; Endrino, J. DLC and DLC-WS2 Coatings for Machining of Aluminium Alloys. *Coatings* 2019, 9, 192.
- [208].Fang, F.Z.; Liu, Y.C. On minimum exit-burr in micro cutting. *J. Micromech. MicroEng.* 2001, 14, 984–988.
- [209].Olvera, O.; Barrow, G. An experimental study of burr formation in square shoulder face milling. *Int. J. Mach. Tools. Manuf.* 1996, 36, 1005–1020.
- [210].Suárez, A.; López De Lacalle, L.N.; Polvorosa, R.; Veiga, F.; Wretland, A. Effects of high-pressure cooling on the wear patterns on turning inserts used on alloy IN718. *Mater. Manuf. Process.* 2017, 32, 678–686.
- [211].Fernández-Lucio, P.; Villarón-Osorno, I.; Pereira Neto, O.; Ukar, E.; López De Lacalle, L.N.; Gil Del Val, A. Effects of laser-textured on rake face in turning PCD tools for Ti6Al4V. *J. Mater. Res. Technol.* 2021, 15, 177–188.
- [212].Riedel, R. *Handbook of Ceramic Hard Materials*; Wiley-Vich Weinheim: New York, NY, USA, 2000.
- [213].Lacalle, N.L.D.; Mentxaka, A.L. *Machine Tools for High Performance Machining*; Springer Verlag London Limited: London, UK, 2008.
- [214].Jamari, J.; Ammarullah, M.I.; Saad, A.P.M.; Syahrom, A.; Uddin, M.; van der Heide, E.; Basri, H. The effect of bottom profile dimples on the femoral head on wear in metal-on-metal total hip arthroplasty. *J. Funct. Biomater.* 2021, 12, 38.
- [215].Grigoriev, S.N.; Volosova, M.A.; Vereschaka, A.A.; Sitnikov, N.N.; Milovich, F.; Bublikov, J.I.; Fyodorov, S.V.; Seleznev, A.E. Properties of (Cr,Al,Si)N-(DLC-Si) composite coatings deposited on a cutting ceramic substrate. *Ceram. Int.* 2020, 46, 18241–18255.
- [216].Huang, L.; Yuan, J.; Li, C.; Hong, D. Microstructure, tribological and cutting performance of Ti-DLC/ α -C:H multilayer film on cemented carbide. *Surf. Coat. Technol.* 2018, 353, 163–170.
- [217].Kumar, C.S.; Majumder, H.; Khan, A.; Patel, S.K. Applicability of DLC and WC/C low friction coatings on Al₂O₃/TiCN mixed ceramic cutting tools for dry machining of hardened 52100 steel. *Ceram. Int.* 2020, 46, 11889–11897.
- [218].Fernández-Abia, A.I.; Barreiro, J.; Fernández-Larrinoa, J.; Lacalle, L.N.L.D.; Fernández-Valdivielso, A.; Pereira, O.M. Behaviour of PVD Coatings in the Turning of Austenitic Stainless Steels. *Procedia Eng.* 2013, 63, 133–141.

- [219].Rodríguez-Barrero, S.; Fernández-Larrinoa, J.; Azkona, I.; López De Lacalle, L.N.; Polvorosa, R. Enhanced Performance of Nanostructured Coatings for Drilling by Droplet Elimination. *Mater. Manuf. Process.* 2016, 31, 593–602.
- [220].de lacalle, L.N.L.; Pérez, J.; Llorente, J.I.; Sánchez, J.A. Advanced cutting conditions for the milling of aeronautical alloys. *J. Mater. Process. Technol.* 2000, 100, 1–11.
- [221].Fernández-Abia, A.I.; Barreiro, J.; López De Lacalle, L.N.; Martínez-Pellitero, S. Behavior of austenitic stainless steels at high speed turning using specific force coefficients. *Int. J. Adv. Manuf. Technol.* 2012, 62, 505–515.
- [222].Polvorosa, R.; de Lacalle, L.N.L.; Egea, A.J.S.; Fernandez, A.; Esparta, M.; Zamakona, I. Cutting edge control by monitoring the tapping torque of new and resharpened tapping tools in Inconel 718. *Int. J. Adv. Manuf. Technol.* 2020, 106, 3799–3808.
- [223].Kumar, C.S.; Patel, S.K. Effect of chip sliding velocity and temperature on the wear behaviour of PVD AlCrN and AlTiN coated mixed alumina cutting tools during turning of hardened steel. *Surf. Coat. Technol.* 2018, 334, 509–525.
- [224].Bhowmick, S.; Banerji, A.; Alpas, A.T. Tribological behavior of Al-6.5%, -12%, -18.5% Si alloys during machining using CVD diamond and DLC coated tools. *Surf. Coat. Technol.* 2015, 284, 353–364.
- [225].Pérez-Ruiz, J.D.; de Lacalle, L.N.L.; Urbikain, G.; Pereira, O.; Martínez, S.; Bris, J. On the relationship between cutting forces and anisotropy features in the milling of LPBF Inconel 718 for near net shape parts. *Int. J. Mach. Tools Manuf.* 2021, 170, 103801.
- [226].Pérez-Ruiz, J.D.; Marin, F.; Martínez, S.; Lamikiz, A.; Urbikain, G.; López De Lacalle, L.N. Stiffening near-net-shape functional parts of Inconel 718 LPBF considering material anisotropy and subsequent machining issues. *Mech. Syst. Signal Process.* 2022, 168, 108675.
- [227].Basso, I.; Voigt, R.; Rodrigues, A.R.; Marin, F.; de Souza, A.F.; de Lacalle, L.N.L. Influences of the workpiece material and the tool-surface engagement (TSE) on surface finishing when ball-end milling. *J. Manuf. Process.* 2022, 75, 219–231.
- [228].Khanna, N.; Shah, P.; de Lacalle, L.N.L.; Rodríguez, A.; Pereira, O. In pursuit of sustainable cutting fluid strategy for machining Ti-6Al-4V using life cycle analysis. *Sustain. Mater. Technol.* 2021, 29, 301.
- [229].Rodríguez, A.; Calleja, A.; de Lacalle, L.N.L.; Pereira, O.; Rubio-Mateos, A.; Rodríguez, G. Drilling of CFRP-Ti6Al4V stacks using CO₂-cryogenic cooling. *J. Manuf. Process.* 2021, 64, 58–66.
- [230].Amigo, F.J.; Urbikain, G.; Pereira, O.; Fernández-Lucio, P.; Fernández-Valdivielso, A.; de Lacalle, L.N.L. Combination of high feed turning with cryogenic cooling on Haynes 263 and Inconel 718 superalloys. *J. Manuf. Process.* 2020, 58, 208–222.
- [231].Pereira, O.; Celaya, A.; Urbikain, G.; Rodríguez, A.; Fernández-Valdivielso, A.; de Lacalle, L.N.L. CO₂ cryogenic milling of Inconel 718: Cutting forces and tool wear. *J. Mater. Res. Technol.* 2020, 9, 8459–8468.
- [232].Klocke, F.; Gerschwiler, K.; Schiffler, M.; Morstein, M.; Dessarzin, P.; Lung, D.; Frank, H. Adapted DLC coatings for increasing tapping performance in TiAl6V4. *Materialwiss. Werkst.* 2013, 44, 710–715.
- [233].Sedlaček, M.; Podgornik, B.; Vizintin, J. Tribological properties of DLC coatings and comparison with test results: Development of a database. *Mater. Charact.* 2008, 59, 151–161.
- [234].Sheeja, D.; Tay, B.K.; Lau, S.P.; Shi, X. Tribological properties and adhesive strength of DLC coatings prepared under different substrate bias voltages. *Wear* 2001, 249, 433–439.
- [235].Robertson, J. Diamond-like amorphous carbon. *Mater. Sci. Eng. R.* 2002, 37, 129–281.

- [236].Chen, K.; Lin, J. The study of adhesion and nanomechanical properties of DLC films deposited on tool steels. *Thin Solid Films* 2009, 517, 4916–4920.
- [237].Aizawa, T.; Masaki, E.; Sugita, Y. Complete ashing of used DLC coating for reuse of the end-milling tools. *Manuf. Lett.* 2014, 2, 1–3.
- [238].Baowan, P.; Saikaew, C.; Wisitsoraat, A. Influence of helix angle on tool performances of TiAlN- and DLC-coated carbide end mills for dry side milling of stainless steel. *Int. J. Adv. Manuf. Technol.* 2017, 90, 3085–3097.
- [239].Silva, W.M.; Jesus, L.M.; Carneiro, J.R.; Souza, P.S.; Martins, P.S.; Trava-Airoldi, V.J. Performance of carbide tools coated with DLC in the drilling of SAE 323 aluminum alloy. *Surf. Coat. Technol.* 2015, 284, 404–409.
- [240].Nemati, N.; Penkov, O.V.; Kim, D. Superior surface protection governed by optimized interface characteristics in WC/DLC multilayer coating. *Surf. Coat. Technol.* 2020, 385, 125446.
- [241].Misra, A.; Hirth, J.P.; Hoagland, R.G. Length-scale-dependent deformation mechanisms in incoherent metallic multilayered composites. *Acta Mater.* 2005, 53, 4817–4824.
- [242].Kot, M.; Major, A.; Lackner, J. The tribological phenomena of a new type of TiN/a-C:H multilayer coatings. *Mater. Des.* 2013, 51, 280–286.
- [243].Liu, L.; Wu, Z.; An, X.; Shao, T.; Xiao, S.; Cui, S.; Lin, H.; Fu, R.K.Y.; Tian, X.; Chu, P.K.; et al. Improved interfacial adhesion between TiAlN/DLC multi-layered coatings by controlling the morphology via bias. *Surf. Coat. Technol.* 2017, 331, 15–20.
- [244].Yang, F.; Lu, Y.; Zhang, R.; Zhang, X.; Zheng, X. Microstructure and tribological properties of WSX/a-C multilayer films with various layer thickness ratios in different environments. *Surf. Coat. Technol.* 2017, 309, 187–194.
- [245].Wei, J.; Li, H.; Liu, L.; Guo, P.; Ke, P.; Wang, A. Enhanced tribological and corrosion properties of multilayer ta-C films via alternating sp³ content. *Surf. Coat. Technol.* 2019, 374, 317–326.
- [246].Lin, Y.; Zhou, Z.; Li, K.Y. Improved wear resistance at high contact stresses of hydrogen-free diamond-like carbon coatings by carbon/carbon multilayer architecture. *Appl. Surf. Sci.* 2019, 477, 137–146.
- [247].Hofmann, D.; Kunkel, S.; Bewilogua, K.; Wittorf, R. From DLC to Si-DLC based layer systems with optimized properties for tribological applications. *Surf. Coat. Technol.* 2013, 215, 357–363.
- [248].Lubwama, M.; Corcoran, B.; Sayers, K.; Kirabira, J.B.; Sebbit, A.; McDonnell, K.A.; Dowling, D. Adhesion and composite micro-hardness of DLC and Si-DLC films deposited on nitrile rubber. *Surf. Coat. Technol.* 2012, 206, 4881–4886.
- [249].Qiang, L.; Bai, C.; Gong, Z.; Liang, A.; Zhang, J. Microstructure, adhesion and tribological behaviors of Si interlayer/Si doping diamond-like carbon film developed on nitrile butadiene rubber. *Diam. Relat. Mater.* 2019, 92, 208–218.
- [250].Henderer, W.; Xu, F. Hybrid TiSiN, CrC/C PVD coatings applied to cutting tools. *Surf. Coat. Technol.* 2013, 215, 381–385.
- [251].Fernández Landeta, J.; Fernández Valdivielso, A.; López de Lacalle, L.N.; Girot, F.; Pérez Pérez, J.M. Wear of Form Taps in Threading of Steel Cold Forged Parts. *J. Manuf. Sci. E-T ASME* 2015, 137, 031002.
- [252].Cheng, L.-C.; Ho, W.-Y. Characteristics of CrAlSiN + DLC double layered coating deposited by cathodic arc evaporation process. In *Proceedings of the 2018 6th International*

- Conference on Mechanical, Automotive and Materials Engineering, Hong Kong, China, 10–12 August 2018; pp. 14–17.
- [253].Gayathri, S.; Krishnan, R.; Ravindran, T.R.; Sundari, S.T.; Dash, S.; Tyagi, A.K.; Raj, B.; Sridharan, M. Spectroscopic studies on DLC/TM (Cr, Ag, Ti, Ni) multilayers. *Mater. Res. Bull.* 2012, 47, 843–849.
- [254].Wei, C.; Wang, Y.; Tai, F. The role of metal interlayer on thermal stress, film structure, wettability and hydrogen content for diamond like carbon films on different substrate. *Diam. Relat. Mater.* 2009, 18, 407–412.
- [255].Wei, C.; Yen, J. Effect of film thickness and interlayer on the adhesion strength of diamond like carbon films on different substrates. *Diam. Relat. Mater.* 2007, 16, 1325–1330.
- [256].Shahsavari, F.; Ehteshamzadeh, M.; Amin, M.H.; Barlow, A.J. A comparative study of surface morphology, mechanical and tribological properties of DLC films deposited on Cr and Ni nanolayers. *Ceram. Int.* 2020, 46, 5077–5085.
- [257].Duminica, F.D.; Belchi, R.; Libralesso, L.; Mercier, D. Investigation of Cr(N)/DLC multilayer coatings elaborated by PVD for high wear resistance and low friction applications. *Surf. Coat. Technol.* 2018, 337, 396–403.
- [258].Sui, X.; Liu, J.; Zhang, S.; Yang, J.; Hao, J. Microstructure, mechanical and tribological characterization of CrN/DLC/Cr-DLC multilayer coating with improved adhesive wear resistance. *Appl. Surf. Sci.* 2018, 439, 24–32.
- [259].Singh, V.; Jiang, J.C.; Meletis, E.I. Cr-diamondlike carbon nanocomposite films: Synthesis, characterization and properties. *Thin Solid Films* 2005, 489, 150–158.
- [260].Jo, Y.J.; Zhang, T.F.; Son, M.J.; Kim, K.H. Synthesis and electrochemical properties of Ti-doped DLC films by a hybrid PVD/PECVD process. *Appl. Surf. Sci.* 2018, 433, 1184–1191.
- [261].Zou, C.W.; Wang, H.J.; Feng, L.; Xue, S.W. Effects of Cr concentrations on the microstructure, hardness, and temperature-dependent tribological properties of Cr-DLC coatings. *Appl. Surf. Sci.* 2013, 286, 137–141.
- [262].Santiago, J.A.; Fernández-Martínez, I.; Sánchez-López, J.C.; Rojas, T.C.; Wennberg, A.; Bellido-González, V.; Molina-Aldareguia, J.M.; Monclús, M.A.; González-Arrabal, R. Tribomechanical properties of hard Cr-doped DLC coatings deposited by low-frequency HiPIMS. *Surf. Coat. Technol.* 2020, 382, 124899.
- [263].Wang, A.; Lee, K.; Ahn, J.; Han, J.H. Structure and mechanical properties of W incorporated diamond-like carbon films prepared by a hybrid ion beam deposition technique. *Carbon* 2006, 44, 1826–1832.
- [264].Daniel, R.; Martinschitz, K.J.; Keckes, J.; Mitterer, C. The origin of stresses in magnetron-sputtered thin films with zone T structures. *Acta Mater.* 2010, 58, 2621–2633.
- [265].Robertson, J. Deposition mechanisms for promoting sp³ bonding in diamond-like carbon. *Diam. Relat. Mater.* 1993, 5–7, 984–989.
- [266].Manninen, N.K.; Ribeiro, F.; Escudeiro, A.; Polcar, T.; Carvalho, S.; Cavaleiro, A. Influence of Ag content on mechanical and tribological behavior of DLC coatings. *Surf. Coat. Technol.* 2013, 232, 440–446.
- [267].Zhou, S.; Wang, L.; Wang, S.C.; Xue, Q. Comparative study of simplex doped nc-WC/a-C and duplex doped nc-WC/a-C(Al) nanocomposite coatings. *Appl. Surf. Sci.* 2011, 257, 6971–6979.
- [268].Ferrari, A.C.; Rodil, S.E.; Robertson, J.; Milne, W.I. Is stress necessary to stabilise sp³ bonding in diamond-like carbon? *Diam. Relat. Mater.* 2002, 11, 994–999.

- [269].Wu, Y.; Chen, J.; Li, H.; Ji, L.; Ye, Y.; Zhou, H. Preparation and properties of Ag/DLC nanocomposite films fabricated by unbalanced magnetron sputtering. *Appl. Surf. Sci.* 2013, 284, 165–170.
- [270].Bhowmick, S.; Alpas, A.T. Minimum quantity lubrication drilling of aluminium–silicon alloys in water using diamond-like carbon coated drills. *Int. J. Mach. Tools Manuf.* 2008, 48, 1429–1443.
- [271].Dai, M.; Zhou, K.; Yuan, Z.; Ding, Q.; Fu, Z. The cutting performance of diamond and DLC-coated cutting tools. *Diam. Relat. Mater.* 2000, 9, 1753–1757.
- [272].Lahres, M.; Müller-Hummel, P.; Doerfel, O. Applicability of different hard coatings in dry milling aluminium alloys. *Surf. Coat. Technol.* 1997, 91, 116–121.
- [273].Enke, K. Dry machining and increase of endurance of machine parts with improved doped DLC coatings on steel, ceramics and aluminium. *Surf. Coat. Technol.* 1999, 116–119, 488–491.
- [274].Dosbaeva, J.; Fox-Rabinovich, G.; Dasch, J.; Veldhuis, S. Enhancement of Wet- and MQL-Based Machining of Automotive Alloys Using Cutting Tools with DLC/Polymer Surface Treatments. *J. Mater. Eng. Perform.* 2008, 17, 346–351.
- [275].Fukui, H.; Okida, J.; Omori, N.; Moriguchi, H.; Tsuda, K. Cutting performance of DLC coated tools in dry machining aluminum alloys. *Surf. Coat. Technol.* 2004, 187, 70–76.
- [276].Santos, G.R.D.; da Costa, D.D.; Amorim, F.L.; Torres, R.D. Characterization of DLC thin film and evaluation of machining forces using coated inserts in turning of Al–Si alloys. *Surf. Coat. Technol.* 2007, 202, 1029–1033.
- [277].Hanyu, H.; Kamiya, S.; Murakami, Y.; Kondoh, Y. The improvement of cutting performance in semi-dry condition by the combination of DLC coating and CVD smooth surface diamond coating. *Surf. Coat. Technol.* 2005, 200, 1137–1141.
- [278].Ucun, I.; Aslantas, K.; Bedir, F. The performance of DLC-coated and uncoated ultra-fine carbide tools in micromilling of Inconel 718. *Precis. Eng.* 2015, 41, 135–144.
- [279].Ammarullah, M.I.; Afif, I.Y.; Maula, M.I.; Winarni, T.I.; Tauviqirrahman, M.; Akbar, I.; Basri, H.; van der Heide, E.; Jamari, J. Tresca stress simulation of metal-on-metal total hip arthroplasty during normal walking activity. *Materials* 2021, 14, 7554.
- [280].Dolinšek, S. Work-hardening in the drilling of austenitic stainless steels. *J. Mater. Process. Technol.* 2003, 133, 63–70.
- [281].Filiz, S.; Conley, C.M.; Wasserman, M.B.; Ozdoganlar, O.B. An experimental investigation of micro-machinability of copper 101 using tungsten carbide micro-endmills. *Int. J. Mach. Tools Manuf.* 2007, 47, 1088–1100.
- [282].Ziberov, M.; de Oliveira, D.; da Silva, M.B.; Hung, W.N.P. Wear of TiAlN and DLC coated microtools in micromilling of Ti-6Al-4V alloy. *J. Manuf. Process.* 2020, 56, 337–349.
- [283].Lin, S.Y.; Yu, S.H.; Wu, M.L. Effect of Different Coating Materials on Cutting Performance in High-Speed Machining of Mold Steels. *Key Eng. Mater.* 2007, 364–366, 1026–1031.
- [284].Badiger, P.V.; Desai, V.; Ramesh, M.R. Performance of DLC coated tool during machining of MDN431 alloyed steel. *Mater. Today Proc.* 2018, 5, 17360–17370.
- [285].Elosegui, I.; Alonso, U.; de Lacalle, L.N.L. PVD coatings for thread tapping of austempered ductile iron. *Int. J. Adv. Manuf. Technol.* 2017, 91, 2663–2672.
- [286].“Surface Roughnes.” Wikipedia, Wikimedia Foundation, 05 July 2022, en.wikipedia.org/wiki/Surface_roughnes.
- [287].Suh, Nam P., and H.-C. Sin. 1981. “The Genesis of Friction.” *Wear* 69 (1): 91–114. [https://doi.org/10.1016/0043-1648\(81\)90315-X](https://doi.org/10.1016/0043-1648(81)90315-X).

- [288].Homola, Andrew M., Jacob N. Israelachvili, Patricia M. McGuiggan, and Michelle L. Gee. 1990. "Fundamental Experimental Studies in Tribology: The Transition from 'Interfacial' Friction of Undamaged Molecularly Smooth Surfaces to 'Normal' Friction with Wear." *Wear* 136 (1): 65–83. [https://doi.org/10.1016/0043-1648\(90\)90072-I](https://doi.org/10.1016/0043-1648(90)90072-I).
- [289].Amrita, M., S.A. Shariq, Manoj, and Charan Gopal. 2014. "Experimental Investigation on Application of Emulsifier Oil Based Nano Cutting Fluids in Metal Cutting Process." *Procedia Engineering* 97: 115–24. <https://doi.org/10.1016/j.proeng.2014.12.231>.

A Brief Biographical Sketch

Ramakant Rana

Ramakant Rana is presently working as an Assistant Professor in the Department of Mechanical and Automation Engineering at Maharaja Agrasen Institute of Technology (affiliated to Guru Gobind Singh Indraprastha University), New Delhi. He obtained his Bachelor's degree in Mechanical and Automation Engineering from Guru Gobind Singh Indraprastha University, New Delhi in 2010 and completed his Masters' degree in Production Engineering from the Department of Mechanical Engineering and Production & Industrial Engineering of Delhi Technological University, Delhi in the year 2014. He has 12 years of experience in the academic sector of teaching undergraduate engineering students. He has taught various subjects like Engineering Drawing (Engineering Graphics), Manufacturing Process, Engineering Mechanics, Metrology, Mechatronics, Robotics, Management of Manufacturing System, Workshop Technology, and Advance Methods of Machining. He is also life-member of the following professional societies viz. Institution of Engineers (India), Indian Society for Technical Education and The Robotics Society. Apart from teaching, he has publications at various international journals and conferences.